SEEPAGE INDUCED INSTABILITY IN WIDELY GRADED SOILS

by

Maoxin Li

B.Eng. Tsinghua University, China, 1991
M.Eng. the National University of Singapore, 2001

A THESIS SUBMITTED IN PARTIAL FULFILMENT OF
THE REQUIREMENTS FOR THE DEGREE OF

DOCTOR OF PHILOSOPHY

in

THE FACULTY OF GRADUATE STUDIES

(Civil Engineering)

THE UNIVERSITY OF BRITISH COLUMBIA
(VANCOUVER)

May 2008

ABSTRACT

Internal instability of a widely graded cohesionless soil refers to a phenomenon in which its finer particles migrate within the void network of its coarser particles, as a result of seepage flow. Onset of internal instability of a soil is governed by a combination of geometric and hydromechanical constraints. Much concern exists for embankment dams and levees built using soils with a potential for internal instability. Migration of finer particles to a boundary where they can exit, by washing out, may cause erosion or piping failure and, occasionally, induce collapse of these soil structures. There is a need, in professional practice, to better understand the phenomenon and to develop improved methods to evaluate the susceptibility of a soil.

A series of permeameter tests was performed on six widely-graded cohesionless materials. The objectives are to assess the geometric indices proposed for evaluation of susceptibility, and examine hydromechanical factors influence the onset of internal instability. A modified slurry mixing technique, with discrete deposition, was found satisfactory for reconstitution of the homogeneous saturated test specimens. The onset of internal instability was founded to be triggered by a combination of effective stress and hydraulic gradient. The finding yields a hydromechanical envelope, unique for a particular gradation shape, at which internal instability initiated.

Three commonly used geometric criteria were comprehensively evaluated with reference to these experimental data and also a database compiled from the literature. The relative conservatism of each criterion was examined and a modified semi-empirical geometric rule then proposed based on the capillary tube model. A theoretical framework for plotting the hydromechanical envelope was established based on an extension of the α concept of Skempton and Brogan, and subsequently verified by test data. Finally, a novel unified approach was proposed to assess the onset of internal instability, based on combining geometric and hydromechanical indices of a soil.

TABLE OF CONTENTS

LIST OF TABLES

LIST OF FIGURES

LIST OF SYMBOLS

A	Cross sectional area of specimen (cm^2)
α	Stress reduction factor in finer fraction
α_D	Shape coefficient
C_u	Coefficient of uniformity
C_c	Coefficient of curvature
D	Diameter of specimen
D_h^c	Kozeny effective diameter in the coarse fraction (mm)
D_n	Grain size corresponding to n % finer by weight (mm)
D'_n	Grain size corresponding to n % finer in coarser fraction (mm)
d'_n	Grain size corresponding to n % finer in finer fraction (mm)
DPT	Differential pressure transducer
F	Mass fraction smaller than D in % (Kenny and Lau, 1985 and 1986)
f	friction parameter between the sidewall and specimen
Gs	Specific gravity
H	Mass fraction measured between D and 4D in % (Kenny and Lau, 1985 and 1986)
h	Water head (cm)
h_{ij}	Water head measured across the length of specimen between ports i and j (cm)
i_{av}	Average hydraulic gradient

i_{cr} Critical hydraulic gradient

i_{ij} Hydraulic gradient between across the length of specimen between ports i and j

k Hydraulic conductivity (cm/s)

k_{ij} Hydraulic conductivity for the length of specimen between port i and j (cm/s)

L Length of the specimen (cm)

LVDT Linear variable differential transformer

n Porosity of a soil

n_c Porosity of coarser fraction

O_{50} Average capillary tube diameter in the coarser fraction (mm)

q Volumetric flow rate (cm^3/s)

TPT Total pressure transducer

v Discharge velocity (cm/s)

σ'_{vm} Mean vertical effective stress (kPa)

$\bar{\sigma}'_{vm}$ Normalized mean vertical effective stress

σ'_{t0} Effective stress on the top of specimen at i = 0 (kPa)

σ'_{b0} Effective stress on the bottom of specimen at i = 0 (kPa)

ACKNOWLEDGEMENTS

I would like to extend sincere thanks and gratitude to my research supervisor, Dr. Jonathan Fannin, for his continued guidance and support throughout the course of this study. I also wish to thank the members of my supervisor committee: Dr. Dawn Shuttle, Dr. Dharma Wijewickreme, Dr. John Howie and Dr. Roger Beckie for their input and constructive comments on this manuscript. Funding support for this research was provided from the Natural Sciences and Engineering Research Council of Canada and British Columbia Hydro and Power Authority.

Thanks are extended to the Civil Engineering Workshop (Bill Leung and Harald Shremp) and to the technical staff (Scott Jackson and John Wong). Thanks are also extended to my colleagues (Ricardo Moffat, Abdul Khan, Jessica Campbell, Ali Khalili, Mavi Sannin, Pascale Rouse, and Lalinda Weerasekara) for their help and insightful conversation with respect to the research.

Finally, I would like to thank my wife, Hui, for her constant encouragement and support over the course of this study.

1 Introduction

1.1 Seepage-induced internal instability

In a soil, internal instability refers to the movement of its finer particles through a network of its coarser particles. The phenomenon is a consequence of seepage-induced forces. Internal instability usually occurs in soils that are widely-graded or gap-graded. The phenomenon is a multidisciplinary issue governed by the principles of soil mechanics and hydraulics. In petroleum engineering, the migration of finer particles may cause clogging of soil reservoirs leading to oil production decline (Valdes, 2002). In geotechnical engineering, particle migration plays a critical role in the performance of filtration and drainage systems, where improper design may cause serious problems, for example, the deterioration of pavement drainage in roadways and airfields. Additionally, much concern exists in embankment dams and levees, where particle migration may result in a piping or erosion failure and a potential for collapse of soil structures (Sherard, 1979; BC Hydro and Hydro Quebec, 2000; Foster et al. 2000; Charles, 2001; Zhang and Chen, 2006).

Onset of internal instability is governed by: (i) the grain size distribution curve, porosity and particle shape of the soil, and (ii) a combination of effective stress and critical hydraulic gradient (Kezdi, 1981; Kenney and Lau, 1985; Moffat, 2005). The first condition represents a geometric criterion that may be used to determine susceptibility to internal instability. The latter condition establishes a hydromechanical relation, which may be used to determine the critical gradient at which the onset of internal instability initiates at a certain effective stress.

1.2 Objectives and scope of the study

Widely-graded and gap-graded soils are present in nature and consequently they are encountered in construction practice. The monitor of large earth dam constructed with these soils indicates performances that differ from design expectations, for instance, higher pore-water pressures developed in the downstream part of the core and sinkhole incident observed in the crest. A notable example is that of at the W.A.C. Bennett Dam (formerly known as Portage Mountain Dam) in British Columbia, as mentioned by Morgan and Harris (1967). For these unexpected performances of earth dam, there is a need for a science-based explanation.

In the literature much focus has been placed on the potential for internal instability, and therefore investigation of the geometric criterion (Kezdi, 1979; Kenney and Lau, 1985; Burenkova, 1993; Honjo, et al., 1996). However, few of these studies are verified independently by the work of others (Skempton and Brogan, 1994, Fannin and Moffat, 2006). In order to use the results of these studies with more confidence in engineering practice, a comprehensive review of the various geometric criteria is necessary. Additionally, since only limited research has been conducted on the onset of internal instability (Skempton and Brogan, 1994; Moffat, 2005), the concept of a hydromechanical criterion has not yet been well-defined.

An intended contribution of the work is to implement a geometric criterion, based on the capillary tube model, and to correlate it to the hydromechanical criterion, based on a concept of stress reduction within the grain assembly. Such a correlation would provide a science-

based explanation of seepage-induced internal erosion, and represent a novel advance in engineering practice.

This thesis consists of seven chapters, which are briefly outlined as follows:

- Chapter 1 gives a brief introduction to the phenomenon of internal instability, as a background to highlighting the objectives and scope of study.
- Chapter 2 reviews existing studies on internal instability, providing a summary of the more commonly-used methods to assess the potential of internal instability together with the findings of limit research on the onset of internal instability.
- Chapter 3 describes the small and large permemeater test device used in this experimental study. Additionally, properties of the materials, the specimen reconstitution technique, and the test procedure are reported.
- Chapter 4 describes the test results, including visual observations as well as measurements obtained from instrumentation scheme.
- Chapter 5 presents an analysis of these experimental results. Particular emphasis is placed on a summary of failure phenomena and characteristics of a hydromechanical envelope for each gradation examined in testing.
- Chapter 6 presents the evaluation of geometric criteria used to evaluate the potential for instability. Thereafter, a theoretical hydromechanical envelope is defined, based on the concept of stress reduction in the finer fraction of a soil. A unified approach to evaluate the initiation of internal instability in a soil is then proposed.
- Chapter 7 concludes the study. Theoretical and experimental works presented in this thesis are summarized, and the recommendations provided for future research.

2 Literature Review

The phenomenon of internal stability of cohesionless soils has been studied by a number of investigators over a period of more than 50 years, commencing with the US Army Corps of Engineers in 1953. This chapter provides a brief review of the findings of those previous investigations, including terminology used to describe behavior, geometric criteria proposed to evaluate susceptibility, and insights into the hydraulic conditions that trigger the onset of instability.

2.1 Terminology

Internal stability is a general term used to describe the migration of finer particles of a soil within its pore spaces. The literature relating to this phenomenon includes other terms: inherent stability, suffusion, suffosion, and suffossion. It is necessary to review these definitions before proceeding further.

The U.S. Army Corps of Engineers (USACE) (1953) first used the term “inherent stability” and “internal stability” to define “the resistance of the filter to segregation and piping within itself”. Later, Kenney and Lau (1985) defined the term “internal stability” as “the ability of a granular material to prevent loss of its own small particles due to disturbing agents such as seepage and vibration”.

Kezdi (1979) used the word “suffusion” to define “a phenomenon where water, while seeping through the pores, carries along the finer particles without destroying the soil

structure". According to the actual location of particle movement within the soil deposit, a distinction should be made between internal suffusion, external suffusion and contact suffusion. Kovacs (1981) also used the word "suffusion" to describe the motion of finer particles. He defined internal suffusion as a "redistribution of fine grains within the layer, when the solid volume of the layer is not changed only the local permeability is altered". In contrast, external suffusion was defined as "the scouring of fines grains when the volume of the solid matrix is reduced, accompanied by an increase in permeability, but the stability of the skeleton composed of the coarse grains is unaffected". Head (1992) affirmed this distinction where suffusion occurs as "movement of fine soil particles from a matrix of coarser particles due to the flow of water through the soil. Fine particles may be either carried away, or moved into another soil horizon".

Kenney and Lau (1985) used the word "suffosion" to describe the "the transport of small particles from a soil", referring to earlier work of Lubochkov (1969, see Kenney and Lau, 1985). Charles (2001) defined suffosion as "mass erosion due to seepage flow in soils which are internally unstable". Jones (1981) reported that use of the word "suffosion" could be attributed to Professor A.P. Pavlov of Moscow University in 1898, and that it appears as a term defined in the Kratkaja Encyclopaedia of Geography.

Chapuis (1992) elected to use the word "suffossion" to describe "the transport of small particles from a soil, which leaves large openings between the large particles of this soil". Later, Chapuis and Aubertin (2004) provided further explanation for its use. They claimed that "suffusion, which is mainly used in medicine, basically refers to a permeating process,

often a fluid movement towards a surface or over a surface, thus, using it would be incorrect". They also claimed that suffosion is not a real word, since it is not found in English and French dictionaries. Therefore, they suggested using "suffossion", with two each of the letters f and s, which comes from the Latin *suffossio*, *onis*, a word that appears in the Oxford English Dictionary. However, in the opinion of this writer, suffossion means "digging under or up; undermining" (online Oxford English Dictionary), and does not properly describe the general migration of finer particles.

Interestingly, the word "suffosion" is found in Wikipedia, where it is defined as "the relocation and the evacuation of fine soil particles in the soil by water" (http://de.wikipeida.org/wiki/suffosion). This definition more properly describes the migration of finer particles of a soil.

In summary, the terms "internal stability", "inherent stability", "suffusion", "suffosion" and "suffossion" have all been used to describe the migration of finer particles of a soil within its own pore spaces. The term "inherent stability" is seldom used. Suffossion has only been used by Chapuis (1992) and Chapuis and Aubertin (2004). Suffusion and suffosion are often used interchangeably in the literature. The term "internal stability" is generally accepted without any confusion. In this thesis, "internal stability" and "suffosion" are used throughout with recognition of "suffusion" as more properly describing the process of permeation. Internal suffosion and external suffosion are distinguished: internal suffosion refers to the redistribution of finer particles within layers that is accompanied by a change in local

hydraulic conductivity, whereas external suffosion refers to the scouring of finer particles that is associated with an overall increase in hydraulic conductivity (Kovacs, 1981).

2.2 Geometric criteria: evaluation of susceptibility

A geometric criterion addresses the comparative sizes of finer and coarser particles in the grain size distribution curve of a soil. In concept, if constrictions in the pore network of the coarse particles are larger than some of the finer particles, these particles can be transported by seepage flow. A series of laboratory studies have been reported that examine the boundary between stable and unstable gradations (see Table 2.1). Several approaches have been proposed in the literature to describe such geometric constraints to instability, and the utility of these various methods has not been critically reviewed.

2.2.1 The U.S Army Corps of Engineers (USACE, 1953)

In order to investigate the feasibility of using a mixture of concrete sand and concrete gravel as a filter, in lieu of a double-layer system of the same materials, the U.S Army Corps of Engineers (1953) tested sand-gravel mixtures to determine which combination was most suitable insofar as inherent stability and permeability characteristics were concerned. They carried out constant-head permeameter tests on four sand-gravel mixtures. The soils were placed rather loosely, and as uniformly as possible, in a 5-in diameter permeameter. No information was provided about any surcharge loading. Unidirectional flow was imposed in the downward direction, starting with a gradient of 0.5, and then increased in steps to 16. Vibration was imposed during the test. Inherent stability was determined from a comparison of grain size distribution before and after testing. Results indicated that materials A (50%

sand + 50% gravel) and D (30% sand + 70% gravel) were inherently unstable, and unsuitable for use as filter material. Materials B (70% sand + 30% gravel) and C (90% sand + 10% gravel) were inherently stable. Material B was declared the better filter material since it had a more suitable permeability than material C.

2.2.2 Istomina (1957)

Istomina (1957; see Kovacs, 1981) put forward a simple method to evaluate internal stability using the coefficient of uniformity (C_u), considered a basic index value for the grain size distribution curve. If $C_u \leq 10$, the soil is internally stable; if $C_u \geq 20$, the soil is internally unstable; if $10 \leq C_u \leq 20$, the soil is deemed a transition material.

2.2.3 Lubochkov (1969)

Lubochkov (1969) found that the likelihood of particle movement depends to a great extent on the shape of the grain size distribution curve, and hence not all materials having uniformity coefficients higher than 20 are susceptible to internal instability. He conceived an analytic method based on the hypothesis that a layer is not susceptible to suffosion if the slope of the grain size distribution curve is equal to, or smaller than, a given limit in each diameter-interval. A simplified mathematical form of this condition can be written as follows (Molenkamp et al, 1979):

$$\frac{1}{\chi^{0.6}} \times \frac{W(\chi d) - W(d)}{W(d) - W(\frac{d}{\chi})} < 1 \qquad (2.1)$$

where, d = any grain size diameter on the gradation curve, W(x) = percentage of weight passing sieve with grain size x; and χ = coefficient associated with the safety factor, shown in Table 2.2 from Kovacs (1981).

2.2.4 Kezdi criterion

Kezdi proposed a method to assess the internal stability of soils in 1969, described in further detail by Kezdi (1979). In this method the grain-size curve is split into its coarse and fine components at an arbitrary grain diameter; the coarser component may be evaluated for its capacity to retain the finer component. If both components satisfy the limiting criterion $D'_{15}/d'_{85} = 4$ advocated by Terzaghi (1939) for soil retention in two adjacent uniformly graded soils, the soil is considered internally stable. In this method, D'_{15} is the diameter of the 15% mass passing in the coarser fraction, and is deemed to characterize the pore size constriction of the coarser fraction; d'_{85} is the diameter of the 85% mass passing in the finer fraction, considered representative of the grain size of the finer fraction (Figure 2.1). Three gap-graded soils were evaluated by Kezdi (1979), which experienced significant internal erosion according to an earlier investigation of Bernatzik in 1947, and used to verify the method.

De Mello (1975) alludes, independently, to the same approach as a "simple test to check unacceptable skip-grading with respect to internal erosion"; Sherard (1979) later suggested a threshold value for the filter ratio $D'_{15}/d'_{85} = 4 \sim 5$. Lowe (1988) advocates the same approach as a criterion for assessment of "the self-filtering ability of broadly graded and skip-graded materials". Accordingly, the method is considered to have achieved general recognition.

Fannin and Moffat (2006) tested five gap-graded and widely-graded soils in a permeameter cell. The test specimens were 10 cm in diameter, with a length of 10 cm, and supported on a metal screen filter (Figure 2.2). A surcharge of 25kPa was applied to the specimen, and unidirectional flow imposed in a downward direction together with automatic vibration. Loss of finer particles and variation of local hydraulic gradient, were used to characterize the internal instability. They found the percentage loss of finer particles increased with increasing $(D'_{15}/d'_{85})_{max}$, see Figure 2.3, from analysis including additional test data from Honjo et al. (1996) and Kenney and Lau (1985). The threshold value of internal stability $D'_{15}/d'_{85} = 4$ advocated by Kezdi (1979) was found consistent with these experimental data.

2.2.5 Capillary tube model (Kovacs, 1981)

Kovacs (1981) adapted a capillary tube model that is widely used in porous media theory to assess internal stability. In the model, pore space of the soil is represented as a bundle of parallel cylindrical tubes (see Figure 2.4). The average pore diameter of the coarse fraction is calculated based on Kozeny's effective diameter and the porosity of the coarse fraction. The grain size distribution curve is divided at a given diameter D_n, from which the effective diameter (D_h^c) of the coarse skeleton is calculated. The average diameter of pipes (d_0) in the idealized soil skeleton is determined based on the following expression:

$$d_0 = 4\frac{n_c}{1-n_c}\frac{D_h^c}{\alpha_D} \qquad (2.2)$$

where α_D = shape coefficient; n_c = porosity of skeleton; and

$$D_h^c = \frac{1}{\sum \frac{\Delta F_i^c}{D_i^c}} \tag{2.3}$$

where D_i^c = average diameter in the i-th interval of the particle size distribution curve of coarse fraction and ΔF_i^c = the weight of grains in the i-th interval of the particle size distribution curve of coarse fraction.

According to the literature on filter design, d'_{85} of finer fraction is generally considered as the representative diameter of the finer fraction. Therefore, Kovacs (1981) proposed a criterion for internal instability $d_0 < d_{85}^{'}$, which is expressed in effective diameter as

$$4\frac{n_c}{1-n_c}\frac{D_h^c}{\alpha_D} < d_{85}^{'} \tag{2.4}$$

This model has not been widely used since it had not been verified based on experimental data.

2.2.6 Kenney and Lau criterion (1985, 1986)

Kenney & Lau (1985) amended Lubochkov's approach and proposed a new criterion based on interpretation of experimental observations. They carried out constant-head permeameter tests on 16 well-graded sandy gravels. The soil was reconstituted by compaction in a cylindrical cell, leading to a specimen with diameter either 245 mm or 580 mm, and length either 450 mm or 860 mm (see Figure 2.5). A low surcharge pressure of 10 kPa was applied, with downward seepage flow at an unspecified gradient. Mild vibration, in the form of

manual tapping, was imposed throughout the test and found to have a profound effect on the response of some gradations. The change in grain size distribution before and after testing was used to determine whether internal instability took place.

A criterion was proposed based on a method of describing the shape of the grain-size distribution curve (see Figure 2.6). In this method, the increment of percent passing (H) that occurs over a designated grain size interval of D to 4D is compared to the percent passing (F) at grain size D. If the grading curve lies below a boundary defined by a stability index H/F, over a portion of its finer end given by $F \leq 0.2$ for soils with a primary fabric that is widely-graded, and by $F \leq 0.3$ for soils with a primary fabric that is narrowly-graded, then it is deemed potentially unstable. The boundary was initially defined as H/F = 1.3 based on Lubochkov (Kenney and Lau, 1985), which upon discussion by Milligan (1986) and Sherard and Dunnigan (1986) was found to be overly conservative, and subsequently revised to H/F = 1.0 (Kenney and Lau, 1986).

2.2.7 Chapuis (1992, 2006)

Chapuis (1992) compared the Kezdi and the Kenney and Lau criteria and demonstrated that the two methods could be expressed as simple but very similar slope criteria. The slope of the gradation curve at any point may be approximated by the slope of the secant line. The secant slope of the grain-size distribution curve indicates the likelihood of internal instability. Therefore, the Kezdi criterion is equivalent to the following: if a soil has in its gradation curve a slope lower than 0.15/log(4) per cycle, it will be unable to stabilize its own particles finer than the grain size at which such a slope occurs. Likewise, the Kenney and Lau method

is equivalent to the following: at a particle size D_y ($y \leq 20$), the slope per cycle of the gradation curve must be higher than y/log(4) to have internal stability. Two examples are presented in a later paper (Chapuis and Tournier, 2006).

Chapuis (1992) also indicated that these criteria must be applied with caution by experienced users. In particular, there is little information on the influence of such factors as (i) the severity of disturbance forces, due to either vibration or seepage; (ii) the stabilizing or destabilizing effects of disturbing forces; (iii) the void ratio; (iv) the initial segregation of the soil.

2.2.8 Burenkova (1993)

Burenkova (1993) proposed a method based on results of laboratory tests on 22 granular materials of maximum particle size up to 100mm, and coefficient of uniformity, C_u, up to 200. For the tests, the soils were divided into various size fractions, and then dry-mixed in a container. The basic assumption is that a smaller size fraction does not form part of the basic soil skeleton if it does not cause a volume increase when mixed with a coarser size fraction. Based on the three representative fractions d_{15}, d_{60}, and d_{90}, the heterogeneity of the soils was described by two ratios called conditional factors of uniformity:

$$h' = d_{90} / d_{60} \qquad (2.5a)$$

$$h'' = d_{90} / d_{15} \qquad (2.5b)$$

Based on these two ratios, Burenkova (1993) presented boundaries separating the "suffosive soils" from "non-suffosive soils" as shown in Figure 2.7. Zones I and III represent suffosive mixes; Zone II represents non-suffosive mixes; Zone IV represents artificial soils. The resulting domain for non-suffosive soils can approximately be evaluated from the ratio d_{90}/d_{60}, where:

$$0.76\log(d_{90}/d_{15})+1 < d_{90}/d_{60} < 1.86\log(d_{90}/d_{15})+1 \qquad (2.6)$$

2.2.9 Honjo et al. (1996)

Honjo et al. (1996) tested gap-graded soils, predominantly sands in which the medium sand fraction was absent. The test specimens were either 150 or 300 mm in diameter, with a length of 100 mm, and supported on a metal screen filter. A light surcharge of 0.9 kPa was applied to the specimen, and unidirectional flow imposed in a downward direction together with gentle tapping to vibrate the specimen. Loss of finer particles was measured and used to determine the occurrence of internal instability. The loss of finer particles increased with increasing gap ratio, which was defined as the ratio of the upper and lower bound particles size bounding the gap. They concluded that a gap ratio of 4 can be considered as an upper bound limit for the stability of gap graded base soils, regardless of the amount of fines present in soil.

2.2.10 Liu (2005) and Mao (2005)

Liu proposed a method to assess the internal stability of cohesionless soils in 1963, described in further detail by Liu (2005). In his method, the soil is again divided into two components, a finer fraction and a coarser fraction. The soil is considered to be internally stable if the finer

particles fully occupy void spaces formed by the coarser particles. Therefore, given a division point on the gradation curve, the finer fraction by mass P (%) is used to evaluate the internal stability of a soil. Based on a combination of theoretical analysis and experimental results, the following criterion was suggested:

$$\begin{aligned} &P < 25, \text{ internally unstable} \\ &P = 25 \sim 35, \text{ transition condition} \\ &P > 35, \text{ internally stable} \end{aligned} \tag{2.7}$$

The division point between finer fraction and coarser fraction is determined based on soil type. Soils are categorized into two types: gap-graded (or discontinuously graded), and continuously graded. For gap-graded soils, P = mass passing at the gap location (%). For continuously graded soils, P = mass passing (%) at the division diameter $d_f = \sqrt{d_{70} d_{10}}$.

A similar method was proposed by Mao in 1981, and described in further detail by Mao (2005). Once again, the finer fraction p_f (%) is also used to evaluate the internal stability of a soil of porosity (n). The criterion was suggested as:

$$\begin{aligned} &p_f < 100 \frac{1}{4(1-n)}, \text{ internally unstable} \\ &p_f \geq 100 \frac{1}{4(1-n)}, \text{ internally stable} \end{aligned} \tag{2.8}$$

For gap-graded soils, p_f = mass passing at the gap location (%). For continuously graded soils, p_f = mass passing (%) at the division diameter $d_f = 1.3\sqrt{d_{85}d_{15}}$.

These methods have widely been used in levee design and sluice design in China, and are accepted in two technical standards: "Design specification for sluice (SL265-2001)" (Ministry of Water Resource, 2001) and "Code of geological investigation for levee project (SL188-2005)" (Ministry of Water Resource, 2005).

2.2.11 Wan and Fell (2004)

Wan and Fell (2004a, 2004b) investigated the internal stability of clay-silt-sand-gravel and silt-sand-gravel mixtures. In total, 14 soils were reconstituted by compaction in a cylindrical cell, yielding a specimen of diameter 300 mm and length 300 mm. The specimen was supported on a drainage layer made of 20 mm single-sized aggregate. The 25 mm single-sized aggregate on top of the specimen served to break up the incoming flow so as to ensure more uniform water pressure on the upper surface of the soil specimen. Unidirectional flow was imposed in a downward direction, at a hydraulic gradient of 10 to 18 across the specimen. No vibration was applied to the specimen. During a test, the colour of the outflow was continuously observed so as to note signs of erosion of fines. The change in grain size distribution before and after testing was used to determine whether internal instability took place.

They assessed those soils using currently available methods and claimed that: (1) the coefficient of uniformity, C_u (the U.S. Army Corps of Engineers (1953), Isomina (1957)), is

not an accurate predictor of internal stability; (2) methods that involve splitting a soil into a coarse fraction and a fine fraction (Kezdi 1969, de Mello 1975, Sherard 1979) are too conservative for assessing internal stability since they tend to classify stable soils as unstable; (3) the Kenney and Lau (1985, 1986) method is conservative in that stable soils are classified as internally unstable soils; (4) the Burenkova (1993) method is less conservative than the Kenney and Lau (1985, 1986) method in that some unstable soils are plotted in the non-suffosive zone.

Among these geometric criteria, the Kezdi (1979), Kenney and Lau (1985, 1986) and Burenkova (1992) criteria are most commonly used in engineering practice. A critical review about these three methods is presented in this thesis.

2.3 Hydraulic conditions: onset of instability

Kovacs (1981) acknowledged that failure to satisfy a geometric criterion "does not imply high susceptibility to suffusion, because the forces at the points of contact of the fine grains hinder their movement and, therefore, a relatively high gradient is necessary to initiate movement". Accordingly, some embankment and hydraulic structures constructed using potentially unstable materials may not experience suffosion in practice. This raises the challenge of confidently assessing the relative safety of soil structures built with potentially unstable materials. In practice, it may be acceptable to use potentially unstable materials in projects where hydraulic gradients are not believed problematic. Previous research related to hydraulic conditions on onset of instability is reviewed in the following section.

2.3.1 Terzaghi's theoretical critical gradient for heave failure

Terzaghi (1939) first formulated a theory about seepage failure in a uniform sand column. The theoretical development is based on a summation of vertical seepage forces exerted by the upward flow of water and the vertical downward weight of the submerged soil particles. When the hydraulic gradient causes a zero effective stress condition, that is the seepage pore water pressure at a certain level equals to the total overburden stress of the soil above that level, then heave failure occurs. The critical hydraulic gradient is given by:

$$i_c = \frac{\gamma'}{\gamma_w} = (G_s - 1)(1 - n) \qquad (2.9)$$

where G_s = specific gravity of soil particles; n = porosity of soil; γ' = submerged unit weight of soil; γ_w = unit weight of water.

2.3.2 Adel et al. (1988)

Adel et al. (1988) tested three minestones, which are commonly used for the slope protection works on banks and dikes in the Netherlands. The test specimen was 105cm long. A mesh confined the bulk of the material (see Figure 2.8). No surcharge was applied to the specimen, and unidirectional flow was imposed in a horizontal direction. Any washout of finer particles was collected in a sandtrap. Rate of loss of finer particles was used to determine a value for critical hydraulic gradient, which was defined as that to transport $1g/m^2 \cdot s$, measured during 30 minutes and averaged over this period. A linear relation was proposed between critical hydraulic gradient (i_{cr}) and $(H/F)_{min}$ (see Figure 2.9).

2.3.3 Skempton and Brogan (1994)

Skempton and Brogan (1994) reported findings from piping tests on well-graded and gap-graded sandy gravels. Test specimens were 139 mm in diameter, with a length of approximately 155 mm (see Figure 2.10). After saturation of the specimen in a permeameter, unidirectional flow was imposed in an upward direction and increased until failure occurred. Internal instability yields a disproportionate increase in the velocity of seepage flow. Interpretation of the results was used to confirm the Kenney and Lau (1985, 1986) criterion for internal stability, and also the Kezdi (1979) criterion. They found that for unstable materials, the critical hydraulic gradient could be roughly 1/3 to 1/5 of the normal threshold of 1.0, based on the theory of Terzahi. A tentative relation was proposed between critical gradient ($i_c < 1$) and Kenney and Lau's stability index $(H/F)_{min}$ (Figure 2.11). It is interesting to note that they re-interpreted a non-linear relation between i_c and $(H/F)_{min}$ in horizontal flow tests reported by Adel et al. (1988) who proposed a linear relation (see Figure 2.9). An important conclusion from this work is that the distribution of internal stress may influence piping potential (Richards and Reddy, 2007).

2.3.4 Liu (2005) and Mao (2005)

Extensive research was conducted in China, from the early 1960's to the late 1970's, on the phenomenon of internal stability in cohesionless soils, since many earthfill dams were constructed during that period. Unfortunately, most of the original experimental work cannot be readily accessed. Some results are reported in a book by Liu (2005) and in a paper by Mao (2005). Personal communication (Li, 2006) indicates that most of the laboratory tests were carried out in a vertical permeameter device. Test specimens were 200 ~ 300 mm in

diameter. No surcharge was applied to the specimen. A unidirectional flow was imposed in the upward direction, and hydraulic gradient gradually increased until failure occurred. Critical gradient was defined to be that at which the slope of gradient ~ seepage velocity curve changed significantly. Based on experimental results, a non-linear relation was proposed by Liu (2005) between the critical gradient (J_{kp}) and finer fraction (P, %). The critical gradient increases with increasing finer fraction. A relation was also proposed by Mao (2005) between the critical gradient (J_c) and a function of the finer fraction (p_f, %). The empirical expression for critical gradient is proposed by Mao (2005):

$$i_{cr} = \frac{7d_5}{d_f}[4p_f(1-n)]^2 \qquad (2.10)$$

where d_5 = 5% mass passing of a soil; $d_f = 1.3\sqrt{d_{85}d_{15}}$ = division diameter between finer and coarser particles; p_f = mass passing (%) at d_f; and n = porosity.

2.3.5 Wan and Fell (2004)

A companion study of hydraulic factors on the internal stability was carried out by Wan and Fell (2004b) on the same 14 clay-silt-sand-gravel and silt-sand-gravel mixtures as their early study. Soil was again reconstituted by compaction in a cylindrical cell yielding a specimen of diameter 300 mm and length 250 mm. In contrast to previous study, unidirectional flow was imposed in an upward direction, and increased until instability occurred or the highest achievable hydraulic gradient, namely 20, was applied. During the test, the colour of the ourflow was continuously observed so as to note signs of erosion of fines.

Wan and Fell (2004b) interpreted their results on the critical hydraulic gradient and concluded that (1) Internally unstable soils began to erode at gradients of 0.8 or less, with several at less than 0.5. The erosion was found to occur at a relatively minor rate, and did not lead to a condition of "extreme cloudiness" at which the erosion would be deemed obvious; (2) No definite mathematical relation was identified between the critical hydraulic gradient and the coefficient of uniformity, the minimum H/F ratio or the fines content; (3) There appeared to be a general trend that soils with higher porosity would start to erode at lower hydraulic gradients. For example, loose, higher porosity soils began to erode at gradients less than 0.3. (4) Soils with clayey (kaolin) fines appear to erode at a relatively higher hydraulic gradient than soils with a similar fines content but without clayey fines; (5) The density of a soil exerts a significant effect on the critical hydraulic gradient. The higher the soil density, the higher the critical gradient. (6) Gap-graded soils erode at relatively lower hydraulic gradient than non gap-graded soils with similar fines content.

2.3.6 Moffat (2005)

Moffat (2005) studied the internal stability of 4 cohesionless gravel-sand and gravel-silt-sand gradations, considered representative of the core and transition zone materials at the W.A.C. Bennett Dam, using a larger permeameter at the University of British Columbia. Test specimens were 279 mm in diameter, with a length of 300 ~ 500 mm. The objective of the research was to examine the effect of vertical effective stress on the onset of internal instability. In contrast to many of the preceding studies (see Table 2.1), a surcharge pressure of 25 ~ 175 kPa was applied to the top of specimen. Unidirectional flow imposed in either a downward or an upward direction, and increased until internal instability occurred. Critical

gradient was determined based on visual observation, and variations in measured local hydraulic gradient. A linear relation was found between critical gradient and vertical effective stress. Each gradation yielded a different hydromechanical boundary, which characterized the onset of internal instability.

2.4 Summary

The selected research of previous investigators is summarized in Table 2.1. It includes a brief description of the test specimen and conditions. It also includes a distinction on whether the research objective was that of a geometric criterion to evaluate the potential for instability, or a hydraulic (gradient only) or hydromechanical (gradient-stress) relation influencing the onset of instability. More specifically, a geometric criterion is used to evaluate the susceptibility to instability in soils where the size of the finer particles is smaller than the size of the constrictions formed by coarser particles. A hydromechanical criterion is used to evaluate the initiation of instability associated with the combination of critical hydraulic gradient and effective stress.

The literature review shows that several geometrical criteria have been developed to assess the potential for internal instability of cohesionless soils. Among them, the Kezdi (1979), Kenney and Lau (1985, 1986) and Burenkova (1992) criteria are most commonly advocated for use in engineering practice. These criteria evaluate the internal stability of granular soils based on different hypotheses and experimental results. Accordingly, they may provide a different assessment of the same gradation. Chapuis (1992) demonstrated that there is a similarity between the Kezdi and the Kenney and Lau criteria, and suggested they be used

with caution. In order to establish the relative conservatism of each criterion, and improve our confidence in the use of these geometric criteria for assessing the potential of instability, it is necessary to compare these criteria with reference to a comprehensive experimental database. This represents one objective of the thesis research.

Limited studies have been conducted on the necessary and companion hydraulic criterion (Adel et al., 1988, Skempton and Brogan, 1994, Richards and Reddy, 2007). Indeed the combined effect of critical gradient and effective stress on the onset of internal instability was first and only studied by Moffat (2005), and it would be reasonable to observe that the relation between critical hydraulic gradient and effective stress (a hydromechanical criterion) has not yet been established in any comprehensive manner. In order to further verify and generalize the previous observations of Moffat (2005), additional testing is needed on various soil gradations. This latter issue, namely, the relation between critical hydraulic gradient and effective stress at the onset of instability, represents the second objective of the thesis research.

Table 2.1 A summary of selected studies

Year	Author	Specimen Size (cm)	Surcharge (kPa)	Water Quality	Hydraulic gradient	Flow direction	Vibration	Criteria
1953	USACE	25.4	0	Tap water	0.5 – 16	downward	Vibration	Geometric
1985	Kenney and Lau	h=20 – 50 d=24.5 or 58	10	Re-circulated water	Re > 10	Downward	Manual tapping	Geometric
1988	Adel et al.	l = 105	0	Not mentioned	0 – 1	Horizontal	No	Hydraulic
1994	Skempton and Brogan	h = 15.5 d = 13.9	0	Not mentioned	0 – 1	Upward	No	Hydraulic
1996	Honjo et al.	h = 10 d=15 or 30	0.9	Tap water	2.5 – 19	Downward	Tapping	Geometric
2004	Wan and Fell	h = 25 - 30 d = 30	0	Not mentioned	10 – 20	Downward/ Upward	No	Geometric/ Hydraulic
2005	Moffat	h = 30 – 50 d = 28	25-175	Distilled and de-aired	1.0 – 65	Downward/ Upward	No	Hydromechanical
2005	Mao	h = 20 – 30	0	Not mentioned	0 – 1	Upward	No	Geometric/ Hydraulic
2005	Liu	h = 20 – 30	0	Not mentioned	0 – 1	Upward	No	Geometric/ Hydraulic
2006	Fannin and Moffat	h = 10 d = 10	25	Distilled and de-aired	0.1 – 15	Downward	Automatic vibration	Geometric

Table 2.2 Factor of safety and χ (after Kovacs, 1981)

Factor of safety	χ
1.0	10
1.5	5
2.3	2.5

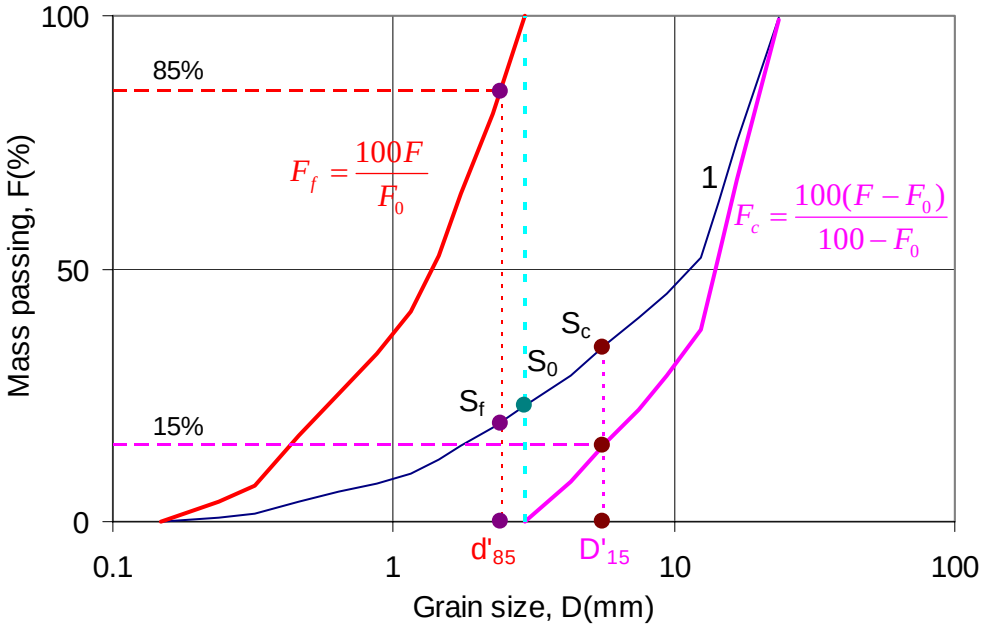

Figure 2.1 Kezdi's method

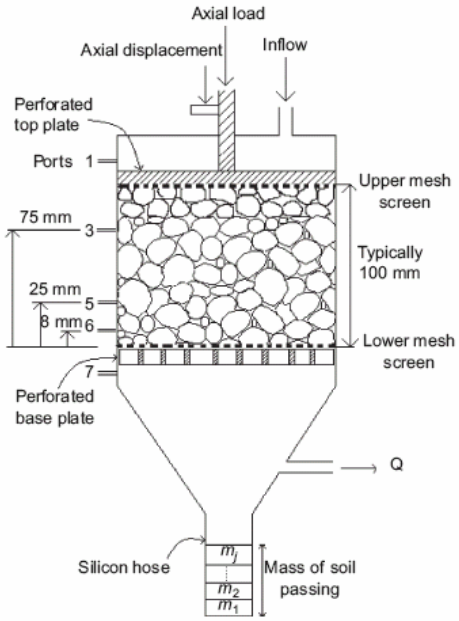

Figure 2.2 Configuration of the permeameter (Fannin and Moffat, 2006, by permission)

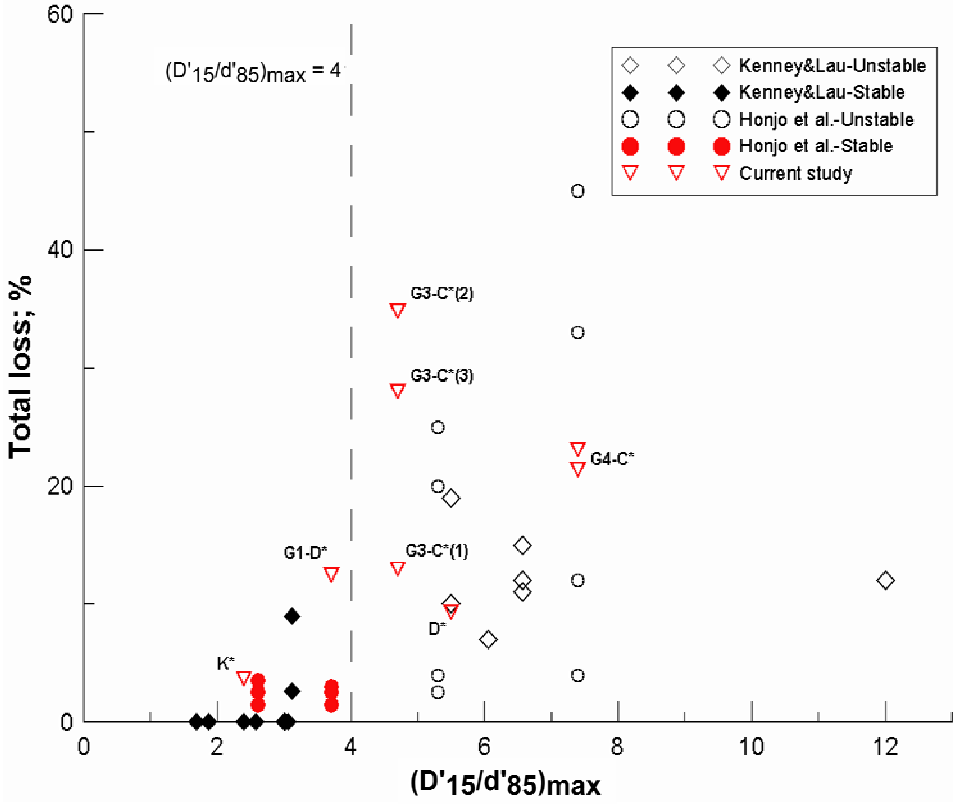

Figure 2.3 Soil loss with $(D'_{15}/d'_{85})_{max}$ (Fannin and Moffat, 2006, by permission)

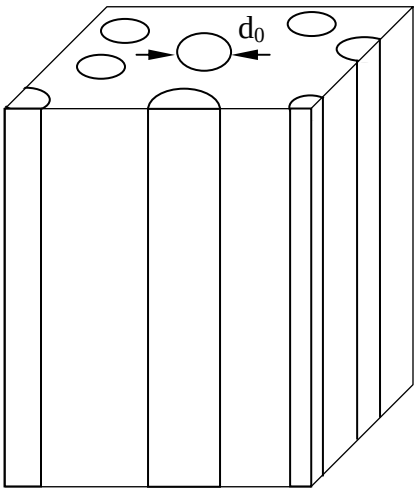

Figure 2.4 Capillary tube model

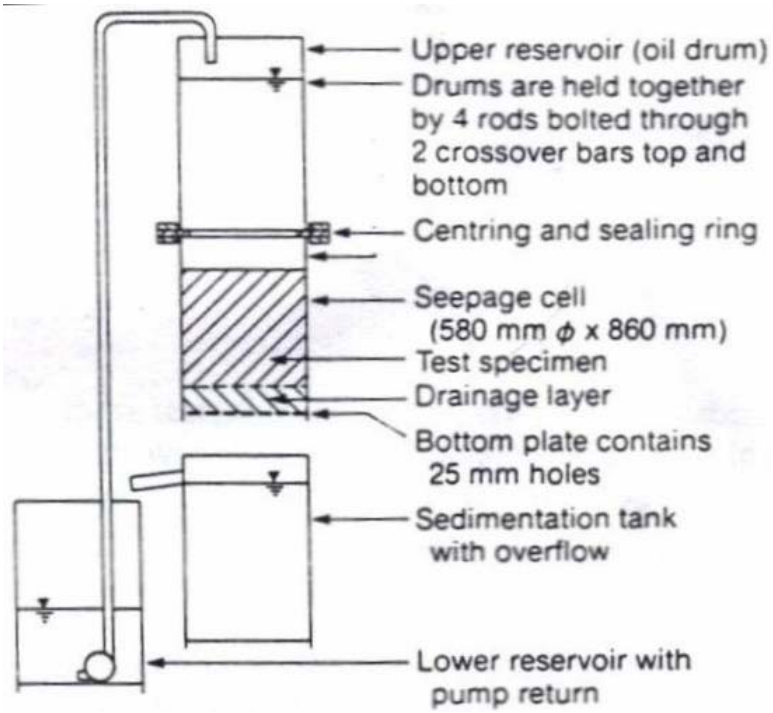

Figure 2.5 Permeameter device (Kenney and Lau, 1985, by permission)

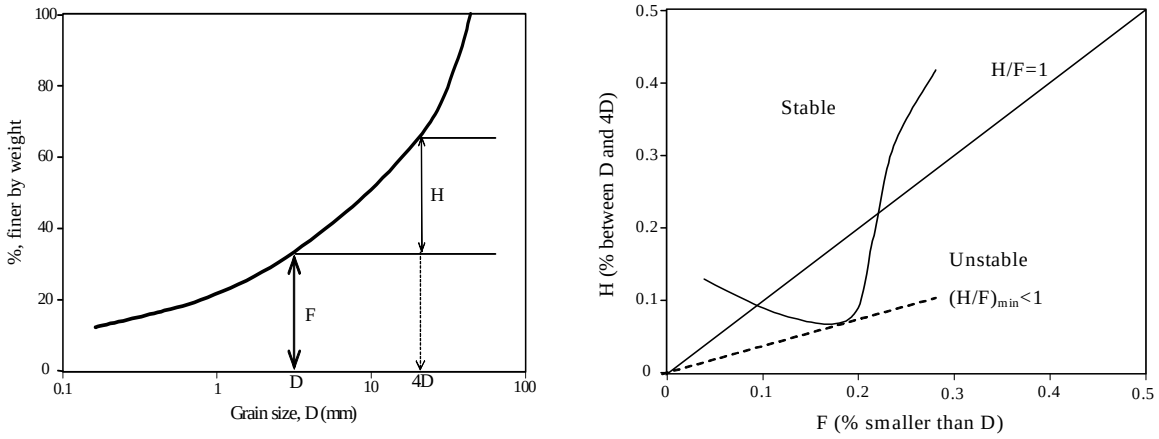

Figure 2.6 Kenney and Lau criterion

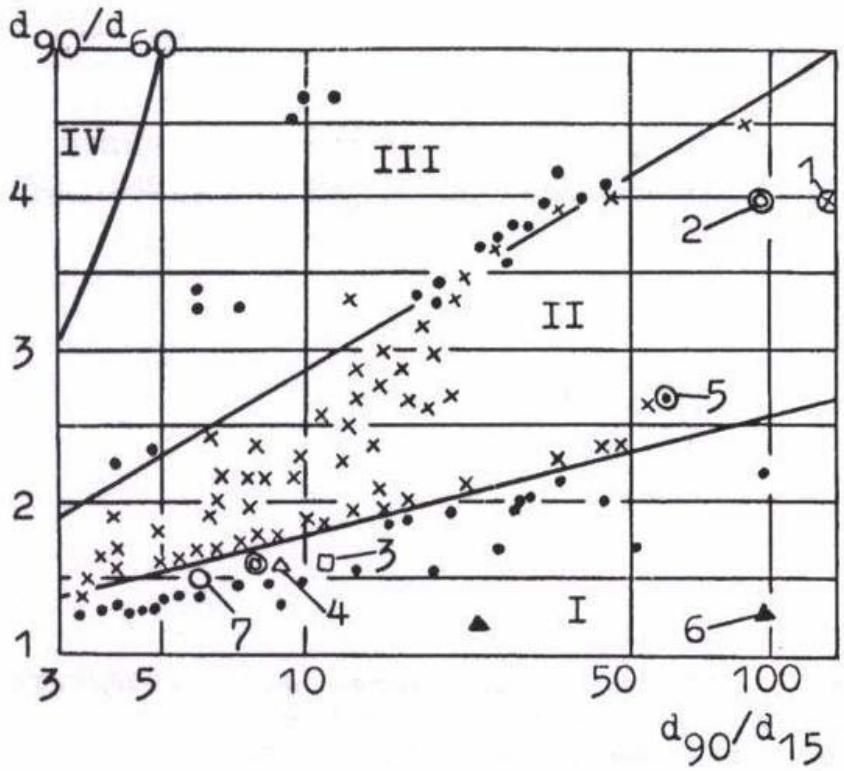

Figure 2.7 Burenkova criterion (Burenkova, 1993, by permission)

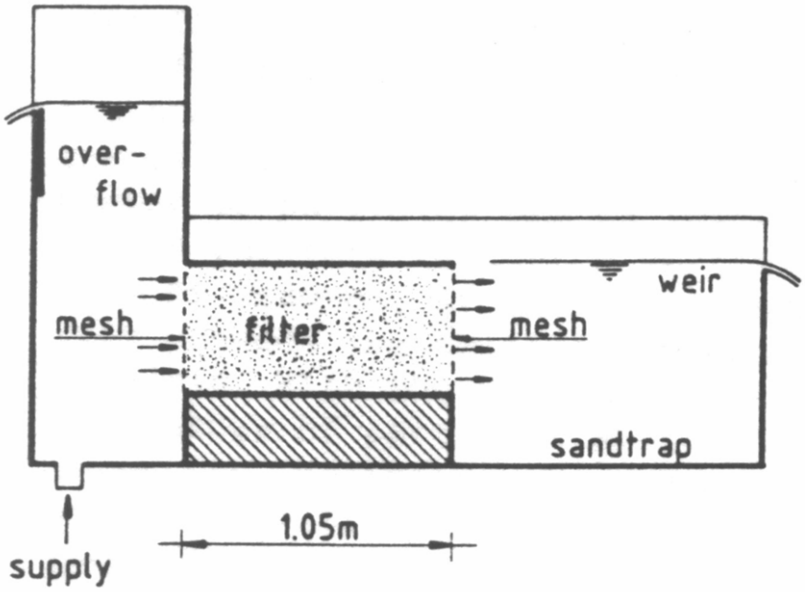

Figure 2.8 Test device (Adel et al., 1988, by permission)

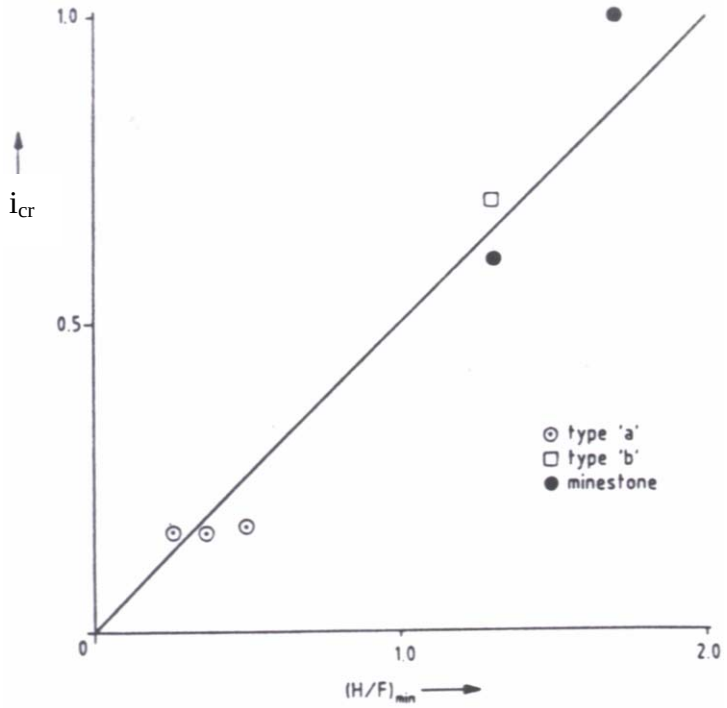

Figure 2.9 Hydraulic criterion for horizontal flow (Adel et al., 1988, by permission)

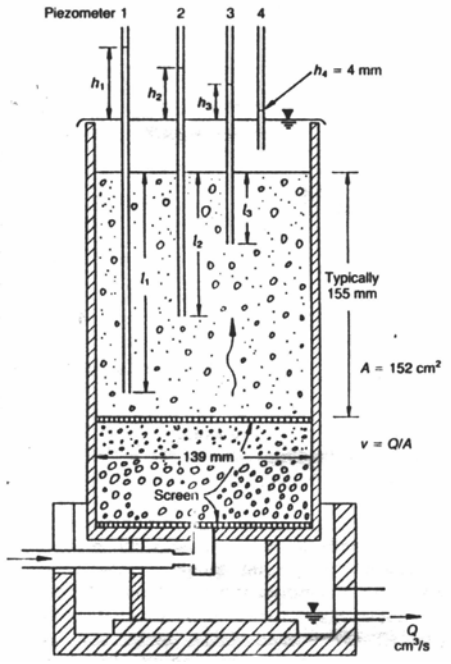

Figure 2.10 Experimental device (Skempton and Brogan, 1994, by permission)

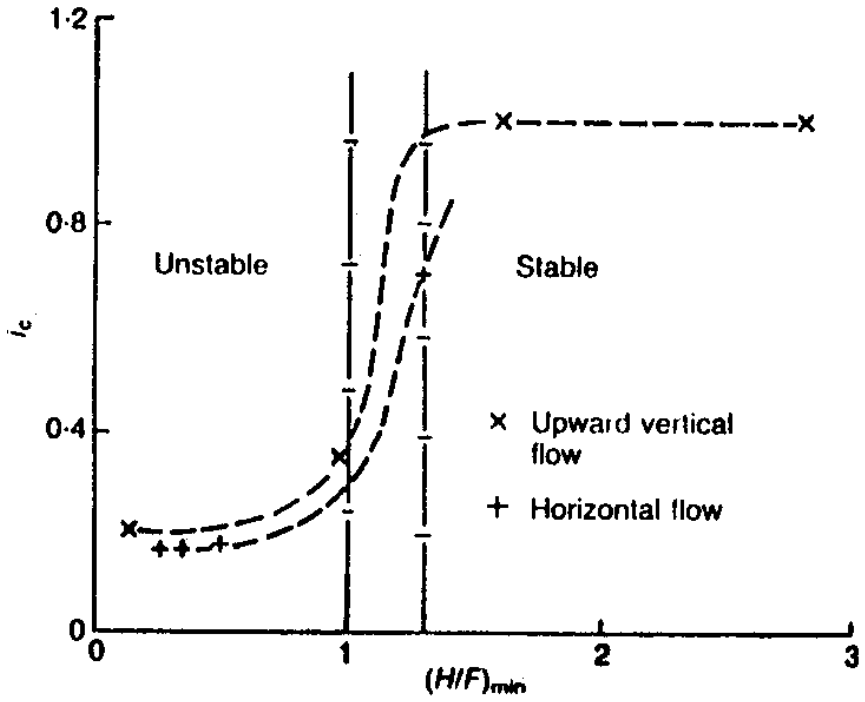

Figure 2.11 Relation between critical gradient and $(H/F)_{min}$ (Skempton and Brogan, 1994, by permission)

3 Apparatus, material and test program

3.1 Introduction

The apparatus, materials and test program used in the laboratory investigation are described in this chapter. Two permeameters were used in testing. The small permeameter is best suited for materials with $D_{100} < 8$ mm, and can accommodate flow conditions bounded by $i_{max} < 15$ and $v_{max} < 0.2$ cm/s. The large permeameter is suitable for materials with $D_{100} < 23$ mm, and can accommodate flow conditions of $i_{max} < 65$ and $v_{max} < 0.1$ cm/s (see Table 3.1). Following a more detailed description of the small permeameter and large permeameter, the test materials, and the specimen reconstitution technique, a summary of the test program is provided.

3.2 The small permeameter device

The small permeameter (a modified ASTM D5101 Gradient Ratio test device) was originally designed for assessment of soil-geotextile filtration compatibility at UBC (Fannin et al., 1996). A schematic diagram of the device is given in Figure 3.1. The permeameter cell assembly is submerged in an outlet tank (m) made of Plexiglas. A photograph of the entire cell assembly is shown as Figure 3.2. The permeameter cell is made of anodized aluminum, with an inner diameter of 102 mm and a wall thickness of 16 mm. The test specimen (a) is laterally confined by the rigid wall of the permeameter (l), and vertical load is applied to the top of the specimen by means of a perforated rigid top plate (c) and piston rod (d). An inlet port (j) in the top of the cell (e) allows water flow to be introduced to the cell, and a top plate

(c) with 5 holes each 5 mm in diameter allows for uniformly distributed seepage flow across the specimen. A wire mesh (b), located between the specimen and the perforated rigid base plate (k), allows throughflow of water. The opening size of the wire mesh was selected based on the grain size of the test specimen (see Table 3.3), so that any finer particles resulting from the internal instability could pass through it. Material passing through the lower wire mesh is captured in a bottom collection trough (g) see Figures 3.2 and 3.3.

The cell diameter restricts the maximum grain size of a material used in testing. The ASTM Gradient Ratio standard test method (ASTM D5101) requires the maximum particle size to be less than 1/10 the diameter of the permeameter cell. Head (1992) stated that "as a general rule the ratio of the cell diameter to the diameter of the largest size of particle in significant quantity should be at least 12". Kenney et al (1985) indicated that the largest particle size was kept to less than 1/10 of the cell diameter in their experimental study. Therefore, the maximum grain size (D_{100}) of the small permeameter was restricted to 8 mm (see Table 3.1) giving a largest particle size to cell diameter of 12.75.

3.2.1 Water supply and control system

Hydraulic gradient across the specimen is applied by means of head-control, using an inlet and outlet tank. A schematic diagram of the flow control system is shown in Figure 3.1. A peristaltic pump, Model 7529-20 manufactured by Masterflex, was used to supply the inlet tank with clean de-aired water from a reservoir tank. De-aired water was manufactured in a custom-made system in the soil laboratory. An overflow on the inlet tank returned excess flow to the reservoir tank, and hence maintained a constant water head on the top of the test

specimen. An overflow flow tube (n) in the outlet tank (m) was used to maintain a constant water head on the base of the specimen. The height of the inlet tank above the outlet tank establishes the applied differential water head (h_0). The specimen length (L) and available head room of the laboratory yielded a maximum average applied hydraulic gradient i_{av} (= h_0/L) of 15.

It is recognized that energy losses through hoses and connections in a permeameter setup reduce the efficiency of a system (Head, 1992). Efficiency is defined as the ratio of measured water head across the specimen (h_{17}) to the applied water head (h_0) (Figure 3.1). Water head is measured at a series of manometer ports (i). Observation showed that an increase in seepage velocity led to greater energy loss through the hoses and connections, i.e., the efficiency decreases. Khan (2003) also reported data on this phenomenon. The relation between the efficiency (h_{17}/h_0) and seepage velocity is shown in Figure 3.4. Inspection indicates that a seepage velocity greater than 1.0 cm/s would yield an efficiency of approximate 60 %, implying nearly half of the energy loss occurs in the hoses and connection of the device. In order to ensure an efficiency of the system greater than 80%, testing should be conducted without causing the seepage velocity to exceed 0.2 cm/s in a small permeameter test.

3.2.2 Instrumentation

The water head distribution along the length of specimen was determined using differential pressure transducers (DPTs). A schematic layout of the port locations is shown in Figure 3.5. Port 1 is located on the top plate to establish the water head at the top of the specimen. Ports

2 to 6 are located on the wall of the cell at the distances of 101.6, 76.2, 50.8, 25.4 and 8 mm above the lower wire mesh on which the test specimen rests (see Figure 3.5). Port 7 is located on the wall of the outlet tank to establish water head at the base (downstream face) of the specimen. In the current study, the test specimen was reconstituted to a length of approximately 10 cm. Hence, port 2 was located above the top surface of specimen and was not used other than to verify the reading at port 1. Differential water pressure is measured across ports 1, 3, 4, 5, 6 and 7 (h_{13}, h_{34}, h_{45}, h_{56} and h_{67} respectively) as illustrated in Figure 3.5. Five differential pressure transducers, model C230 manufactured by Setra, were used to measure differential water pressure between the ports. Four transducers had a range of ±7 kPa (h_{13}, h_{45}, h_{56}, h_{67}) and one a range of ±17 kPa (h_{34}). The resolution of these transducers was found to be ±1 mm of water head. Local hydraulic gradient (i_{jk}) was computed from measured differential water pressure, knowing the spacing between the ports.

Axial load was applied to the specimen through the piston rod (d), to impose a target value of vertical effective stress (Figure 3.1). It was measured using a compression load cell of either 50 or 400 kgf capacity, yielding a resolution of ± 0.5 kPa or 2.5 kPa respectively. Axial displacement was measured using a linear variable differential transformer (LVDT) that is mounted on the loading piston rod (Figure 3.1). It recorded displacement to a resolution of ±0.1 mm.

Any finer particles that washed out from the specimen were captured in a collection trough (g) located below the permeameter cell (Figure 3.1). The collection trough comprises two removable pans mounted on a frame that rotates into position below the perforated base plate

(Figure 3.3). The arrangement allows for one pan to collect soil particles passing through the lower wire mesh, while the other is removed to allow weighing of any material previously collected. This configuration enables collection of finer particles at any stage of a test, which can then be dried and weighed after the test is completed.

Volumetric flow of the water is measured by intercepting the outflow and collecting in a graduated cylinder for a specific time interval. The hydraulic conductivity of the reconstituted soil, and its variation with time during a test, was deduced from the volumetric flow.

3.2.3 Data acquisition system

An electronic data logger records all output voltages from the differential pressure transducers (DPTs), load cell, and LVDT. This system comprises a power supply, a signal-conditioning unit that amplifies the output signal from the transducers, and a Metrabyte DAS-16 board connected to a desktop computer. The DAS-16 board is a multifunction board with a 12-bit resolution and digital input and output. Voltage in the transducers is amplified in the signal-conditioning box manufactured at UBC. Data from the 7 channels is collected at a rate of 2 Hz, and written to an output file. The software used is Labtech Notebook, a product of the Laboratory Technologies Corporation.

3.3 The large permeameter device

The large permeameter was specifically designed at UBC for the assessment of internal stability in soils of the core and transition materials of the WAC Bennett dam (Moffat, 2005;

Moffat and Fannin, 2006). A schematic diagram of the large permeameter apparatus is given in Figure 3.6. A photograph of the permeameter cell assembly is shown as Figure 3.7, together with a schematic drawing of it in Figure 3.8. The permeameter cell is made of acrylic, with an inner diameter of 279 mm and a wall thickness of 13 mm. The test specimen (a) is laterally confined by the rigid wall of permeameter (l), allowing axial vertical load to be applied to the top of specimen by means of a perforated rigid top plate (c) and piston rod (d). In unidirectional downward flow tests, an inlet port (j) on the top of the cell (e) allows water flow to be introduced to the cell, and a perforated top plate (c) allows for uniformly distributed seepage flow across the specimen. Conversely, in unidirectional upward flow tests, an inlet port (j) in the base of the cell (f) allows water flow to be introduced to the cell, and a perforated base frame (k) allows for uniformly distributed seepage flow across the specimen. A wire mesh (bt) was placed between the specimen (a) and the perforated rigid top plate (c) and a wire mesh (bb) was placed between the specimen (a) and the perforated rigid base frame (k). The opening size of the wire mesh was selected based on the grain size of the test specimen, so that finer particles could pass through freely in the event of any internal instability (Table 3.3).

Like the small permeameter, the cell diameter in the large permeameter restricts the maximum grain size of a material used in the testing. Based on the requirements of ASTM D5101, and the observations of Kenny et al. (1985) and Head (1992), the maximum grain size (D_{100}) was restricted to 23 mm (see Table 3.1) giving a largest particle size to cell diameter of 12.1.

3.3.1 Water supply and control system

The water supply system includes one storage reservoir, one inlet tank and one outlet tank. Like the small permeameter, the large permeameter uses de-aired water but in a relatively large quantity. De-aired water for this device is manufactured using (1) a two-stage filter system of the laboratory tap water and (2) a dedicated de-airing system (Figure 3.6). In the two-stage filter system, manufactured by Millipore Corporation, tap water is first passed through a sand filter (Millipore Backwashable Multimedia Filter), which removes all particles larger than 10 μm. Water is then passed through a carbon filter (model P72017), which removes particles larger than 3 μm. The filtered water is then held in a storage reservoir (model JW805TF1, manufactured by GSW Water Heating), with a capacity of 270 liters, where a vacuum of approximately 80 kPa is imposed for approximately 24 hours to remove air. Thereafter, the de-aired water is supplied to the inlet water tank for use in testing.

Seepage flow through the test specimen is controlled by means of an inlet and outlet tank (model AP-260/302, manufactured by JACUZZI), with a maximum capacity of 320 liters. Each tank has an internal membrane that acts as an air-water interface. Like the small permeameter, the large permeameter operates on a principle of head control; more specifically, the differential head across the specimen is controlled by the differential air pressure on the inlet and outlet tank, using a servo-controlled electro-pneumatic regulator (TA6000-505, manufactured by Fairchild). The National Instruments LabVIEW software was used to control the signal in the regulator, and impose a constant hydraulic gradient across the specimen. A demand signal is sent by means of LabVIEW to the regulator, yielding an air pressure in the inlet tank; the measured hydraulic gradient across the specimen

generates a signal to the software, which then adjusts the demand signal to maintain a target value of hydraulic gradient by means of a feedback control system.

The large permeameter allows for a maximum hydraulic gradient of 65. The 320 liter capacity of inlet water tank acts to restrict the seepage velocity across the test specimen. For instance, if a minimum test stage of one hour interval is desired, the seepage velocity through the soil specimen should be less than,

$$v = \frac{Q}{At} = \frac{320 \times 1000\ cm^3}{\frac{\pi}{4}(27.9)^2\ cm^2 \times (60 \times 60)\ s} = 0.14\ cm/s\ .$$

This seepage velocity does not consider energy losses in the pipes and connections. As discussed in the small permeameter tests, the energy loss increases with the seepage velocity.

3.3.2 Instrumentation

Measurements of the water head along the length of specimen were made using differential pressure transducers (DPTs) and also using total pressure transducers (TPTs). A schematic layout of the port locations is shown in Figure 3.8. Ports 2 to 6 are located on the wall of the cell at the distance of 530, 405, 280, 155 and 30 mm from the lower wire mesh. Port 7 is also located on the wall of the cell below the lower wire mesh screen, and measures water head on the bottom of specimen.

The total pressure transducers (TPTs) are a Schaevitz model PS10000 with a pressure range between 0 and 350 kPa. The differential pressure transducers (DPTs) are a model PDW/E972-05-01, manufactured by Sensotec. The range of these sensors is -70 to 70 kPa.

The TPTs and DPTs are believed to have a resolution of ± 0.5 kPa and ± 0.1 kPa, respectively.

Axial load was applied to the specimen through the piston rod (d). A top load cell is located on the loading rod, above the top plate and therefore outside of the permeameter cell. The base load cell (g) is located inside the permeameter, between the base frame (k) and cell base (f), see Figure 3.8. The top and base load cells have a full scale capacity of 2250 kgf and yield a resolution of ± 0.5 kPa in the value of vertical stress.

Axial displacement is measured using a linear variable differential transformer (LVDT) which mounted the loading rod in contact with top of the specimen (Figure 3.8). This LVDT was custom-manufactured and recorded displacement to a resolution of ± 0.1 mm.

The volumetric flow of water was measured by means of recording the change in mass of water held in the inlet and outlet tanks (Figure 3.6). These water tanks were each mounted on a weigh scale that measured the total mass, and hence volumes of seepage flow, over the duration of a test. The weigh scales are Mars Scales MSG series, with a capacity of 900 kgf and an accuracy of ± 0.1 kg. Output of the load cell in each weigh scale is directly read by the data logger.

3.3.3 Data acquisition system

An automatic data acquisition system reads the output of the instrumentation (transducers, regulator, load cells, LVDT and weigh scales) and writes the data to the storage. The

acquisition system comprises: (1) a power supply for the A/D board and the transducers; (2) an A/D board; (3) an ethernet network module; (4) a personal computer with LabVIEW software. Power to the A/D board was provided by power supply model PS-4 manufactured by National Instruments. Power to the transducers was provided by a custom-made power supply with an output voltage of approximately 15 V.

The A/D board comprises different modules manufactured by National Instruments. The FP-AI-100 module includes 8 single-ended analog input channels. These are 16 bits resolution channels with a current input range between 0 to 20 mA or voltage between -10.4 to 10.4 volts, and a maximum reading frequency of 6 Hz. There is an electronic filter on each channel, which can be configured for 50 Hz or 60 Hz. The FP-TC-120 module includes 8 inputs in the milli-volts range. This module has the same resolution and filter capabilities as the FP-AI-100. The FP-TB-10 model has two 0-5 V analog output channels, generated with 12-bits of resolution; one of these channels controls the electronic regulator used to apply air pressure to the inlet water tank.

The Ethernet network interface connects a node of a module to a high-speed Ethernet network. It manages communications between the host PC and inlet and outlet modules. A personal computer was used to collect and save all data read through the A/D board, using the software LabVIEW. It has a user-friendly graphical interface that enables all the transducers and control systems to be displayed on screen by a virtual instrument (VI), yielding an attractive ease of operation.

3.4 Materials Tested

Test specimens were prepared by reconstituting using two materials: glass beads and soils (see Table 3.3). The rationale for performing tests on glass beads in the small permeameter is that they are very round and have proved beneficial in detecting anomalies in the experiments. The majority of the permeameter tests were performed in the large permeameter on reconstituted specimens of soil. In order to provide a basis for comparison between the two permeameters, some tests were also performed in the large permeameter using glass beads.

3.4.1 Glass beads

The glass beads are made of cerium oxide manufactured by Rotair Industries and Potters Industries. The particles are perfectly spherical and clear (Figure 3.9). The specific gravity is approximately 2.5. Test specimens were prepared by mixing different size ranges (0.1 to 2.0 mm) of beads to obtain the target gradation curve.

3.4.2 Soils

The soils used for testing were taken from the site of an embankment dam and supplied to the project by the BC Hydroelectric and Power Authority. Visual inspection shows the soil particles have a sub-angular shape (Figure 3.10). A specific gravity of 2.7 was measured for the fine sand fraction of the soil, and is assumed valid for the coarse fraction (Moffat, 2005). The soil was processed by washing and sieving into target grain sizes. Test specimens were prepared by mixing different size ranges to obtain the target gradation curve.

3.5 Specimen reconstitution

The objective of the reconstitution technique is to replicate a uniform and saturated specimen. This was achieved through a modified slurry-mixing preparation (Kuerbis, 1989; Moffat, 2005) and a technique of discrete deposition (Moffat, 2005). This modified slurry deposition technique was used both in the small and the large permeameters.

The specimen was reconstituted in a series of layers. Each layer was prepared using a batch of dry soils or glass beads according to the target grain size distribution. In small permeameter tests, the specimen was reconstituted in three layers each about 35 mm thick (approximately 600 g of glass beads per batch). In large permeameter tests, it was reconstituted in 12 layers each about 25 mm thick (approximately 3000 g of soils or glass beads per batch). In preparing the materials, each batch of soil/glass beads was boiled in clean de-aired water for at least 30 ~ 60 minutes. After cooling to room temperature, it was placed under vacuum for more than 12 ~ 24 hours to evacuate any entrained air.

When each batch of saturated material was ready, it was placed directly into the permeameter cell using a discrete deposition technique. Before placing the first batch, the permeameter was filled with de-aired water to yield a thin film of 5 mm or less of standing water over the lower wire mesh screen. After thorough mixing, discrete quantities of the material were then deposited under this thin layer of standing water using a spoon. The first layer was placed directly onto the lower wire mesh. Placement of successive layers was done under the same thin film of standing water, to ensure the resulting specimen is saturated and also to ensure

minimal segregation. Specimen reconstitution for a small permeameter test took about 1 day, and that for a large permeameter took test about 10 days.

Upon deposition of the last batch, the top surface of specimen was leveled. In the small permeameter, excess soil particles were removed using a siphon (Figure 3.11). In the large permeameter, the maximum particle size is too large for this technique. Hence, a spoon was used. An upper wire mesh was placed on top of the level specimen. The opening size was selected based on the grain size of the test specimen and the direction of seepage flow (Table 3.3). The top loading plate was then placed in contact with the wire mesh in readiness for testing.

3.6 Test procedure

The main objective of this study was to examine the relation between vertical effective stress and critical hydraulic gradient at the onset of internal instability in cohensionless soils. The test procedure comprised two main phases: (1) consolidation; and (2) multi-stage seepage flow. The purpose of consolidation was to obtain the target vertical effective stress on the specimen. The purpose of multi-stage seepage flow was to determine the critical gradient at which internal instability occurs.

3.6.1 Consolidation

During the consolidation stage, a target value of effective stress (σ'_{t0}) was applied to the top of specimen. Any excess pore water pressure dissipates at both ends of the specimen, yielding a condition of double-drainage in the specimen. It is important to control the

magnitude of these transient hydraulic gradients in order to avoid a potential for internal migration during the consolidation stage. Hence, the target value of σ'_{t0} was applied slowly in increments of 5kPa. Pore water pressure was monitored to ensure the excess pore pressure diminished to a near-zero value. Experience revealed that excess pore pressure dissipated relatively quickly, and usually within a minute in all gradations. Successive increments of load were applied until the target effective stress was reached.

3.6.2 Seepage flow

The purpose of the test program was to determine the critical gradient at which onset of the internal instability took place. Therefore a multi-stage test procedure was used in which hydraulic gradient was increased to failure. Upon completion of consolidation, unidirectional seepage flow was imposed at an average gradient, $i_{av} \approx 0.5$ in the small permeameter tests and $i_{av} \approx 1.0$ in the large permeameter tests. Thereafter, the hydraulic gradient was increased in defined increments, until the onset of instability was observed or the capacity of apparatus was reached. The increment of each hydraulic gradient depended on the gradation of the test specimen and the effective stress applied to it. Typically, the hydraulic gradient was increased in increments of $i_{av} \approx 1$ or 2. The duration of each stage was generally 30 minutes for specimens of glass beads, and one or two hours for soil specimens so that sufficient volume of water can be measured for calculation of seepage flow.

3.7 Test program

A primary objective of this study was to examine the relation between the vertical effective stress and critical hydraulic gradient, and establish how those relations may be affected by

grain size distribution of the soil. Therefore, three test variables were examined in testing: (1) grain size distribution, (2) vertical effective stress, and (3) hydraulic gradient across the specimen.

As noted in the literature review, the preceding study (Moffat, 2005) characterized the instability of four gradations of soils and established the relation between the effective stress and critical hydraulic gradient for each gradation. The four soils had $0.29 < (H/F)_{min} < 0.67$ and $7.7 < D'_{15} / d'_{85} < 14.3$. In order to broaden the scope of that work, six gradations were tested in this study in order to verify and supplement the database of that previous research. The six gradations were selected to yield a geometric index $(H/F)_{min}$ from 0 to 1.0 with reference to the Kenney & Lau criterion, and a D'_{15} / d'_{85} from 4 to 11 with reference to the Kezdi criterion. All the gradations are summarized in Table 3.2 and shown in Figure 3.12.

An overview of the test program is given in Figure 3.13. The test code defines the gradation of soil or glass beads, vertical effective stress on the top of specimen, and the direction of seepage flow. In quantifying the gradation, HF stands for the Kenney and Lau index $(H/F)_{min}$, while FR stands for the Kezdi filter ratio D'_{15} / d'_{85}. For example, HF03-25-U represents the test on gradation HF03, at an effective stress of 25 kPa, with upward seepage flow.

3.7.1 Small permeameter tests

All preliminary tests, and some tests in the main test program, were performed in the small permeameter. Glass beads were used in those tests. Gradation FR3, which is believed to be internally stable, was used in preliminary tests to commission the small permeameter.

Gradation FR8, which is believed to be internally unstable and indeed close to physically unstable by means of segregation, was used to demonstrate the repeatability of the test method at a relatively low vertical stress of 25 kPa. In the main test program, the gradation FR8 was tested at vertical stresses of 50, 100 and 200 kPa. Gradation FR7 was tested at vertical effective stresses of 25, 50, and 100 kPa.

The test on gradation FR7 at an effective stress of 100 kPa nearly reached the capacity of the small permeameter. Since restrictions of maximum gradient (<15) and particle size (< 8 mm) govern operation of the small permeameter, the tests on relatively stable gradations with a maximum particle size greater than 10 mm were conducted in the large permeameter.

3.7.2 Large permeameter tests

Most of main test program was performed in the large permeameter because large soil particle sizes (up to 23 mm) and large gradients (up to 65) could be accommodated in this test device. More importantly, the distribution of vertical effective stress along the length of the specimen could be more accurately defined based on direct measurement of axial load on the top and bottom surface of the specimen.

Two tests were performed using glass beads on gradation FR7. The objectives of these tests were two-fold: first to commission the large permeameter, and second to establish a connection between tests performed in the small and large permeameter. The latter issue proved important: comparison of the small and large permeameter tests results yields a dimensionless approach to unify the two sets of test data. More specifically, it proved very

important to establishing a relation between critical gradient and normalized mean vertical effective stress, namely, the hydromechanical envelope (see section 5.3).

Given the concept of a hydromechanical envelope for a particular gradation, the effect of grain size distribution on the location of that hydromechanical envelope became a prime focus of the study. Four different gradations of soils with geometric index $(H/F)_{min}$ ranging from 0.1 to 1.0, and D'_{15} /d'_{85} ranging from 4 to 11, were tested in the large permeameter (gradations HF01, HF03, HF05 and HF10). Each gradation was tested with various effective stresses ranging from 0 to 50 kPa. The test on gradation HF01 was conducted in order to replicate a test of Skempton and Brogan (1994); therefore, no vertical effect stress was applied on the top of specimen (see Figure 3.13).

3.8 Summary

The program of testing was performed on six gradations of two materials using two permeameters (Figure 3.13 and Table 3.3). The materials comprise a rounded glass bead and a sub-angular soil. Three gradations of glass beads (one internally stable and two unstable) and four gradations of soils (one internally stable and three unstable) were tested. Tests were performed in either a small permeameter or a large permeameter, both of which were operated using a principle of head control.

A total of 21 tests were performed. In each test, a modified slurry-mixing specimen preparation and discrete deposition technique was used to yield a saturated and homogenous

specimen. A multi-stage procedure was then executed to assess the onset of seepage failure at a target value of vertical effective stress.

Table 3.1 Comparison of the small and the large permeameters

Comparison		Small permeameter	Large permeameter
Material	Maximum particle size (mm)	8	23
	Maximum seepage velocity (cm/s)	0.2	0.12
	Specimen volume (cm^3)	820	18340
Water flow control	Maximum gradient	15	65
	Gradient control	Varying elevation	Varying air pressure
	Flow direction	Downward	Downward or Upward
Measurement and Observation	Load measurement	Top surface	Top and Bottom surface
	Fine particle collection	Each stage	Final stage
	Visual observation	No	Yes

Table 3.2 Characteristics of the test gradations

Gradation	D_5 (mm)	D_{10} (mm)	D_{15} (mm)	D_{30} (mm)	D_{50} (mm)	D_{60} (mm)	D_{85} (mm)	C_u	C_c	D'_{15}/d'_{85}	$(H/F)_{min}$
FR3	0.116	0.126	0.138	0.380	0.611	0.775	1.401	6.1	1.5	2.8	1.3
FR7	0.112	0.119	0.126	0.150	1.118	1.327	1.775	11.2	0.1	7.1	0
FR8	0.112	0.119	0.126	0.150	1.219	1.346	1.724	11.3	0.1	7.9	0
HF01	0.135	0.178	0.300	2.451	3.786	4.316	6.919	24.2	7.8	11.0	0.14
HF03	0.112	0.150	0.178	0.300	1.741	2.427	5.652	16.2	0.2	4.9	0.3
HF05	0.010	0.027	0.043	0.238	0.425	0.601	3.434	22.2	3.5	5.5	0.5
HF10	0.050	0.185	0.427	1.662	4.750	6.637	13.325	35.9	2.2	-	0.98

Note: FR3 used only in a test to commission the small permeameter

Table 3.3 Test conditions on gradations

Gradation	Permeameter	Material	Flow direction	Wire mesh (mm)	
				Lower	Upper
FR3*	Small	Glass beads	Downward	0.6	0.3
FR8				0.6	0.3
FR7	Small / Large	Glass beads	Downward or Upward	0.6 or 0.3	0.3 or 0.6
HF01	Large	Soils	Upward	0.15	NA
HF03				0.15	1.14
HF05				0.043	1.14
HF10				0.15	1.14

Note: * Commission test

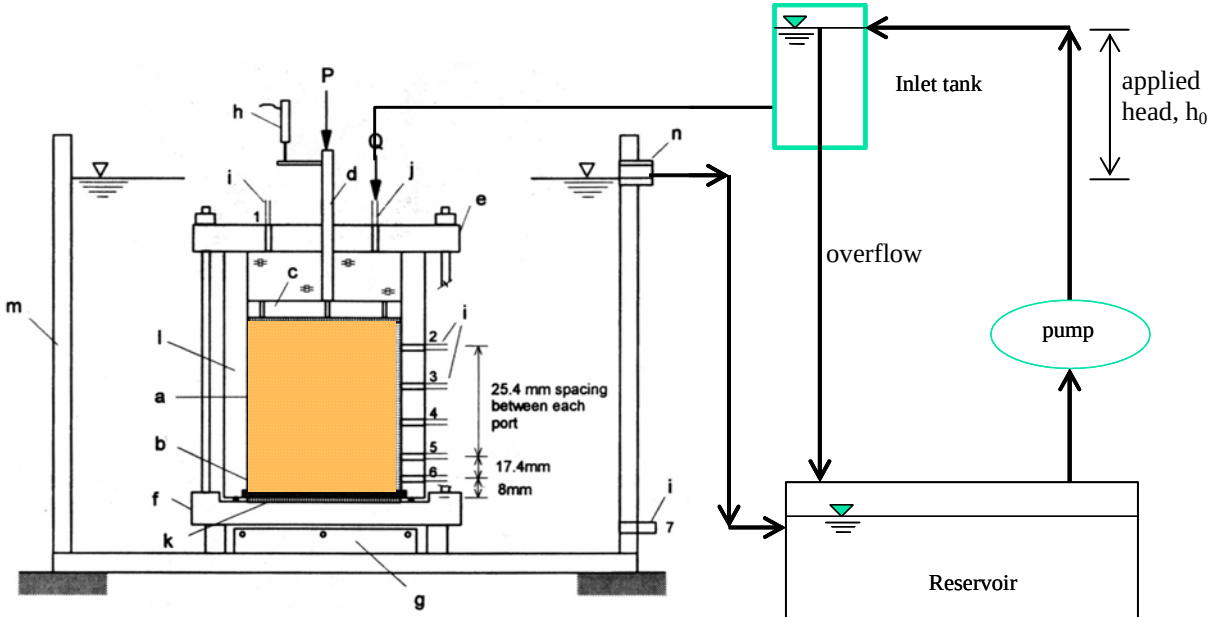

a – test specimen	i – ports 1 to 7
b – wire mesh	j – water inlet
c – perforated top plate	k – perforated base plate
d – piston rod	l – permeameter cell wall
e – cell top	m – outlet tank
f – cell base	n – constant head overflow tube
g – collection trough	P – axial load
h – LVDT	Q – inlet flow rate

Figure 3.1 Generalized layout of the small permeameter (after Fannin et al., 1996, by permission)

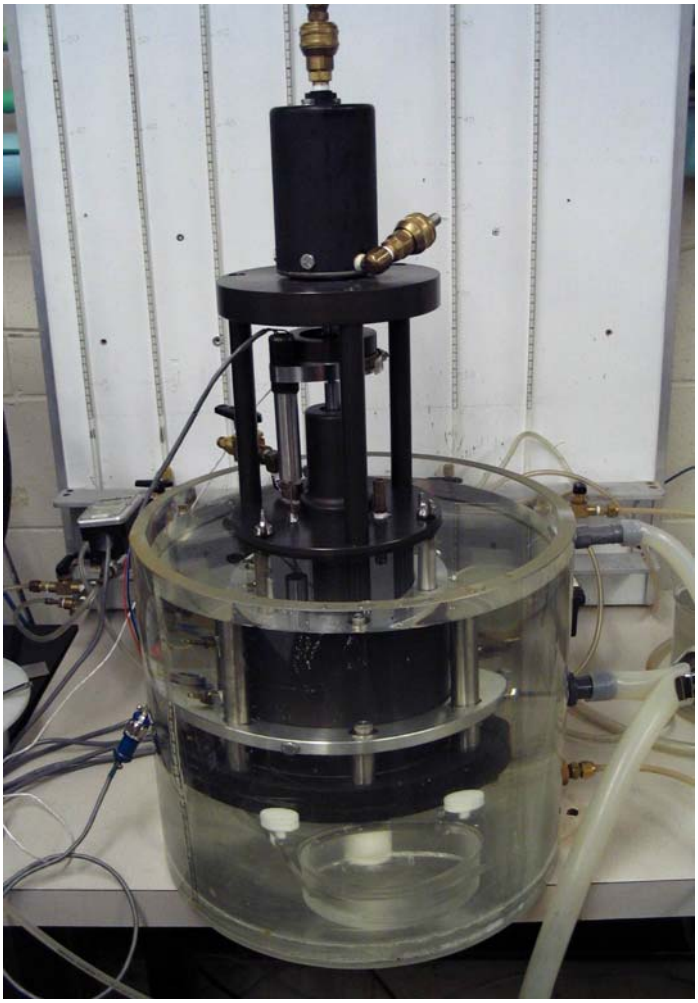

Figure 3.2 The small permeameter

Figure 3.3 Collection trough

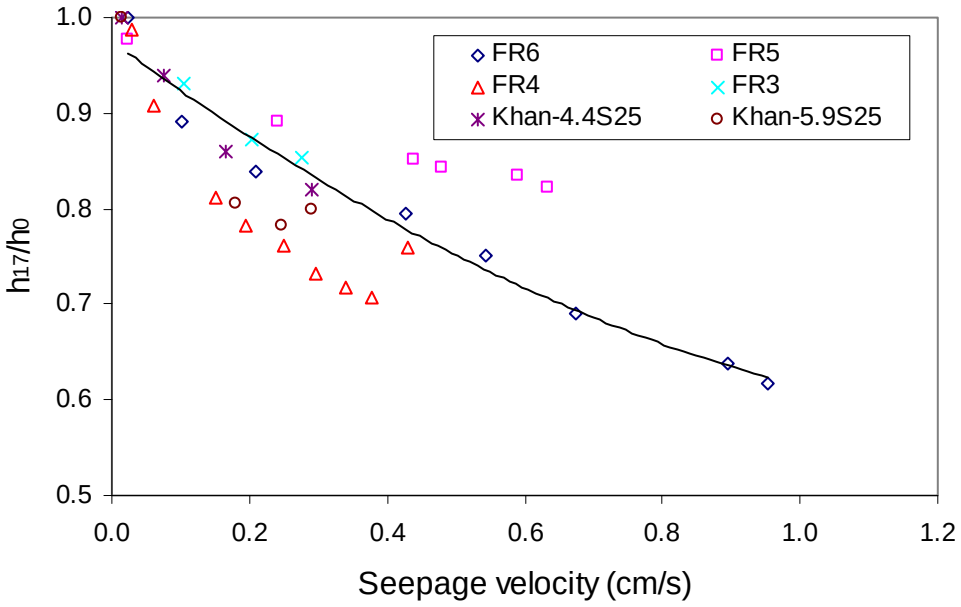

Figure 3.4 Efficiency of small permeameter

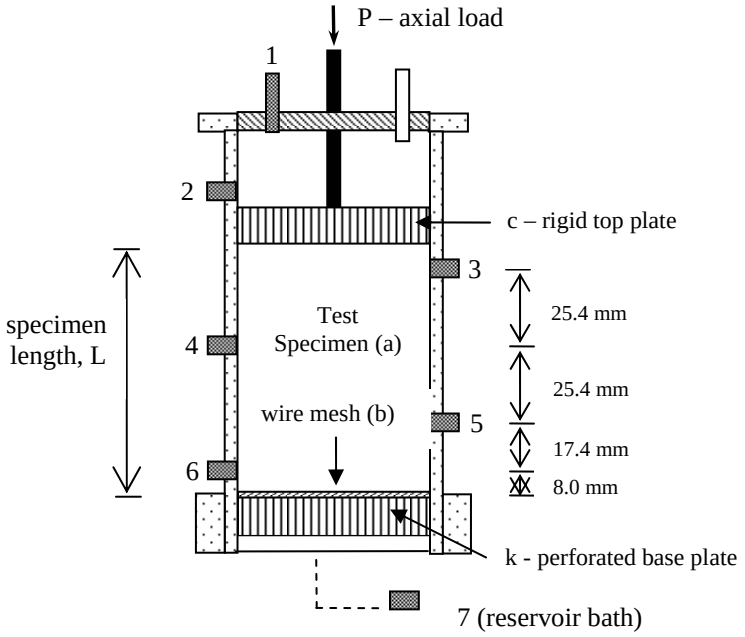

Figure 3.5 Manometer port locations and specimen for current study

Figure 3.6 has been removed due to copyright restrictions. This figure is Figure 3.1 from “experiments on the internal stability of widely graded cohensionless soils” (PhD thesis, the University of British Columbia, Ricardo Moffat, 2005).

Figure 3.6 Layout of Large Permeameter (after Moffat, 2005)

Figure 3.7 The large permeameter

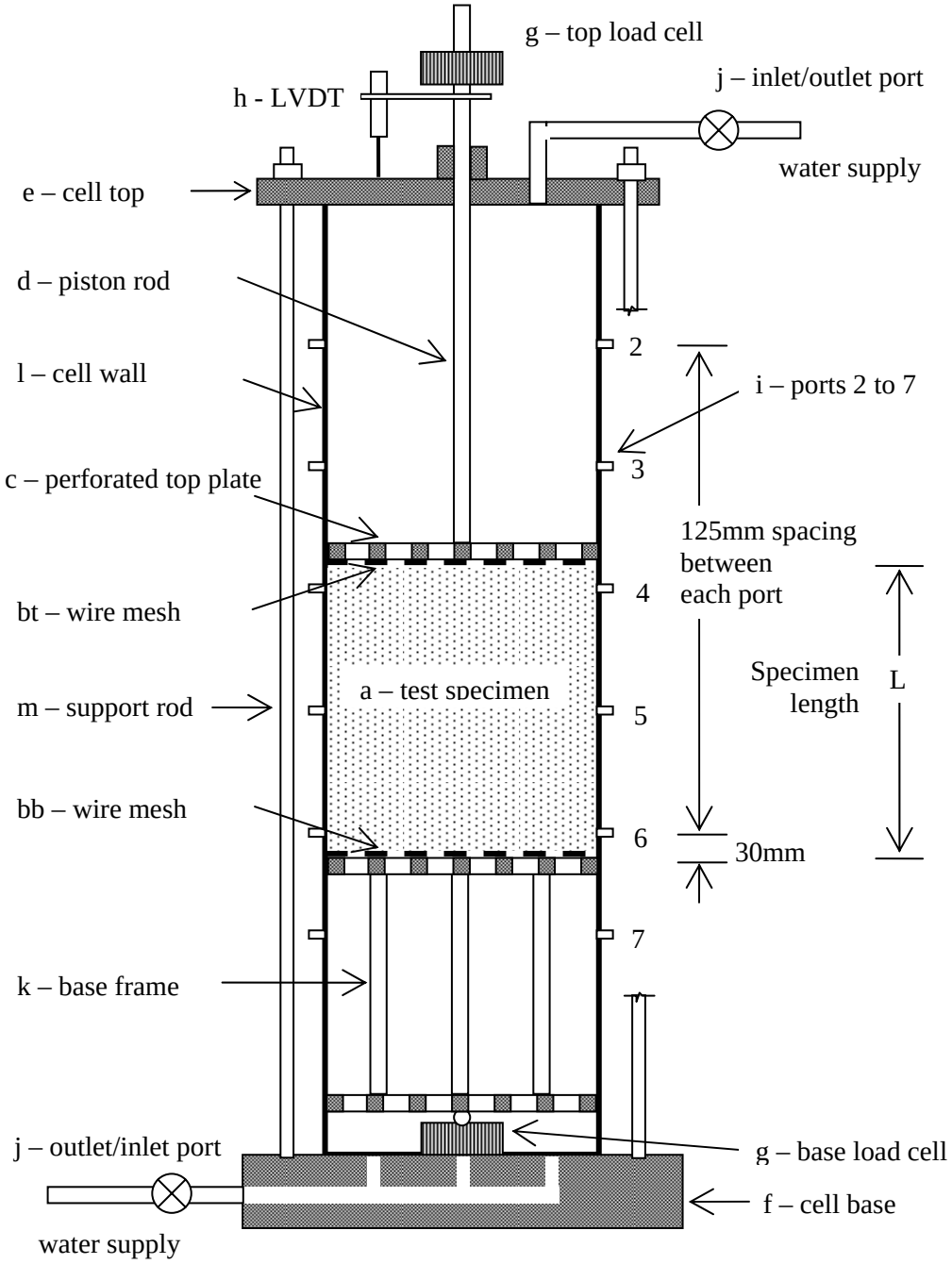

Figure 3.8 Manometer port locations and specimen in the large permeameter

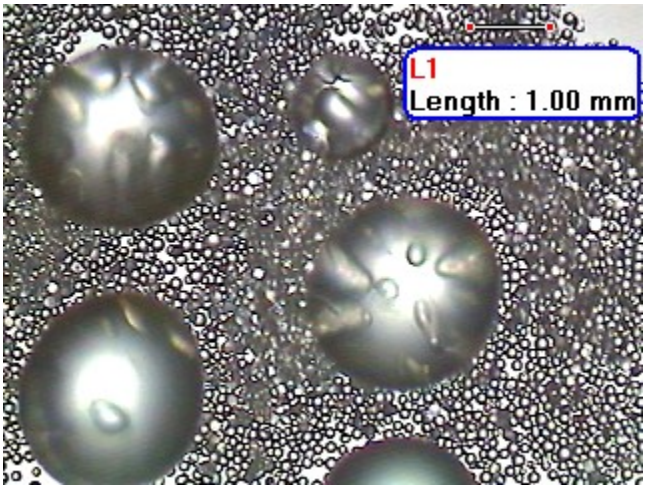

Figure 3.9 Illustrative view of the glass beads

Figure 3.10 Illustrative coarse portion of soils from the W.A.C. Bennett Dam

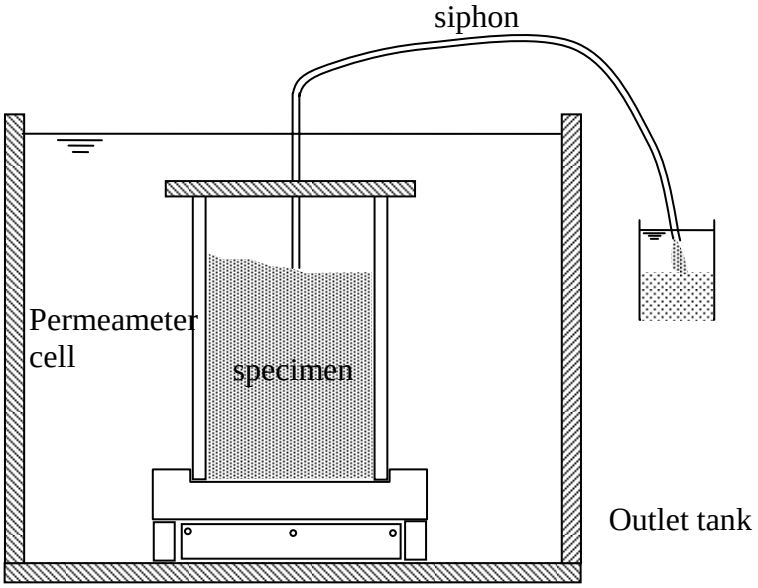

Figure 3.11 Level the top surface using siphon

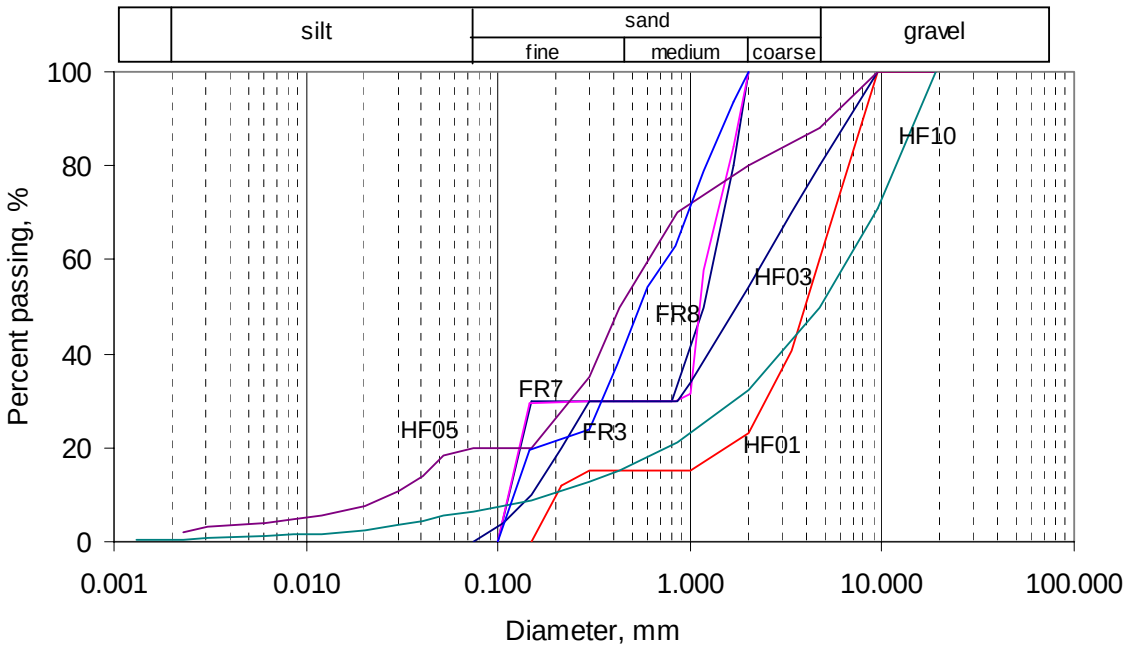

Figure 3.12 Gradations

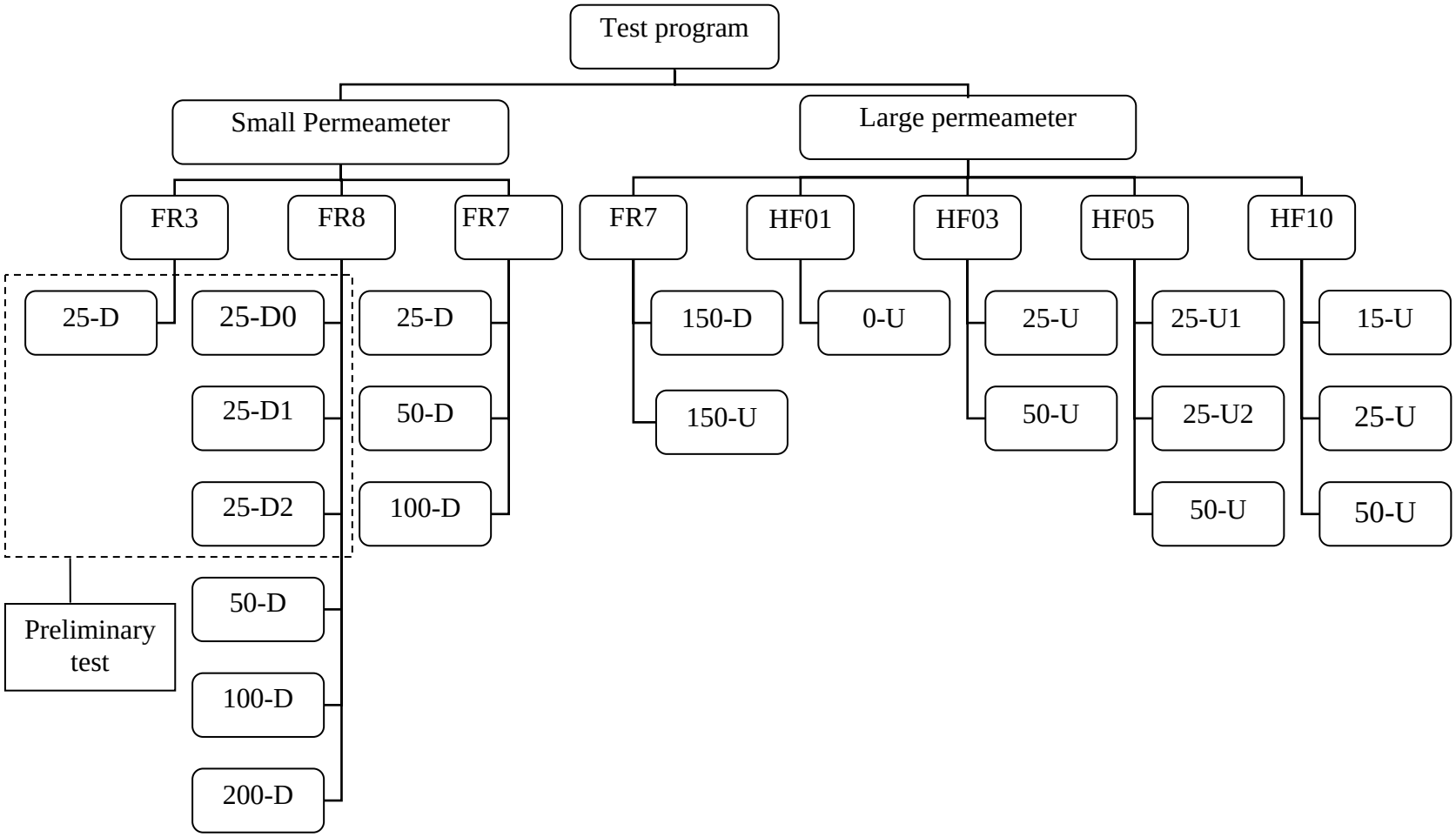

Figure 3.13 Overview of test program

4 Results

A series of permeameter tests was conducted using both the small permeameter and the large permeameter. Following some definitions, results obtained using the small permeameter and the large permeameter are presented. Each test is described with reference to measurements of axial displacement and mass loss, with reference to deduced values of seepage velocity, hydraulic gradient and hydraulic conductivity, and also with reference to observations of finer particle movement. A total of seven gradations (Figure 3.12), including a commission test, were selected for testing, of which two were internally stable and five were internally unstable.

4.1 Some definitions

4.1.1 Hydraulic gradient

Hydraulic gradient (i_{jk}) is defined as head loss per unit distance:

$$i_{jk} = \frac{h_{jk}}{l_{jk}} \tag{4.1}$$

where, l_{jk} and h_{jk} are the distance and head loss between ports j and k, respectively. Therefore the average gradient (i_{av}) is defined as $i_{av} = h_{17}/L$ for the small permeameter and $i_{av} = h_{37}/L$ for the large permeameter, where L = length of the specimen (Figure 3.5 and Figure 3.8).

The critical gradient (i_{cr}) is defined as the local hydraulic gradient (i_{jk}) between two port locations that bound the zone (j-k) where the onset of any seepage-induced internal

instability is interpreted to first occur. In a multi-stage test, if the specimen fails in the n^{th} stage, based on the following conditions, the critical gradient is defined as:

(a) hydraulic gradient in the n^{th} stage if the local gradient is sustained for a certain period of time in the n^{th} stage;

(b) hydraulic gradient in the $(n-1)^{th}$ stage if the local gradient immediately dropped in the n^{th} stage.

4.1.2 Hydraulic conductivity

Hydraulic conductivity is defined as the flow rate per unit hydraulic gradient per unit area:

$$k_{jk} = \frac{q}{Ai_{jk}} \tag{4.2}$$

where, q = volumetric flow rate, cm^3/s; A = cross sectional area of permeameter, cm^2; k_{jk} = hydraulic conductivity of the specimen between ports j and k, cm/s.

4.1.3 Mass of soil passing

Mass of soil passing (or mass loss) is defined as dry mass of the fine fraction washed from the test specimen expressed as a percentage of its initial dry mass (%). This parameter could only be quantified in the small permeameter, by collecting, drying and weighing of materials that settled on the collection trough, at different times during multi-stage testing (Figure 3.3).

4.1.4 Definition of the onset of instability

There is no widely-accepted means to define the onset of instability in seepage flow tests. Accordingly, the onset of internal instability is usually determined based on one or more of

the following attributes: (1) a gradation change of the test specimen before and after testing (eg. Kenney and Lau, 1985); (2) a slope change in the seepage velocity (v) versus hydraulic gradient (*i*) curve (eg. Skempton and Brogan, 1994); (3) rate of loss of finer particles (eg. Honjo et al., 1996); (4) visual observations (eg. Skempton and Brogan, 1994; Honjo et al., 1996; Moffat, 2005); (5) a variation in local hydraulic gradient with time (eg. Moffat, 2005).

In this study, the onset of internal instability is evaluated primarily on the basis of three of these attributes, namely a slope change in the relation between velocity (v) and hydraulic gradient (*i*), a temporal variation of local hydraulic gradient, and companion visual observations. A slope change in the $v \sim i$ curve usually results from migration of finer particles. The moving particles are either trapped by the adjacent downstream layer, leading to a decrease in hydraulic conductivity (internal suffosion), or washed out, leading to an increase in hydraulic conductivity (external suffosion). Both of these phenomena are detected from measurements of a variation of local hydraulic gradient (i_{jk}) between port locations on the wall of the permeameter. Additionally, visual observations can detect particle movement at the sidewall of the large permeameter, or through the exit wire mesh of either the large or small permeameter.

4.2 Experiments tests in the small permeameter

The objectives of tests performed in the small permeameter include: (a) commission of the apparatus, (b) demonstration of the repeatability of the test method, and (c) to study the effect of top vertical effective stress (σ'_{t0}) and hydraulic gradient (*i*) on the onset of internal instability in specimens of different grain size distribution. Gradation FR3 with a filter ratio

D'_{85}/d'_{15} = 2.8 was selected to commission the apparatus (FR3-25-D) because it is internally stable. Gradation FR8 with D'_{85}/d'_{15} = 7.9 was selected for repeatability tests because it is internally unstable and has been found susceptible to segregation (Khan, 2003). Two potentially internally unstable gradations (FR7 and FR8) were selected for the main test program in the expectation that a maximum hydraulic gradient less than 15 would be sufficient to cause failure. A total of 10 tests were conducted for 25 kPa $\leq \sigma'_{t0} \leq$ 200 kPa (see Table 4.1). In these tests, volumetric flow rate of water, distribution of water head along the specimen length, axial displacement and mass of soil passing were measured. Values of seepage velocity, hydraulic gradient and hydraulic conductivity were deduced from these measurements.

4.2.1 Commission test (FR3-25-D)

Test FR3-25-D was conducted on a gradation of filter ratio D'_{85}/d'_{15} = 2.8 to commission the small permeameter. This gradation was expected to be internally stable. A vertical effective stress 25 kPa was applied to the top of the specimen. The specimen was reconstituted to a length of 10.2 cm, yielding a void ratio after consolidation of 0.37. A negligible mass loss of 0.22% was measured during specimen reconstitution (Table 4.1).

Downward flow was imposed at i_{av} = 0.7 and sequentially increased to i_{av} = 1.3, 5.0, 10.0 and finally 14.0, at which point the maximum capacity of the small permeameter was reached. Each stage lasted 30 minutes. A negligible cumulative mass loss (0.16%) was measured during these stages. Seepage velocity was found proportional to hydraulic gradient, indicating the flow regime satisfied Darcy's law (Figure 4.1). A nearly linear distribution of

water head along the specimen length demonstrated the homogeneity of the reconstituted specimen (Figure 4.2). Identical initial and post-test grading curves indicate that the technique of specimen preparation (Chapter 3) is appropriate for reconstitution of a homogeneous specimen (Figure 4.3). From this test to commission the apparatus, it was concluded the specimen preparation, water supply system and data acquisition system work well and provide satisfactory results.

4.2.2 Repeatability tests

The purpose of repeatability tests is to ensure the method of specimen reconstitution, and the responses to seepage flow, are both repeatable and reliable. The modified slurry preparation and discrete deposition technique were used for specimen reconstitution, as described in section 3.5. Three separate tests were conducted with an identical FR8 soil gradation, at the same vertical stress, σ'_{t0} = 25 kPa. The main results of these three tests, FR8-25-D0, FR8-25-D1 and FR8-25-D2, are summarized in the Table 4.1.

Each specimen revealed an identical void ratio (0.37) after specimen consolidation, and hence dry density (1.82 ~ 1.83 g/cm^3). Each specimen exhibited a similar quantity of mass loss (10.6 ~ 11.1 %) during the specimen reconstitution. Likewise, a comparable water head distribution was measured at i_{av} = 1.3 (see Figure 4.4). These results confirm the replication of specimen reconstitution technique used in the tests. Upon further increases in seepage flow to failure, a similar quantity of mass passing (4.0 ~ 6.9%) was induced by seepage flow. A more detailed description of the response of each test specimen now follows, from which it is concluded the test method is repeatable and the results are reliable.

4.2.3 Tests on gradation FR8

A total of six tests were performed on gradation FR8 (with a filter ratio D'_{85}/d'_{15} = 7.9). In addition to the three repeatability tests at σ'_{t0} = 25 kPa mentioned above, another three tests were conducted at a vertical stress σ'_{t0} = 50, 100, and 200 kPa to study the relation between effective stress and critical hydraulic gradient. Downward seepage flow was applied in all the tests. A summary of results for each test is presented in the following paragraphs.

4.2.3.1 FR8-25-D0

Test FR8-25-D0 was performed with a top vertical effective stress σ'_{t0} = 25 kPa. The specimen was 9.2 cm long and the void ratio after consolidation was 0.37. A mass loss of 10.6% was measured during specimen reconstitution (see Table 4.1).

Downward flow was imposed at i_{av} = 0.4 and sequentially increased to 1.3 and 2.9. Distribution of water head over the course of test is shown in Figure C.1: the relatively lower head loss in the lowermost layer between ports 6 and 7 (for port locations, see Figure 3.5) at i_{av} = 0.4 is attributed to the mass loss during specimen reconstitution. Negligible mass loss and axial displacement were observed during these flow stages to i_{av} = 2.9, and the seepage velocity increased proportionally with hydraulic gradient (Figure 4.5). Upon imposing a small increase in hydraulic gradient to i_{av} = 3.2, a modest amount of finer particles (6.9%) was lost from the specimen (see Table 4.1). A total downward axial displacement of 2.5 mm was measured, resulting in an axial strain of 2.6%. Seepage velocity increased disproportionately. Hydraulic conductivity k_{35} increased nearly ten-fold, from 0.04 to 0.39 cm/s, as i_{av} was increased from 2.9 to 3.2 (Figure D.1). The increase in slope of the velocity

(v) ~ gradient (i_{av}) curve, the downward displacement and the mass loss are collectively attributed to the onset of instability.

The variation of local hydraulic gradient i_{jk} with elapsed time since the beginning of the test stage, at i_{av} = 2.9 and then 3.2, is shown in Figure 4.6. The stage at i_{av} = 2.9 lasted from 60 to 88 min, and the stage at i_{av} = 3.2 from 88 to 118 min. At i_{av} = 2.9, the applied hydraulic gradient i_{av} was essentially constant, and the local gradient between ports 3 and 5 was measured as i_{35} = 3.8. At 88 min, an effort was made to increase i_{av} from 2.9 to about 3.2, triggering an immediate drop in the value of i_{35}. As a marked amount of finer particles was lost, the seepage velocity increased greatly (see Figure 4.5), and it proved impossible to maintain i_{av} at 3.2. About 5 minutes later, i_{av} stabilized at a value of 2.3. With the decrease in i_{35}, a companion increase was measured in i_{56} and i_{67}: these increases are attributed to the system of head control, and also to a relative change in permeability of each layer ($\Delta k_{35} > \Delta k_{56} > \Delta k_{67}$) yielding a redistribution of hydraulic gradient among the layers (Figure D.1). This change in local hydraulic gradient in layer 3-5 is attributed to the onset of internal instability. The local gradient at the stage i_{av} = 2.9, immediately previous to the stage of onset of instability, is defined as the critical local gradient, yielding a value of i_{35} = 3.8 (see Figure 4.6) and reported in Table 4.1.

4.2.3.2 FR8-25-D1

Test FR8-25-D1 was also performed with a top vertical effective stress σ'_{t0} = 25 kPa. The specimen was 9.2 cm long and the void ratio after consolidation was 0.37. A mass loss of 11.1% was measured during specimen reconstitution (see Table 4.1).

Downward flow was imposed at i_{av} = 0.4 and sequentially increased to i_{av} = 1.3. Distribution of water head over the course of test is shown in Figure C.2: the relatively lower head loss in the lowermost layer between ports 6 and 7 at i_{av} = 0.4 is attributed to this mass loss during specimen reconstitution. Negligible mass loss and axial displacement were measured during these stages to i_{av} = 1.3, and the seepage velocity increased proportionally with hydraulic gradient (Figure 4.7). Upon imposing a large increase in hydraulic gradient to i_{av} = 3.1, a modest amount of finer particles (4.0%) was lost from specimen (see Table 4.1). A total downward axial displacement of 1.0 mm was measured, resulting in an axial strain of 0.9 %. Seepage velocity increased disproportionately. Hydraulic conductivity k_{35} again increased nearly ten-fold, from 0.015 to 0.2 cm/s, as i_{av} was increased from 1.3 to 3.1 (Figure D.2). The increase in slope of the velocity (v) ~ gradient (i_{av}) curve, the downward displacement and the mass loss are attributed to the onset of instability.

The variation of local hydraulic gradient i_{jk} with elapsed time since the beginning of the test stage, at i_{av} = 1.3 and then 3.1, is shown in Figure 4.8. The stage at i_{av} = 1.3 lasted from 40 to 80 min, and the stage at i_{av} = 3.1 from 80 to 95 min. At i_{av} = 1.3, the applied hydraulic gradient i_{av} was essentially constant, and the local gradient between ports 3 and 5 was measured as $i_{35} \approx 2.0$. At 80 min, i_{av} was increased from 1.3 to about 3.1, and i_{35} was measured to increase from 2.0 to 4.4 before experiencing an immediate drop. As a marked amount of finer particles was lost, the seepage velocity increased greatly (see Figure 4.7), and it proved impossible to maintain i_{av} at 3.2. About 5 minutes later, i_{av} stabilized at a value of 2.2. With the decrease in i_{35}, a companion increase was measured in i_{56} and i_{67}. Those

increases are again attributed to the system of head control, and also to a relative change in permeability of layers ($\Delta k_{67} > \Delta k_{35} > \Delta k_{56}$) yielding a redistribution of hydraulic gradient among the layers (Figure D.2). This change in local hydraulic gradient in layer 3-5 is attributed to the onset of internal instability. Figure 4.8 indicates that the increment in i_{35} in the last stage was too large to precisely define the critical hydraulic gradient; however, its range can be determined, between 2 and 4.4. This test suggested keeping a small increment in a multi-stage test, which was performed in the following tests.

4.2.3.3 FR8-25-D2

Test FR8-25-D2 was performed with a top vertical effective stress σ'_{t0} = 25 kPa. The specimen was 9.2 cm long and the void ratio after consolidation was 0.37. A mass loss of 10.8% was measured during specimen reconstitution (see Table 4.1).

Downward flow was imposed at i_{av} = 0.4 and sequentially increased to 1.3, 1.8, 2.3 and then 2.8. Distribution of water head over the course of test is shown in Figure C.3: the relatively lower head loss in the lowermost layer between ports 6 and 7 at i_{av} = 0.4 is attributed to the mass loss during the specimen reconstitution. Negligible mass loss and displacement were measured during the stages to i_{av} = 2.8, and the seepage velocity increased proportionally with hydraulic gradient (Figure 4.9). Upon imposing an increase in hydraulic gradient to the stage i_{av} = 3.2, a modest amount of finer particles (4.4%) was lost from specimen (see Table 4.1). A total downward axial displacement of 1.7 mm was measured, resulting in an axial strain of 1.6%. Seepage velocity increased disproportionately. Hydraulic conductivity k_{35} increased nearly four-fold from 0.04 to 0.15 cm/s, as an attempt to increase i_{av} from 2.8 to 3.2

(Figure D.3). The increase in slope of velocity (v) ~ gradient (i_{av}) curve, downward displacement and mass loss are attributed to the onset of instability.

The variation of local hydraulic gradient i_{jk} with elapsed time since the beginning of the test stage, at i_{av} = 2.8 and then 3.2, is shown in Figure 4.10. At i_{av} = 2.8, the applied hydraulic gradient i_{av} was essentially constant, and the local gradient between ports 3 and 5 was measured as i_{35} = 3.0. At 152 min, an effort was made to increase i_{av} from 2.8 to 3.2: a small variation in hydraulic gradient was attributed to the manual adjustment of the elevation of the constant head tank. As i_{av} was increased to achieve 3.2, i_{35} was measured to drop immediately. As a marked amount of finer particles was lost, the seepage velocity increased greatly (Figure 4.9), and it proved impossible to maintain i_{av} at 3.2 and stabilized at a value of 2.4. With the decrease in i_{35} and i_{56}, a companion increase was measured in i_{67} that is attributed to the system of head control. The change in local hydraulic gradient in layer 3-5 is attributed to the onset of internal instability. The local gradient at the stage i_{av} = 2.8, immediately previous to the stage of onset of instability, is defined as the critical local gradient yielding a value of i_{35} = 3.0 (see Figure 4.10).

Visual inspection of each specimen after the tests of FR8-25-D0, FR-25-D1 and FR-25-D2 revealed an extensive area without finer particles. The affected areas included nearly all of the cross-section of the specimen, implying the sidewall boundary was not a preferential zone for soil migration.

4.2.3.4 FR8-50-D

Test FR8-50-D was performed with a top vertical effective stress σ'_{t0} = 50 kPa. The specimen was 9.3 cm long and the void ratio after consolidation was 0.37. A mass loss of 11.1% was measured during specimen reconstitution (see Table 4.1).

Downward flow was imposed at i_{av} = 0.6 and sequentially increased to 1.4, 2.3, and 3.1. Distribution of water head over the course of test is shown in Figure C.4: the relatively lower head loss in the lowermost layer between ports 6 and 7 at i_{av} = 0.6 is attributed to this mass loss during specimen reconstitution. Negligible mass loss and axial displacement were measured during these stages to i_{av} = 3.1. The seepage velocity increased proportionally with hydraulic gradient (Figure 4.11). Upon imposing a small increase in hydraulic gradient to i_{av} = 3.3, a modest amount of finer particles (2.9%) was lost from the specimen (see Table 4.1). A total downward axial displacement of 0.7 mm was measured, resulting in an axial strain of 0.7%. Seepage velocity increased disproportionately. Hydraulic conductivity k_{35} increased nearly four-fold from 0.02 to 0.08 cm/s, as i_{av} increased from 3.1 to 3.3 (Figure D.4). The increases in slope of the velocity (v) ~ gradient (i_{av}) curve, the downward displacement and the mass loss are attributed to the onset of instability.

The variation of local hydraulic gradient i_{jk} with elapsed time since the beginning of the test stage, at i_{av} = 3.1 and then 3.3, is shown in Figure 4.12. The stage at i_{av} = 3.1 lasted from 90 to 120 min, and the stage at i_{av} = 3.3 from 120 to 150 min. At i_{av} = 3.1, the applied hydraulic gradient i_{av} was essentially constant, and the local gradient between ports 3 and 5 was measured as i_{35} = 4.5. At 120 min, as i_{av} was increased from 3.1 to 3.3, the local hydraulic

gradients followed with the exception of i_{35}, due to the manual adjustment of elevation of inlet water tank. At i_{av} = 3.3, i_{35} and i_{56} were observed to drop immediately. As a marked amount of finer particles was lost, and the seepage velocity increased greatly (Figure 4.11), it proved impossible to maintain i_{av} at 3.3 which then stabilized at the preceding value of 3.1. With the decrease in i_{35} and i_{56}, a companion increase was measured in i_{67}. Those increases and decreases are attributed to the system of head control, and also to a relative change in permeability of layers ($\Delta k_{35} \approx \Delta k_{56} > \Delta k_{67}$) yielding a redistribution of hydraulic gradient among these layers. This change in local hydraulic gradient in layer 3-5 is attributed to the onset of internal instability. The local gradient at the stage i_{av} = 3.1, immediately previous to the stage of onset of instability is defined as the critical local gradient yielding a value of i_{35} = 4.5 (see Figure 4.12).

Inspection of the specimen after the test indicated a large area without finer particles. Like the tests on gradation FR8 at 25 kPa, the affected areas included most of the cross-section of the specimen, implying the sidewall boundary is not a preferential zone for soil migration.

4.2.3.5 FR8-100-D

Test FR8-100-D was performed with a top vertical effective stress σ'_{t0} = 100 kPa. The specimen was 9.2 cm long and the void ratio after consolidation was 0.36. A mass loss of 8.6% was measured during specimen reconstitution (see Table 4.1).

Downward flow was imposed at i_{av} = 0.7 and sequentially increased to 1.2, 1.8 and then 2.3. Distribution of water head over the course of test is shown in Figure C.5: the relatively lower

head loss in the lowermost layer between ports 6 and 7 at i_{av} = 0.7 is attributed to this mass loss during specimen reconstitution. Negligible mass loss and axial displacement were measured during these stages to i_{av} = 2.3, and the seepage velocity increased proportionally with hydraulic gradient (Figure 4.13). Upon imposing a small increase in hydraulic gradient to i_{av} = 2.7, a small amount of finer particles (1.0%) was lost from specimen (see Table 4.1). Although a negligible axial displacement was measured, the seepage velocity increased disproportionately (see Figure 4.13). Hydraulic conductivity k_{34} increased from 0.012 to 0.04 cm/s, as i_{av} was increased from 2.3 to 2.7 (Figure D.5). Increases in the slope of velocity (v) ~ gradient (i_{av}) curve and the small mass loss are attributed to the onset of instability. The test was continued thereafter to i_{av} = 4.1, leading to a total displacement of 4.3 mm and a finer particles loss of 12.2% due to seepage flow.

The variation of local hydraulic gradient i_{jk} with elapsed time since the beginning of the test, at i_{av} = 2.7, is shown in Figure 4.14. At 120 min, i_{av} was increased from 2.3 to 2.7. At 140 min, i_{34} experienced a decrease. As finer particles were lost, the seepage velocity approximately doubled. The value of i_{av} stabilized at about 2.6 within 2 to 3 minutes. With the decrease in i_{34}, companion increases were measured in i_{45} and i_{56}: they are attributed to the system of head control, and also to the relative change in permeability of the layers ($\Delta k_{34} > \Delta k_{45} > \Delta k_{56}$) yielding a redistribution of hydraulic gradient (Figure D.5). This change i_{34} is attributed to the onset of internal instability. The local gradient at this stage is defined as the critical local gradient yielding i_{34} = 5.0 (see Figure 4.14).

Inspection of the specimen after the test revealed an extensive area without finer particles (Figure E.1). The affected areas included nearly all of the cross-section of the specimen, implying the sidewall boundary is not a preferential zone for soil migration.

4.2.3.6 FR8-200-D

Test FR8-200-D was performed with a top vertical effective stress σ'_{t0} = 200 kPa. The specimen was 9.0 cm long and the void ratio after consolidation was 0.33. A mass loss of 8.5% was measured during the specimen reconstitution (see Table 4.1).

Downward flow was imposed at i_{av} = 0.7 and sequentially increased to 1.1, 1.7, 2.2, 2.7 and then 3.2. Distribution of water head over the course of test is shown in Figure C.6: the relatively lower head loss in the lowermost layer between ports 6 and 7 at i_{av} = 0.7 is attributed to this mass loss during specimen reconstitution. Negligible mass loss and axial displacement were measured during these stages to i_{av} = 3.2, and the seepage velocity increased proportionally with hydraulic gradient (Figure 4.15). Upon imposing a small increase in hydraulic gradient to i_{av} = 3.5, a large amount of finer particles (11.5%) was lost from specimen (see Table 4.1). A total downward axial displacement of 3.7 mm was measured, resulting in an axial strain of 3.9%. Seepage velocity increased disproportionately. Hydraulic conductivity k_{34} increased from 0.018 to 0.79 cm/s as i_{av} increased from 3.2 to 3.5 (Figure D.6). Increases in the slope of velocity (v) ~ gradient (i_{av}) curve, downward displacement and the significant mass loss are attributed to the onset of instability.

The variation of local hydraulic gradient i_{jk} with elapsed time since the beginning of the test, at i_{av} = 3.2 and then 3.5, is shown in Figure 4.16. The stage at i_{av} = 3.2 lasted from 150 to 175 min, and the stage at i_{av} = 3.5 from 175 to 210 min. At i_{av} = 3.2, the applied hydraulic gradient i_{av} was essentially constant, and the local gradient between ports 3 and 4 (see Figure 3.5) was measured as i_{34} = 6.6. At 160 min, a disturbance caused re-adjustment between the layers 3-4 and 4-5 yielding a reduction in i_{34} from 6.6 to 6.0 and an increase in i_{45} from 2.0 to 2.5. At 175 min, i_{av} was increased from 3.1 to 3.5, whereupon the local hydraulic gradients were measured to increase correspondingly. Very shortly thereafter, i_{34} exhibited a steady drop over a period 1 ~ 2 minutes. As a large amount of finer particles was lost, the seepage velocity increased greatly, and it proved impossible to maintain i_{av} at 3.5. It stabilized at $i_{34} \approx$ 1.0; i_{45} and i_{56} were also measured to decrease. This change in local hydraulic gradient in layer 3-4 is attributed to the onset of internal instability. The local gradient at the stage i_{av} = 3.2, immediately previous to the stage of onset of instability is defined as the critical local gradient yielding a value of i_{34} = 6.6 (see Figure 4.16).

Inspection of the specimen after the test revealed a large area without finer particles (Figure E.2). The affected areas include most of the cross-section of the specimen, implying the sidewall boundary is not a preferential zone for soil migration.

4.2.4 Tests on gradation FR7

A total of three tests were conducted on gradation FR7 (with a filter ratio D'_{85}/d'_{15} = 7.1). A vertical effective stress, ranging from 25 to 100 kPa was applied to the top surface of

specimen. Downward seepage flow was imposed in all of the tests. A summary of results for each test is presented in the following paragraphs.

4.2.4.1 FR7-25-D

Test FR7-25-D was performed with a top vertical effective stress σ'_{t0} = 25 kPa. The soil specimen was 10.3 cm long and the void ratio after consolidation was 0.34. A mass loss of 3.5% was measured during specimen reconstitution (see Table 4.1).

Downward flow was imposed at i_{av} = 1.1 and sequentially increased to 2.0, 3.0, 3.9, 4.8, 5.7 and then 6.6. Distribution of water head over the course of test is shown in Figure C.7: the relatively lower head loss in the lowermost layer between ports 5 and 7 is attributed to this mass loss during the specimen reconstitution. Negligible mass loss and axial displacement were measured during the seepage stages to i_{av} = 6.6, and the seepage velocity increased proportionally with hydraulic gradient (Figure 4.17). Upon imposing a small increase in hydraulic gradient to i_{av} = 7.3, seepage velocity increased disproportionately and a total downward axial displacement of 0.6 mm was measured, resulting in an axial strain of 0.6%. A small amount of finer particles (0.2%) was lost from specimen (see Table 4.1). Hydraulic conductivity k_{13} increased from 0.014 to 0.046 cm/s as i_{av} was increased from 6.6 to 7.3 (Figure D.7). Increases in the slope of velocity (v) ~ gradient (i_{av}) curve and the associated downward displacement are attributed to the onset of instability. The test was continued to the value of i_{av} = 9.0, yielding a modest amount of mass loss (6.5%) (see Figure E.3) and a total displacement of 3.5 mm at the end of the test.

The variation of local hydraulic gradient i_{jk} with elapsed time since the beginning of the test, at i_{av} = 6.6 and then 7.3, is shown in Figure 4.18. The stage at i_{av} = 6.6 lasted from 210 to 240 min, and the stage at i_{av} = 7.3 from 240 to 270 min. At i_{av} = 6.6, the applied hydraulic gradient i_{av} was essentially constant, and the local gradient between ports 1 and 3 (see Figure 3.5) was measured as i_{13} = 8.7. At 240 min, i_{av} was increased from 6.6 to 7.3, and the local hydraulic gradients were measured to increase correspondingly. As soon as the target gradient was reached, the local hydraulic gradient i_{13} was measured to drop immediately, while the applied hydraulic gradient i_{av} was essentially constant. With the decrease in i_{13}, a companion increase was measured in i_{34} and i_{45}. Those increases are attributed to the system of head control, and also to a relative change in permeability of layers ($\Delta k_{13} > \Delta k_{45} > \Delta k_{34}$) yielding a redistribution of hydraulic gradient among these layers (Figure D.7). This change in local hydraulic gradient across layer 1-3 is attributed to the onset of internal instability. The local gradient at the stage i_{av} = 6.6, immediately previous to the stage of onset of instability, is defined as the critical local gradient yielding a value of i_{13} = 8.7 (see Figure 4.18).

Inspection of the specimen after the test revealed several areas without finer particles (Figure E.4). The affected area includes both central and boundary segments of the cross-section, implying the boundary is not a preferential zone for soil migration.

4.2.4.2 FR7-50-D

Test FR7-50-D was performed with a top vertical effective stress σ'_{t0} = 50 kPa. The soil specimen was 10.2 cm long and the void ratio after consolidation was 0.33. A mass loss of 4.3% was measured during specimen reconstitution (see Table 4.1).

Downward flow was imposed at i_{av} = 0.6 and sequentially increased to 1.1, 2.0, 3.4, 5.2, 7.1, 8.0, and then 8.9. Distribution of water head over the course of test is shown in Figure C.8: the relatively lower head loss in the lowermost layer between ports 5 and 7 at i_{av} = 0.6 is attributed to this mass loss during specimen reconstitution. Negligible mass loss and axial displacement were measured during the seepage stages to i_{av} = 8.9, and the seepage velocity increased proportionally with hydraulic gradient (Figure 4.19). Upon imposing a small increase in hydraulic gradient to i_{av} = 9.5, a modest amount of finer particles (4.8%) was lost from the specimen (see Figure E.5 and Table 4.1). A total downward axial displacement of 1.0 mm was measured, resulting in an axial strain of 0.1%. Seepage velocity increased disproportionally. Hydraulic conductivity k_{13} increased from 0.012 to 0.022 cm/s as i_{av} increased from 8.9 to 9.5 (Figure D.8). Increases in the slope of velocity (v) ~ gradient (i_{av}) curve, downward displacement and mass loss are attributed to the onset of instability.

The variation of local hydraulic gradient i_{jk} with elapsed time since the beginning of test, at i_{av} = 8.9 and then 9.5, is shown in Figure 4.20. The stage at i_{av} = 8.9 lasted from 200 to 230 min, and the stage at i_{av} = 9.5 from 230 to 260 min. At i_{av} = 8.9, the applied hydraulic gradient i_{av} was essentially constant, and the local gradient between ports 1 and 3 (see Figure 3.5) was measured as i_{13} = 15.4. At 230 min, i_{av} was increased from 8.9 to 9.5 yielding a

corresponding increase in the local hydraulic gradients; i_{13} was increased from 15.4 to 16.5. About 2 minutes later, i_{13} was measured to drop very rapidly, while the applied hydraulic gradient i_{av} was essentially constant. With the decrease in i_{13}, a companion increase was measured in i_{34} and i_{45}. About 10 minutes later, i_{34} was measured to drop, and a companion increase occurred in i_{13} and i_{45}. These changes in hydraulic gradient are attributed to the system of head control, and also to the relative change in permeability of layers ($\Delta k_{13} > \Delta k_{34} > \Delta k_{45}$) yielding a redistribution of hydraulic gradient among the layers (Figure D.8). The change in local hydraulic gradient in layer 1-3 is attributed to the onset of internal instability. The local gradient at this stage $i_{av} = 9.5$ is defined as the critical local gradient yielding a value of $i_{13} = 16.5$ (see Figure 4.20).

Inspection of the specimen after the test revealed nearly 50% of the cross-section without finer particles (Figure E.6). The affected area included central and boundary segment of the specimen, implying the side-wall boundary is not a preferential zone for soil migration.

4.2.4.3 FR7-100-D

Test FR7-100-D was performed with a top vertical effective stress σ'_{t0} = 100 kPa. The soil specimen was 10.8 cm long and the void ratio after consolidation was 0.32. A mass loss of 3.7% was measured during specimen reconstitution (see Table 4.1).

Downward flow was imposed at $i_{av} = 0.6$ and sequentially increased to 1.0, 1.9, 3.7, 6.4, 9.0 and 10.7. Distribution of water head over the course of test is shown in Figure C.9: the relatively lower head loss in the lowermost layer between ports 5 and 7 at $i_{av} = 0.6$ is

attributed to this loss during specimen reconstitution. Negligible mass loss and axial displacement were measured with seepage flow to i_{av} = 10.7, and the seepage velocity increased proportionally with increasing the hydraulic gradient (Figure 4.21). In order to impose a hydraulic gradient in excess of 10.7, the reservoir bath was lowered from the bench to the floor (see Figure 3.2). The action caused some disturbance to the specimen, and minor finer particles loss was observed at i_{av} = 12.0. However, negligible finer particles loss and axial displacement were measured at i_{av} = 14.4. Upon imposing an increase to i_{av} = 15.5, a modest amount of finer particles (6.5%) was lost from specimen (see Figure E.7 and Table 4.1). A total downward axial displacement of 1.8 mm was measured, resulting in an axial strain of 1.6%. Seepage velocity increased disproportionately. Hydraulic conductivity k_{34} increased from 0.012 to 0.034 cm/s, as i_{av} was increased from 14.4 to 15.5 (Figure D.9). Increases in the slope of velocity (v) ~ gradient (i_{av}) curve, downward displacement and mass loss are attributed to the onset of instability.

The variation of local hydraulic gradient i_{jk} with elapsed time since the beginning of test, at i_{av} = 14.4 and then 15.5, is shown in Figure 4.22. The stage at i_{av} = 14.4 lasted from 240 min to 268 min; the applied hydraulic gradient i_{av} was essentially constant, and the local gradient between ports 3 and 4 was measured as i_{34} = 27.1. At 268 min, i_{av} was increased from 14.4 to 15.5. Manual adjustment of inlet water tank caused the initial systematic drop in local hydraulic gradients. As the inlet water tank was then positioned at the target elevation, i_{34} was observed to drop immediately. As a marked amount of finer particles was lost, the seepage velocity increased greatly: i_{av} could not be maintained at 15.5 and dropped immediately. Since the seepage velocity exceeded 0.6 cm/s, it is difficult to control the

seepage flow and the test was stopped. With the decrease in i_{34} and i_{13}, a companion increase was measured in i_{45}. This change in local hydraulic gradient in layer 3-4 is attributed to the onset of internal instability. The local gradient at the stage i_{av} = 14.4, immediately prior to the stage of onset of instability, is defined as the critical local gradient yielding a value of i_{34} = 27.1 (see Table 4.1).

Inspection of the specimen after the test revealed several areas without finer particles (Figure E.8). The affected areas included central and boundary segments of the specimen, implying the side-wall boundary is not a preferential zone for soil migration.

4.3 Experimental tests in the large permeameter

To further study the effect of grain size distribution and effective stress on the critical hydraulic gradient to trigger the onset of instability, a series of tests was performed on widely-graded soils with a component of gravel. In order to accommodate a maximum particle size of 19 mm (¾ in), the tests were performed in the large diameter permeameter (see Figure 3.7).

Four gradations of soils were examined in testing. The permeameter test data were used to supplement the findings of Moffat (2005). The four gradations (HF01, HF03, HF05 and HF10) yield a geometric index $(H/F)_{min}$ from 0 to 1.0, and 'bound' the work of Moffat (2005). Upward seepage flow was imposed on most of the reconstituted test specimens, since experience has shown that downward flow tends to reach the maximum capacity of apparatus (Moffat, 2005). In the large permeameter tests, volumetric flow rate of water, distribution of

water head along the specimen length and axial displacement were measured. Values of seepage velocity, hydraulic gradient and hydraulic conductivity were deduced from these measurements. In addition to the tests on reconstituted soils, one gradation of glass bead (FR7) was tested to unify interpretation of the small and the large permeameter test data.

4.3.1 Tests on gradation FR7

Strictly, there were two purposes to testing gradation FR7 in the large permeameter. One was to commission the apparatus, and the other was to verify the data analysis and consistency of findings between the small permeameter (of diameter 100 mm) and the large permeameter (of diameter 279 mm). Two identical specimens were tested, one with downward flow and the other with upward flow, at the same value of top vertical effective stress.

4.3.1.1 FR7-150-D

Test FR7-150-D was performed with a top vertical effective stress σ'_{t0} = 150 kPa. Downward seepage flow was applied to the specimen in order to compare its response to that of gradation FR7 in the small permeameter, in which all tests were also subject to downward flow. The reconstituted specimen was 31.0 cm long and the void ratio after consolidation was 0.32 (see Table 4.2). A modest mass loss was observed during specimen reconstitution.

Downward flow was imposed at i_{av} = 1.1 and sequentially increased to 2.0 and then 3.0. Distribution of water head over the course of test is shown in Figure C.10: the relatively lower head loss in the lowermost layer between ports 6 and 7 (see Figure 3.8) at i_{av} = 1.1 is attributed to the mass loss during the specimen reconstitution. A negligible mass loss was

observed, and minor axial displacement was measured, during the seepage stages to i_{av} = 3.0, and the seepage velocity increased proportionally with hydraulic gradient (Figure 4.23). Upon imposing an increase in hydraulic gradient to i_{av} = 4.0, finer particles were observed to move from side-wall starting within layers 3-5. The action propagated towards the basal outlet of the specimen, with continued wash-out of finer particles from the specimen (Figure E.9). Visual observations after testing showed that a marked amount of finer particles were lost (Figure E.10). A total downward axial displacement of 1.9 mm was measured, resulting in a cumulative axial strain of 0.6%. Seepage velocity increased disproportionately (Figure 4.23). Hydraulic conductivity k_{35} increased from 0.01 to 0.03 cm/s as i_{av} increased from 3.0 to 4.0 (Figure D.10). Increases in the slope of velocity (v) ~ gradient (i_{av}) curve, downward displacement and mass loss are attributed to the onset of internal instability.

The variation of local hydraulic gradient i_{jk} with time since the beginning of the stage at i_{av} = 4.0 is shown in Figure 4.24. At 100s, i_{av} attained its target increment from the previous stage. At 300s, i_{35} was recorded to drop, yielding a companion increase in i_{56}. These increases and decrease in hydraulic gradient are attributed to the system of head control, and also to a relative change in permeability of each layer ($\Delta k_{35} > \Delta k_{56}$) yielding a redistribution of hydraulic gradient among these layers (Figure D.10). A change in local hydraulic gradient in layer 3-5 is attributed to the onset of internal instability. The hydraulic gradient in this stage immediately prior to the onset of instability is defined as the critical hydraulic gradient yielding a value of i_{35} = 5.0 (see Figure 4.24).

4.3.1.2 FR7-150-U

Test FR7-150-U was subject to upward flow in order to compare with the previous test using downward flow. An identical vertical effective stress σ'_{t0} = 150 kPa was applied on the top surface of specimen. The specimen was 31.0 cm long and the void ratio after consolidation was 0.32 (see Table 4.2). Minor mass loss was observed during the specimen constitution.

Upward flow was imposed at i_{av} = 0.7 and sequentially increased to 1.1, 1.5 and then 1.9. Distribution of water head over the course of test was shown in Figure C.11: a nearly linear water head distribution at i_{av} = 0.7 confirms the reconstituted specimen was homogenous. Minor finer particle loss was observed at top surface of specimen and minor downward displacement was measured during these stages to i_{av} = 1.7, and the seepage velocity increased proportionally with hydraulic gradient (Figure 4.25). Upon increasing the hydraulic gradient to i_{av} = 1.9, a displacement of 3.5 mm was recorded, together with observation of local "boiling" finer particles at several locations of top surface above exit mesh. However, the seepage velocity is noted to still increase proportionally with hydraulic gradient. Further imposing a small increase in hydraulic gradient to i_{av} = 2.5, trigged a large mass loss at the surface of specimen (Figure E.11). Post-test inspection of the specimen revealed that a large amount of finer particles were lost (Figure E.12). A total axial displacement of 9.0 mm was measured, resulting in a cumulative axial strain of 3.0% (see Table 4.2). The seepage velocity increased disproportionally. Hydraulic conductivity k_{56} increased from 0.012 to 0.020 cm/s as i_{av} increased from 1.9 to 2.5 (Figure D.11). Increases in the slope of velocity (v) ~ gradient (i_{av}) curve, downward displacement and mass loss are attributed to the onset of instability.

The variation of local hydraulic gradient i_{jk} with time since the beginning of the stage at i_{av} = 2.5 is shown in Figure 4.26. At 200s, i_{av} attained its target increment from the previous stage. At about 400s, the local hydraulic gradient i_{56} was observed to slowly diminish, and a slow companion increase was measured in i_{45}. At about 620s, i_{56} started to drop significantly. At about 750s, both i_{45} and i_{56} started to drop. As a large amount of finer particles was lost, the seepage velocity increased greatly, it proved difficult to maintain i_{av} at 2.5. The test was then stopped at 1000s. A change in local hydraulic gradient is attributed to the onset of internal instability. The hydraulic gradient in this stage immediately prior to the initiation of instability is defined as the critical hydraulic gradient yielding a value of i_{56} = 3.0 (see Figure 4.26).

4.3.2 Test on gradation HF01

Gradation HF01 was reconstituted from soils to the same grain size distribution as material A tested by Skempton and Brogan (1994). The geometric indices are $(H/F)_{min}$ = 0.1 and D'_{85}/d'_{15} = 11.0. The specimen is 30.0 cm long and the void ratio was 0.32 (see Table 4.2). Minor mass loss was observed during the specimen reconstitution. Originally, a vertical effective stress σ'_{t0} = 25 kPa was applied to the top surface of specimen. However its hydraulic conductivity was found greater than 0.5 cm/s, and therefore most of the imposed differential water head was consumed by pipes and connections (see Chapter 3), leading to a maximum hydraulic gradient across the specimen less than 0.4. Thus, the vertical stress was released, and the test was conducted with σ'_{t0} = 0, thereby replicating exactly the test conditions of Skempton and Brogan (1994).

Upward flow was imposed at i_{av} = 0.08 and sequentially increased to 0.1, 0.13, 0.14, and then 0.16. Distribution of water head over the course of test is shown in Figure C.12: a nearly linear distribution of water head in the specimen at i_{av} = 0.08 indicated the specimen was homogenous. A "boiling"-like movement of finer particles was observed at a few places on the side of specimen, and slight "boiling" was observed at a few locations on the surface of specimen during these stages. The seepage velocity increased proportionally with hydraulic gradient (Figure 4.27). However, at i_{av} = 0.17, the seepage velocity was noted to increase disproportionately, and upon imposing an increase in hydraulic gradient to i_{av} = 0.22, a substantive boiling action was observed on the top surface of specimen (Figure E.13). Hydraulic conductivity k_{56} increased from 0.6 to 1.1 cm/s and k_{45} increased from 0.5 to 0.8 cm/s as i_{av} increased from 0.16 to 0.22 (Figure D.12). Post-test observations reveal the nature of finer particles washed out and settled on the top surface of specimen (Figure E.14). Increases in the slope of velocity (v) ~ gradient (i_{av}), and mass loss indicated the onset of instability.

The variation of local hydraulic gradient i_{jk} with time since the beginning of the stage at i_{av} = 0.22 is shown in Figure 4.28. i_{45} and i_{56} was measured to decrease. As a large amount of finer particles was lost, the seepage velocity increased greatly, i_{av} could not be maintained at 0.22 and dropped gradually. This variation of hydraulic gradient indicated the onset of internal instability. The critical gradient is defined as the average hydraulic gradient i_{46} = 0.17, at which the slope of $v \sim i_{av}$ curve changes. This value is very close to that of 0.20 reported by Skempton and Brogan (1994).

4.3.3 Tests on gradation HF03

Two upward flow tests were conducted on gradation HF03, with $(H/F)_{min}$ = 0.3, at a vertical effective stress σ'_{t0} = 25 and 50 kPa respectively. All tests exhibited internal instability. A summary of results for each test is presented in the following paragraphs.

4.3.3.1 HF03-25-U

Test HF03-25-U was performed with a top vertical effective stress σ'_{t0} = 25 kPa. The soil specimen was 30.0 cm long and the void ratio after consolidation was 0.31 (see Table 4.2). Negligible mass loss was observed during specimen reconstitution.

Upward seepage flow was imposed at i_{av} = 0.9 and sequentially increased to 1.9, 2.6, 3.7, 4.7 and then 5.6. Distribution of water head over the course of the test is shown in Figure C.13: a nearly linear distribution of water head at i_{av} = 0.9 indicates the specimen was homogenous. Negligible mass loss was observed and minor axial displacement was measured during these stages up to i_{av} = 5.6, and the seepage velocity increased proportionally with hydraulic gradient (Figure 4.29). A “boiling”-like movement of finer particles was observed at several places on the sides of the specimen, at its lowermost part between ports 5 and 7. Additionaly, minor “boiling” was observed on the top surface of specimen. Upon imposing an increase in hydraulic gradient to i_{av} = 6.6, finer particle loss was observed between ports 4 and 5 (Figure E.15). There was no through channel observed along the sidewall of permeameter, implying the sidewall boundary was not a preferential zone for soil migration. Vigorous “boiling” was observed on the top surface of specimen (Figure E.16b). A total axial displacement of 0.7 mm displacement was measured, resulting in an axial strain of 0.23%. Seepage velocity

increased disproportionately, although the change was more subtle than in other tests. Hydraulic conductivity k_{45} increased from 0.01 to 0.012 cm/s as i_{av} increased from 5.6 to 6.6 (Figure D.13). Increases in the slope of velocity (v) ~ gradient (i_{av}) curve, downward displacement and mass loss are attributed to the onset of instability. The test was continued to i_{av} = 7.5, whereupon strong "boiling" continued to develop at the top surface of specimen. Post-test observations indicate the preferential locations of finer particles collected at the top surface (Figure E.16a).

The variation of local hydraulic gradient i_{jk} with time since the beginning of the stage at i_{av} = 6.6 is shown in Figure 4. 30. Hydraulic gradient was gradually increased to the previous stage at i_{av} = 5.6, as it is stable at 175s, i_{av} was increased from zero to the targeted gradient 6.6. About 100s later, the local hydraulic gradient i_{45} was measured to drop, and a companion increase was measured in i_{56} and i_{67}. At about 500s, i_{67} also started to drop. A change in local hydraulic gradient is attributed to the onset of internal instability. The hydraulic gradient immediately prior to the initiation of instability in the layer 4-5 is defined as the critical hydraulic gradient, yielding a value of i_{45} = 6.9 (see Figure 4.30).

4.3.3.2 HF03-50-U

Test HF03-50-U was performed with a top vertical effective stress σ'_{t0} = 50 kPa. The soil specimen was 28.7 cm long and the void ratio after consolidation was 0.29 (see Table 4.2). Minor finer particle loss was observed during specimen reconstitution.

Upward seepage flow was imposed at i_{av} = 2.0 and sequentially increased to 3.9, 5.9, 7.9, 9.8, 11.7 and then 13.7. Distribution of water head over the course of test is shown in Figure C.14: a nearly linear distribution of water head at i_{av} = 2.0 indicates the specimen was homogenous. During i_{av} = 2.0 ~ 5.9, negligible mass loss was observed and negligible axial displacement was measured, and the seepage velocity increased proportionally with hydraulic gradient (Figure 4.31). During i_{av} = 5.9 ~ 13.7, a small "boiling"-like movement of finer particles was observed at one to four distinct locations on the sides of the specimen between ports 5 and 7. Slight "boiling" was also observed on the top surface of specimen. A total downward displacement of 0.1 ~ 0.4 mm was measured. However, the seepage velocity still increased proportionally with hydraulic gradient (Figure 4.31). Upon imposing an increase in hydraulic gradient to i_{av} = 15.7, Vigorous "boiling" was observed on the top surface of specimen (Figure E.17). Seepage velocity increased disproportionately (Figure 4.31), albeit in a subtle manner. Hydraulic conductivity k_{45} increased from 0.01 to 0.012 cm/s as i_{av} increased from 13.7 to 15.7 (Figure D.14). Increases in the slope of velocity (v) ~ gradient (i_{av}) curve and mass loss are attributed to the onset of instability. Two more stages were performed to increase the hydraulic gradient to i_{av} = 17.6 and 19.6, each of which yielded continued "boiling" on the top surface of specimen and a subsequent post-test collection of finer materials at the top surface (Figure E.18)

The variation of local hydraulic gradient i_{jk} with time since the beginning of the stage at i_{av} = 15.7 is shown in Figure 4. 32. At 400s, i_{av} reached the targeted gradient 15.7 from an initial value of zero at the beginning of the stage. The stage lasted 3.5 hours. The applied hydraulic gradient i_{av} was essentially constant. The local hydraulic gradient i_{56} was measured to

increase gradually and i_{45} diminish gradually. A change in local hydraulic gradient is attributed to the onset of internal instability. The hydraulic gradient immediately prior to the initiation of instability in the layer 4-5 is defined as the critical hydraulic gradient yielding a value of i_{45} = 12.9 (see Figure 4.32).

4.3.4 Tests on gradation HF05

Three upward flow tests were conducted on gradation HF05, with $(H/F)_{min}$ = 0.5, at a vertical effective stress σ'_{t0} = 25 and 50 kPa respectively. A summary of results for each test is presented in the following paragraphs.

4.3.4.1 HF05-25-U1

Test HF05-25-U1 was performed with a top vertical effective stress σ'_{t0} = 25 kPa. The soil specimen was 31.0 cm long and the void ratio after consolidation was 0.32 (see Table 4.2). Modest mass loss was observed during specimen reconstitution.

Upward flow was imposed at i_{av} = 1.3 and sequentially increased to 2.2, 3.3, 4.4, 5.5, 6.5 and then 7.6, at which stage internal instability occurred. The test was continued until heave fail occurred at i_{av} = 16.8. Distribution of water head over the course of test is shown in Figure C.15: the very small head loss in the lowermost layer between ports 6 and 7 at i_{av} = 1.3 is attributed to the mass loss during specimen reconstitution. At values of i_{av} = 1.3 to 6.5, negligible mass loss was observed with seepage flow, no axial displacement was measured, and the seepage velocity increased with hydraulic gradient (Figure 4.33). Inspection reveals the increase is not proportional at low gradient, which is attributed to the low permeability of

the specimen and a resolution of measurement in the experiment. Upon imposing a small increase in hydraulic gradient to i_{av} = 7.6, no finer particles loss was observed (Figure E.19), and again no axial displacement was measured. However, the slope of v ~ i_{av} curve was observed to decrease (Figure 4.33). The response is attributed to a migration of finer particles within the soil specimen, and is believed indicative of the onset of internal instability.

The test was continued, and the gradient increased sequentially to i_{av} = 13.6, whereupon a short horizontal crack was observed in the layer 5-6, about 6 cm above the basal inlet of specimen, and an upward displacement of 0.1 mm was measured. At i_{av} = 15.0, the horizontal crack developed more fully (Figure E.20), and a further upward displacement of 0.1 mm was measured. At i_{av} = 16.8, the portion of the test specimen above the horizontal crack rose quickly causing the horizontal crack to open to a significant gap. Soil particles were observed to precipitate from the top surface of the gap, and test was stopped (Figure E.21). Seepage velocity increased disproportionately (see Figure 4.33). Hydraulic conductivity in the layer k_{56} increased from 1.2×10^{-4} to 3.4×10^{-3} cm/s as i_{av} increased from 15.0 to 16.8 (Figure D.15). A total upward displacement of 23.5 mm was measured.

The variation of local hydraulic gradient i_{jk} with time since the beginning of the stage at i_{av} = 7.6 is shown in Figure 4.34. The stage lasted for 45 minutes. The applied hydraulic gradient i_{av} was essentially constant. The local hydraulic gradient i_{56} was observed to drop gradually and i_{45} increase gradually. This change in local hydraulic gradient is attributed to migration of finer particles within specimen and indicates the onset of internal instability. This process is time dependent, as the change in hydraulic gradient is slow and continuous. The critical

gradient is defined as the average gradient in the central portion of specimen yielding a value of i_{46} = 9.0.

The variation of local hydraulic gradient i_{jk} with time since the beginning of the stage at i_{av} = 16.8 is shown in Figure 4.35. At 1000s, i_{56} was measured to drop immediately, yielding a companion increase in i_{45} and i_{34}. At about 1500s, i_{45} dropped dramatically. As the lowermost portion of the specimen liquefied, the length of intact specimen shortened, leading to an increase in average hydraulic gradient across it. The hydraulic gradient in layer 5-6 immediately prior to the onset of heave failure is defined as the critical gradient, yielding a value of i_{56} = 15.3.

4.3.4.2 HF05-25-U2

Test HF05-25-U2 was also performed with a top vertical effective stress σ'_{t0} = 25 kPa. The soil specimen was 31.0 cm long and the void ratio after consolidation was 0.32 (see Table 4.2). Modest mass was observed during specimen reconstitution.

Upward flow was imposed at i_{av} = 1.4 and sequentially increased to 2.1, 3.1, 4.1, and then 5.0, at which stage internal instability occurred. As for the previous test, this test was also continued to i_{av} = 9.9. Distribution of water head over the course of test is shown in Figure C.16: the relative lower head loss in the lowermost layer between ports 6 and 7 at i_{av} = 1.4 is attributed to the mass loss during specimen reconstitution. At values of i_{av} = 1.4 to 4.1, negligible mass loss was observed and no axial displacement was measured, and the seepage velocity increased proportionally with hydraulic gradient (Figure 4.36). Upon imposing a

small increase in hydraulic gradient to i_{av} = 5.0, no mass or axial displacement was measured, yet the slope of v ~ i_{av} curve was observed to decrease (Figure 4.36). This response is again attributed to a migration of finer particles, the onset of internal instability. The test was continued until i_{av} = 9.9, throughout which there was no axial displacement or particle loss observed (Figure E.22).

The variation of local hydraulic gradient i_{jk} with time since the beginning of the stage at i_{av} = 5.0 is shown in Figure 4.37. This stage lasted for 4.5 hours. The applied hydraulic gradient i_{av} was essentially constant. The local hydraulic gradient i_{45} was measured to diminish very gradually and i_{56} increased likewise. This change in local hydraulic gradient is attributed to migration of finer particles within the specimen and indicates the phenomenon of internal instability. This process is time dependent, as the change in hydraulic gradient is slow and continuous. The critical gradient is defined as the average gradient in the central portion of specimen yielding a value of i_{46} = 5.6.

4.3.4.3 HF05-50-U

Since the central portion of specimen in the test HF05-25-U2 was nearly intact, it was decided to perform an additional test on the same specimen but at higher stress. Test HF05-50-U was performed with a top vertical effective stress σ'_{t0} = 50 kPa.

Upward flow was imposed at i_{av} = 2.2 and sequentially increased to 4.1, 6.1, 8.1, 10.0, 12.0, 15.0 and then 18.0, at which stage internal instability occurred. The test was continued until

to heave failure at i_{av} = 31.0. Distribution of water head over the course of test was shown in Figure C.17: a nearly linear distribution of water head at i_{av} = 2.2 indicated that the specimen was homogenous. At values of i_{av} = 2.2 to 15.0. negligible mass loss was observed and no axial displacement was measured, and the seepage velocity increased proportionally with hydraulic gradient (Figure 4.38). Upon imposing an increase in hydraulic gradient to i_{av} = 18.0, no finer particles loss was observed (Figure E.23), and again no axial displacement was measured. However, the slope of v ~ i_{av} curve decreased (Figure 4.38). Hydraulic conductivity in local layers experienced a slow decrease (Figure D.17). The decrease in slope of the velocity (v) ~ gradient (i_{av}) is attributed to migration of finer particles within the specimen and the onset of internal instability.

The test was continued, and the gradient increased sequentially to i_{av} = 29.0, whereupon a short horizontal crack was observed in the layer 5-6, about 3 cm above the bottom of specimen (Figure E.24), and an upward displacement of 0.1 mm was measured. At i_{av} = 31.0, the portion of test specimen above the horizontal crack rose quickly causing the horizontal crack to open to a significant gap. Soil particles were observed to precipitate from the top surface of the gap, and test was stopped (Figure E.25). Seepage velocity increased disproportionately (see Figure 4.38). Hydraulic conductivity in the layer k_{56} increased from 2.2×10^{-5} to 1.8×10^{-3} cm/s as i_{av} increased from 29.0 to 31.0 (Figure D.17). A total upward displacement of 26.7 mm was measured (Table 4.2).

The variation of local hydraulic gradient i_{jk} with time at i_{av} = 18.0 is shown in Figure 4.39. The stage lasted for 4.5 hours. The applied hydraulic gradient i_{av} was essentially constant.

The local hydraulic gradient i_{45} was measured to diminish gradually and i_{56} increased likewise (Figure 4.39). This change in local hydraulic gradient indicated the onset of internal instability. This process is time dependent, as the change in hydraulic gradient is slow and continuous. The critical gradient is defined as the average gradient in the central portion of specimen yielding a value of $i_{46} = 17.1$.

The variation of local hydraulic gradient i_{jk} with time at $i_{av} = 31.0$ is shown in Figure 4.40. At 180s, i_{56} was measured to drop dramatically, and a companion increase was measured in i_{45} and i_{67}. At about 300s, i_{67} dropped quickly to the same level as i_{56}, and i_{45} gradually dropped to approach the i_{av}. The hydraulic gradient in the layer 5-6 immediately prior to the onset of heave failure is defined as the critical gradient yielding a value of $i_{56} = 34.0$.

4.3.5 Tests on gradation HF10

Three tests were conducted on a Fuller curve gradation, for which $(H/F)_{min} = 1.0$. The maximum particle size $D_{max} = 19$ mm (3/4 in). Vertical effective stress on the top surface of the respective specimens was σ'_{t0} = 15, 25 and 50 kPa. Despite taking considerable care to create a homogeneous specimen; unfortunately, segregation occurred during specimen reconstitution in all three cases. In spite of this, these tests can still provide some insight to the failure mechanism of heave. A summary of results for each test is presented in the following paragraphs.

4.3.5.1 HF10-15-U

Test HF10-15-U was performed with a top vertical effective stress σ'_{t0} = 15 kPa. The soil specimen was 31.0 cm long and the void ratio after consolidation was 0.24 (see Table 4.2). Minor mass loss was observed during specimen reconstitution.

Upward flow was imposed at i_{av} = 1.0 and sequentially increased to 2.0, 3.0, 4.0, 5.0, 6.0, 7.0, 8.0, 9.0, 10.0, 12.0, 14.0, 16.0, 19.0, 20.2 and then 22.3. Distribution of water head over the course of test is shown in Figure C.18: the relatively lower head loss in the lowermost layer between ports 6 and 7 at i_{av} = 1.0 is attributed to the mass loss during specimen reconstitution. The relatively lower head loss in the uppermost layer between ports 3 and 4 at i_{av} = 1.0 is probably attributed to segregation during specimen reconstitution. Negligible mass loss was observed and no axial displacement was measured with seepage flow to i_{av} = 12.0, and the seepage velocity increased proportionally with hydraulic gradient (Figure 4.41). Upon imposing a small increase in hydraulic gradient to i_{av} = 14.0, episodic movement of soil particles was observed in the lowermost layer between ports 5 and 6 (Figure E.26). In contrast to previous tests, an upward displacement of 0.1 mm was measured. No finer particle loss was observed from the top of specimen. Hydraulic conductivity in layer k_{56} increased from 3.3×10^{-4} to 5.1×10^{-4} cm/s as i_{av} increased from 12.0 to 14.0 (Figure D.18). A further increase in hydraulic gradient to i_{av} = 19.0, the whole specimen was lifted up, and an upward displacement of 0.5 mm was measured. Seepage velocity increased disproportionately. Test was continued to i_{av} = 22.3 and stopped. The increases in the slope of velocity (v) ~ gradient (i_{av}) and upward displacement is attributed to the onset of heave failure.

The variation of local hydraulic gradient i_{jk} with time since the beginning of the stage at i_{av} = 14.0 is shown in Figure 4.42. The applied hydraulic gradient i_{av} was essentially constant. At about 460s, the local hydraulic gradient i_{56} was measured to drop dramatically, and a companion increase occurred in i_{45}. This increase in hydraulic gradient is attributed to the system of head control, and also to the relative change in permeability of each layer ($\Delta k_{56} > \Delta k_{45}$), yielding a redistribution of hydraulic gradient among the layers (Figure D.18). The change in local hydraulic gradient indicated the onset of heave failure. The hydraulic gradient in the layer 5-6 immediately prior to the onset of heave failure is defined as the critical gradient yielding a value of i_{56} = 33.3 (Figure 4.42).

4.3.5.2 HF10-25-U

Test HF10-25-U was performed with a top vertical effective stress σ'_{t0} = 25 kPa. The soil specimen was 32.5 cm long and the void ratio after consolidation was 0.27 (see Table 4.2). Minor loss was observed during the specimen reconstitution.

Upward flow was imposed at i_{av} = 1.4 and sequentially increased to 2.3, 5.1, 8.0, 10.5, 12.4, 15.0 and then 16.0. Distribution of water head over the course of test was shown in Figure C.19: the relatively lower head loss in the lowermost layer between ports 5 and 7 at i_{av} = 1.4 is attributed to the mass loss during specimen reconstitution. Negligible mass loss was observed and no axial displacement was measured with seepage flow to i_{av} = 10.5, and the seepage velocity increased proportionally with hydraulic gradient (Figure 4.43). A further increase in hydraulic gradient to i_{av} = 12.4 and 15.0, an upward displacement of 0.1 and 0.6

mm were measured, the seepage velocity still increased proportionally with hydraulic gradient. Upon imposing an increase in hydraulic gradient to i_{av} = 16.0, episodic movement of soil particles was observed in the uppermost layer between ports 4 and 5 (Figure E.27), and a large upward displacement of 4.2 mm was measured, resulting in a strain of 1.3%. Seepage velocity increased disproportionately. Hydraulic conductivity k_{45} increased from $1.0x10^{-3}$ to $6.0x10^{-3}$ cm/s as i_{av} increased from 15.0 to 16.0 (Figure D.19). Increases in the slope of velocity (v) ~ gradient (i_{av}) and upward displacement are attributed to the onset of heave failure.

The variation of local hydraulic gradient i_{jk} with time since the beginning of the stage at i_{av} = 16.0 is shown in Figure 4.44. The applied hydraulic gradient i_{av} was essentially constant during this stage. At about 95s, i_{45} was measured to drop dramatically, and a companion increase occurred in i_{34}. This increase in hydraulic gradient is attributed to the system of head control, and also to the relative change in permeability of each layer ($\Delta k_{45} > \Delta k_{34}$) yielding a redistribution of hydraulic gradient among the layers (Figure D.19). This change in local hydraulic gradient indicated the onset of heave failure. The hydraulic gradient in the layer 4-5 immediately prior to the onset of heave failure is defined as the critical gradient yielding a value of i_{45} = 35.3 (Figure 4.44).

4.3.5.3 HF10-50-U

Test HF10-50-U was performed with a top vertical effective stress σ'_{t0} = 50 kPa. The soil specimen was 32.5 cm long and the void ratio after consolidation was 0.26 (see Table 4.2). Minor mass loss was observed during specimen reconstitution.

Upward flow was imposed at i_{av} = 1.5 and sequentially increased to 5.2, 10.5, 14.5, 18.6, 22.5, 24.5, and then 26.3. Distribution of water head over the course of test was shown in Figure C.20: the relatively lower head loss in the lowermost layer between ports 5 and 7 at i_{av} = 1.5 is attributed to the mass loss and segregation during specimen reconstitution. Negligible mass loss was observed and no axial displacement was measured with seepage flow to i_{av} = 14.5, and the seepage velocity increased proportionally with hydraulic gradient (Figure 4.45). A further increase in hydraulic gradient to i_{av} = 18.6 ~ 24.5, an upward displacement of 0.3 ~ 0.8 mm were measured, the seepage velocity still increased proportionally with hydraulic gradient. Upon imposing an increase in hydraulic gradient to i_{av} = 26.3, episodic movement of soil particles was observed in the uppermost layer between ports 4 and 5 (Figure E.28), and a large upward displacement of 4.0 mm was measured, resulting in a strain of 1.2%. Hydraulic conductivity k_{45} increased from 1.8×10^{-4} to 1.4×10^{-2} cm/s as i_{av} increased from 24.5 to 26.3 (Figure D.20). Increase in the slope of velocity (v) ~ gradient (i_{av}) curve and upward displacement are attributed to the onset of heave failure.

The variation of local hydraulic gradient i_{jk} with time since the beginning of the stage at i_{av} = 26.3 is shown in Figure 4.46. The applied hydraulic gradient i_{av} was essentially constant during this stage. At about 200s, i_{45} was measured to drop dramatically, and a companion increase occurred in i_{34}. This increase in hydraulic gradient is attributed to the system of head control, and also to the relative change in permeability of each layer ($\Delta k_{45} > \Delta k_{34}$) yielding a redistribution of hydraulic gradient among these layers (Figure D.20). This change in local hydraulic gradient indicated the onset of heave failure. The hydraulic gradient in the layer 4-

5 immediately prior to the onset of heave failure is defined as the critical gradient yielding a value of $i_{45} = 58.6$ (Figure 4.46).

4.4 Summary

A total of 20 tests have been reported on 6 gradations in the main program. Specifically, 9 tests were performed in the small permeameter and 11 tests in the large permeameter. Altogether, 11 tests were conducted on glass beads and 9 tests on soils. And 10 tests were conducted in downward flow and 10 tests in upward flow.

Seepage failure is described from visual observations and instrument measurements. The onset of seepage failure was defined from visual observations, slope change in the $v \sim i_{av}$ curve and variations in local hydraulic gradient with time. Changes in other variables are also used to characterize the seepage response, such as the axial displacement and mass passing of finer particles, and thereby distinguish between internal instability and heave phenomena. Based on these detailed test-by-test descriptions, a summary of these tests is presented in Chapter 5.

Table 4.1 Summary of test results in the small permeameter

Code	After reconstitution				Onset of internal instability					Final stage		
	Length L (cm)	Dry unit weight γ_d, (g/cm^3)	Void ratio e	Mass loss (%)	Displace-ment (mm)	Mass loss (%)	Average gradient i_{av}	Local gradient i_{ik}	Initiation zone	Displace-ment (mm)	Mass loss (%)	Average gradient i_{av}
FR3-25-D*	10.2	1.83	0.37	0.22	-	-	-	-	-	-	0.16	14.2
FR8-25-D0	9.2	1.82	0.37	10.6	2.5	6.9	3.2	3.8	3-5	-	-	-
FR8-25-D1	9.2	1.83	0.37	11.1	1.0	4.0	3.1	2 ~ 4.4	3-5	-	-	-
FR8-25-D2	9.2	1.83	0.37	10.8	1.7	4.4	3.2	3.0	3-5	-	-	-
FR8-50-D	9.3	1.82	0.37	11.1	0.7	2.9	3.3	4.5	3-5	-	-	-
FR8-100-D	9.2	1.84	0.36	8.6	0	1.0	2.7	5.0	3-4	4.3	12.2	4.1
FR8-200-D	9.0	1.87	0.33	8.5	3.7	11.5	3.5	6.6	3-4	-	-	-
FR7-25-D	10.3	1.87	0.34	3.5	0.6	0.2	7.3	8.7	1-3	3.5	6.5	9.0
FR7-50-D	10.2	1.88	0.33	4.3	1.0	4.8	9.5	16.5	1-3	-	-	-
FR7-100-D	10.8	1.90	0.32	3.7	1.8	6.5	15.5	27.1	3-4	-	-	-

Note: FR3-25-D is a commission test.

Table 4.2 Summary of test results in the large permeameter

Code	After reconstitution				Onset of internal instability					Heave failure / Final stage				
	Length L (cm)	Dry unit weight γ_d (g/cm^3)	Void ratio e	Mass loss (%)	Displace-ment (mm)	Mass loss (%)	Average gradient i_{av}	Local gradient i_{jk}	Initiation zone	Displace-ment (mm)	Mass loss (%)	Average gradient i_{av}	Local gradient i_{jk}	Initiation zone
FR7-150-D	31.0	1.90	0.32	Yes	1.9	Yes	4.0	5.0	3-5	-	-	-	-	-
FR7-150-U	31.0	1.90	0.32	Minor	9.0	Yes	2.5	3.0	5-6	-	-	-	-	-
HF01-0-U	30.0	2.00	0.32	Minor	-	Yes	0.22	0.16	4-6	-	-	-	-	-
HF03-25-U	30.0	2.00	0.31	Minor	0.7	Yes	6.6	6.9	4-5	0.7	Yes	7.5	-	-
HF03-50-U	28.7	2.05	0.29	Minor	0.4	Yes	14.0	12.9	4-5	0.9	Yes	19.6	-	-
HF05-25-U1	31.0	2.00	0.32	Yes	0	No	6.5	9.0	4-6	-23.5	No	16.8	15.3	5-6
HF05-25-U2	31.0	2.00	0.32	Yes	0	No	4.1	5.6	4-6	0	No	9.9	-	-
HF05-50-U	30.9	2.00	0.32	NA	0	No	15.0	17.1	4-6	-26.7	No	31.0	34.0	5-6
HF10-15-U	31.0	2.13	0.24	Yes	-	-	-	-	-	-0.1	-	14	33.3	5-6
HF10-25-U	32.5	2.09	0.27	Yes	-	-	-	-	-	-4.2	-	16	35.3	4-5
HF10-50-U	32.5	2.10	0.26	Yes	-	-	-	-	-	-4.0	-	26.3	58.6	4-5

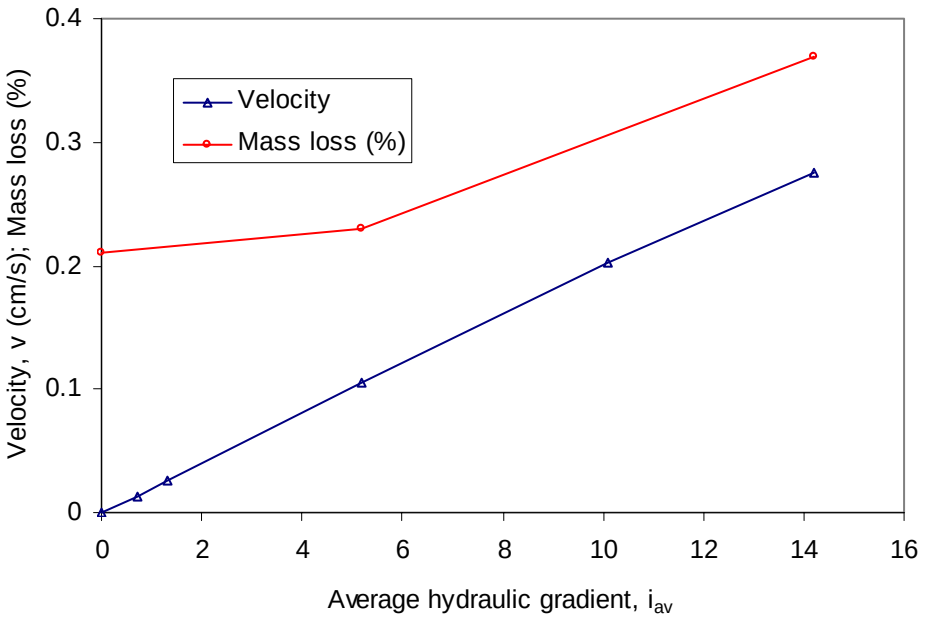

Figure 4.1 Variation of velocity/mass loss with hydraulic gradient in test FR3-25-D

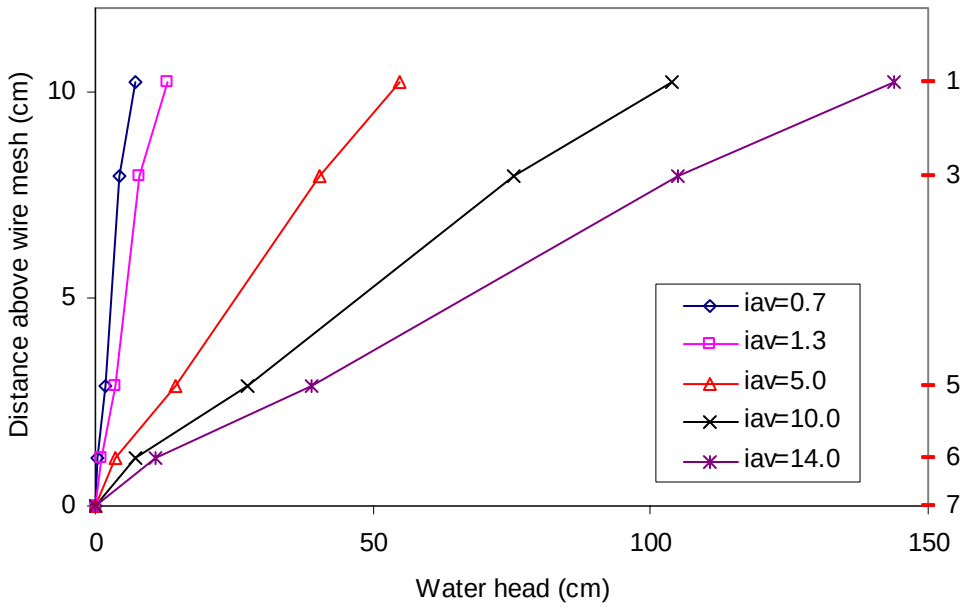

Figure 4.2 Water head distribution in test FR3-25-D

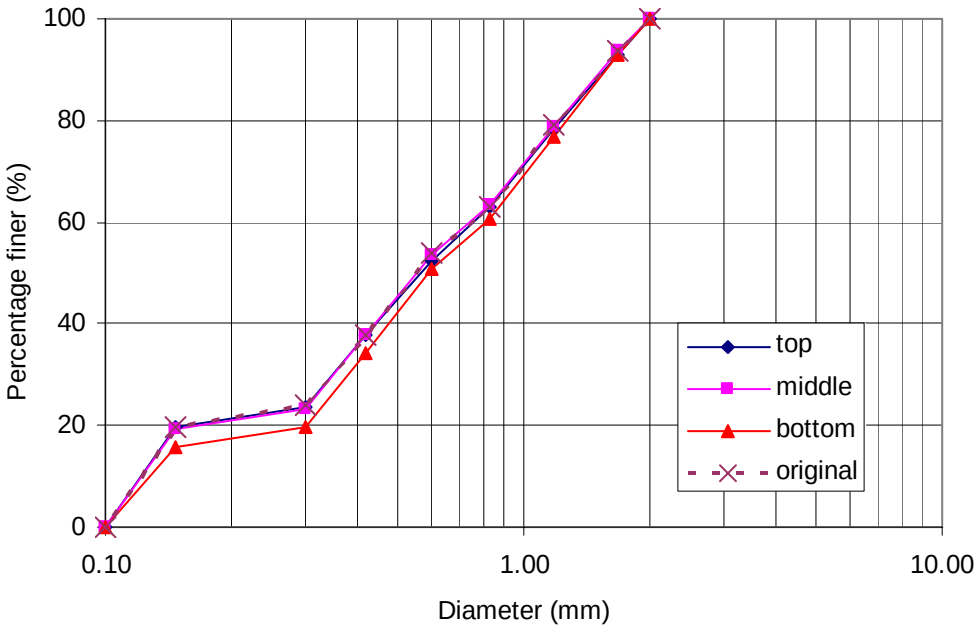

Figure 4.3 Grain size distribution after the test in test FR3-25-D

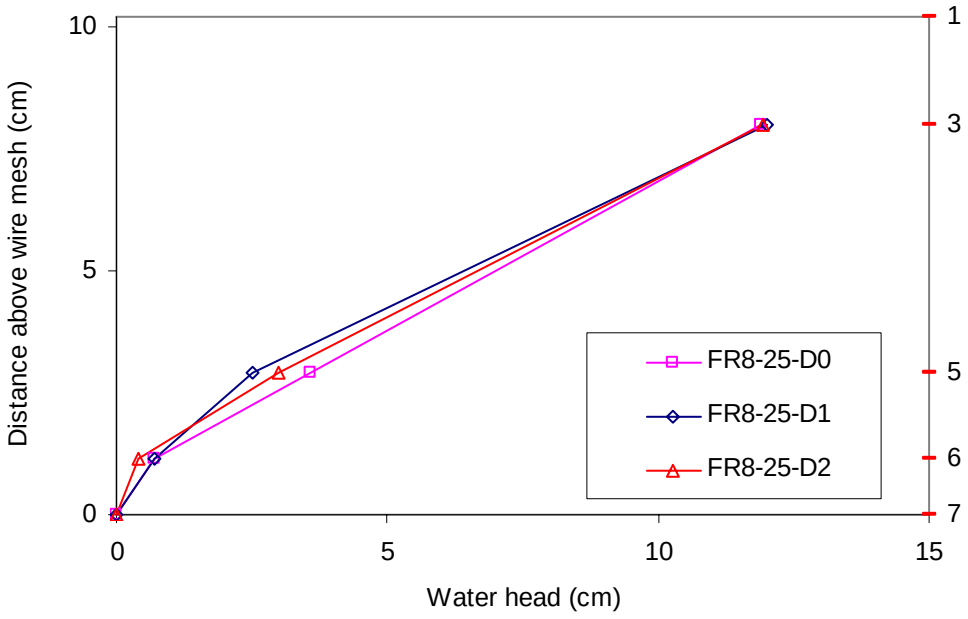

Figure 4.4 Initial water head distribution in the tests on gradation FR8 (i_{av} = 1.3)

(note: data for port #1 unavailable)

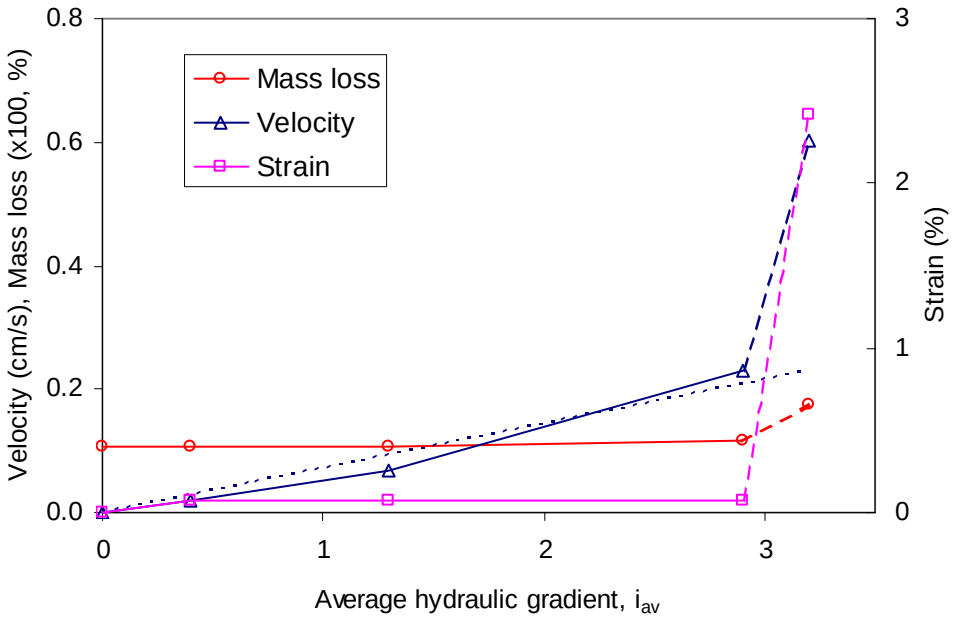

Figure 4.5 Variation of velocity/mass loss/axial strain with hydraulic gradient in test FR8-25-D0

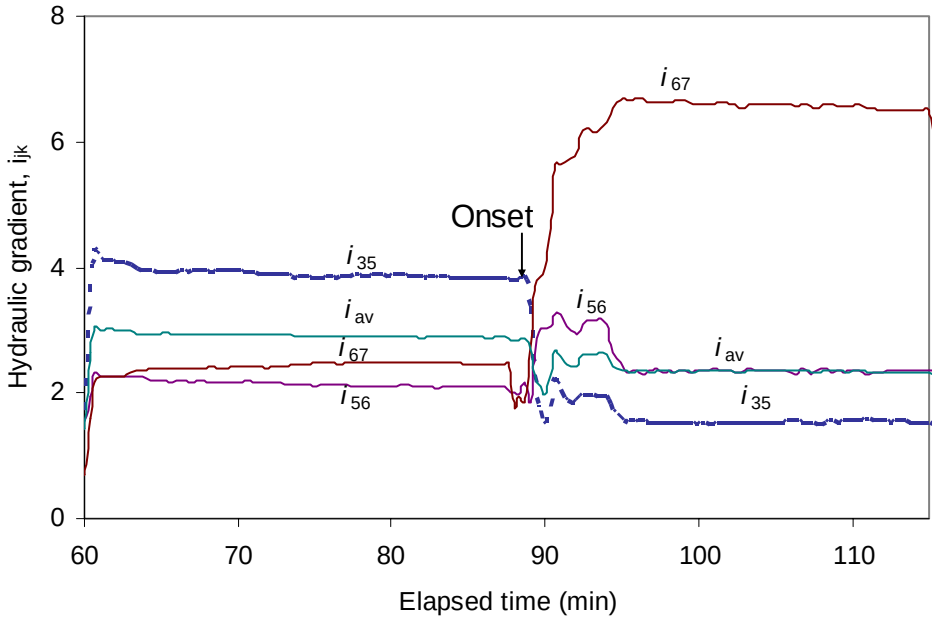

Figure 4.6 Onset of instability in test FR8-25-D0 (i_{av} = 2.9 and 3.2)

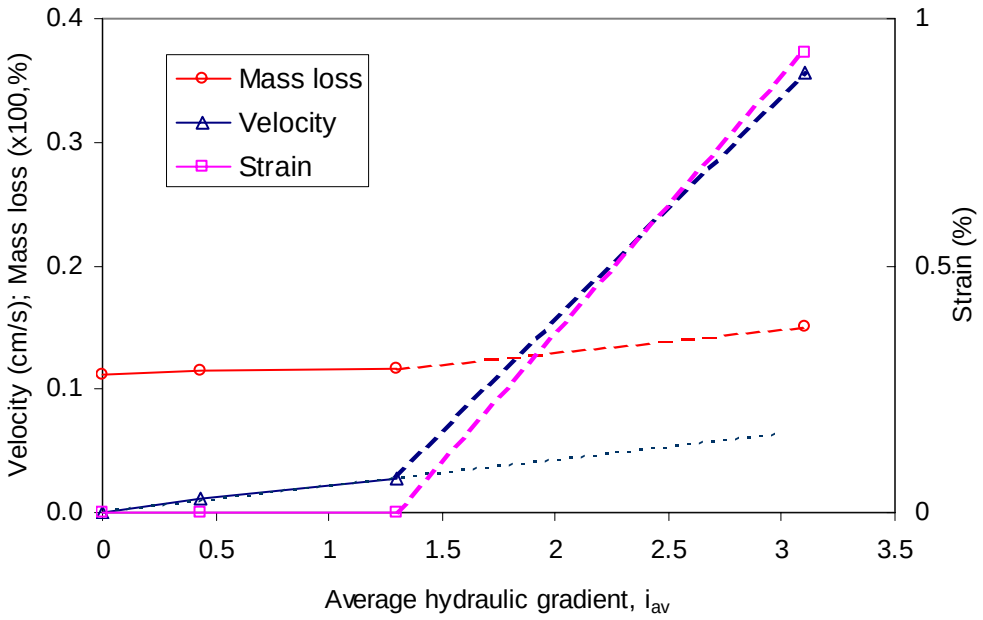

Figure 4.7 Variation of velocity/mass loss/strain with hydraulic gradient in test FR8-25-D1

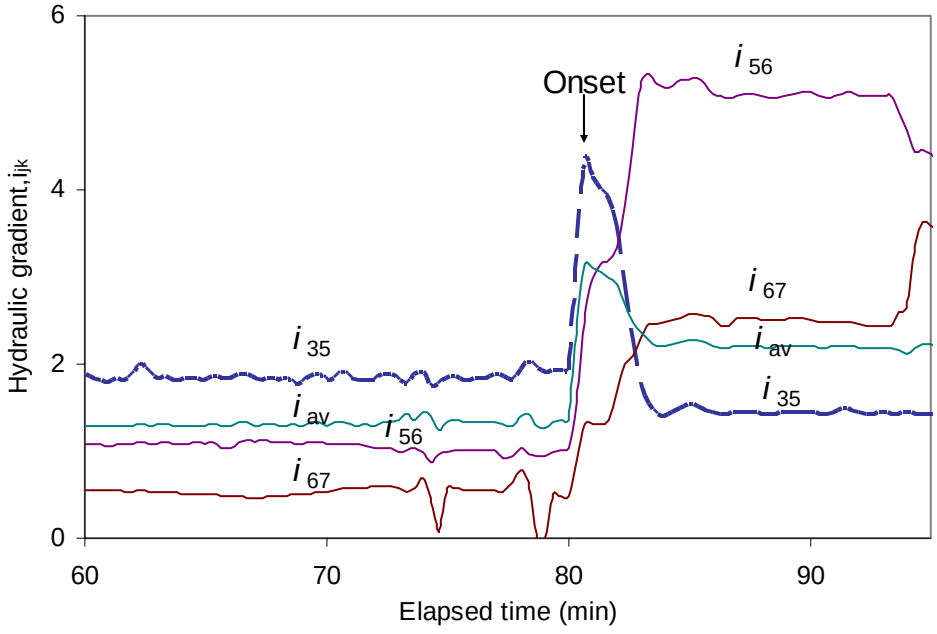

Figure 4.8 Onset of instability in test FR8-25-D1 (i_{av} = 1.3 and 3.1)

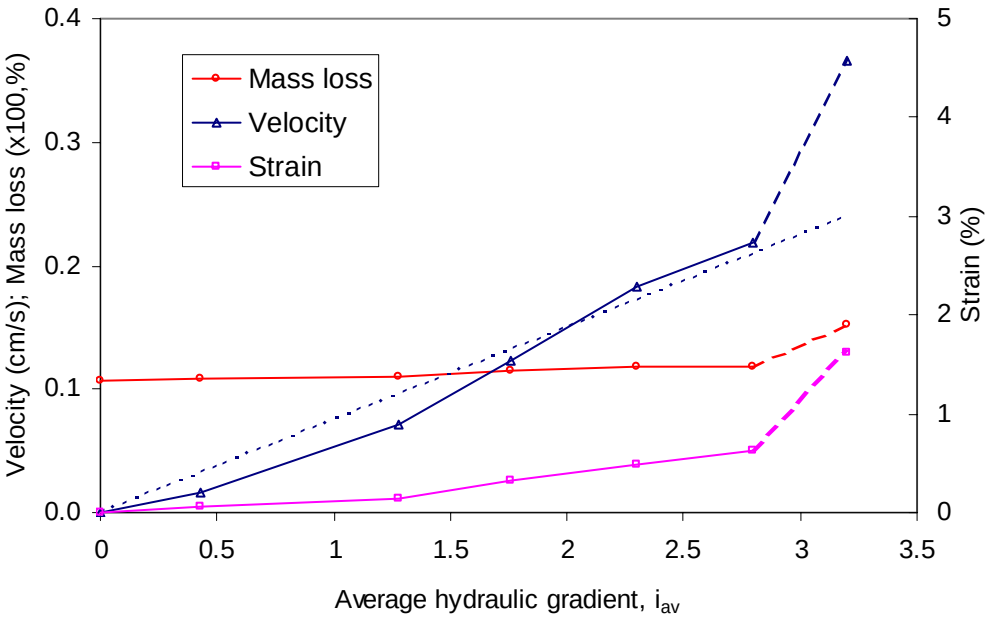

Figure 4.9 Variation of velocity/mass loss/strain with hydraulic gradient in test FR8-25-D2

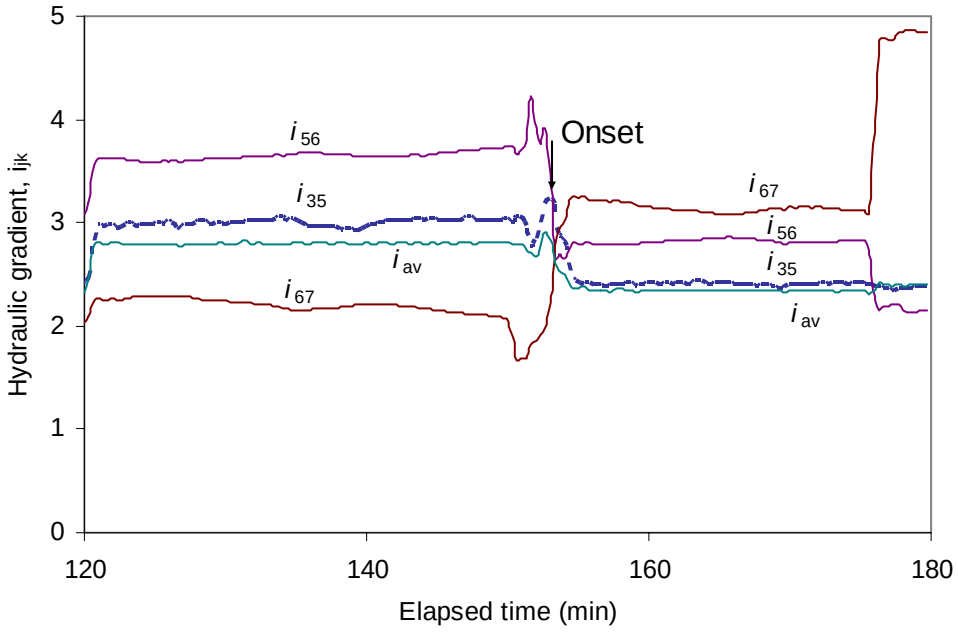

Figure 4.10 Onset of instability in test FR8-25-D2 (i_{av} = 2.8 and 3.2)

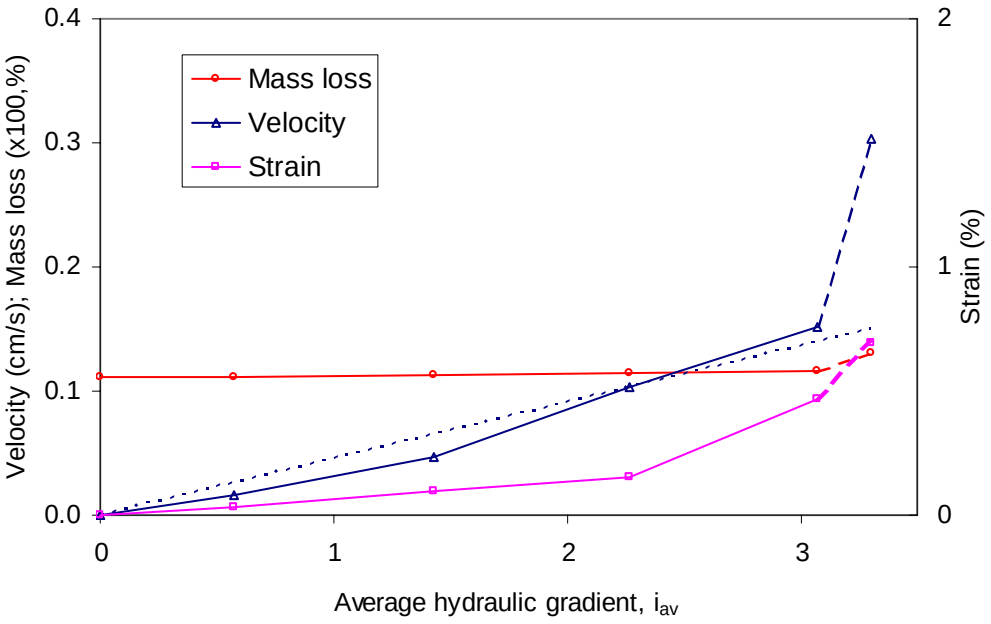

Figure 4.11 Variation of velocity/mass loss/strain with hydraulic gradient in test FR8-50-D

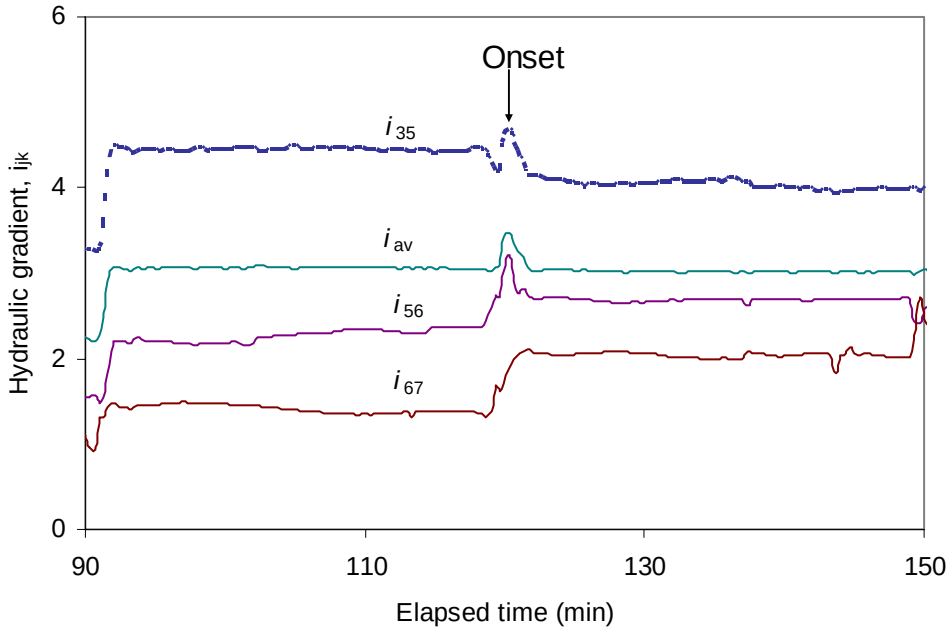

Figure 4.12 Onset of instability in test FR8-50-D (i_{av} = 3.1 and 3.3)

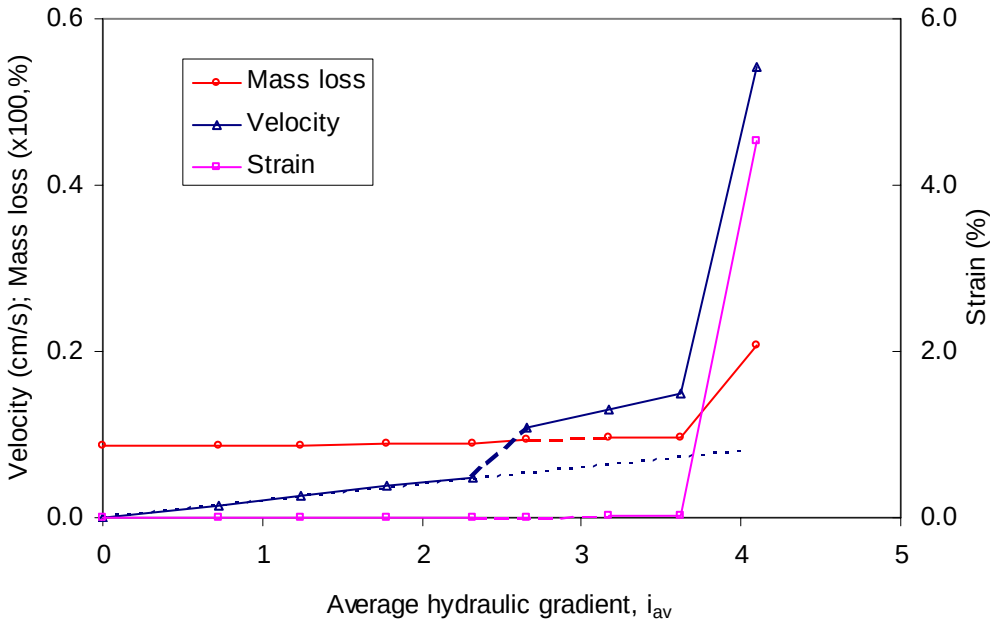

Figure 4.13 Variation of velocity/mass loss/strain with hydraulic gradient in test FR8-100-D

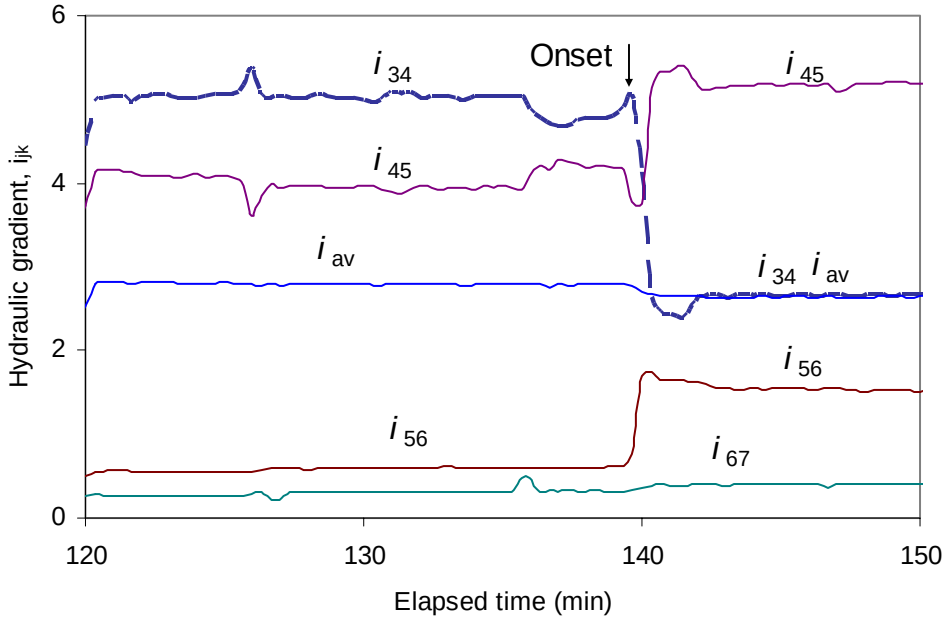

Figure 4.14 Onset of instability in test FR8-100-D (i_{av} = 2.7)

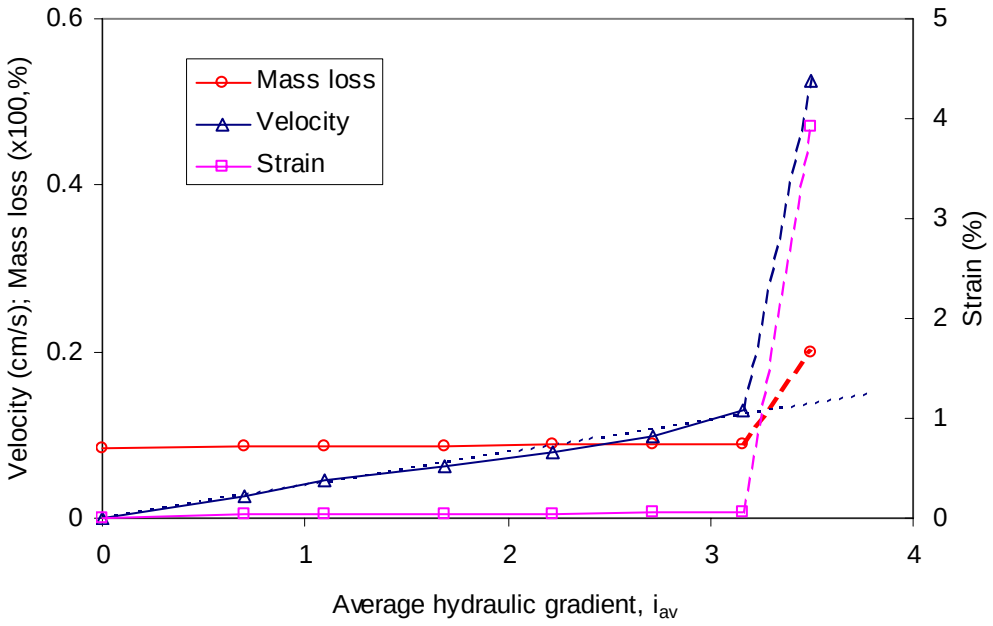

Figure 4.15 Variation of velocity/mass loss/strain with hydraulic gradient in test FR8-200-D

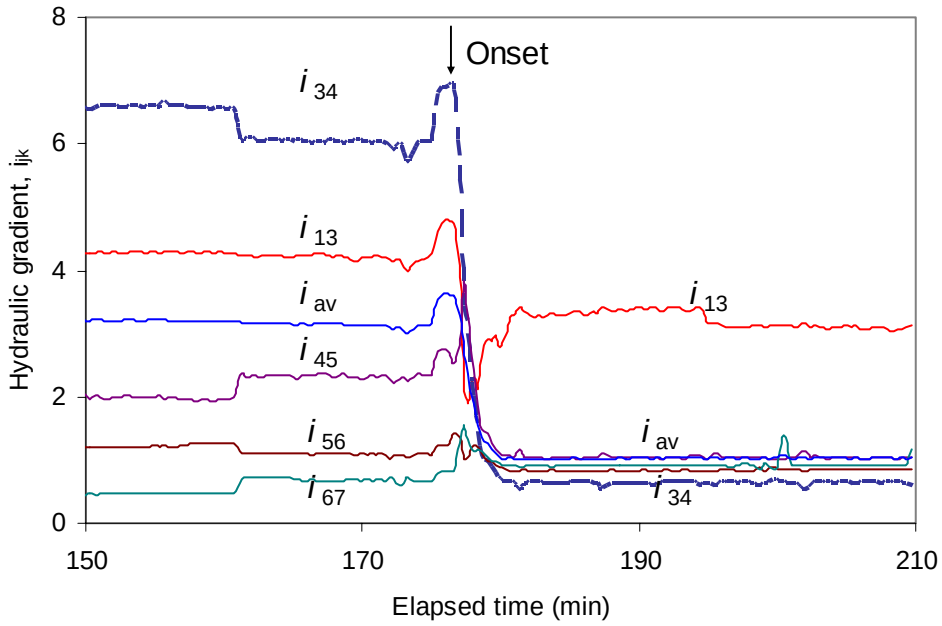

Figure 4.16 Onset of instability in test FR8-200-D (i_{av} = 3.2 and 3.5)

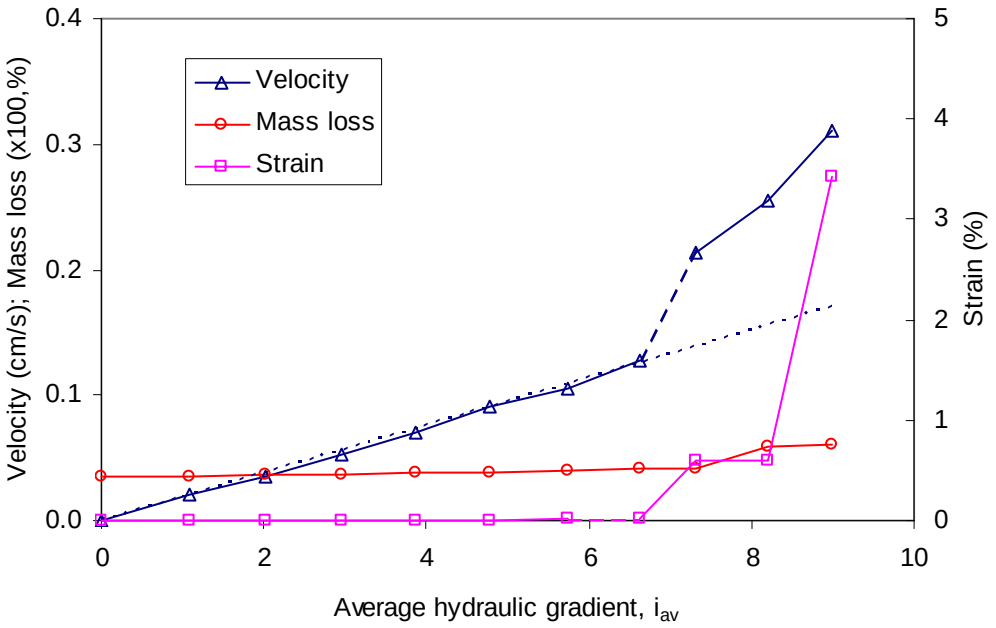

Figure 4.17 Variation of velocity/mass loss/strain with hydraulic gradient in test FR7-25-D

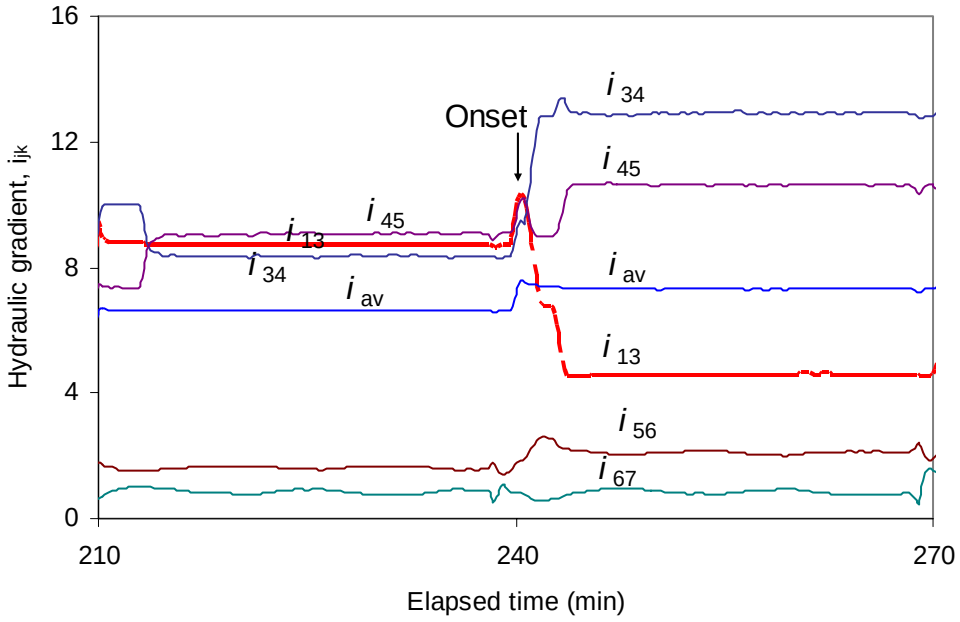

Figure 4.18 Onset of instability in test FR7-25-D (i_{av} = 6.6 and 7.3)

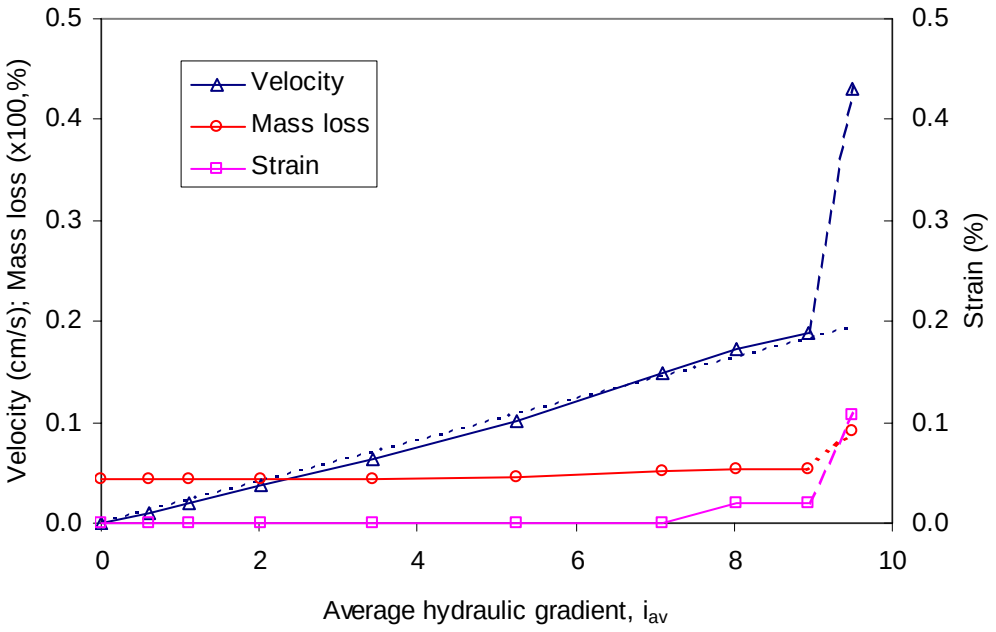

Figure 4.19 Variation of velocity/mass loss/strain with hydraulic gradient in test FR7-50-D

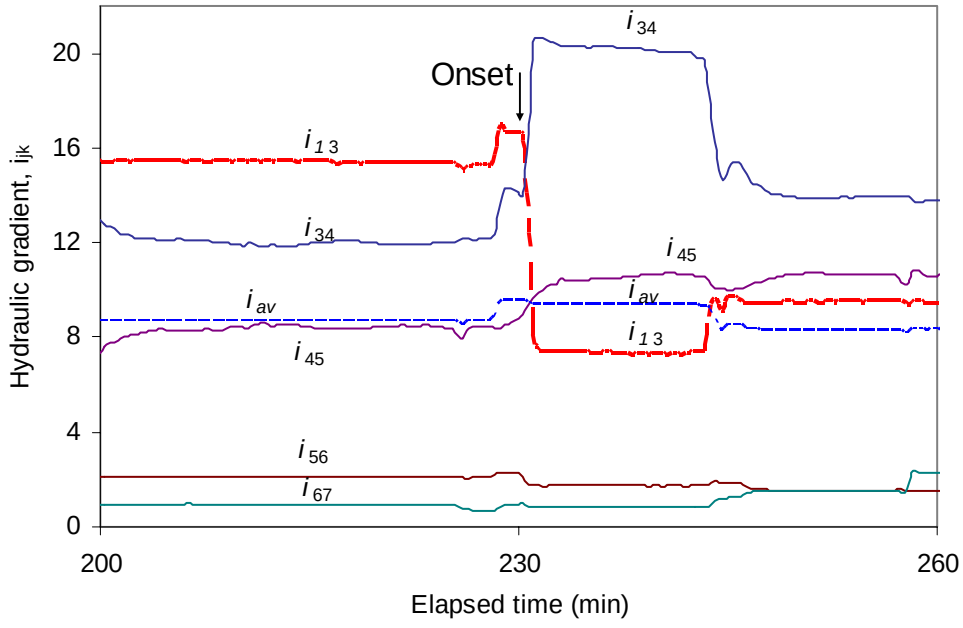

Figure 4.20 Onset of instability in test FR7-50-D (i_{av} = 8.9 and 9.5)

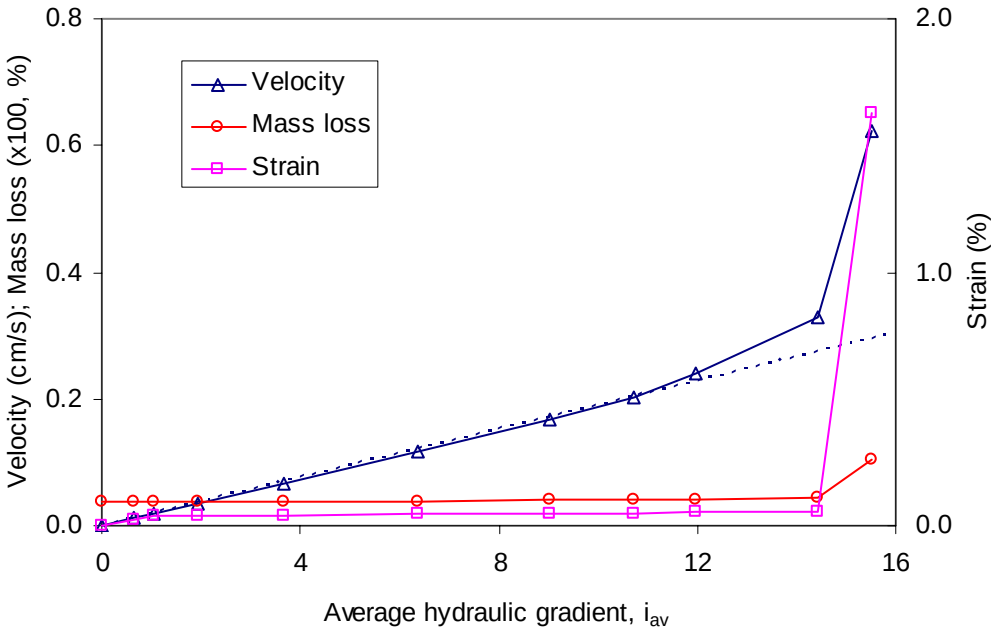

Figure 4.21Variation of velocity/mass loss/strain with hydraulic gradient in test FR7-100-D

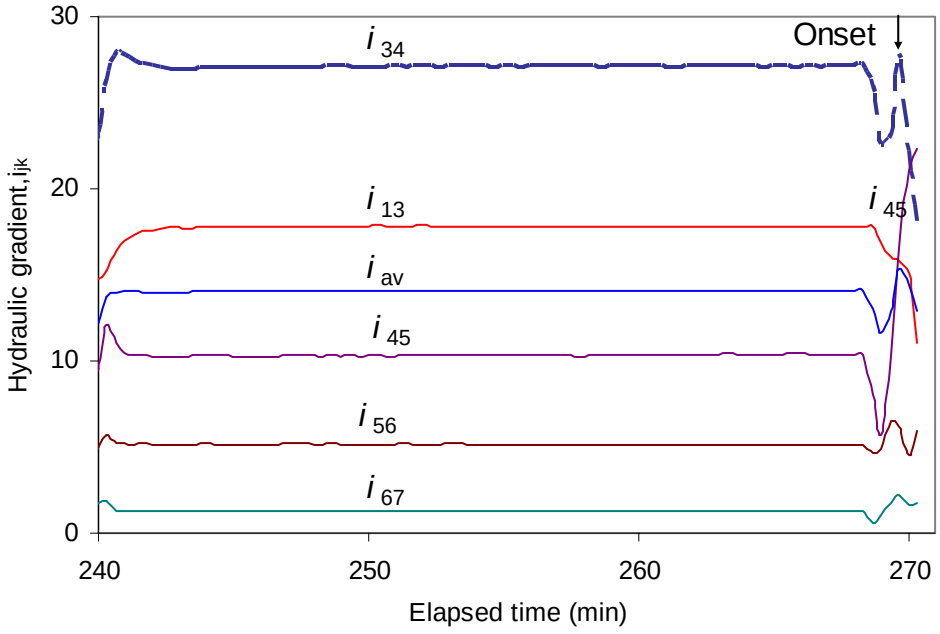

Figure 4.22 Onset of instability in test FR7-100-D (i_{av} = 14.4 and 15.5)

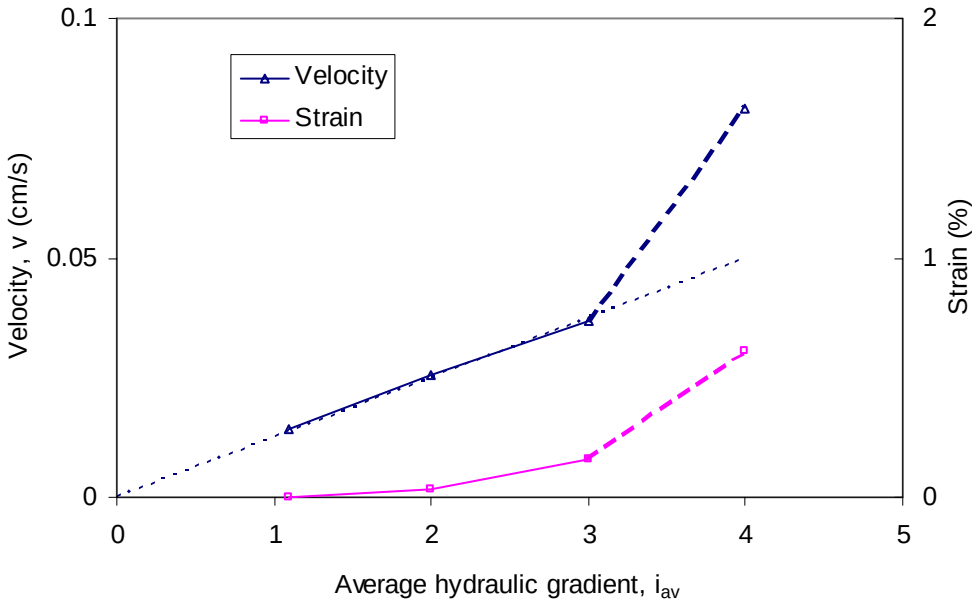

Figure 4.23 Variation of velocity/strain with hydraulic gradient in test FR7-150-D

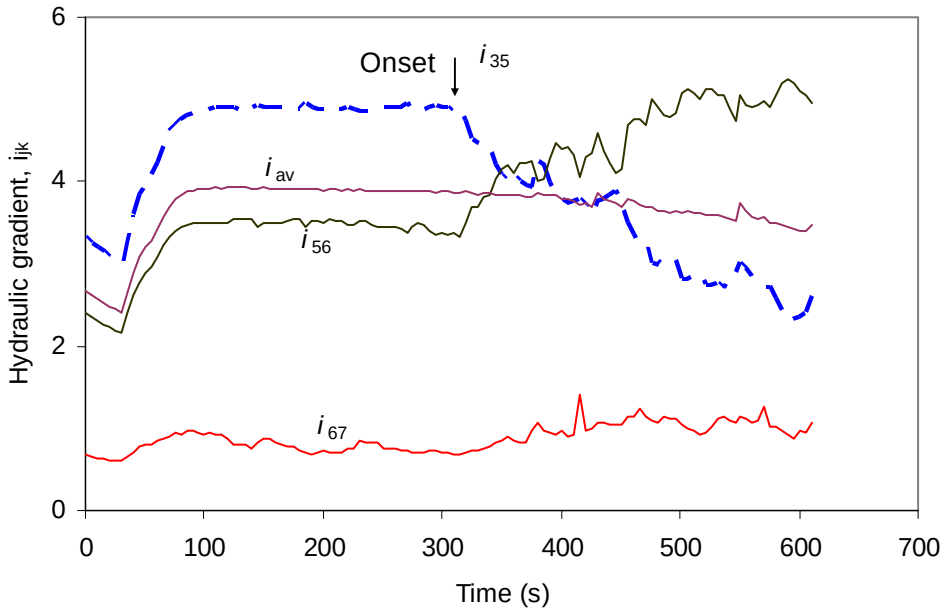

Figure 4.24 Onset of instability in test FR7-150-D (i_{av} = 4.0)

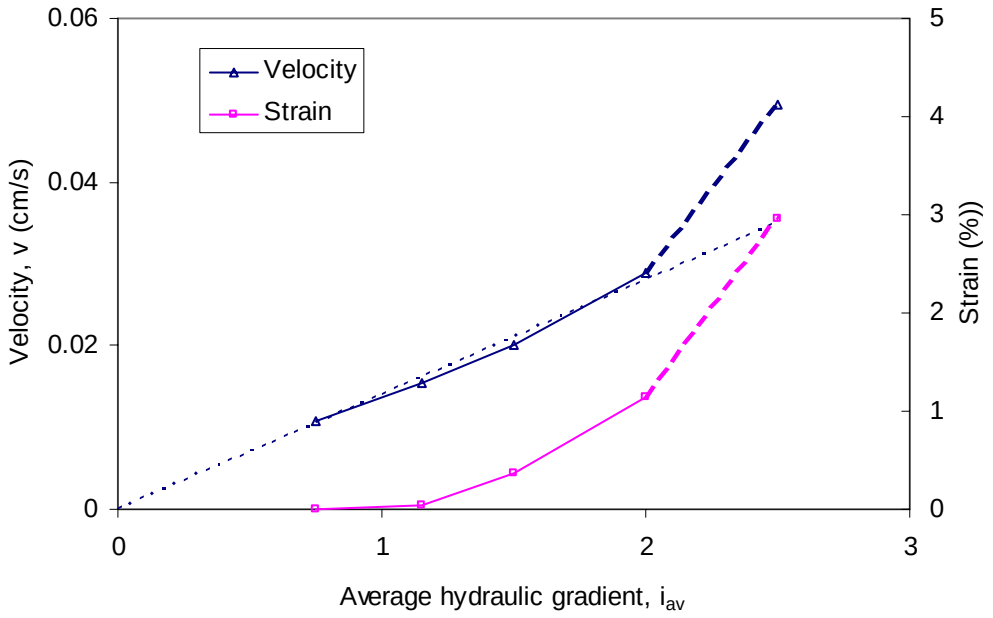

Figure 4.25 Variation of velocity/strain with hydraulic gradient in test FR7-150-U

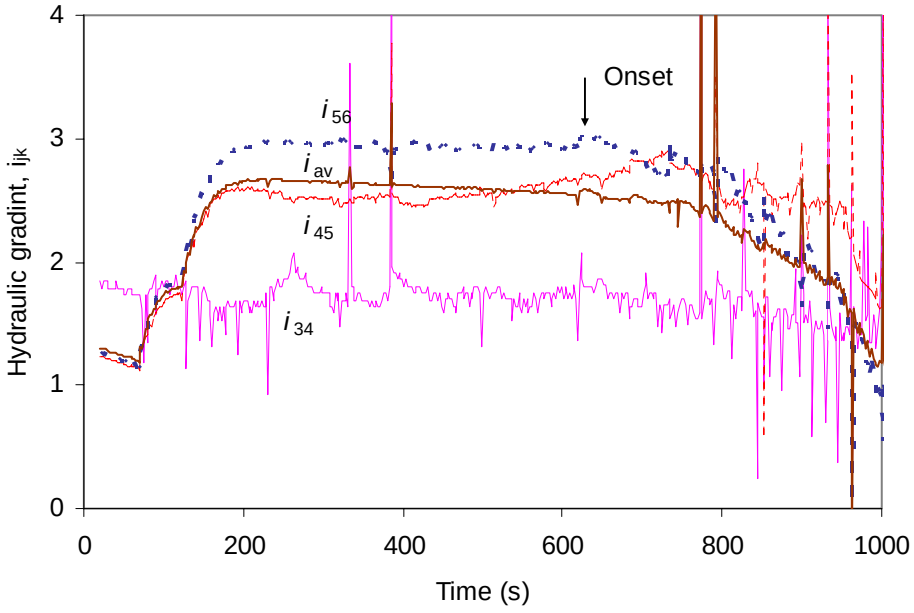

Figure 4.26 Onset of instability in test FR7-150-U (i_{av} = 2.5)

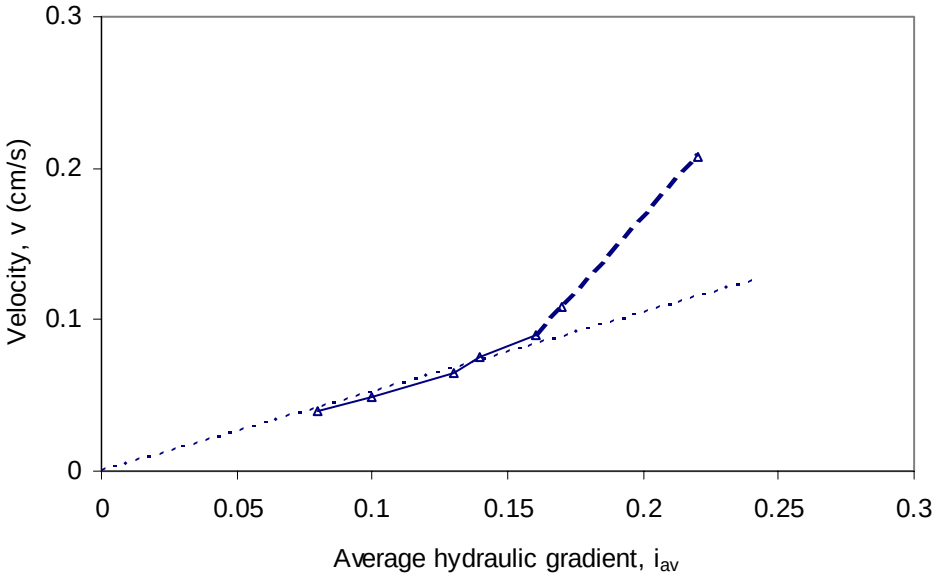

Figure 4.27 Variation of velocity with hydraulic gradient in test HF01-0-U

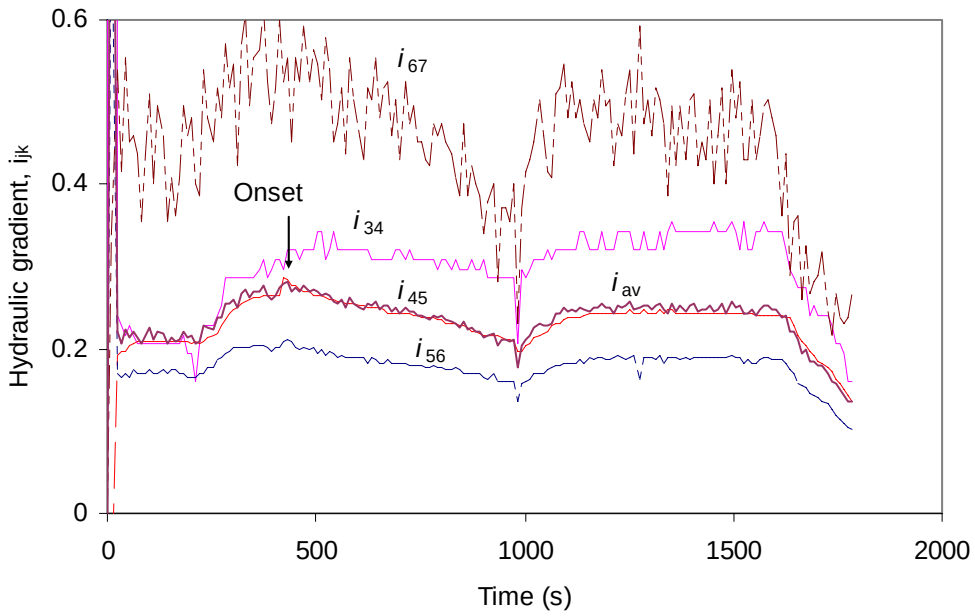

Figure 4.28 Onset of instability in test HF01-0-U (i_{av} =0.22)

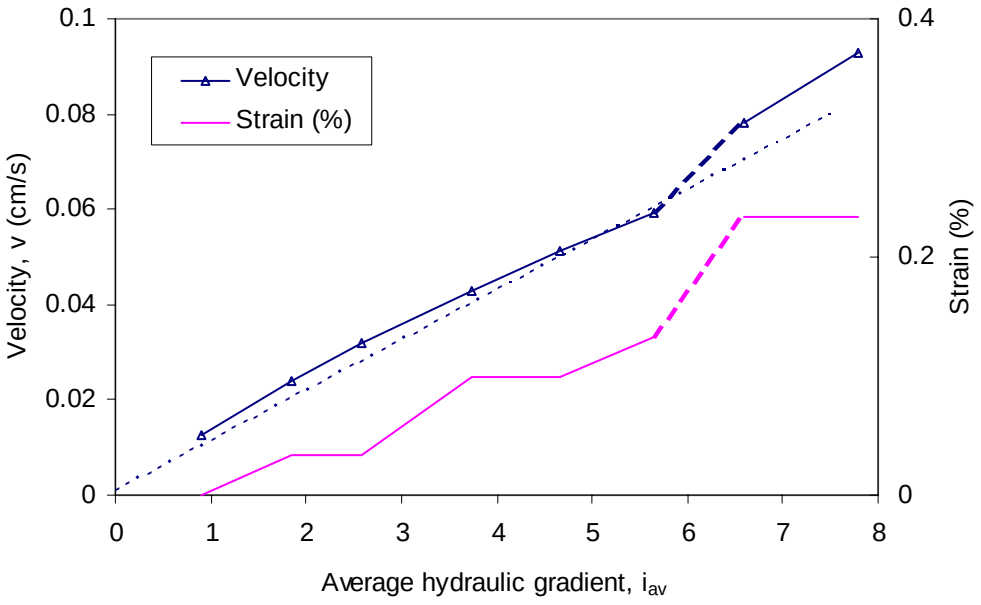

Figure 4.29 Variation of velocity/strain wtih hydraulic gradient in test HF03-25-U

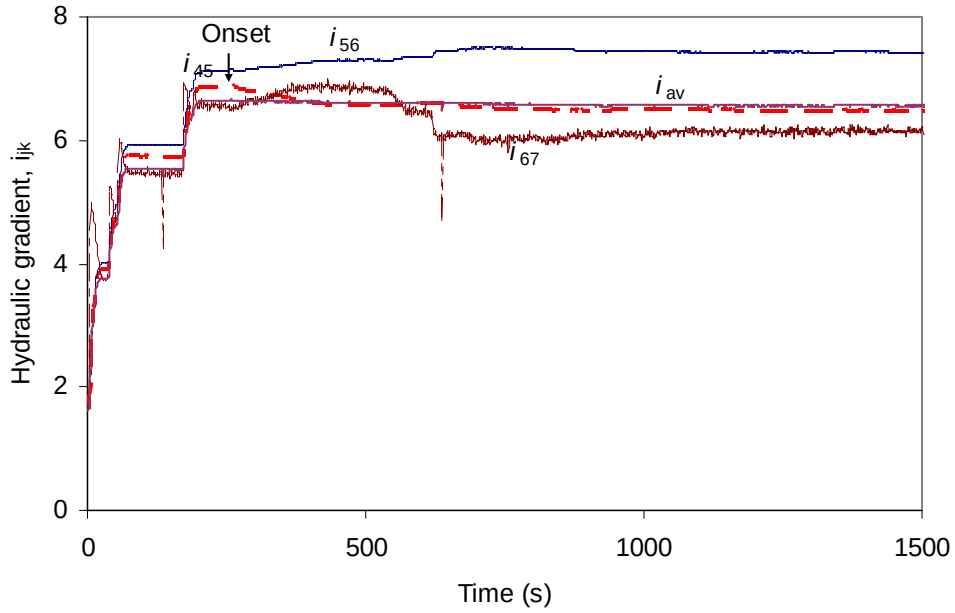

Figure 4.30 Onset of instability in test HF03-25-U (i_{av} = 6.6)

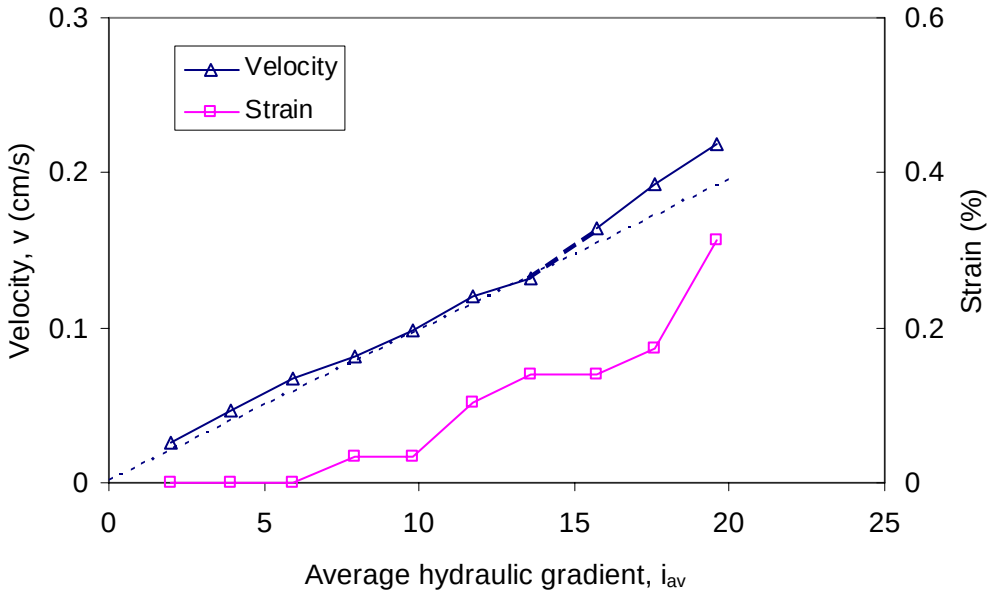

Figure 4.31Variation of velocity/strain with hydraulic gradient in test HF03-50-U

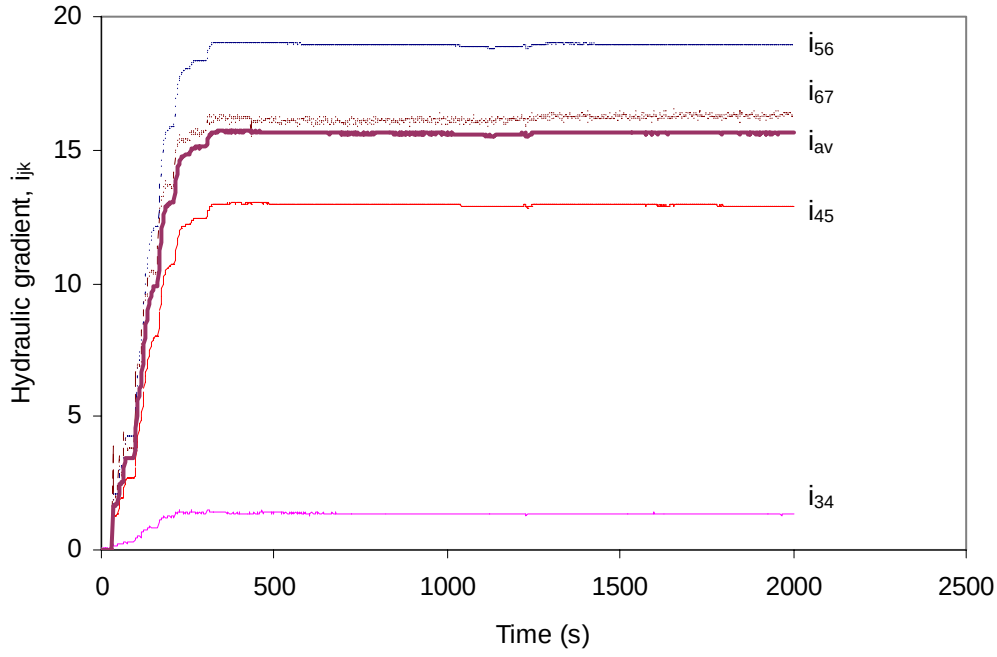

Figure 4.32 Onset of instability in test HF03-50-U (i_{av} = 15.7)

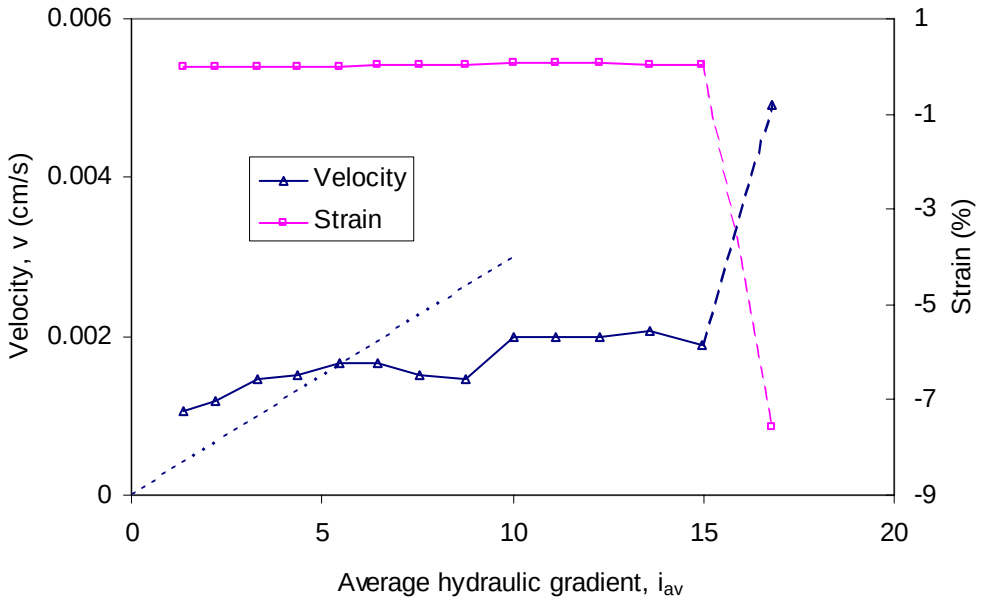

Figure 4.33 Variation of velocity/strain with hydraulic gradient in test HF05-25-U1

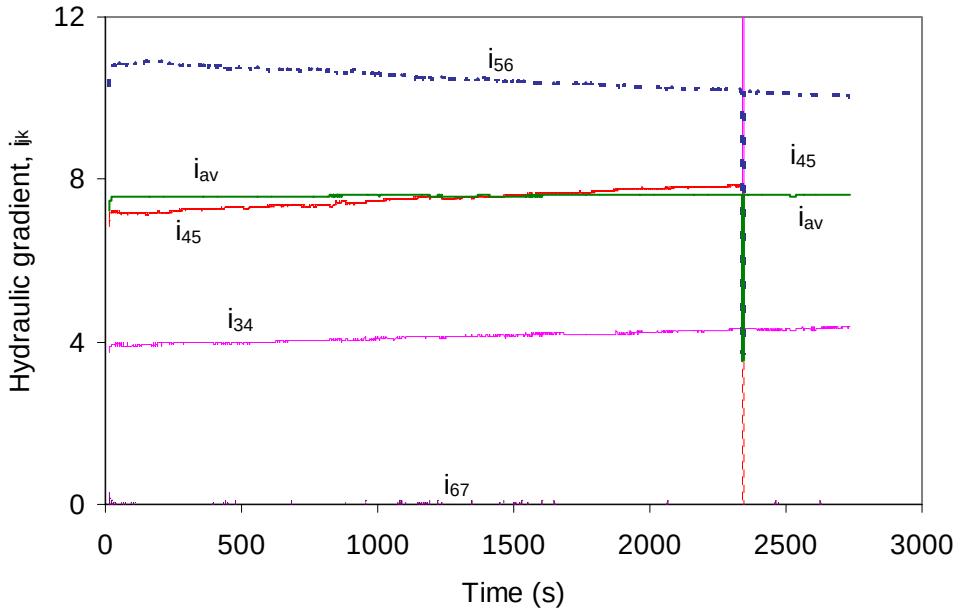

Figure 4.34 Onset of instability in test HF05-25-U1 (i_{av} = 7.6)

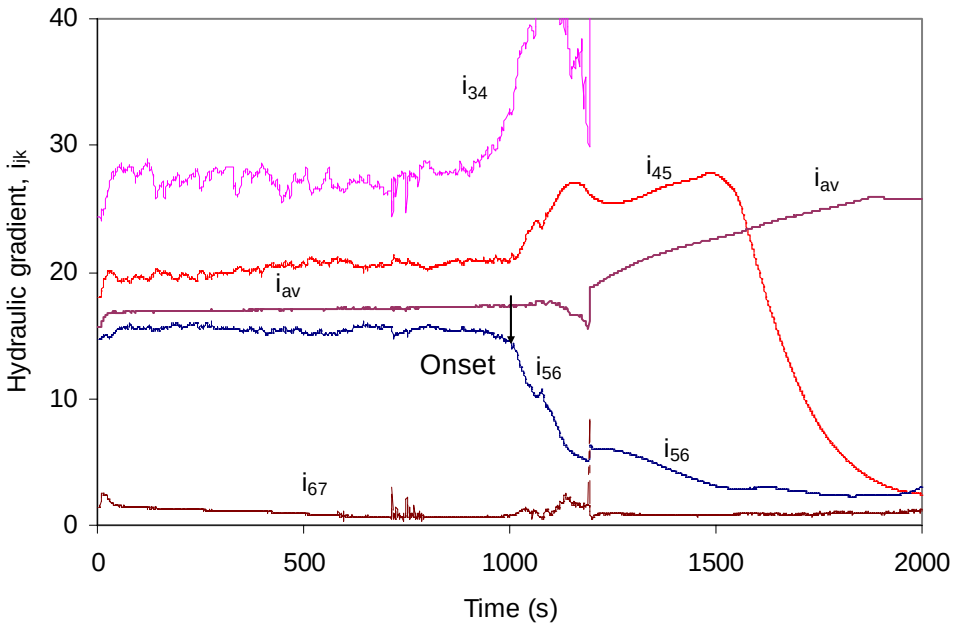

Figure 4.35 Onset of heave failure in test HF05-25-U1 (i_{av} = 16.8)

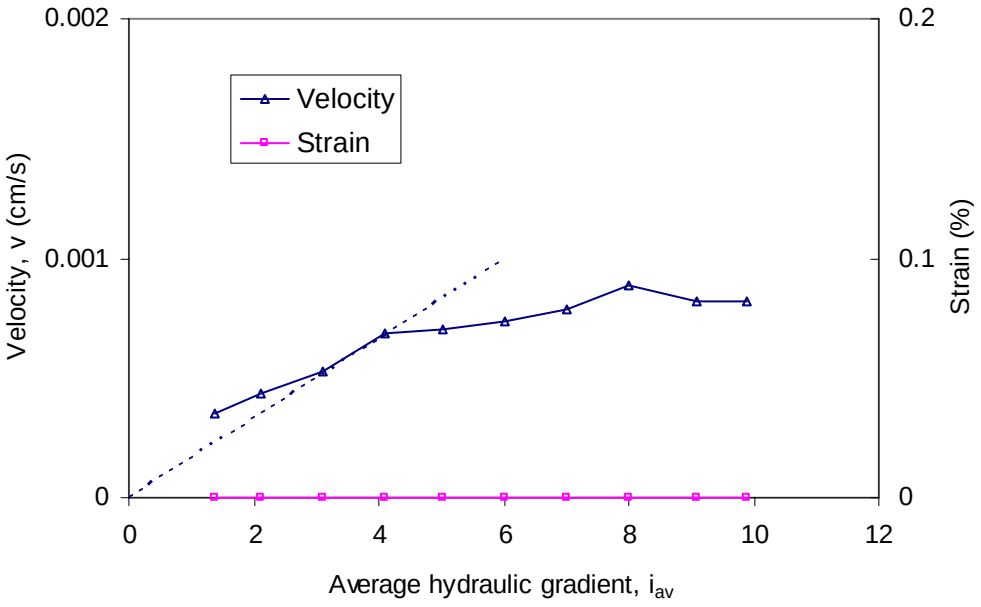

Figure 4.36 Variation of velocity/strain with hydraulic gradient in test HF05-25-U2

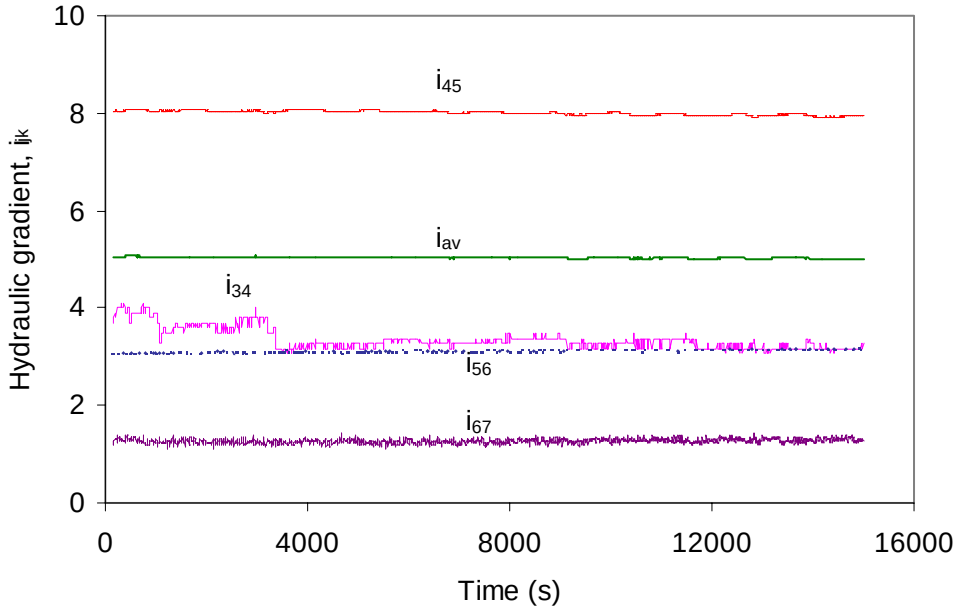

Figure 4.37 Onset of instability in test HF05-25-U2 (i_{av} = 5.0)

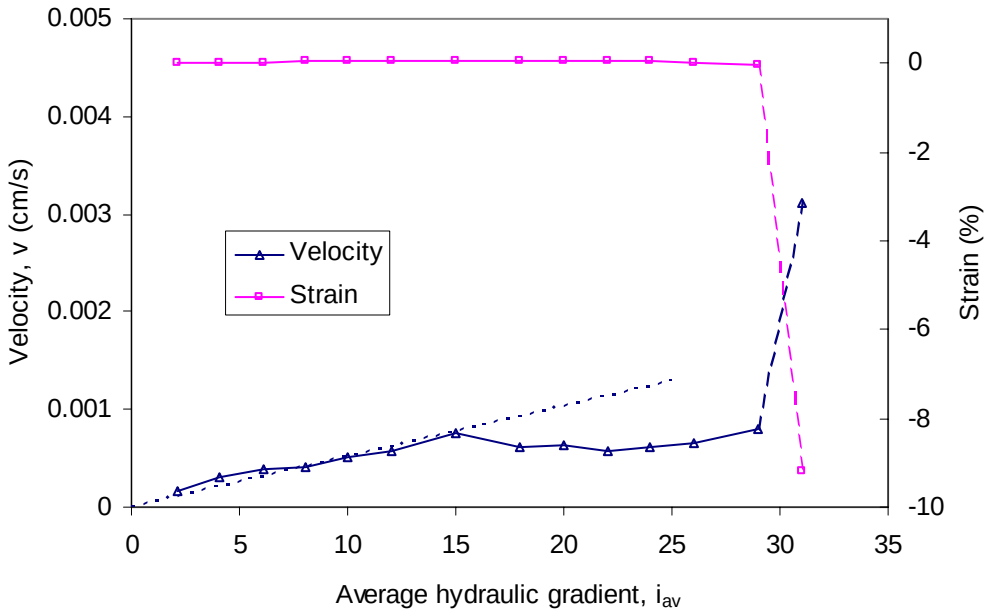

Figure 4.38 Variation of velocity/strain with hydraulic gradient in rest HF05-50-U

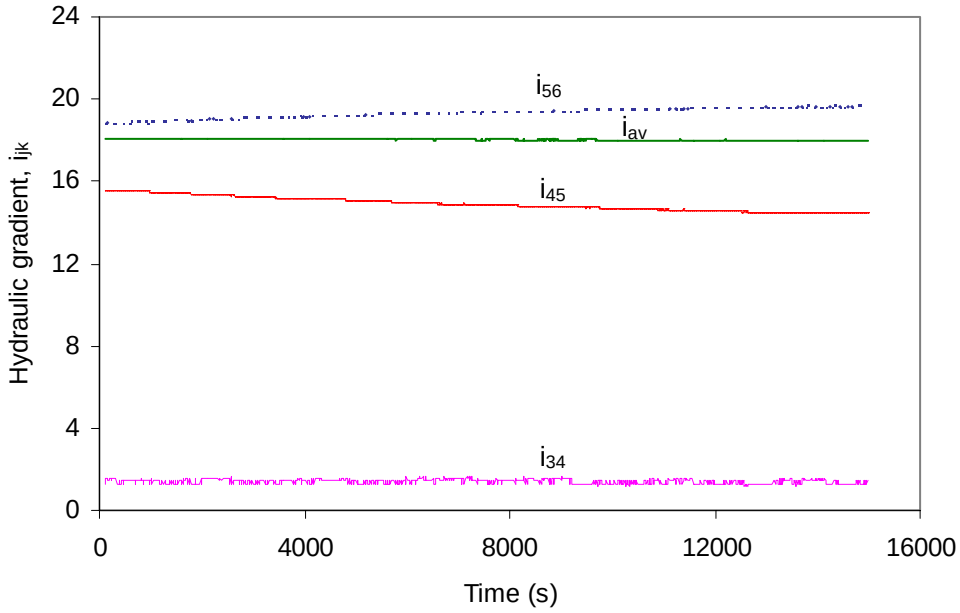

Figure 4.39 Onset of instability in test HF05-50-U (i_{av} = 18.0)

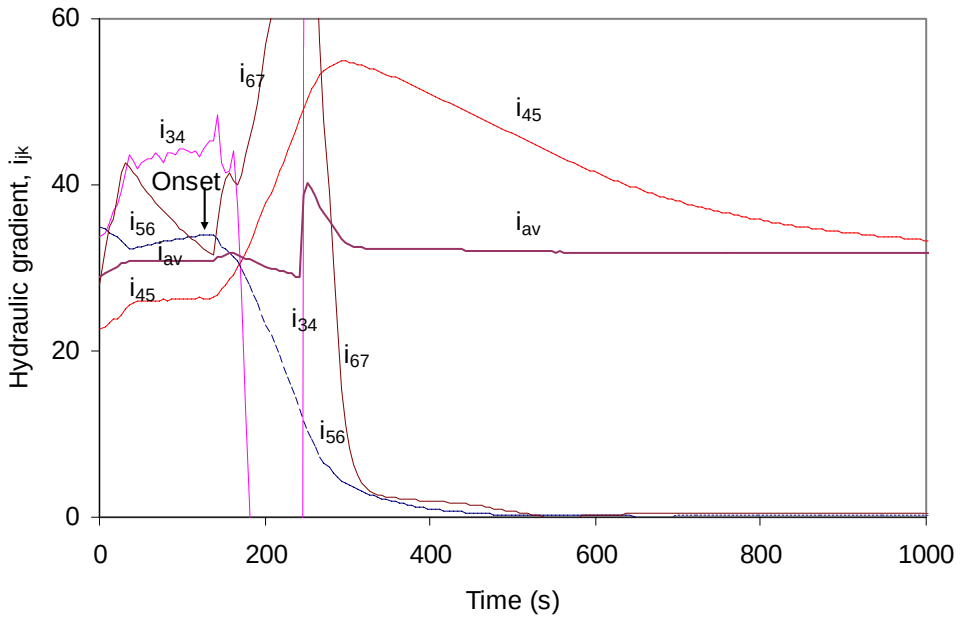

Figure 4.40 Onset of heave failure in test HF05-50-U (i_{av}=31.0)

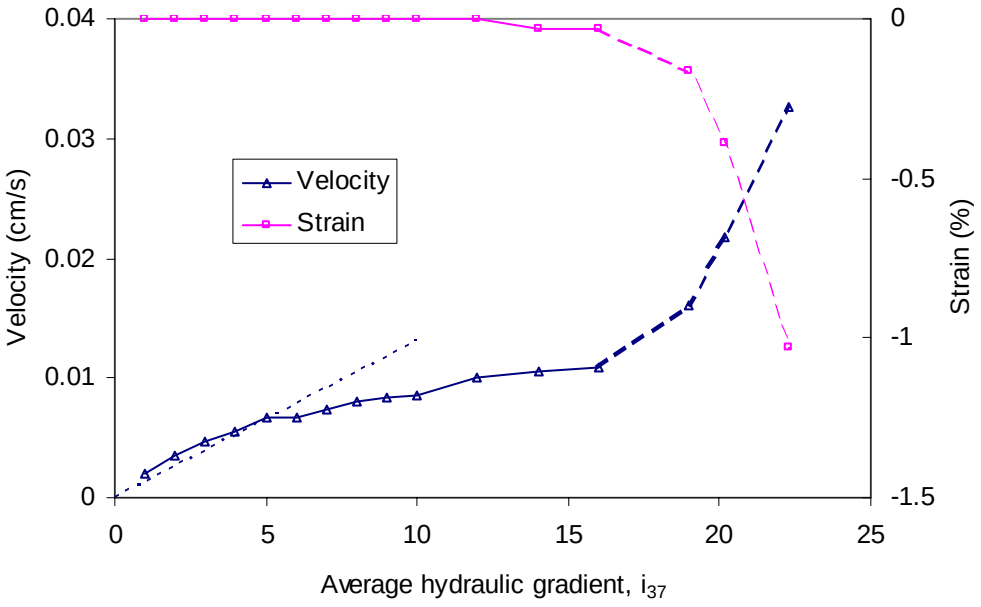

Figure 4.41Variation of velocity/strain with hydraulic gradient in test HF10-15-U

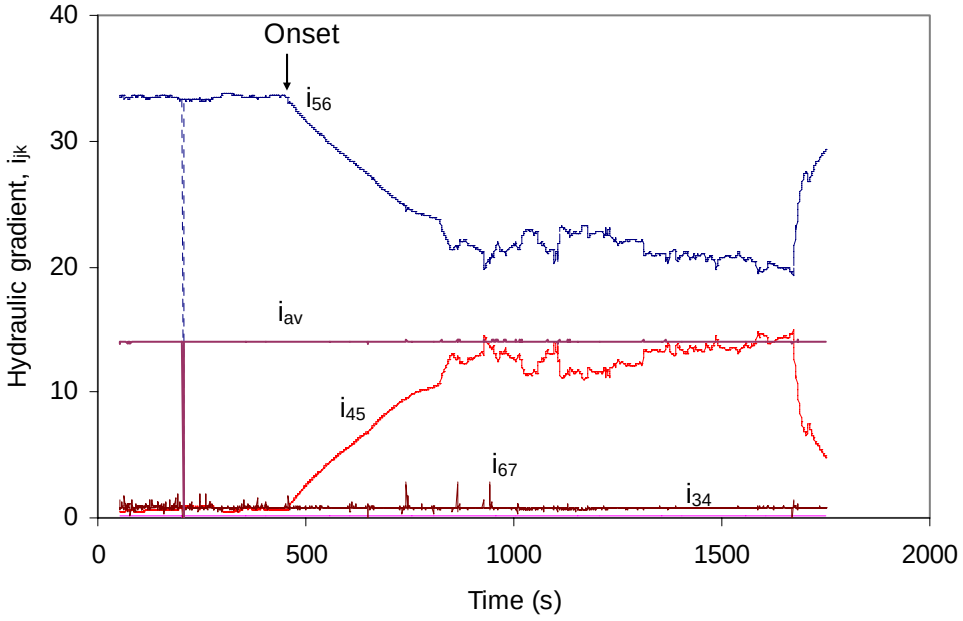

Figure 4.42 Onset of heave failure in test HF10-15-U (i_{av} = 14.0)

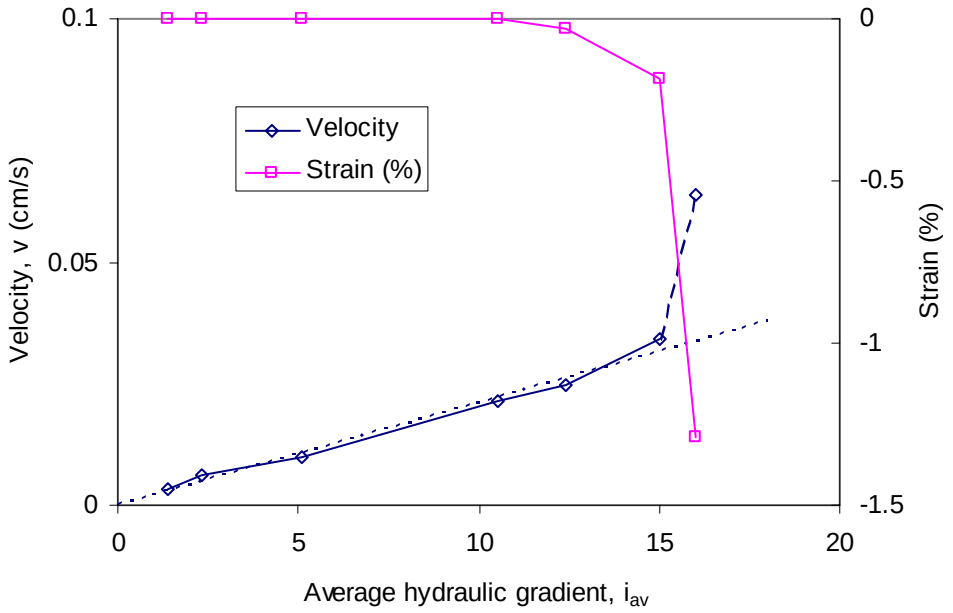

Figure 4.43 Variation of velocity/strain with hydraulic gradient in test HF10-25-U

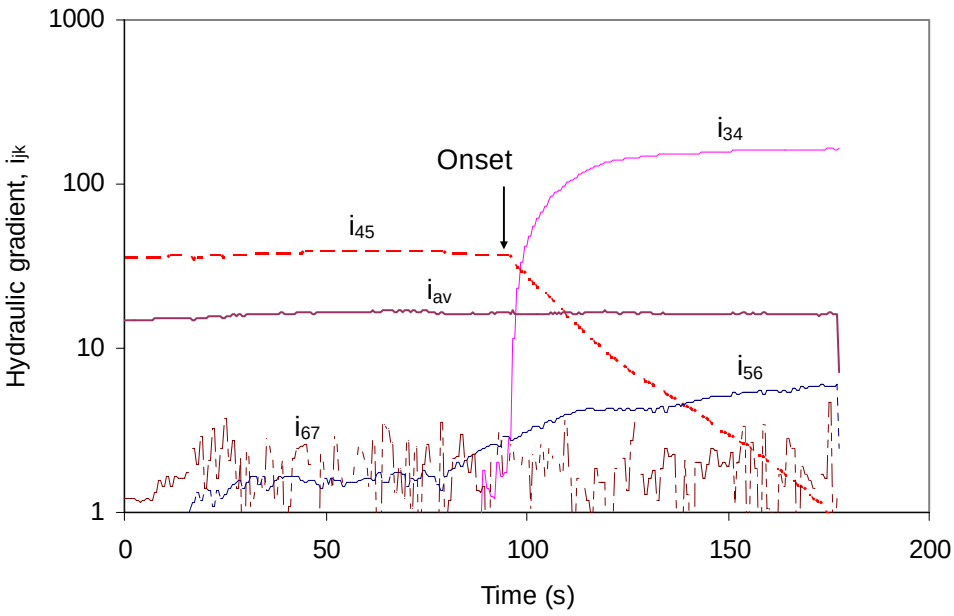

Figure 4.44 Onset of heave failure in test HF10-25-U (i_{av} = 16.0)

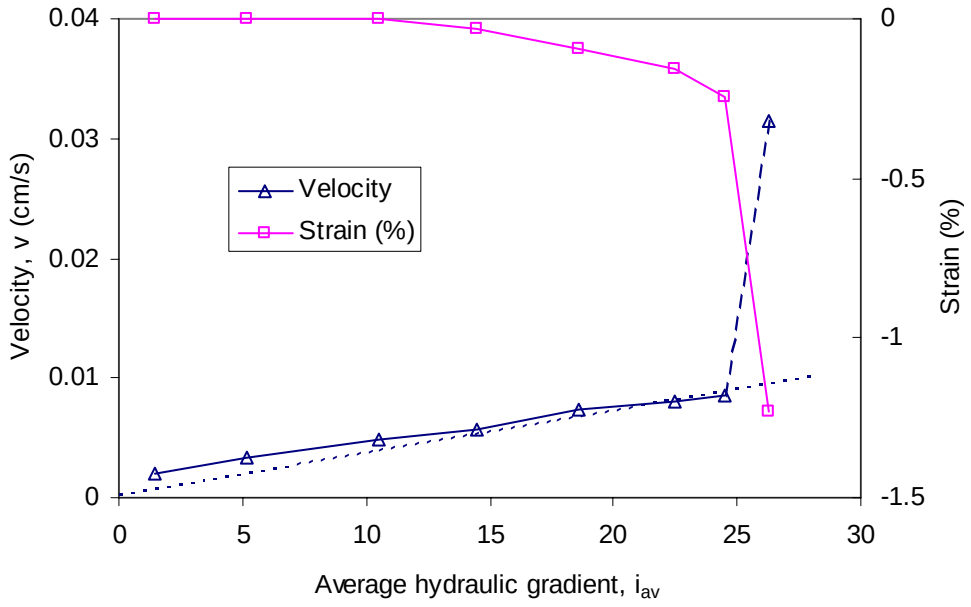

Figure 4.45 Variation of velocity/strain with hydraulic gradient in test HF10-50-U

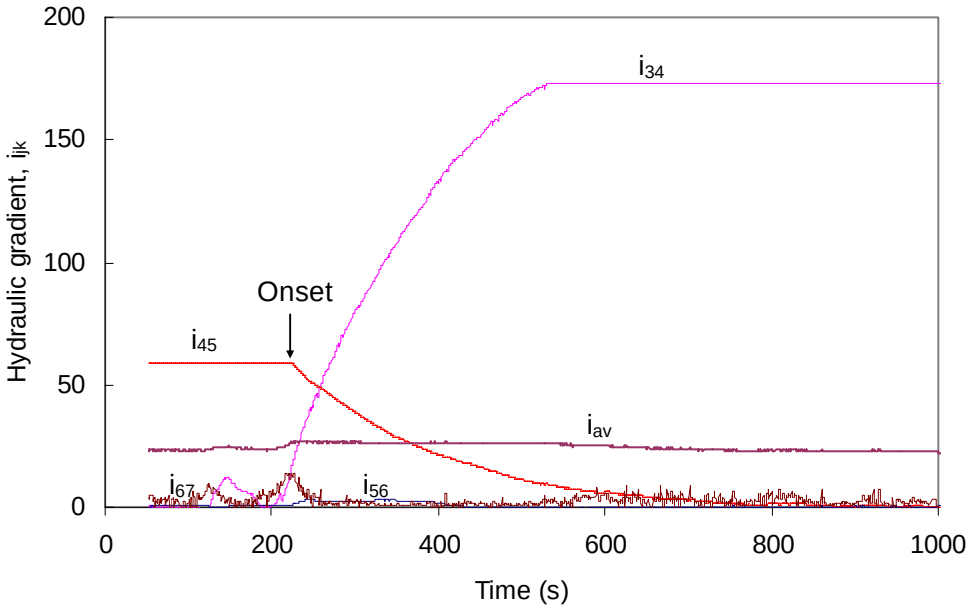

Figure 4.46 Onset of heave failure in test HF10-50-U (i_{av} = 26.3)

5 Analysis: hydromechanical response

Test data and visual observations from the laboratory study are summarized to better understand the nature of seepage-induced failure in cohesionless materials. The combined influence of effective stress and critical hydraulic gradient on the onset of seepage failure is examined in this chapter. Following a description of the nature of the seepage-induced failure, the variation of effective stress along the specimen length is established. Thereafter, the concept of a normalized effective stress is proposed. Finally, the relation between the normalized effective stress and critical hydraulic gradient, which establishes a hydromechanical envelope to internal stability, is described for each gradation.

5.1 Generalized nature of seepage-induced failure

The main objective of the permeameter test is to determine the onset of any seepage-induced failure in the specimen. A detailed description of each test was given in Chapter 4. Those results are now grouped by gradation type, in order to establish qualitative patterns evident in the generalized response and failure mode.

Two types of failure mode were observed in the tests (Table 5.1). Suffosion was typically associated with an internally unstable material, while heave was found to occur in internally stable material. In discussing the generalized nature of seepage-induced failure, these two failure modes are distinguished.

5.1.1 Nature of internal instability

Internal instability (suffosion) was observed in tests on five of the six gradations (FR8, FR7, HF01, HF03 and HF05). Recall that a distinction has been made in the literature between external suffosion and internal suffosion (see Chapter 2). In external suffosion, the finer particles are washed out from the specimen, resulting in an increase in hydraulic conductivity. In contrast, internal suffosion involves an accumulation of migrated finer particles within adjacent layers resulting in a decrease in hydraulic conductivity. In summarizing the nature of internal instability, the five gradations were distinguished according to the respective values of geometric stability index $(H/F)_{min}$ or (D'_{15}/d'_{85}) reported in Table 3.2.

5.1.1.1 Gradation FR8

A total of six tests were conducted on gradation FR8. The tests were performed in the small permeameter on specimens of glass beads. A relatively large amount of finer particle loss (≈ 10%) was measured during specimen reconstitution (Figure 5.1), which is attributed to the high potential for segregation in such gap-graded materials. Downward seepage flow was imposed until seepage-induced failure occurred. The applied gradient ranged from 2.7 to 3.5. All specimens exhibited an axial strain less than 1% before failure, most but not all exhibited an axial strain greater than 1% at failure, and all specimens contracted upon failure (Figure 5.2).

Variation of discharge velocity with the average hydraulic gradient is shown in Figure 5.3. Prior to instability, seepage velocity increased proportionally with average hydraulic gradient

for all specimens. At the onset of instability, the slope of $v \sim i_{av}$ curve increased sharply. The temporal variation of local hydraulic gradients within the specimen can be found in Chapter 4 (see Figures 4.6, 4.8, 4.10, 4.12, 4.14 and 4.16): local hydraulic gradient in the critical layer was measured to drop at the onset of instability in all tests. The onset of instability occurred relatively quickly, typically in less than 1 min. (Table 5.1).

Gradation FR8, for which stability indices $(D'_{15}/d'_{85}) = 7.9$ and $(H/F)_{min} = 0$, is characterized as highly internally unstable based on the Kezdi and the Kenney and Lau criteria. This finding conforms to the observation of Khan (2003). All specimens exhibited loss of finer particles at the onset of internal instability leading to an increase in average hydraulic conductivity (Figure 5.3). This instability is categorized as external suffosion. Average critical hydraulic gradients ranged from 2.5 to 3.5 as the applied top effective stress increased from 25 to 200 kPa, which implies critical hydraulic gradient is not very sensitive to applied vertical stress for the FR8 gradation (Figure 5.3).

5.1.1.2 Gradation FR7

A total of five tests were conducted on gradation FR7. The tests were performed on specimens of glass beads, three of them in the small permeameter and two in the large permeameter. A modest amount of finer particle loss (≈ 4%) was measured during specimen reconstitution in the small permeameter, which is attributed to a modest potential for segregation in the gap-graded material (Figure 5.4). Seepage flow was imposed until failure occurred (four of five tests in the downward direction and one in the upward direction). The maximum applied gradient ranged from 2.5 to 15.5. Four of five specimens exhibited an

axial strain less than 0.5% before failure, four of five specimens exhibited an axial strain greater than 0.5% at failure, and all specimens contracted upon failure (Figure 5.5).

Variation of discharge velocity with the average hydraulic gradient is shown in Figure 5.6. Prior to instability, seepage velocity increased proportionally with increase of hydraulic gradient. Upon instability, the slope of $v \sim i_{av}$ curve increased very significantly. The temporal variation of local hydraulic gradient within each specimen can be found in Chapter 4 (see Figures 4.18, 4.20, 4.22, 4.24, 4.26 and 4.28). In all cases, the local hydraulic gradient in the critical layer was observed to drop at the onset of instability. Again, onset of instability was initiated relatively quickly, typically in less than 1 minute (Table 5.1).

Gradation FR7, for which stability indices $(D'_{15}/d'_{85}) = 7.1$ and $(H/F)_{min} = 0$, is characterized as internally unstable based on the Kezdi and the Kenney and Lau criteria. All specimens exhibited loss of finer particles at the onset of internal instability leading to an increase in average hydraulic conductivity (Figure 5.6). This instability is categorized as external suffosion. Average critical hydraulic gradients ranged from 7.3 to 15.5 as the applied top effective stress increased from 25 to 100 kPa in the small permeameter tests, which shows that critical hydraulic gradient increased with effective stress (Figure 5.6). It was also observed that average critical hydraulic gradient in the large permeameter (FR7-150-D and FR7-150-U) was much lower than in small permeameter, which is attributed to the influence of specimen size (discussed later in Section 5.3).

5.1.1.3 Gradation HF01

One test was conducted on gradation HF01, which has the same grain size distribution as material A tested by Skempton and Brogan (1994). The specimen was reconstituted using soils from the site of WAC Bennett Dam, and tested in the large permeameter. No effective stress was applied to the top of the specimen, to replicate the test conditions of Skempton and Brogan (1994). Some mass losses were observed during the specimen reconstitution. Upward seepage flow was imposed until seepage-induced failure occurred. The maximum applied gradient was 0.22.

The variation of seepage velocity with average hydraulic gradient can be found in Chapter 4 (Figure 4.27). Prior to instability, seepage velocity increased proportionally with hydraulic gradient. Upon instability, the slope of $v \sim i_{av}$ curve greatly increased, and a vigorous boiling of finer particles was observed at the exit boundary (Figure E.13). The temporal variation of local hydraulic gradients within the specimen can also be found in Chapter 4 (Figure 4.28). The local hydraulic gradient in the critical layer was observed to drop at the onset of instability. It initiated relatively slowly, in less than 10 min (Table 5.1).

Gradation HF01, for which stability indices $(D'_{15}/d'_{85}) = 11.0$ and $(H/F)_{min} = 0.14$, is deemed internally unstable. The specimen exhibited loss of finer particles at the onset of internal instability leading to an increase in average hydraulic conductivity. This instability is categorized as external suffosion.

5.1.1.4 Gradation HF03

A total of two tests were conducted on gradation HF03. The tests were performed in the large permeameter on specimens of soil obtained from the site of WAC Bennett Dam. Some mass losses were observed during specimen reconstitution. Upward seepage flow was imposed until seepage-induced failure occurred. The maximum applied gradients range from 6.6 to 14.0. All specimens exhibit an axial strain of less than 0.2% before failure and greater than 0.2% at failure, and all specimens contracted upon failure (Figure 5.7).

Variation of discharge velocity with the average hydraulic gradient is shown in Figure 5.8. Prior to instability, seepage velocity increased proportionally with hydraulic gradient. Upon instability, the slope of $v \sim i_{av}$ curve increased. The temporal variation of local hydraulic gradients within the specimen for each test can be found in Chapter 4 (see Figures 4.30 and 4.32). Upon instability, the local hydraulic gradient in the critical layer was observed to drop. It initiated relatively quickly, in less than 5 ~ 10 minute (Table 5.1).

Gradation HF03, for which stability indices $(D'_{15}/d'_{85}) = 4.9$ and $(H/F)_{min} = 0.3$, is internally unstable. The specimen exhibited loss of finer particles at the onset of internal instability leading to an increase in average hydraulic conductivity (Figures E.15 and E.17). This instability is categorized as external suffosion. Average critical hydraulic gradients ranged from 6.6 to 14.0 as the applied top effective stress increased from 25 to 50 kPa, which shows that critical hydraulic gradient increased with effective stress (Figure 5.8).

5.1.1.5 Gradations HF05

A total of three tests were conducted on gradation HF05, which possesses 20% silt (<75μm). The tests were performed in the large permeameter on soils from the site of WAC Bennett Dam. No significant finer particle losses were observed during specimen reconstitution. Upward flow was imposed until seepage-induced failure occurred. The maximum applied gradients ranged from 4.1 to 15.0. All specimens exhibited negligible axial strain before and at internal instability (Figure 5.9).

Variation of discharge velocity with hydraulic gradient is shown in Figure 5.10. Prior to instability, seepage velocity increased proportionally with hydraulic gradient. Upon instability, the slopes of $v \sim i_{av}$ curves were observed to decrease, which are attributed to the migration of finer particles within the specimen. The temporal variation of hydraulic gradients within the specimen for each test can be found in Chapter 4 (see Figures 4.34, 4.37 and 4.39). Upon instability, the local hydraulic gradient in the critical layer was observed to decrease gradually. It implies the migration of finer particles in these tests was time-dependent, and the process was slow and continuous.

Gradation HF05, for which stability indices (D'_{15}/d'_{85}) = 5.5 and $(H/F)_{min}$ = 0.5, is characterized as internally unstable. The specimen exhibited migration of finer particles at the onset of internal instability leading to a decrease in average hydraulic conductivity (Figures 5.10). This instability is categorized as internal suffosion. Average critical hydraulic gradients ranged from 4.1 to 15.0 as the applied top effective stress increased from 25 to 50 kPa, which suggests the critical hydraulic gradient increased with effective stress (Figure

5.10).

5.1.2 Heave failure

Heave failure was observed in tests on two of the six gradations (HF05 and HF10). Although gradation HF05 has been characterized as internally unstable in the previous section, this process of internal suffosion was slow and time-dependent. After the onset of internal suffosion, two of the tests on gradation HF05 were continued until a heave failure took place. The test results are presented in the following sections.

5.1.2.1 Gradation HF05

After experiencing internal suffosion, two of the tests on gradation HF05 (HF05-25-U1 and HF05-50-U) were continued until heave failure occurred. The maximum applied gradient ranged from 16.8 to 31.0. All specimens exhibited negligible axial strain before failure and a strain greater than 6% at failure, and all specimens expanded upon failure (Figure 5.9). Horizontal crack was observed at the lowermost layer 5-6 (Figures E.20 and E.24).

Variation of seepage velocity with the average hydraulic gradient is shown in Figure 5.10. Upon the heave failure, the slope of $v \sim i_{av}$ curve increased very significantly. The temporal variation of local hydraulic gradient within each specimen can be found in Chapter 4 (see Figures 4.35 and 4.40). At failure, the local hydraulic gradient in the critical layer was observed to drop dramatically. It initiated relatively quickly, in less than 5 ~ 15 min. (Table 5.1).

Both specimens exhibited heave failure and upward displacement was observed (Figure 5.9). Average critical hydraulic gradients were 16.8 and 31.0 as the applied top effective stress increased from 25 to 50 kPa, which again suggests the critical hydraulic gradient increased with effective stress (Figure 5.10).

5.1.2.2 Gradation HF10

A total of three tests were conducted on gradation HF10. The tests were performed in the large permeameter on specimens of soils from the site of WAC Bennett Dam. Upward flow was imposed until failure occurred. The maximum applied gradients range from 14.0 to 26.3. All specimens exhibited negligible axial strain before failure and a strain of greater than 1% at failure, and all specimens expanded upon failure (Figure 5.11)

Variation of seepage velocity with the average hydraulic gradient is shown in Figure 5.12. Prior to failure, seepage velocity increased proportionally with hydraulic gradient. Upon failure, the slope of $v \sim i_{av}$ curve increased significantly. The temporal variation of local hydraulic gradient within each specimen can be found in Chapter 4 (see Figures 4.42, 4.44 and 4.46). At failure, local hydraulic gradient in the critical layer was observed to drop dramatically at the onset of heave failure. It was initiated relatively quickly, typically in less than 5 min. (Table 5.1).

Gradation HF10, for which stability index $(H/F)_{min} = 1.0$, is internally stable. All specimens exhibited episodic movements of soil particles and an upward displacement (Figure 5.11). Average critical hydraulic gradients ranged from 14.0 to 26.3 as the applied top effective

stress increased from 15 to 50 kPa, which shows that critical hydraulic gradient varied with effective stress (Figure 5.12).

5.1.3 Summary of nature of seepage failure

The nature of seepage failure for each test is summarized in Table 5.1. This preceding qualitative analysis of the data by grain size distribution has clearly shown two types of failure: suffosion and heave failure. External suffosion was observed in tests on FR8, FR7, HF01 and HF03. In these tests, the slope of $v \sim i_{av}$ curve was observed to increase (i.e., increase in hydraulic conductivity), and local gradient was observed to decrease at the onset of internal instability. A contractive displacement and a mass loss typically accompanied the onset of external suffosion. Internal suffosion was observed in the tests on gradation HF05. In these tests, the slope of $v \sim i_{av}$ curve was observed to decrease (i.e., decrease in hydraulic conductivity) and local hydraulic gradient was observed to decrease gradually when internal suffosion occurred. No displacement or mass loss was observed at the onset of internal suffosion.

Heave failure was observed in tests on gradation HF05 and HF10. Like the case for external suffosion, heave failure is associated with an increase in the slope of $v \sim i_{av}$ curve and a decrease in local hydraulic gradient. In contrast to external suffosion, an expansive displacement was observed during heave.

In all cases, critical hydraulic gradient was found to increase with effective stress in both heave failure and internal instability. The relation appears to depend on gradation type. A

highly unstable gradation, such as FR8, is not very sensitive to change in effective stress; a relatively stable gradation, such as HF03, is very sensitive to change in effective stress. The quantitative relation between critical gradient and effective stress is now discussed in the following sections.

5.2 Distribution of effective stress along the specimen

Effective stress has been shown to play an important role in the onset of internal stability, and appears to exert a great influence on critical hydraulic gradient. In order to establish a relation between local hydraulic gradient and effective stress in the initiation location, the variation of effective stress along the specimen must be accurately described.

In the permeameter tests, vertical effective stress (σ'_{t0}) was applied to the top surface of specimen and kept constant during the testing. With no flow (i = 0), vertical effective stress will vary along the specimen because of sidewall friction, yielding a different value of effective stress at the bottom of the specimen (σ'_{b0}). With seepage flow (i > 0), effective stress on the top σ'_t was again kept constant as σ'_{t0}, while effective stress on the bottom σ'_b either increases (under downward flow) or decreases (under upward flow).

An analysis of vertical effective stress in the test specimen was carried out using a piece-wise 1D effective stress model (see Appendix A). The soil specimen is divided into n sub-layers. An equilibrium equation for each sub-layer is established. In a layer j, the governing equation can be expressed as (Figure 5.13):

$$\frac{\sigma'_{t,j} - \sigma'_{b,j}}{\Delta z_j} + \frac{4 f_j}{D} \sigma'_{vm,j} + \gamma' + i_j \gamma_w = 0 \qquad (5.1)$$

where,

$\sigma'_{t,j}$ = vertical effective stress at the top of layer j;

$\sigma'_{b,j}$ = vertical effective stress at the bottom of layer j;

$\sigma'_{vm,j}$ = vertical mean effective stress in the layer j;

f_j = $\mu_j K_0$ = soil-wall friction between the specimen and side wall in layer j; μ_j = friction coefficient between sidewall and soil = $\tan(\delta)$; K_0 = coefficient of earth pressure at rest;

i_j = local hydraulic gradient in the layer j;

D = diameter of the specimen;

Δz_j = thickness of layer j;

γ' = submerged unit weight of the soil specimen;

γ_w = unit weight of water.

To solve this problem, two assumptions are made:

(i) interface friction coefficient does not vary with sub-layers location, $f_j = f$ (j = 1, 2, … , j, … n);

(ii) effective stress in the sub-layer j is linearly distributed, $\sigma'_{vm,j} = 0.5\,(\sigma'_{t,j} + \sigma'_{b,j})$.

In a system of n sub-layers, there are (2n+1) unknown variables, including top and bottom effective stresses in each sub-layer (2n) and soil-wall friction (1) (see Eq. 5.1). To solve this problem, (2n+1) equations are needed. Equilibrium equations and boundary conditions for a

system of n sub-layers are summarized as follows:

(i) n equilibrium equations (see Eq. 5.1)

(ii) (n-1) stress continuities at the interface of two sub-layers:

$$\sigma'_{b,j} = \sigma'_{t,j+1} \tag{5.2}$$

In total, there are (2n-1) equations for (2n+1) unknown variables; therefore, two additional equations are needed to specify stress distribution along the specimen length. In the large permeameter, effective stress is measured at the top and bottom of specimen (σ'_{t0} and σ'_{b0}), hence the distribution of stress along the specimen length can be determined (see Figure 5.14). In the small permeameter, since only the effective stress at the top of specimen (σ'_{t0}) is measured, the soil-wall friction (*f*), has to be assumed in order to calculate the stress distribution along the specimen length (see Figure 5.14).

5.2.1 Stress distribution in the large permeameter

In the large permeameter, values of σ'_{t0} and σ'_{b0} were calculated directly from measurements of the top and bottom load cell, respectively. As discussed in the previous section, values of vertical effective stress at the middle ports along the specimen were deduced using the piece-wise effective stress model. Values of soil-wall friction (*f*) were also obtained by trial-and-error, to ensure the vertical effective stress on both surfaces of the specimen were consistent with the measurements. The results are summarized in Tables 5.2.

5.2.1.1 Stress distribution at $i_{av} = 0$

The force of friction will always act opposite to the direction of the soil movement. At i = 0, the friction force acted opposite to the applied effective stress (σ'_{t0}), leading to a decrease of effective stress along the specimen from top to bottom. The bottom effective stresses were measured as 35 ~ 64% of the top effective stresses, for different soil types (see Table 5.2). For glass beads (gradation FR7), the stress ratio $\sigma'_{b0}/\sigma'_{t0} \approx 64\%$. For soils gradations (HF3, HF5 and HF10), the stress ratio $35 \leq \sigma'_{b0}/\sigma'_{t0} \leq 62$ %. Interface friction coefficients (f_0) were back-calculated and found to range from 0.10 to 0.26. For glass beads, $f_0 \approx 0.11$, while for soils, $0.14 \leq f_0 \leq 0.26$. Based on the piece-wise model, the deduced distributions of initial vertical effective stress (solid line) are as shown in Figures 5.15 ~ 5.19.

5.2.1.2 Stress distribution at $i_{av} > 0$

Stress distribution along the specimen length changed as seepage flow was imposed. Figures 5.15 ~ 5.19 also show the deduced value of vertical effective stress immediately prior to the onset of instability (pre-critical) and heave failure (pre-heave). Tests for FR7 experienced a relatively small increase (downward flow) and decrease (upward flow). Tests for HF03, HF05 and HF10 (all upward flow) experienced a large decrease in effective stress at the bottom of specimen. Inspection revealed that the effective stress at the pre-critical condition was greater than zero (Figures 5.15 to 5.17). In contrast, for heave failure, effective stress at the pre-heave condition is close to zero (Figures 5.18 ~ 5.19).

Inspection further reveals the magnitude and direction of sidewall friction may vary during seepage flow (see Table 5.2). Specifically, the variation of sidewall friction is illustrated in

Figure 5.20 for test HF05-50-U. At i_{av} = 0, the sidewall friction and overburden pressure were in opposite directions, and $f_0 \approx 0.17$. When the soil specimen was subjected to upward seepage flow, the sidewall friction started to decrease with increasing hydraulic gradient. At $i_{av} \approx 18.0$, the direction of friction force had become the same as that of overburden pressure in order to balance the seepage force (and $f \approx 0$). Thereafter, the magnitude of the sidewall friction increased with increasing the hydraulic gradient. When the sidewall friction reached the maximum permissible value, the overburden pressure and the sidewall friction could no longer resist the seepage force, causing the soil specimen to lift up and heave failure to occur ($f \approx -0.26$). Variations of deduced sidewall friction in magnitude and direction at static, pre-critical and pre-heave conditions are shown in Tables 5.2.

5.2.2 Stress distribution in the small permeameter

In the small permeameter, values of σ'_{t0} were calculated directly from the top load cell measurement. To obtain the distribution of effective stress along the specimen length, the soil-wall friction (f) must to be assumed. Given the back-calculated soil-wall friction (f) in the large permeameter is approximately 0.10 ~ 0.12 (Table 5.2), it is reasonable to assume the same interface friction coefficient in the small permeameter since the same materials (glass beads) were tested. Parameters used in the calculation of stress in the small permeameter tests are shown in Table 5.3.

The deduced distributions of initial vertical effective stress (solid line) are shown in Figures 5.21 and 5.22. Since the stress distributions in tests FR8-25-D0, FR8-25-D1 and FR8-25-D2 are quite similar, only the test FR8-25-D0 is shown in Figure 5.21. The deduced values of

vertical effective stress immediately prior to the onset of instability (dashed line) are also shown in Figures 5.21 and 5.22. Compared with the static condition, stress at the pre-critical condition exhibits a small increase in the tests on gradation FR8, and a large increase in the tests on gradation FR7.

5.3 Hydromechanical envelope

5.3.1 The concept of normalized effective stress ($\overline{\sigma}'_{vm}$)

Knowing the local hydraulic gradient (i_{jk}) and mean vertical effective stress (σ'_{vm}) in the 'onset' layer where instability first occurs allows for study of the relation between these two parameters. Based on observations in the large permeameter tests performed by Moffat (2005), it was hypothesized that the critical hydraulic gradient would increase with effective stress. The finding was also evident from tests in the small permeameter in the current study. However, further evaluation of the data sets show that the relation is more complex than originally conceived.

Five tests were conducted on gradation FR7, in both the small and large permeameter. The critical hydraulic gradient and mean vertical effective stress at the 'onset' layer for each test are plotted in Figure 5.23. A linear relation was observed between critical gradient and mean vertical effective stress in results from the small and large permeameter tests. However, the relation is not unique. The slope formed in data from the small permeameter tests is much steeper than that from in the large permeameter tests. The difference is attributed to scale effects, given the length of the local failure zone is 2.5 cm in the small permeameter and 12.5

cm in the large permeameter.

In order to unify the two sets of data, a dimensionless approach was taken to eliminate the scale effect. Consider, for example, a soil element in the failure zone where σ'_{vm} = mean vertical effective stress, Δz = the length of failure zone and A = the cross sectional area of specimen (Figure 5.24). Seepage force is the body force associated with the volume of soil; the seepage force, $F_{seepage}$, can be expressed as,

$$F_{seepage} = i\gamma_w V = i\gamma_w A\Delta z \tag{5.3}$$

where γ_w = unit weight of water.

The vertical resistant force on this element, $F_{apply} = \sigma'_{vm} A$ (5.4)

As the resistant force equals to the seepage force, $F_{seepage} = F_{apply}$, the critical hydraulic gradient is obtained. Therefore,

$$i_{critical} = \frac{\sigma'_{vm} A}{\gamma_w A\Delta z} = \frac{\sigma'_{vm}}{\gamma_w \Delta z} = \overline{\sigma}'_{vm} \tag{5.5}$$

where $\overline{\sigma}'_{vm}$ is the normalized mean vertical effective stress. From this definition, the critical hydraulic gradient is found to be a function of $\overline{\sigma}'_{vm}$.

The data in Figure 5.23 were re-plotted in Figure 5.25 using the normalized mean vertical effective stress. They yield a good relation between critical gradient and normalized effective stress, which appears unique for the two sets of data. Scatter about the linear fit is attributed to the different methods used to determinate effective stress in the large and small permeameter tests (see Section 5.2 and Figure 5.14). Therefore, the critical hydraulic gradient

is proportional to normalized mean vertical effective stress rather than mean vertical effective stress, and this will form basis of test interpretation.

The influence of flow direction (upward or downward seepage flow) on the envelope can be examined with reference to tests on gradation FR7, which was subject to four downward flow tests and one upward test (see Table 3.2). Downward and upward flow tests appear to be bounded by the same envelope (Figure 5.25). The same finding was also reported by Moffat (2005) from large permeameter tests on his gradation T-5.

5.3.2 Hydromechanical path and envelope

To further examine the relation between critical gradient and normalized effective stress, hydromechanical paths for each gradation are plotted in Figures 5.26 to 5.30. Hydromechanical path is defined as the variation of normalized mean vertical effective stress $\overline{\sigma}'_{vm}$ ($\sigma'_{vm} / \gamma_w \Delta z$) with local hydraulic gradient (i_{jk}) across the 'onset' layer for each test. The plot of hydromechanical path for each test terminates at the critical hydraulic gradient i_{cr}.

The hydromechanical paths for each gradation appeared to be bounded by an envelope at which the onset of instability occurs. The envelope is generally defined by a relation between $\overline{\sigma}'_{vm}$ and i_{cr} for each gradation. A linear envelope is strongly evident in gradations FR7, HF03, HF05 and HF10. It is less apparent in gradation FR8, which was found to be the most susceptible to segregation in laboratory testing. Forensic inspection revealed that about 10% of finer particles were lost during specimen reconstitution of the gradation FR8, which likely explains the data scatter (Figure 5.1).

The slope of each hydromechanical envelope is assumed to depend on the geometric characteristics of respective materials. To better examine this assumption, the hydromechanical envelopes for all materials are plotted in Figure 5.31. Inspection shows the relative slope of the envelopes to follow the order given by: F8 < F7 < HF03 < HF05 < HF10. Referring to the geometric index $(H/F)_{min}$ of materials, it is identical to the geometrical ranking of susceptibility to internal instability given by F8 < F7 < HF03 < HF05 < HF10 (see Table 3.2). It seems reasonable to conclude that the slope of hydromechanical envelope increased with the stability index $(H/F)_{min}$, thus implying the hydromechanical envelope depends on the gradation shape. Inspection also reveals that, at any effective stress, initiation of instability requires a larger hydraulic gradient in a material with higher value of $(H/F)_{min}$ than one with a lower value of $(H/F)_{min}$. Referring to the geometric index (D'_{15}/d'_{85}) of materials, it is similar, but not identical to, the geometrical ranking of susceptibility to internal instability given by F8 < F7 < HF05 < HF03 < HF10 (see Table 3.2). In order to further explore the relation between these geometric indexes and the slope of hydromechanical envelope, data from the current study are compared with other experimental data reported in the literature in Chapter 6.

5.4 Summary

In this chapter, the experimental results are summarized for each gradation. Two types of seepage-induced failure were observed in the tests: heave failure and suffosion. Hydromechanical envelope, the relation between critical hydraulic gradient and normalized mean vertical effective stress, governs the onset of seepage-induced failure of each gradation.

The hydromechanical envelope is not unique, and the slope of envelope is dependent on geometric characteristics of each gradation. The factors influencing the slope of hydromechanical envelope will be examined in the Chapter 6.

Table 5.1 Summary characterization of seepage failure

Failure mode	Test code	$v \sim i_{av}$ slope	Local gradient	Displace-ment	Mass loss	Initiation	
						zone	time (min)
		(Δk)	(Δi)	(ΔL)	(Δm)		
Suffosion	FR8-25-D0	↑	↓	↓	↑	3-5	<1
	FR8-25-D1	↑	↓	↓	↑	3-5	<1
	FR8-25-D2	↑	↓	↓	↑	3-5	<1
	FR8-50-D	↑	↓	↓	↑	3-5	<1
	FR8-100-D	↑	↓	×	↑	3-4	<20
	FR8-200-D	↑	↓	↓	↑	3-4	<1
	FR7-25-D	↑	↓	↓	↑	1-3	<1
	FR7-50-D	↑	↓	↓	↑	1-3	<1
	FR7-100-D	↑	↓	↓	↑	3-4	<1
	FR7-150-D	↑	↓	↓	↑	3-5	<1
	FR7-150-U	↑	↓	↓	↑	5-6	<5
	HF01-0-U	↑	↓	NA	↑	4-6	<10
	HF03-25-U	↑	↓	↓	↑	4-5	<5
	HF03-50-U	↑	↓	↑	↑	4-5	<10
	HF05-25-U1	↓	↓	×	×	4-6	NA
	HF05-25-U2	↓	↓	×	×	4-6	NA
	HF05-50-U	↓	↓	×	×	4-6	NA
Heave	HF05-25-U1	↑	↓	↑	×	5-6	<15
	HF05-50-U	↑	↓	↑	×	5-6	<5
	HF10-15-U	↑	↓	↑	×	5-6	<10
	HF10-25-U	↑	↓	↑	×	4-5	<2
	HF10-50-U	↑	↓	↑	×	4-5	<5

Note: ↑ = increase; ↓ = decrease; × = no change; NA = Not available

Table 5.2 Stress calculation in the large permeameter

Code	Static condition ($i_{av} = 0$)				Pre-critical/heave condition ($i_{av} > 0$)			
	σ'_{t0}	σ'_{b0}	$\sigma'_{b0} / \sigma'_{t0}$	f_0	σ'_t	σ'_b	σ'_b / σ'_t	f
FR7-150-D	157.9	99.5	63.0	0.11	155.7	102.7	66.0	0.12
FR7-150-U	146.8	93.4	63.6	0.11	145.9	92.5	63.4	0.10
HF03-25-U	29.4	18.4	62.6	0.14	29.4	8.9	30.3	0.05
HF03-50-U	46.7	22.0	47.2	0.20	45.2	8.8	19.5	0
HF05-25-U1	25.8	13.7	53.1	0.18	26.5	5.5	20.8	0.05
					27.5*	1.5*	5.4*	-0.27*
HF05-25-U2	26.5	15.4	58.1	0.16	26.5	8.3	31.3	0.10
HF05-50-U	50.2	26.4	52.6	0.17	52.5	8.1	15.4	0.03
					56.5*	0.4*	0.7*	-0.26*
HF10-15-U	16.0	7.2	45.0	0.25	16.0*	0.9*	5.6*	-0.25*
HF10-25-U	28.5	11.9	42.8	0.24	28.5*	3.1*	10.9*	-0.36*
HF10-50-U	49.2	17.3	35.2	0.26	49.2*	1.7*	3.5*	-0.32*

Note: Pre-critical/heave condition refers to the condition immediately prior to the onset of internal instability/heave failure, respectively. * denotes heave failure.

Table 5.3 Stress calculation in the small permeameter

Code	Static condition ($i_{av} = 0$)			Pre-critical/heave condition ($i_{av} > 0$)		
	σ'_{t0}	σ'_{b0}	f_0	σ'_t	σ'_b	f
FR8-25-D0	25.2	18.8	0.1	25.2	19.8	0.1
FR8-50-D	51.7	37.8	0.1	51.7	40.2	0.1
FR8-100-D	108.2	78.2	0.1	108.2	79.9	0.1
FR8-200-D	201.0	144.6	0.1	201.0	146.9	0.1
FR7-25-D	25.2	18.4	0.1	25.2	23.9	0.1
FR7-50-D	51.3	36.6	0.1	51.3	43.8	0.1
FR7-100-D	100.9	69.2	0.1	100.9	81.4	0.1

Note: Pre-critical/heave condition refers to the condition immediately prior to the onset of internal instability/heave failure, respectively. * denotes heave failure

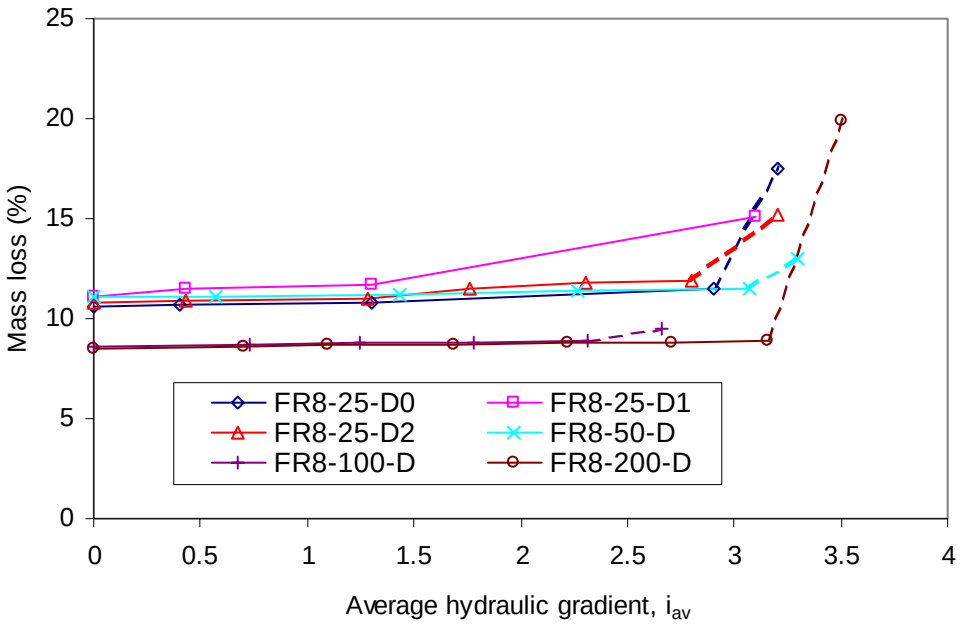

Figure 5.1 Variation of mass loss with average hydraulic gradient for gradation FR8

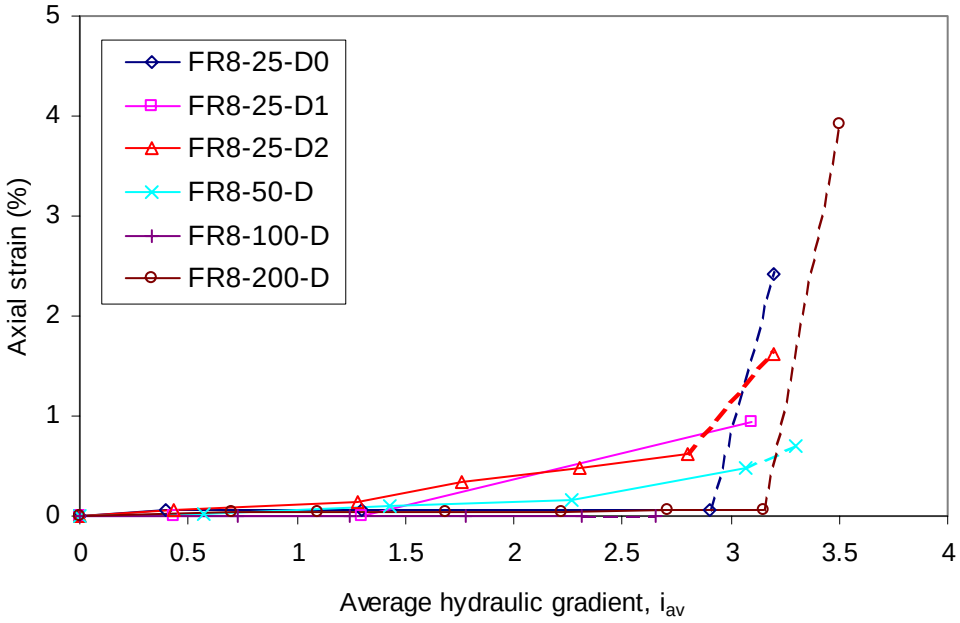

Figure 5.2 Variation of axial strain with average hydraulic gradient for gradation FR8

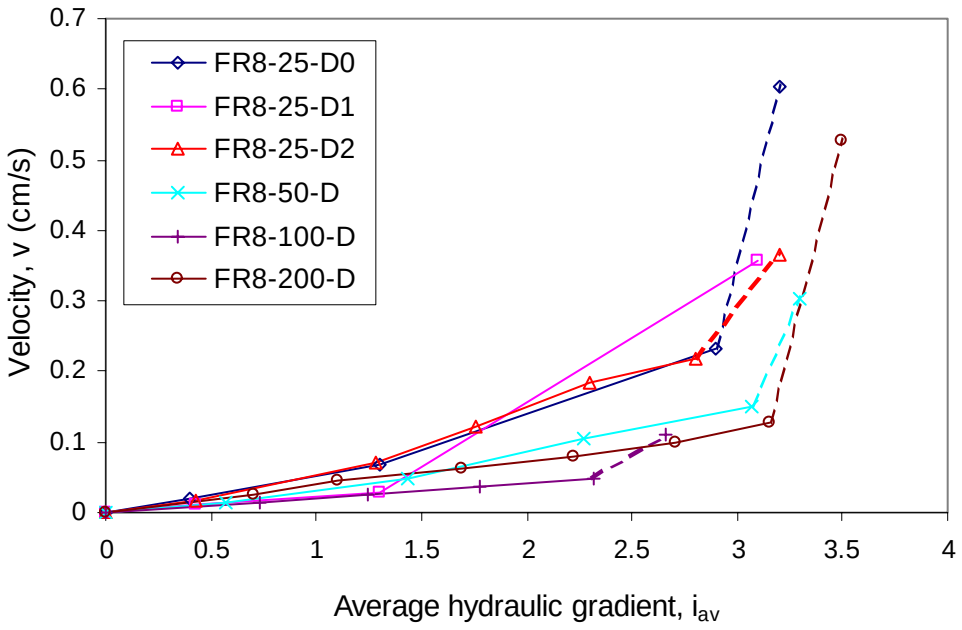

Figure 5.3 Variation of velocity with average hydraulic gradient for gradation FR8

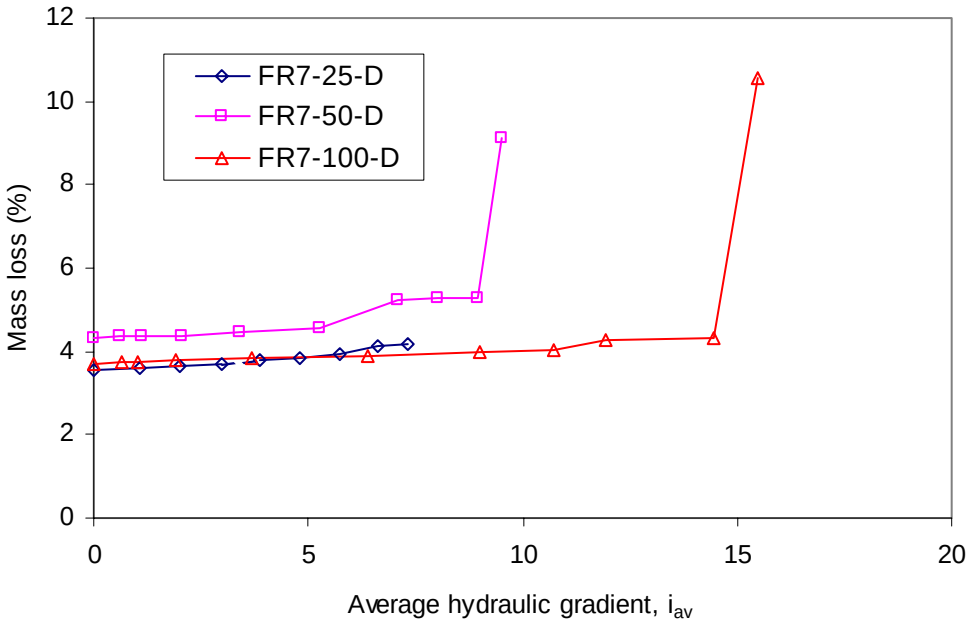

Figure 5.4 Variation of mass loss with average hydraulic gradient for gradation FR7

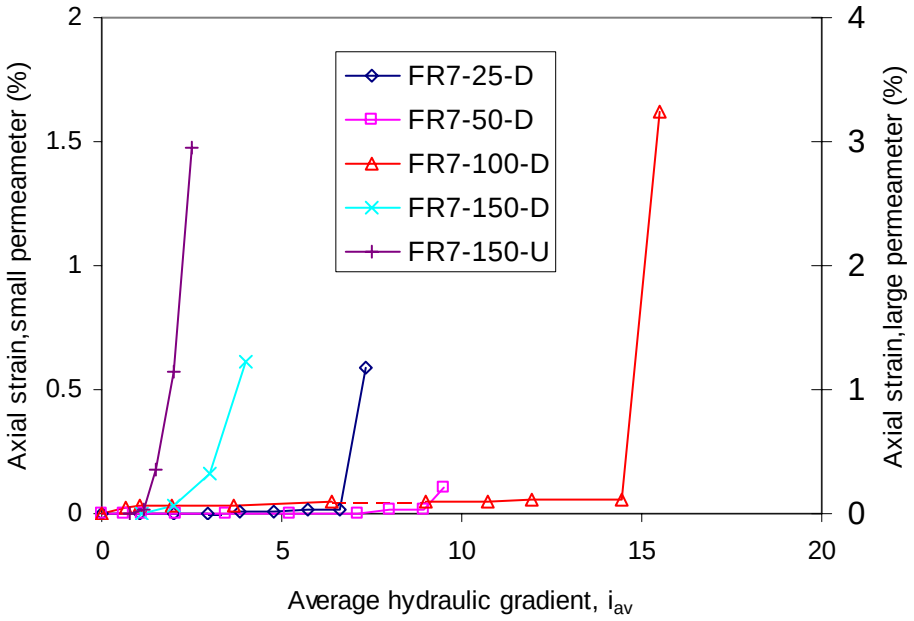

Figure 5.5 Variation of axial strain with average hydraulic gradient for gradation FR7

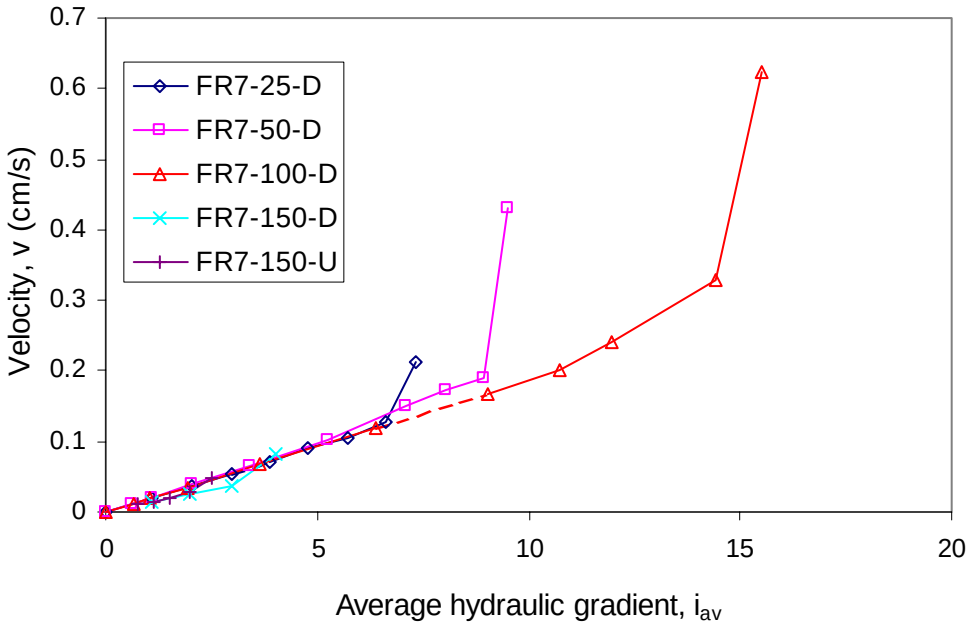

Figure 5.6 Variation of velocity with average hydraulic gradient for gradation FR7

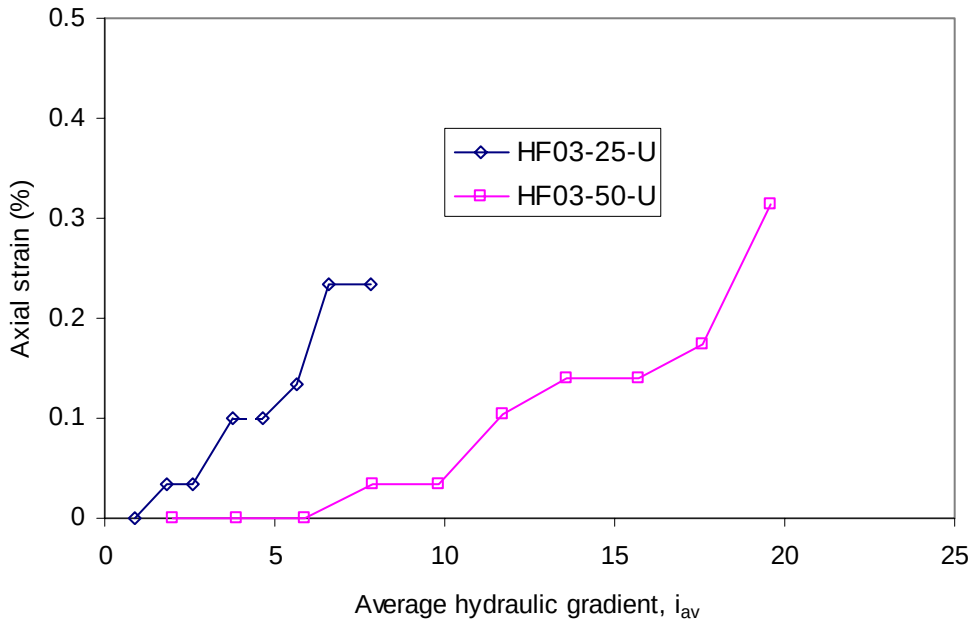

Figure 5.7 Variation of axial strain with average hydraulic gradient for gradation HF03

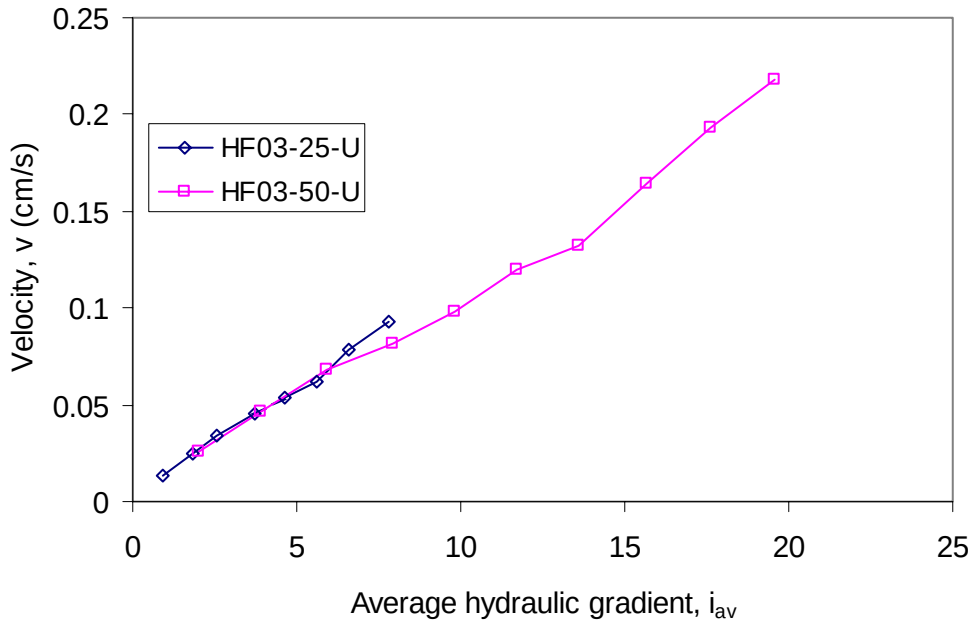

Figure 5.8 Variation of velocity with average hydraulic gradient for gradation HF03

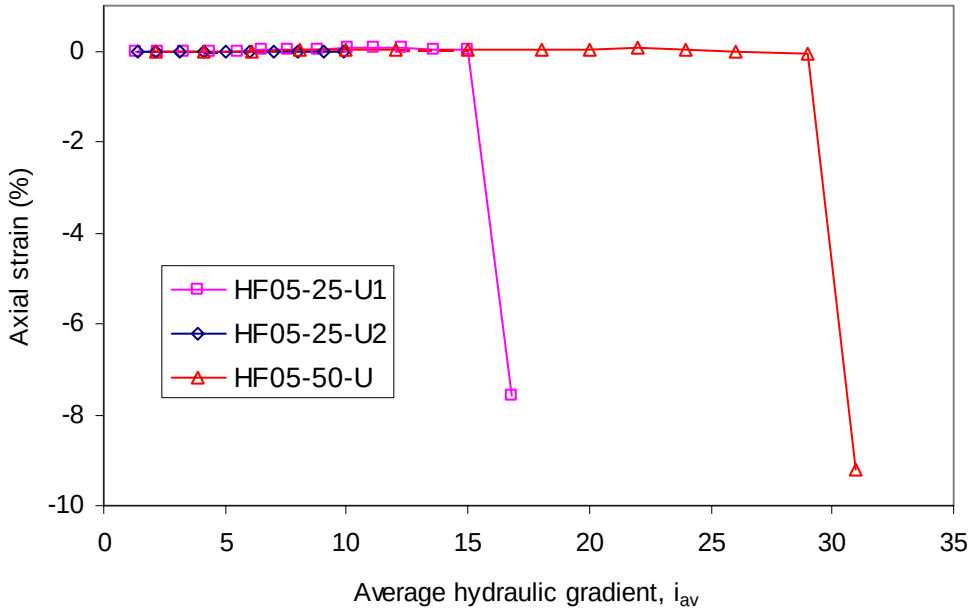

Figure 5.9 Variation of axial strain with average hydraulic gradient for gradation HF05

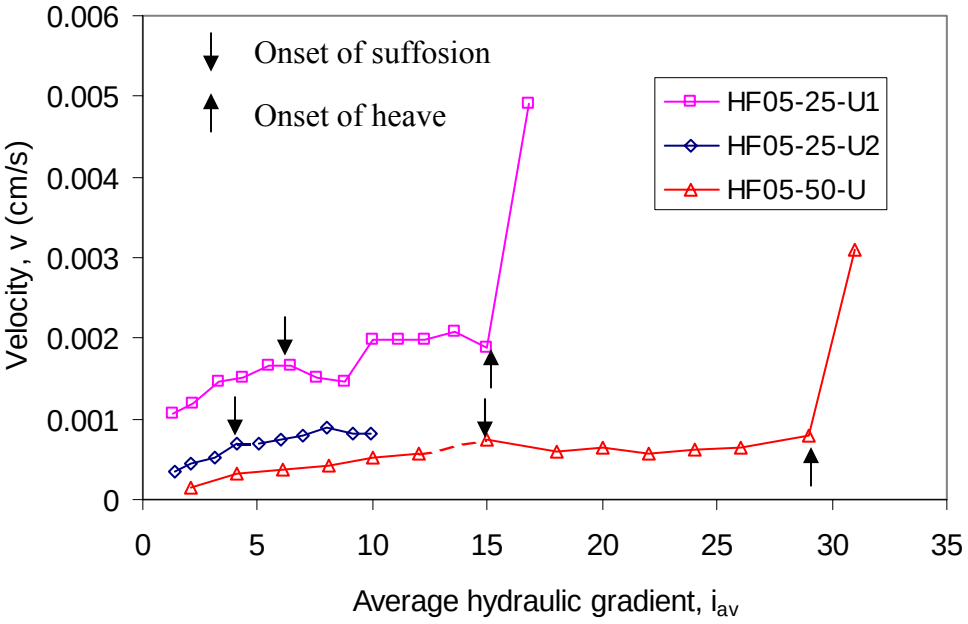

Figure 5.10 Variation of velocity with average hydraulic gradient for gradation HF05

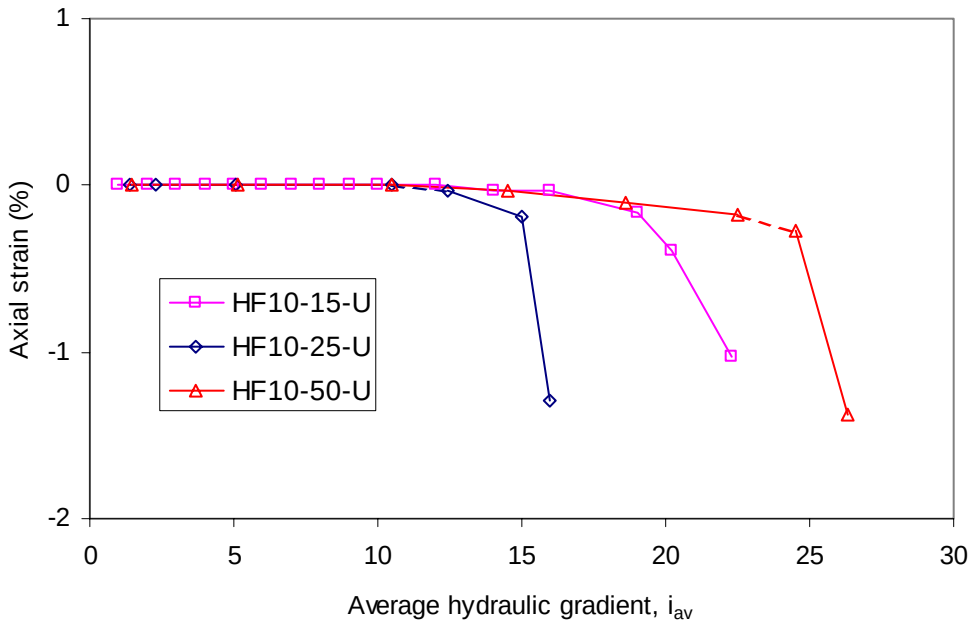

Figure 5.11 Variation of velocity with average hydraulic gradient for gradation HF10

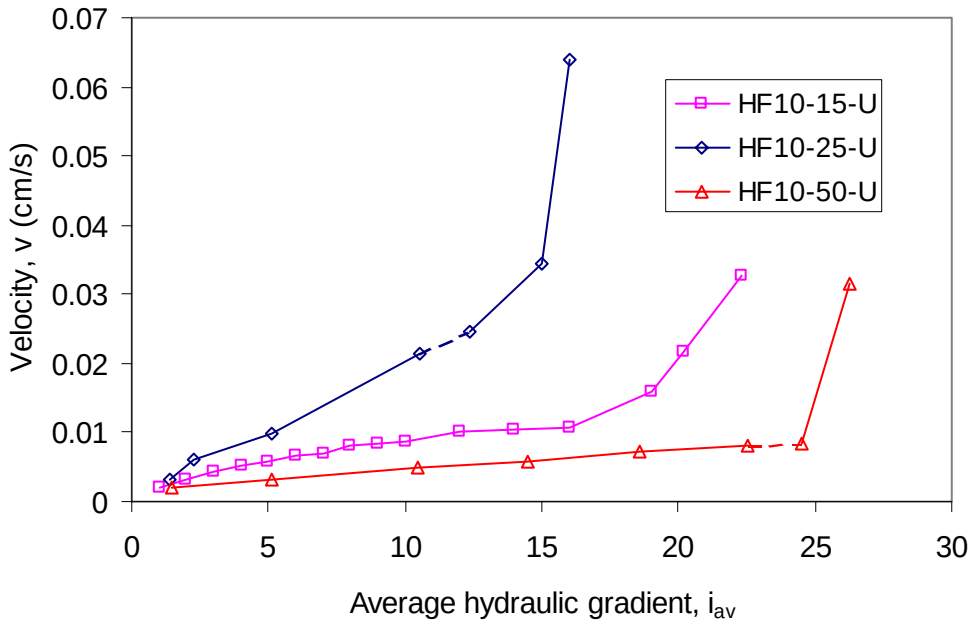

Figure 5.12 Variation of velocity with average hydraulic gradient for gradation HF10

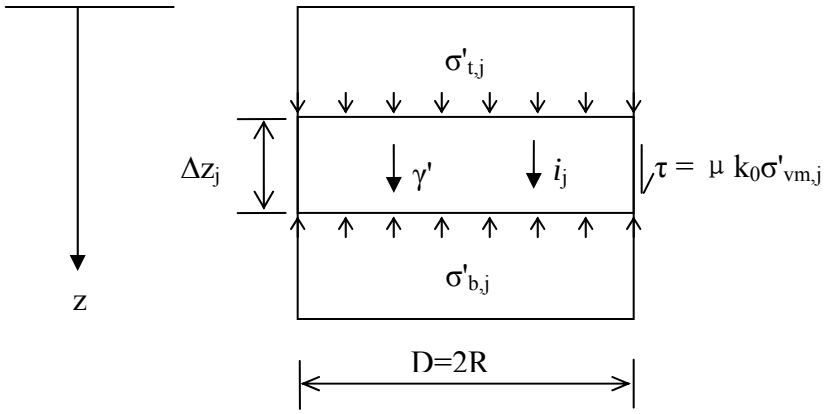

Figure 5.13 Forces in a sub-layer j

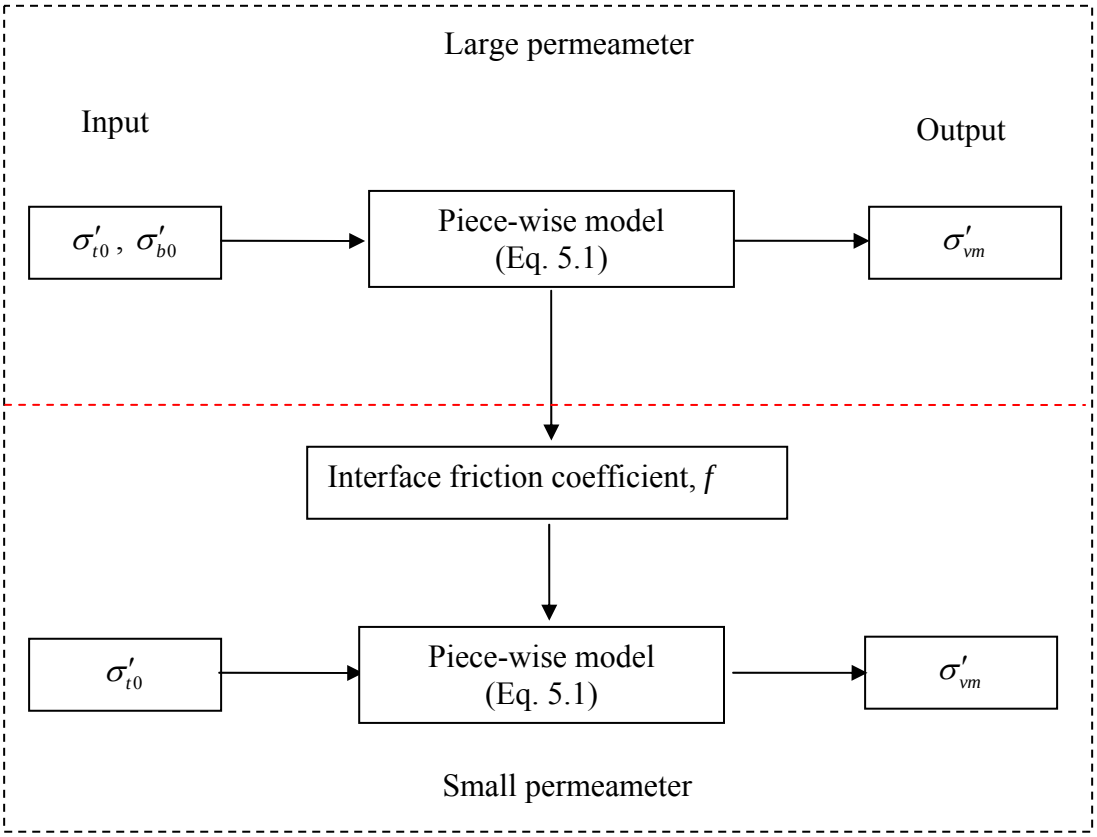

Figure 5.14 Calculation of stress distribution in the test specimens

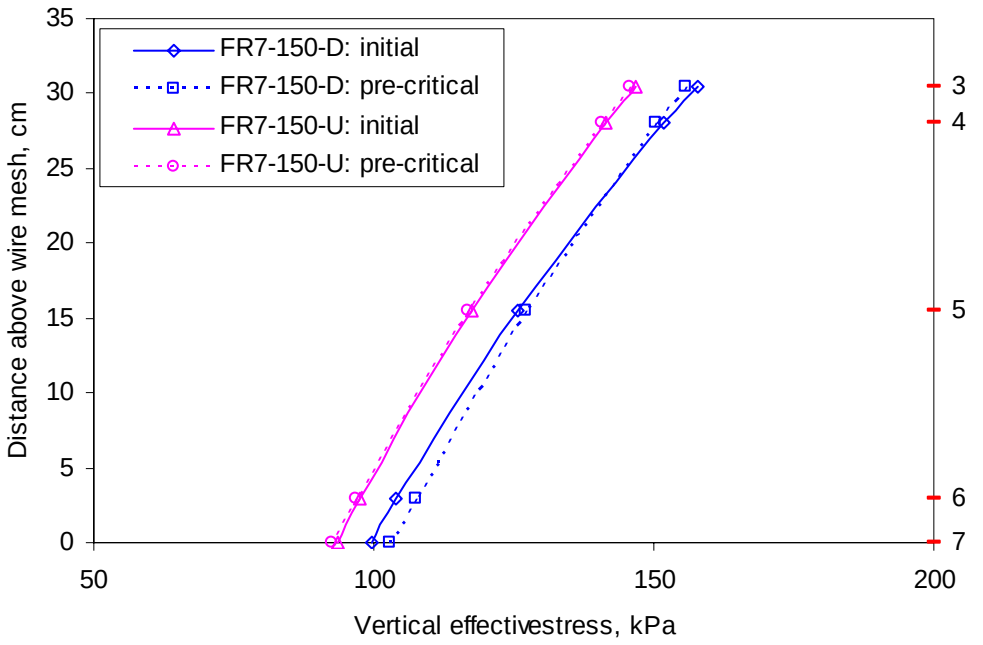

Figure 5.15 Stress distribution for gradation FR7 in large permeameter

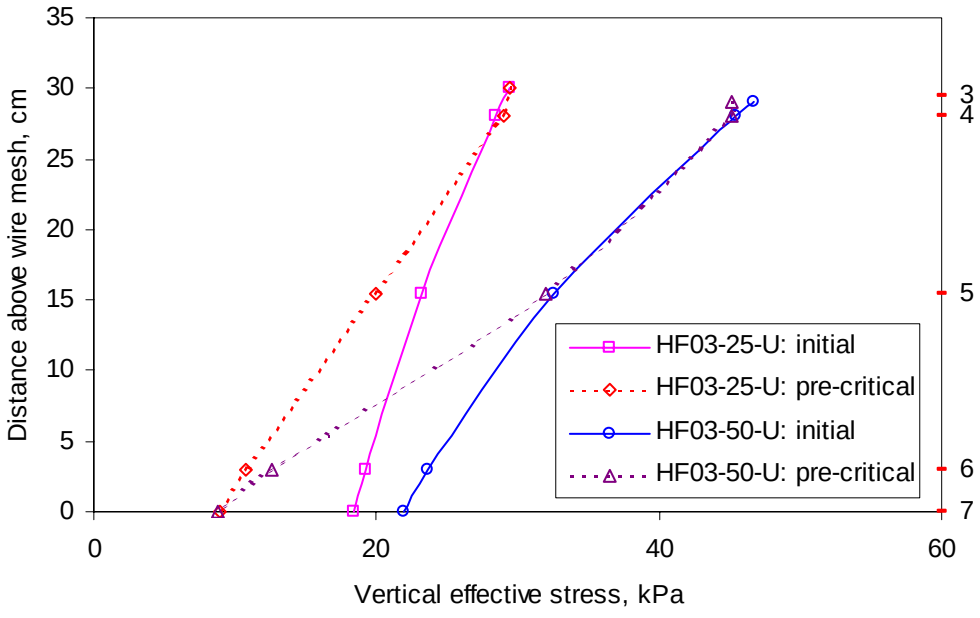

Figure 5.16 Stress distribution for gradation HF03

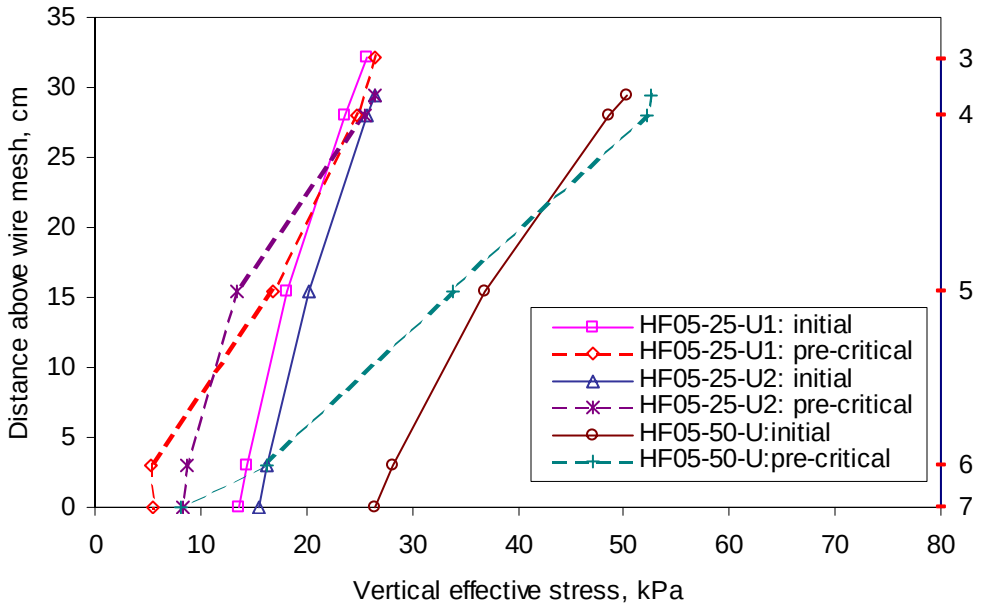

Figure 5.17 Stress distribution on gradation HF05 (internal instability)

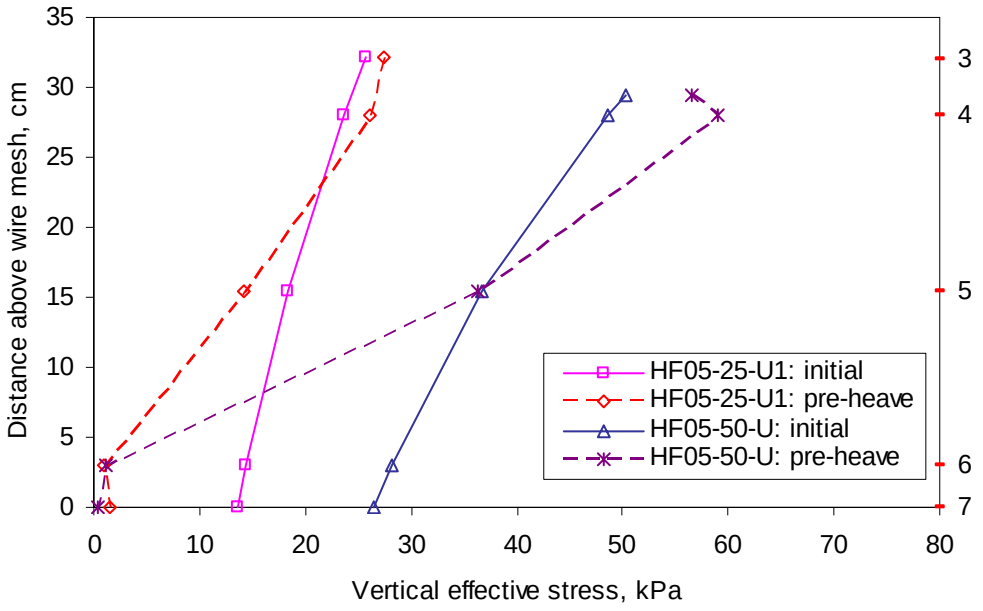

Figure 5.18 Stress distribution on HF05 (heave failure)

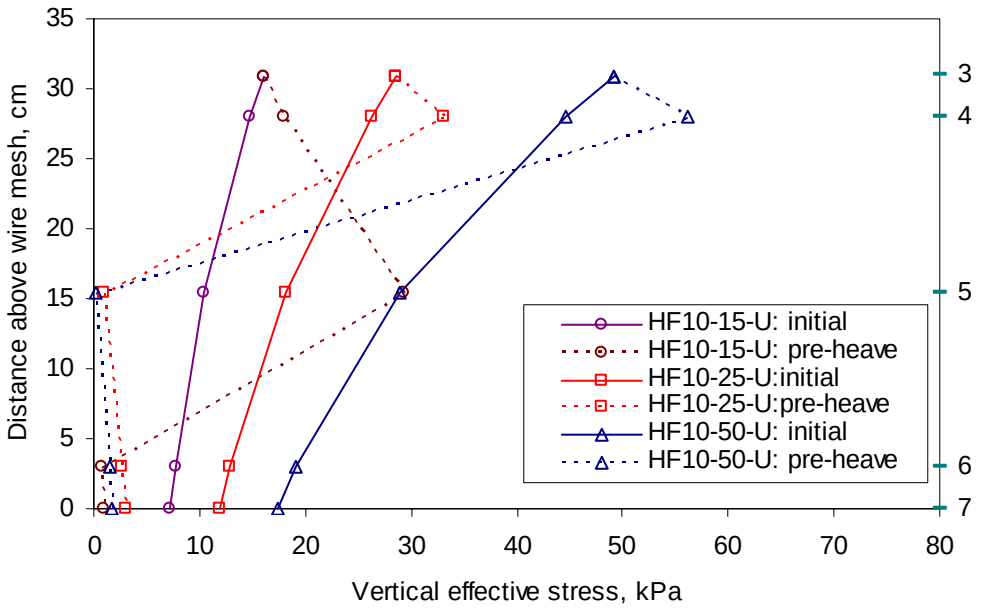

Figure 5.19 Stress distribution on gradation HF10 (heave failure)

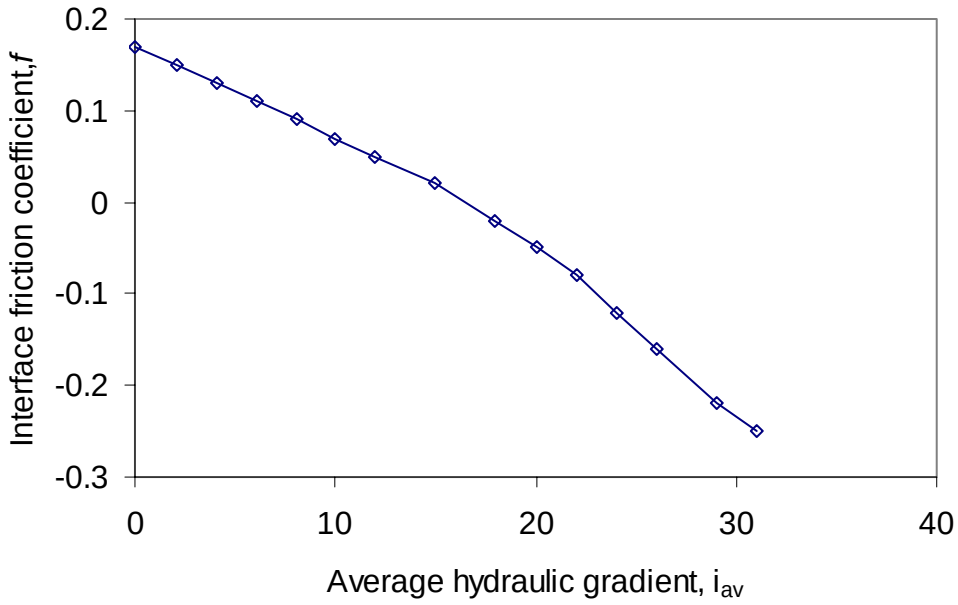

Figure 5.20 Variation of sidewall friction during seepage flow

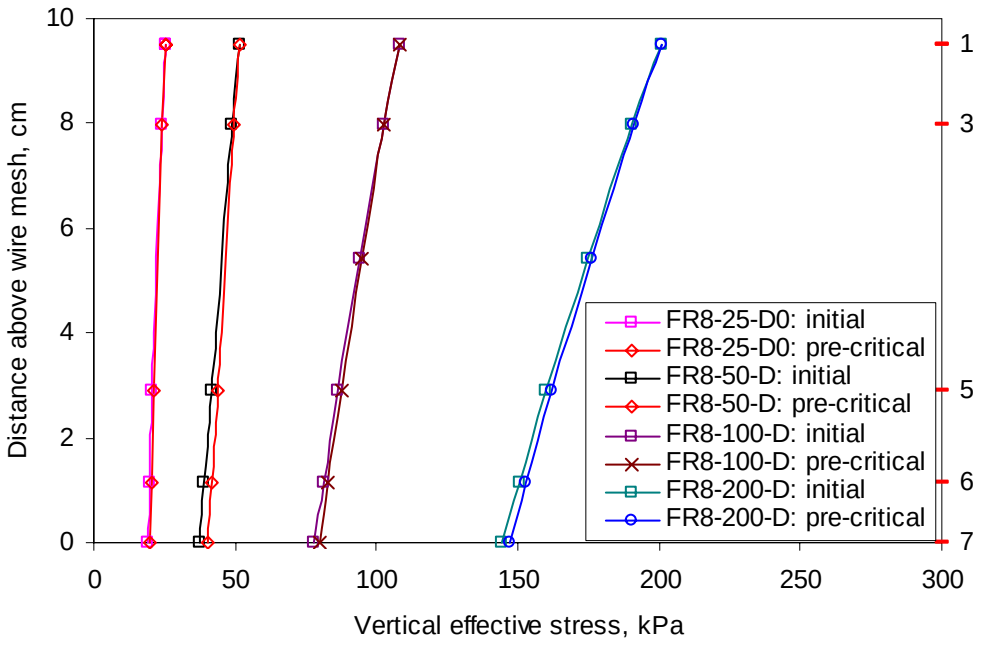

Figure 5.21 Deduced stress distribution for gradation FR8 in small permeameter

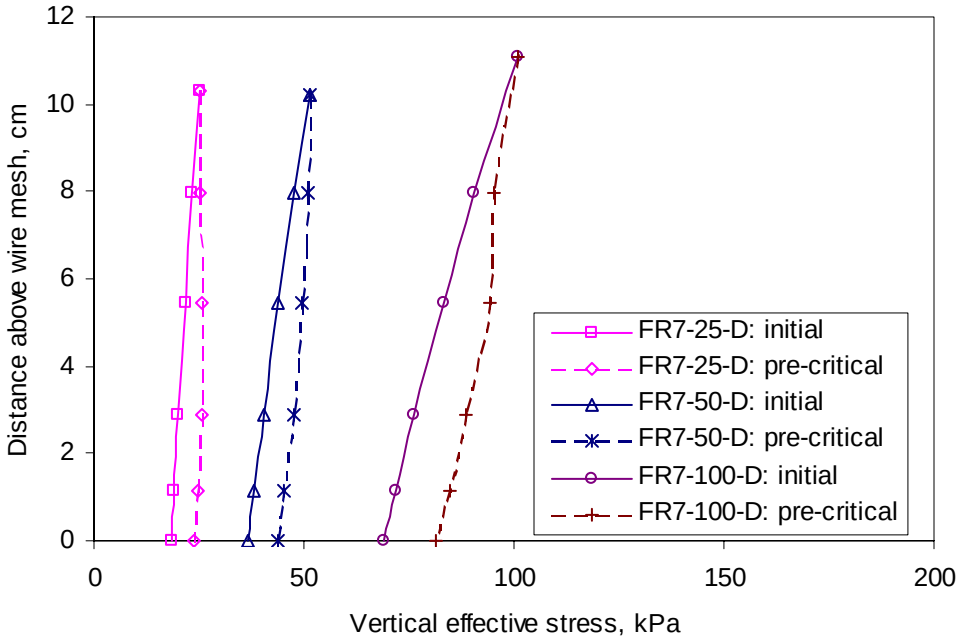

Figure 5.22 Deduced stress distribution for gradation FR7 in small permeameter

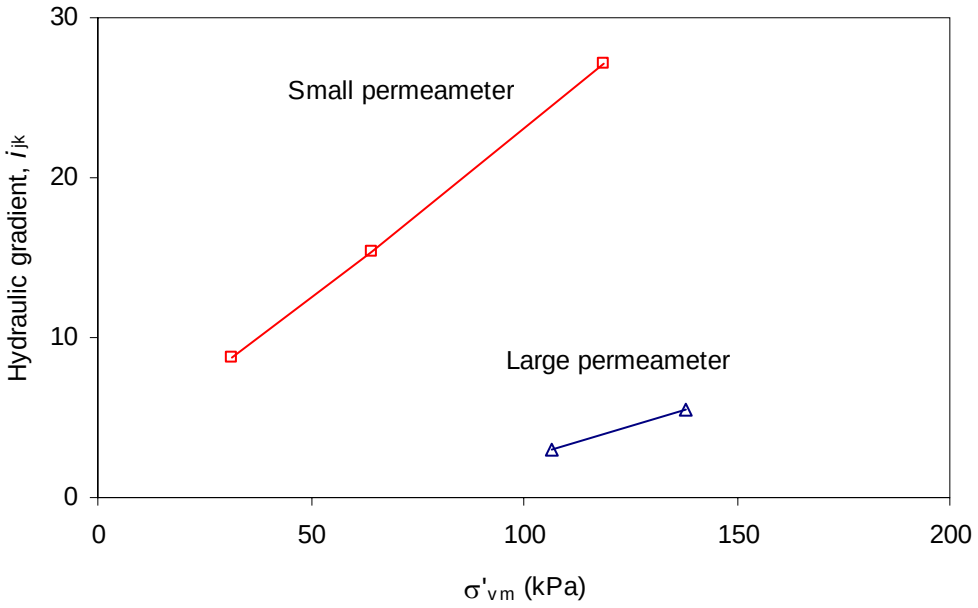

Figure 5.23 Relation between critical gradient and vertical effective stress for gradation FR7

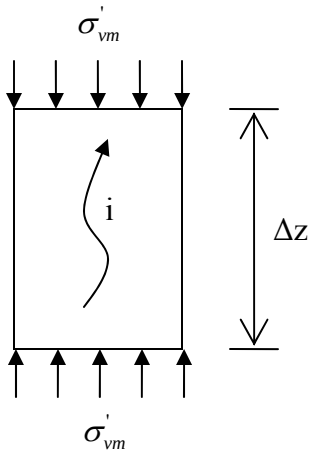

$$F_{seepage} = i\,\gamma_w V = i\gamma_w A\Delta z$$

$$F_{apply} = \sigma'_{vm} A$$

$$F_{seepage} = F_{apply}$$

$$\overline{\sigma}'_{vm} = \frac{\sigma'_{vm}}{\gamma_w \Delta z} = i_{critical}$$

Figure 5.24 Definition and physical nature of normalized effective stress

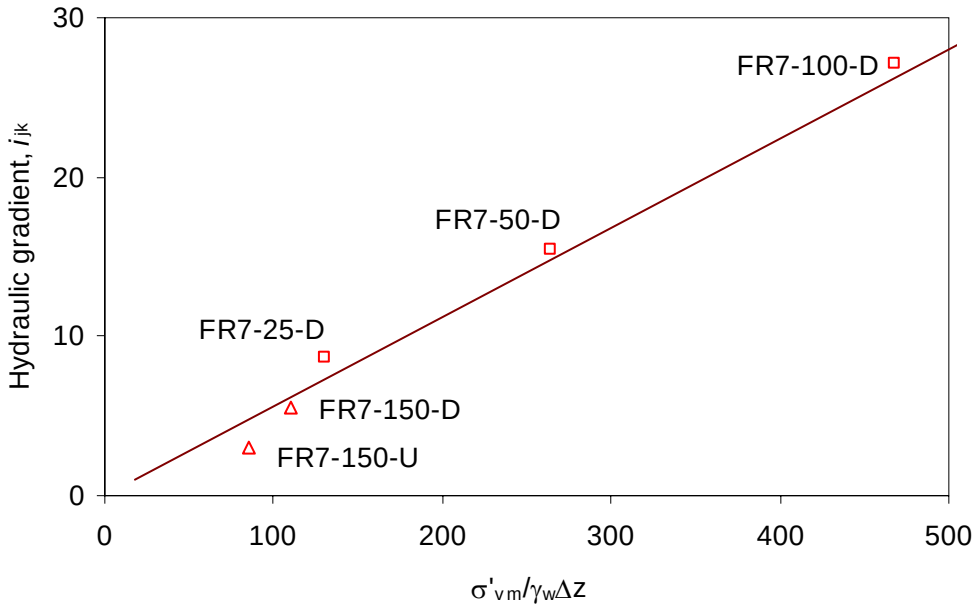

Figure 5.25 Relation between the normalized effective stress and critical gradient for gradation FR7

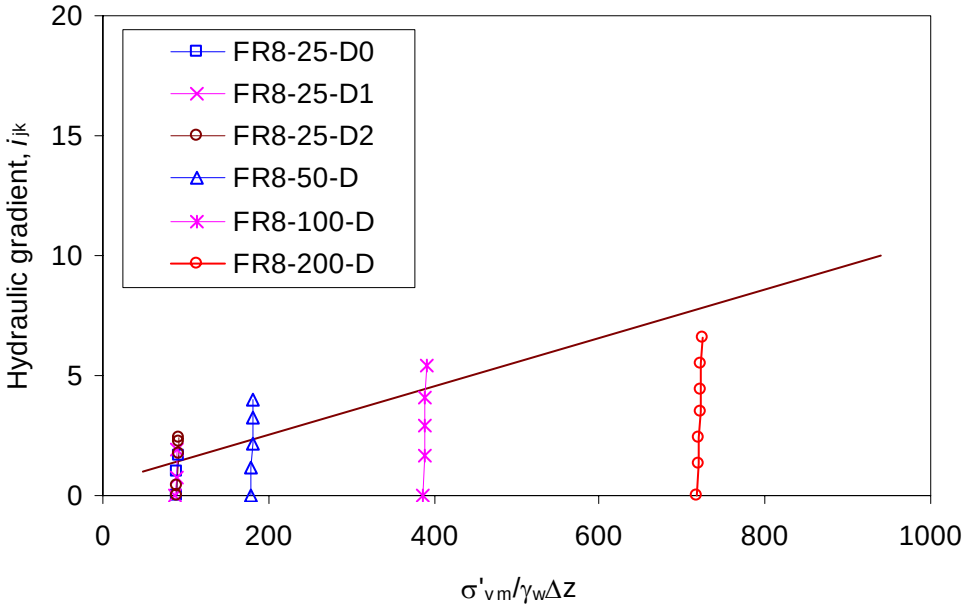

Figure 5.26 Hydromechanical paths for gradation FR8

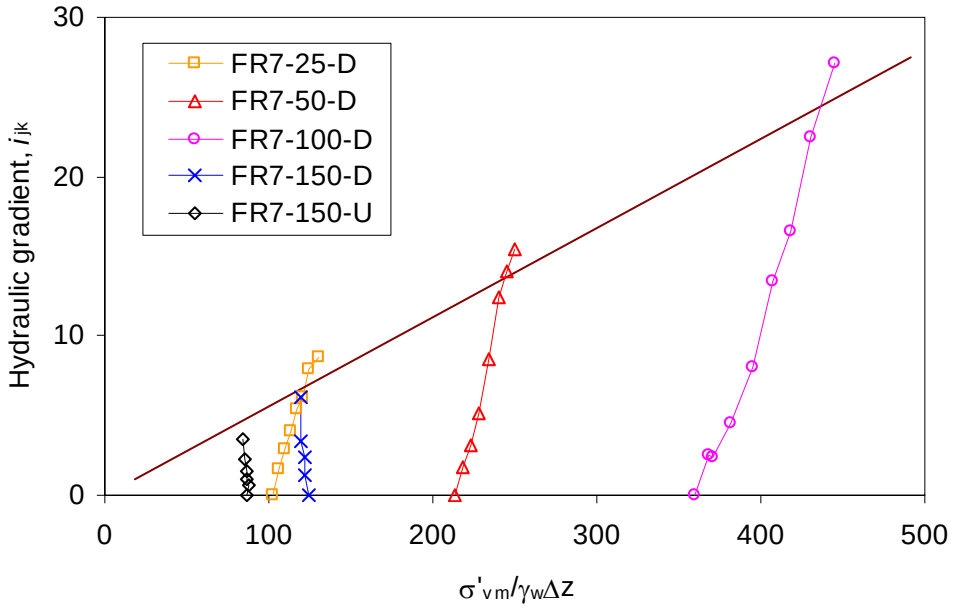

Figure 5.27 Hydromechanical paths for gradation FR7

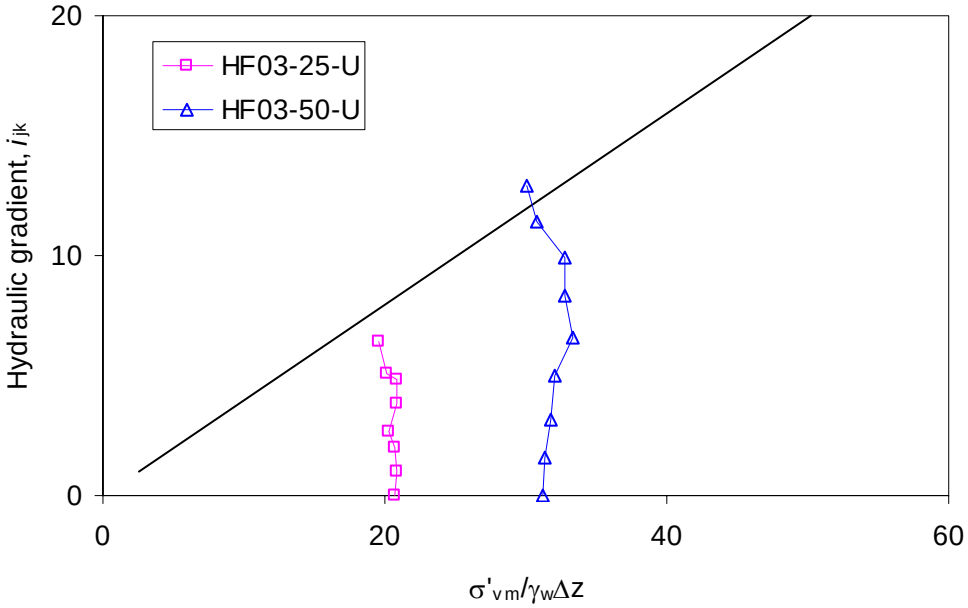

Figure 5.28 Hydromechanical paths for gradation HF03

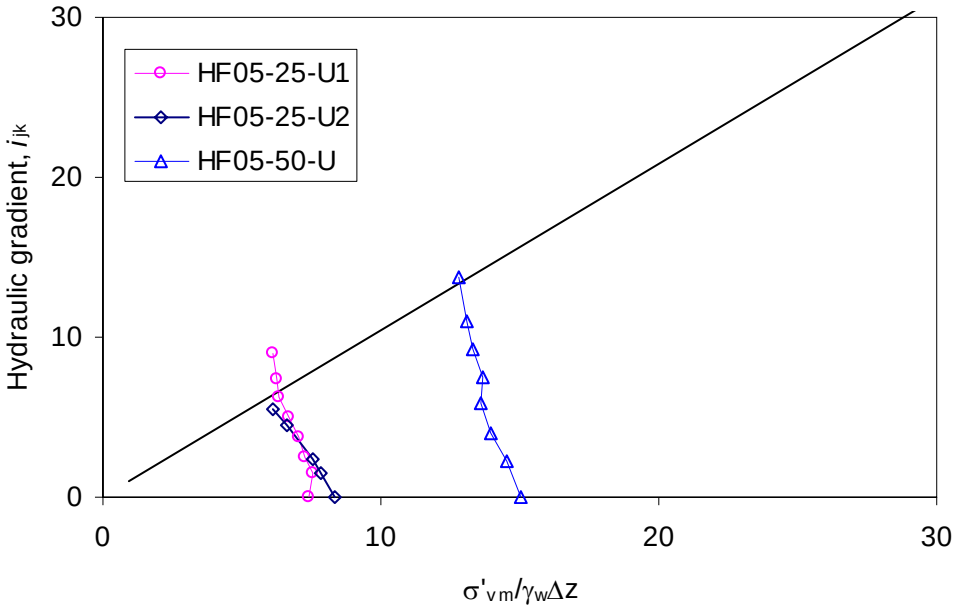

Figure 5.29 Hydromechanical paths for gradation HF05

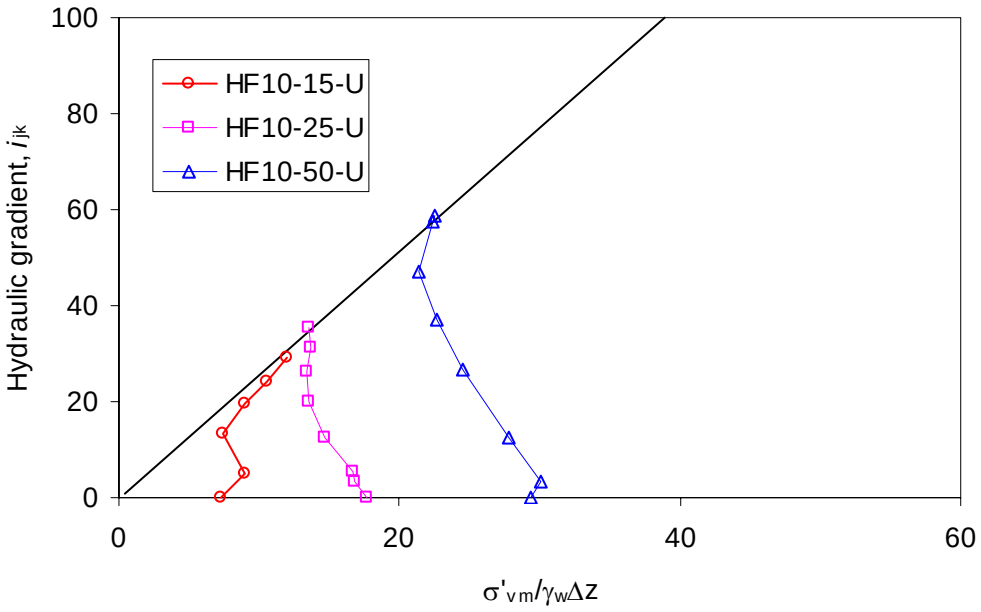

Figure 5.30 Hydromechanical paths for gradation HF10

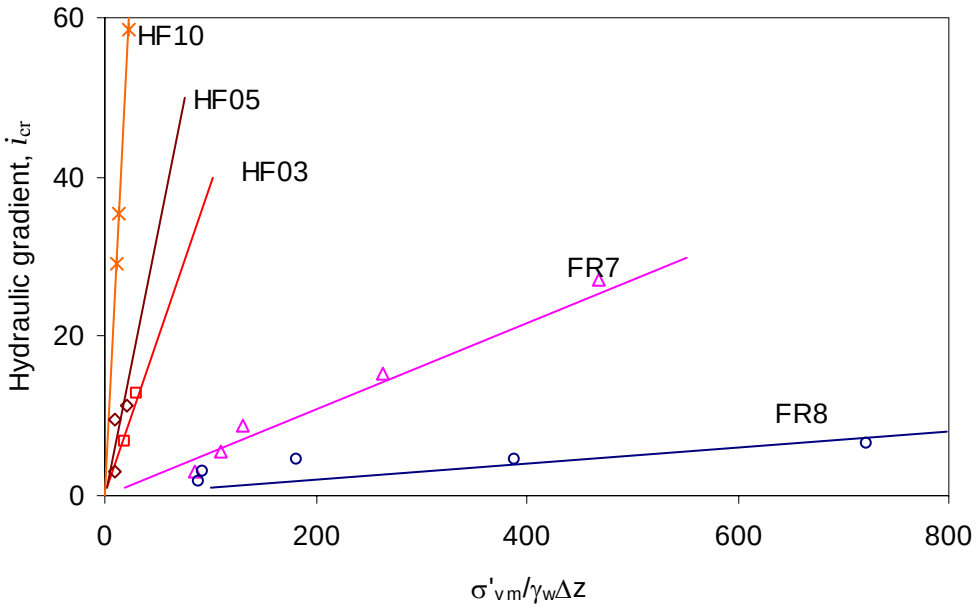

Figure5.31 Summary of hydromechanical envelopes

6 Discussion of the results

6.1 Introduction

To evaluate the internal stability of cohesionless soils, two questions have to be addressed: (i) Is the soil susceptible to internal instability? (ii) If the soil is susceptible, will internal instability be triggered by seepage flow? A framework for this process of evaluation is given in Figure 6.1. When considering susceptibility to internal instability, comparative sizes of finer particles (d) and pore size constrictions of coarser particles (D_c) should be examined. If $d < D_c$, the finer particles have potential to be transported by seepage flow. For potentially unstable materials, a gradient in excess of a critical value is necessary to initiate movement ($i > i_c$).

To address the first question, empirical geometric criteria are typically used in engineering practice. Several criteria exist such as the Kezdi (1979) criterion, the Kenney and Lau (1985, 1986) criterion or the Burenkova (1993) criterion. However, few of them have been verified independently (Skempton and Brogan, 1994; Fannin and Moffat, 2006). In order to gain more confidence in using these criteria, a systematic study is conducted in this chapter. By comparing these criteria on the basis of theoretical and experimental evaluations, the relative conservatism of each method is established. The findings reported in this chapter lead to a proposed unified approach, drawing upon the Kezdi and the Kenney and Lau methods.

To address the second question, it is proposed to use the hydromechanical criterion examined in Chapter 5. The concept was first identified by Moffat (2005), who postulated a hydromechanical envelope for four soils at which the onset of internal instability initiated. The idea of a hydromechanical criterion has not yet been well established. In this chapter, beyond Moffat's work, use of the hydromechanical envelope is further advanced based on the stress reduction concept of Skempton and Brogan (1994). A novel unified approach combining a hydromechanical index and geometric indices is then proposed to evaluate internal instability.

6.2 Susceptibility of a soil to internal instability

To evaluate the susceptibility of a soil to internal instability, empirical geometric criteria have been widely used in professional practice. In this section, experimental data from the current study (section 6.2.1) and other studies in the literature (section 6.2.2) are used to evaluate these geometrical criteria. Comparing these empirical rules allows the relative conservatism of each approach to be established, which has some implications for their application to engineering practice. Finally, a new semi-empirical method based on a capillary tube model is proposed to evaluate the potential for internal instability.

6.2.1 Geometric analysis: current study

The six gradations examined in this study are evaluated using the Kezdi method, the Kenney and Lau method, and the Burenkova method. A summary of the evaluations of internal stability using these methods is given in Tables 6.1 – 6.5.

6.2.1.1 Kezdi method (1979)

The Kezdi method involves splitting a gradation into a coarser fraction and a finer fraction at any arbitrary point along its grain size distribution curve, and checking Terzaghi's filter criterion is satisfied for an internally stable soil (see Chapter 2):

$D'_{15}/d'_{85} < 4$ (6.1)

where, D'_{15} is the diameter for 15% mass passing in the coarser fraction and d'_{85} is the diameter for 85% mass passing in the finer fraction. It has also formed the basis for Sherard's (1979) recommendation that D'_{15}/d'_{85} be less than 4 to 5. Accordingly, both methods are essentially the same, and the latter being less severe.

In reality, it is not necessary to separate the original gradation curve into two parts, because the d'_{85} and D'_{15} can be obtained directly from the original gradation curve. At an arbitrary point S_0 (see Figure 6.2), the corresponding mass passing is F_0. According to the definition, the mass passing (%) for the finer fraction can be expressed as, $F_f = 100F / F_0$, and the mass passing for the coarser fraction can be expressed as $F_c = 100(F - F_0)/(100 - F_0)$. Therefore, at d'_{85}, the mass passing $F = 0.85F_0$, and at D'_{15}, the mass passing $F = 0.85F_0 + 15$. Accordingly, the grain size d'_{85} of the finer fraction and D'_{15} of the coarser fraction can be read from the original gradation curve using

$$d'_{85} = D_{0.85F_0} \quad (6.2)$$

and

$$D'_{15} = D_{0.85F_0+15} \quad (6.3)$$

and providing the filter ratio D'_{15}/d'_{85} along the gradation curve. It is noted that mass increment H over D'_{15} and d'_{85} is constant and equal to 15% (Figure 6.2).

The variation of filter ratio D'_{15}/d'_{85} with mass passing for each of the six gradations tested (see Figure 3.12) is shown to F = 40% in Figure 6.3. The maximum value of filter ratio D'_{15}/d'_{85} is summarized in Tables 6.2 and 6.3. Inspection shows $(D'_{15}/d'_{85})_{max} > 4$ for each gradation. Accordingly, they are all classified as internally unstable by the Kezdi method. It is interesting to note that gradation HF10, which satisfies the gradation requirement of a 'Fuller' curve, was classified as internally unstable. Milligan (1986) pointed out that 'Fuller' curve should be internally stable. Kenney and Lau (1986), and the current test study, confirm the 'Fuller' curve is internally stable. However, the Kezdi method condemns it as internally unstable, as does the Sherard criterion. This raises an interesting question for use of the Kezdi method.

To summarize, the Kezdi method produces 5 correct evaluations for the 6 gradations examined in this study. The method condemns one stable gradation (HF10) as unstable; therefore, it appears to be a little conservative in its evaluation of potential for internal instability.

6.2.1.2 Kenney and Lau method (1986)

The Kenney and Lau (1985, 1986) criterion was proposed to assess the internal stability of granular soils by analyzing the shape of the grain size distribution curve. Its shape is described using the mass increment (H) that occurs over a designated grain size interval of D

to 4D compared to the mass passing (F) at grain size D. If the grading curve (the H-F plot) lies below a boundary defined by H = 1.0F (Kenney and Lau, 1986), over a portion of its finer fraction given by F ≤ 20% for soils with a primary fabric that is widely-graded ($C_u > 3$), and by F ≤ 30% for soils with a primary fabric that is narrowly-graded ($C_u \leq 3$), then it is deemed potentially unstable.

H-F curves for the six gradations are shown in Figure 6.4. Since $C_u \leq 3$ in the primary fraction of all gradations except HF10, internal instability is evaluated to F ≤ 30%. All H-F curves, except HF10, plot below the Kenney and Lau boundary. HF10, a 'Fuller' curve, defines the empirical boundary between internally stable and unstable gradations (Kenney and Lau, 1986). The five gap-graded gradations lie below the boundary, two of them yielding $(H/F)_{min} = 0$. All unstable soil gradations are correctly classified as unstable by the Kenney and Lau method (see Table 6.1). The method, therefore, appears to be successful in its evalutation of potential for internal stability.

6.2.1.3 Burenkova method (1993)

Burenkova (1993) proposed a method to assess the internal stability of granular soils, wherein a soil was deemed stable if the finer particles fully filled the voids of the coarse fraction that constitutes the primary fabric (see Chapter 2). Two conditional factors of uniformity, h' and h", are used in the evaluation. If h' and h" satisfy the following relation, the soil is considered internally stable:

$$0.76\lg(h'') + 1 < h' < 1.86\lg(h'') + 1 \qquad (6.4)$$

where,

$$h' = d_{90} / d_{60} \quad (6.5a)$$

$$h'' = d_{90} / d_{15} \quad (6.5b)$$

The plot of h" versus h' for each of the six gradations is shown in Figure 6.5. Gradations FR7, FR8, HF01 and HF05 plot in the unstable zones, while gradations HF03 and HF10 plot in the stable zone. It is interesting to note that gradation HF10, a "Fuller" Curve, again lies on one of the boundaries. Consider now the five unstable soil gradations, four of which are correctly evaluated by the Burenkova method (see Table 6.4). The exception is the unstable gradation HF03, which is classified as stable (Figure 6.5). Although the method works reasonably well, it appears to be a little unconservative in its evaluation of potential for internal stability.

6.2.2 Geometric analysis: literature database

The preceding discussion of data from the current study suggests we can have reasonable confidence in using the Kezdi (1979), Kenney and Lau (1986), and Burenkova (1993) methods to evaluate the internal stability of soils. To gain more confidence in using these methods, experimental data reported in the literature are evaluated using these same three methods in this section. As a result, a total of 56 gradations from 7 studies, in addition to the 6 gradations of the current study, are reviewed in this section.

The 56 gradations comprise 14 from Kenney and Lau (1985), 4 from Skempton and Brogan (1994), 13 from Honjo et al. (1996), 4 from Khan (2003), 9 from Liu (2005), 8 from Mao (2005) and 4 from Moffat (2005). Gradations from these studies are shown in Figures 6.6 -

6.12. Kenney and Lau (1985) conducted permeameter tests on widely-graded sandy gravels. A low surcharge pressure of 10 kPa was applied, with downward seepage at an unspecified gradient. Mild vibration, in the form of manual tapping, was imposed throughout the test. Honjo et al. (1996) tested gap-graded soils with a finer fraction less than 40 %, predominantly sands in which the medium sand fraction was absent. A light surcharge of 0.9 kPa was applied to the specimen, and unidirectional flow was imposed in a downward direction together with gentle tapping to vibrate the specimen. Skempton and Brogan (1994), Mao (2005), and Liu (2005) report findings from tests on sandy gravels using a similar test methodology: upon saturation of the reconstituted specimen in a permeameter, unidirectional flow was imposed in an upward direction and increased until piping occurred. Khan (2003), Moffat (2005) and the current study examined gap-graded and widely-graded specimen of glass beads or soil. A surcharge pressure between 25 and 150 kPa was applied, and unidirectional flow was imposed in an upward or downward direction and increased until internal instability occurred.

The 62 gradations of the combined experimental database, including 6 gradations from the current study, are categorized into two groups: 29 gap-graded specimens (see Tables 6.2 and 6.4) and 33 widely-graded specimens (see Tables 6.3 and 6.5). A gap-graded soil is one defined by a broad gradation in which a distinct portion is significantly under-represented or completely absent. An evaluation of these gradations using the Kezdi (1979), Kenney and Lau (1986) and Burenkova (1993) methods is presented below.

6.2.2.1 Kezdi method (1979)

Gap-graded test specimens

A total of 29 gap-graded soils are evaluated using the Kezdi method. The value of $(D'_{15}/d'_{85})_{max}$ and its corresponding mass passing F (%) are reported for each gradation in Figure 6.13. Inspection shows that a value of $(D'_{15}/d'_{85})_{max} \geq 4$ in all of 22 unstable gradations, and $(D'_{15}/d'_{85})_{max} \leq 4$ in 5 of 7 stable gradations (see Table 6.2).

Consider now the two exceptions, namely G1-a and G1-b, both of which are gap-graded materials from Honjo et al. (1996). It is noted that $(D'_{15}/d'_{85})_{max}$ in these two gradation occurs within the finer fraction (F = 5 and 6%, respectively). It is believed that a gap location is the intrinsically correct division point between the coarser fraction and finer fraction of a gap-graded material. Re-evaluating the filter ratio D'_{15}/d'_{85} at the gap location yields the plot of Figure 6.14. Inspection shows that a value of $(D'_{15}/d'_{85})_{gap} > 4$ in all 22 unstable gradations, and $(D'_{15}/d'_{85})_{gap} < 4$ in all 7 stable gradations (see Table 6.2). The evaluation is in complete agreement with the outcome of all the laboratory tests. This seems entirely reasonable, given the origin of Terzaghi's filter rule for a uniform filter against a uniform base. Therefore, the Kezdi method provides a suitable guide to evaluate the internal stability of gap-graded soils in which there is clear division point between the finer and coarser particles.

Widely-graded test specimens

A total of 33 widely-graded soils are evaluated using the Kezdi method. The value of $(D'_{15}/d'_{85})_{max}$ and its corresponding mass passing F (%) are reported for each gradation in Figure 6.15. Inspection shows a value of $(D'_{15}/d'_{85})_{max} > 4$ in 18 of 19 unstable gradations,

and $(D'_{15}/d'_{85})_{max} \leq 4$ in 8 of 14 stable gradations (see Table 6.3). This represents a variable success, in which most of the unstable soils are correctly identified, and also many but not all of the stable soils.

Consider now the one exception for the unstable gradations, namely Soil A from Kenney and Lau (1985). This gradation was the subject of some discussion since an attempt to replicate the test by Sherard and Dunnigan (1986) suggested it was stable, while an additional test by Kenney and Lau (1986) on the same gradation confirmed it to be unstable. Consider now the six exceptions for the stable gradations, namely Soils 1, 2, 3 from Kenney and Lau (1985), Soil C from Skempton and Brogan (1994), Soil 5' from Liu (2005) and HF10 from the current study. It is interesting to note that $(D'_{15}/d'_{85})_{max} > 4$ occurs within $F < 10\%$ for all these stable gradations (see Figure 6.15 and Table 6.3).

The Kezdi method correctly evaluates most of the unstable gradations, but it condemns 6 stable gradations as unstable. Thus, the Kezdi method appears a little conservative in evaluating the potential for internal stability in widely-graded soils.

6.2.2.2 Kenney and Lau method (1986)

Gap-graded test specimens

A total of 29 gap-graded soils are similarly evaluated using the Kenney and Lau method. The $(H/F)_{min}$ point on the H-F curves is plotted in Figure 6.16. Inspection shows a value of $(H/F)_{min} < 1$ in all 22 unstable gradations, and $(H/F)_{min} \geq 1$ in 5 of 7 stable gradations (see also Table 6.2). The evaluation is not in complete agreement with the laboratory tests,

because two stable soils are deemed to be unstable. Consider these two exceptions, namely G1-c and G1-d from Honjo et al. (1996): the $(H/F)_{min}$ occurs at F = 30% for both gradations.

The Kenney and Lau method correctly evaluates all unstable gradations, while it condemns two stable gradations as unstable. Therefore, the Kenney and Lau method is deemed to provide a conservative assessment of potential for internal stability in gap-graded soils.

Widely-graded test specimens

A total of 33 widely-graded soils are also evaluated using the Kenney and Lau method. The $(H/F)_{min}$ point on the H-F curve is plotted in Figure 6.17. Inspection shows a value of $(H/F)_{min} \leq 1$ for all 19 unstable gradations, and $(H/F)_{min} \geq 1$ in 12 of 14 stable gradations (see also Table 6.3). Consider now the two exceptions: one is gradation A_s from Kenney and Lau (1986) and the other is gradation 5' from Liu (2005). It is interesting to note that Kenney and Lau (1986) acknowledge gradation A_s, for which $(H/F)_{min} = 0.9$ at F = 25 %, is an exception to the formulation of their original empirical boundary to stability at H/F = 1.0. Yet the Kezdi method correctly established it as internally stable given a value of $(D'_{15}/d'_{85})_{max} = 3.7$ at F = 5% (see Table 6.3). This raises the interesting possibility of combining some aspects of the two empirical methods. The combination of two methods is discussed in Section 6.2.3.

The Kenney and Lau method correctly evaluates all unstable gradations, while it condemns two stable gradations as unstable. Therefore, the method appears a little conservative in evaluating the potential for internal stability in widely-graded soils.

6.2.2.3 Burenkova method (1993)

Gap-graded test specimens

Once again the total of 29 gap-graded soils is evaluated using the Burenkova method. The plot of h" versus h' for each gradation is shown Figure 6.18. Inspection reveals that 19 of 22 unstable gradations plot within the unstable zones, and 2 of 7 stable gradations plot within the stable zone. Accordingly, the evaluation is not in complete agreement with the outcome of the laboratory tests. Three unstable gradations plot within in the stable zone (HF03 of the current study, and Moffat's T0 and T5) (see Table 6.4). This method, therefore, appears to be somewhat unconservative in evaluating the potential for internal stability in gap-graded soils.

Widely-graded test specimens

Finally, the 33 gap-graded soils are evaluated using the Burenkova method. The plot of h" versus h' for each gradation is shown Figure 6.19. Inspection shows that 17 of 19 unstable gradations plot within the unstable zones, and 8 of 14 stable gradations plot within the stable zone. The evaluation is not in complete agreement with the laboratory test results. Two unstable gradations (the Liu (2005) gradation 26 and the Mao (2005) gradation b) plot within the stable zone. This method, therefore, also appears to be unconservative in evaluating the potential for internal stability in widely-graded soils.

In totality, the Burenkova method correctly evaluates 36 of 41 unstable gradations and 10 of 21 stable gradations. The findings suggests there is not a clear boundary between the internally stable and unstable gradations in the plot of h" versus h' (Figures 6.18 and 6.19).

Hence, the Burenkova method appears to be less successful than the Kezdi method and the Kenney and Lau method.

6.2.3 Comparison of the Kezdi and the Kenney and Lau methods

The preceding evaluation of experimental data from 8 studies in 4 countries (Section 6.2.2) has found the Kezdi method to be most successful in evaluating gap-graded soils if the method is applied to the gap location, while the Kenney and Lau method proves more successful in evaluating widely-graded soils. Both of the methods are a little conservative: in particular, the Kezdi method is conservative at $F < 15\%$, while the Kenney and Lau method is conservative at $F > 20$ %. A theoretical comparison of the two methods is now considered in order to give more confidence in their use.

Both methods are based on analysis of the grain size distribution curve. Chapuis (1992) has demonstrated that the two methods take similar mathematical expressions, where the secant slope of the grain-size distribution curve indicates the likelihood of internal instability. More specifically, the Kezdi criterion can be expressed as “the slope is steeper than 15% per 4 times change in grain size”, and the Kenney and Lau criterion can be expressed as “the slope is steeper than F% per 4 times change in grain size” (see Figure 6.20). An evaluation of the similarities and differences of the two methods is reported below, and used to better understand the relative conservatism of each approach.

The common feature of both methods is the examination of the slope of the gradation curve over a discrete interval of its length. The difference arises from the criterion used to establish

the size of that interval: one approach uses a constant increment of percent finer by mass while, in contrast, the other uses a variable increment of grain size. More specifically, the D'_{15}/d'_{85} filter ratio of Kezdi (1979) is calculated, by its very definition, over the constant increment of H = 15 % at any point along the gradation curve (see Figure 6.20). It implies a theoretical boundary to instability that is a linear relation on the semi-log plot of grain size. In contrast, the H/F stability index of Kenney and Lau (1985, 1986) is calculated over the increment 4D - D, which increases in magnitude with progression along the gradation curve. It therefore implies a theoretical boundary to instability that is a non-linear relation and concave upwards in shape.

A plot of the respective Kezdi and Kenney and Lau boundaries, in F: H space, is given in Figure 6.21. At values of F > 15 %, the method of Kenney and Lau defines a boundary curve to internal instability that locates above that of the Kezdi method. Conversely, the method of Kezdi defines a boundary above that of the Kenney and Lau method at F < 15 %. The suggested limit values to stability of D'_{15}/d'_{85} = 4 and H/F = 1 yield a unique point on the gradation curve, where the both criteria converge at F ≈ 15 % (see Figure 6.21). By inspection, the Kenney and Lau criterion is the more conservative of the two methods at F > 15 %, while the Kezdi criterion is more conservative at F < 15 %.

6.2.4 Combination of the Kezdi and the Kenney and Lau methods

Theoretical comparison of the Kezdi and the Kenney and Lau methods has shown each method exhibits a degree of conservatism. Application of the two methods to the literature database also shows the two methods have mixed success in assessment of internal stability

for gap-graded and widely-graded soils (see section 6.2.2). These observations raise the interesting possibility of combining some aspects of the two empirical methods.

6.2.4.1 On a revision to the Kezdi method

The Kezdi method is very successful in evaluating internal stability of gap-graded soils when the filter ratio D'_{15}/d'_{85} is calculated at the gap location, rather than taken as the maximum D'_{15}/d'_{85} ratio (see Figures 6.13 and 6.14). This suggests that, if there is a fairly clear division point between the coarser and finer fractions, the method is a good guide to instability potential (Skempton and Brogan, 1994). However, for the case of a widely-graded soil, there is not such a clear division point between coarser and finer fraction. Furthermore, the method has proven conservative in evaluating internal stability in widely-graded soils because it condemns 6 of 14 stable gradations as unstable (at the lower finer fraction F < 10%) (see Figure 6.15). In particular it condemns the 'Fuller' Curve as an unstable gradation, which is believed to be internally stable (Kenney and Lau, 1986).

Consider now the argument that the point where the H/F ratio is minimum is the most critical point on the grain size curve, and therefore its potential to identify the most influential division point between coarser and finer fraction. Accordingly, a new technique to evaluate an index value of filter ratio D'_{15}/d'_{85} is proposed here: calculate the filter ratio D'_{15}/d'_{85} at the point (F_n, %) on the grain size curve defined by the minimum of H/F, $(H/F)_{min}$ (see Table 6.3, columns 5 and 9), rather than the reporting of $(D'_{15}/d'_{85})_{max}$ wherever it occurs on the curve (see Table 6.3, columns 3 and 7). The value of D'_{15}/d'_{85} at $(H/F)_{min}$ is plotted against the corresponding mass passing F (%) for widely-graded soils is shown in Figure 6.22. The

stable and unstable gradations are clearly separated by the Kezdi threshold value. This qualifier on the Kezdi method leads to 18 of the 19 unstable soils again yielding a $D'_{15}/d'_{85} \geq 4$, but also 13 of 14 of the stable soils yielding a $D'_{15}/d'_{85} \leq 4$. Comparison with the original technique (see Figure 6.15 and Table 6.3) indicates this qualifier to the Kezdi method, drawn from the Kenney and Lau technique, yields a significant improvement to the agreement between empirical rule and experimental observation in testing.

In summary, the Kezdi method is demonstrated to be very successful in evaluating the internal stability of both gap-graded and widely graded soils using the proposed qualifier (Figures 6.14 and 6.22) whereby the filter ratio D'_{15}/d'_{85} is evaluated either at the gap location for the gap-graded soils or at the $(H/F)_{min}$ location for widely-graded soils. This revision leads to 40 of the 41 unstable soils yielding a $D'_{15}/d'_{85} \geq 4$ and 20 of 21 stable soils yielding a $D'_{15}/d'_{85} \leq 4$.

6.2.4.2 On a revision to the Kenney and Lau method

Merits of unifying some aspects of the Kezdi and Kenney and Lau methods are further examined in Figure 6.23, where the respective values of H and F obtained at $(H/F)_{min}$ are plotted, together with a depiction of the two boundaries to instability established by means of the respective empirical rules (see Figure 6.21). The data are those reported for gap-graded soil in Table 6.2 and widely-graded soils in Table 6.3, from 8 experimental studies (Kenney and Lau, 1985; Skempton and Brogan, 1994; Honjo et al., 1996, Khan, 2003, Liu, 2005, Mao, 2005, Moffat, 2005, Li, current), for a total of 41 unstable soils and 21 stable soils.

Additionally, six unstable sandy gravels reported by Skempton and Brogan (1994) are also included (Table 6.6).

Inspection suggests the Kenney and Lau criterion of $H/F \leq 1$ yields a more precise distinction between stable and unstable gradations at $F < 15$ %. At higher values of F (%) it provides an overly conservative evaluation, since four gradations are deemed unstable but found to be stable from testing. In contrast, the Kezdi criterion yields a more precise distinction at $F > 15$ %. There is only one overly conservative evaluation of a gradation deemed unstable and found stable (Liu's soil 5', see Table 6.3). The other exception is an unstable gradation that locates above the $H = 15$ % boundary and is therefore deemed stable (Soil A, see Table 6.3). Interestingly this gradation was the subject of some discussion because an attempt to replicate the test by Sherard and Dunnigan (1986) suggested a very similar gradation was indeed stable, and yet an additional test by Kenney and Lau (1986) on the same gradation confirmed it to be unstable.

In summary, the Kenney and Lau method appears very successful in evaluating the internal stability of a soil with inclusion of a modified boundary (Figure 6.23) defined by $H = F$, when $F \leq 15\%$, and $H=15\%$, when $F \geq 15\%$. This revision produces 40 correct evaluations of the 41 unstable soils, and 20 correct evaluations of the 21 stable soils.

6.2.5 Modified Kovacs criterion - capillary tube model

As illustrated in Figure 6.1, internal stability of a soil is evaluated by comparing a particle size of the finer fraction (d) and pore size constriction of the coarser fraction (D_c). If $d < D_c$, the finer particles have potential to be transported within the void network constituted by the coarser particles. The Kenney and Lau and the Kezdi criteria are empirical methods, which indirectly measure the pore size of the coarser fraction. In this section, a more comprehensive and semi-empirical approach is proposed to evaluate the phenomenon of internal stability. It involves the theoretical capillary tube model to describe the pore size constriction of the coarse fraction (see Chapter 2). This model has some advantages over empirical rules, because it considers the effects of (1) grain size distribution; (2) particle shape and (3) soil porosity.

Kovacs (1981) first suggested the capillary tube model to assess the internal stability of granular soils (see Chapter 2). The boundary between the stable and unstable can be expressed as,

$$d'_{85} = BO_{50}; \tag{6.6}$$

where, d'_{85} = a representative diameter of the finer fraction, O_{50} = the average capillary tube diameter of the coarser fraction, and B = a constant, taken as 1.

As before,

$$d'_{85} = D_{0.85F_n} \tag{6.7}$$

and Kovacs (1981) suggested,

$$O_{50} = 4\frac{n_c}{1-n_c}\frac{D_h^e}{\alpha_D} \tag{6.8}$$

where α_D = shape coefficient (6 for rounded particle, 7 ~ 9 for angular particle); n_c = porosity of skeleton; F_n = mass passing (%) at diameter D_n, which separates the finer fraction and coarser fraction; and D_h^c = Kozeny effective diameter of the coarse fraction. More details on the formulation of Eq. 6.8 can be found in Appendix F. D_h^c and n_c can be calculated using,

$$n_c = n + F_n (1-n) \tag{6.9}$$

$$D_h^c = \frac{1}{\sum \frac{\Delta F_i^c}{D_i^c}} \tag{6.10}$$

where n = porosity of a soil, D_i^c = average diameter in the i-th interval of the particle size distribution curve of the coarse fraction, and ΔF_i^c = the weight of grains in the i-th interval of the particle size distribution curve of the coarse fraction.

To apply the model, we need to know where to split a gradation (F_n) and where to establish the boundary location (B) between stable and unstable gradations. Kovacs (1981) suggested splitting a gradation into a coarser fraction and a finer fraction at any arbitrary point along its grain size distribution curve, and finding the minimum d'_{85}/O_{50} ratio to assess internal stability. This technique is time-consuming. The boundary suggested by Kovacs (B = 1) does not consider differences between the ideal straight capillary tube model and the actual soil sample. These differences may be caused by (1) tortuosity of porous media, (2) the interconnectivity of pores and (3) variation of cross-sectional areas of pores (Kovacs, 1981). Therefore, this suggested approach for evaluation of internal stability is only conceptual and

has not verified by experimental data. A new technique to determine F_n, and a new boundary between the internal stable and unstable gradations, is proposed in this section.

As noted previously, in qualifying the use of the Kezdi method, it appears the most influential point on the gradation curve is at the gap location for a gap-graded soil and at $(H/F)_{min}$ location for a widely-graded soil. Exactly the same technique is now adopted for the capillary tube model, thereby enabling a representative diameter of the finer fraction (d'_{85}) and the average capillary tube diameter of the coarser fraction (O_{50}) to be calculated using Eqs.6.7 – 6.10. Details of the procedure for calculation of d'_{85} of the finer fraction and O_{50} of the coarser fraction are shown in Figure 6.24.

Consider the boundary between the stable and unstable gradations. Its location for the capillary tube model is determined with reference to the experimental database that has been compiled in this study from the literature (Kenney and Lau, 1985, Skempton and Brogan, 1994, Honjo et al., 1996, Khan, 2003, Moffat, 2005, Liu, 2005 and the current study). The analysis is carried out using only database results for specimens whose density or porosity is given in the references. The maximum finer fraction of interest is taken as less than 35 %, since for $F \geq 35$ %, the coarser grains are believed to float in a matrix of finer grains (Skempton and Brogan, 1994; Vallejo, 2001), rendering Eq. 6.9 invalid. Accordingly, the experimental database is reduced from 62 to 40 test results.

A summary of results obtained using the capillary tube model is reported in Table 6.7. The variation of O_{50} with d'_{85} is plotted in Figure 6.25. A narrow boundary is defined between the internally stable and unstable test specimens, defined by:

$$d'_{85} = 0.42 O_{50} \qquad (6.11)$$

implying B = 0.42.

The theoretical capillary tube model with the empirical rule for gradation-splitting, seems to provide an excellent assessment of potential for internal stability of these granular soils. Two stable gradations plot just below the boundary, which is, therefore, a little conservative. In summary, the constriction ratio d'_{85}/O_{50} can be used to evaluate internal instability: if $d'_{85}/O_{50} > 0.42$, the soil is considered potentially internally stable.

6.3 Hydromechanical index and hydromechanical envelope

Given an improved geometric index to evaluate the potential for internal instability, the challenge becomes one of developing a companion hydromechanical index to evaluate the susceptibility and, ideally, then unifying it with the geometric index. Experimental work has demonstrated the onset of internal instability is governed by the combined effect of critical hydraulic gradient (i) and effective stress (σ') (Moffat, 2005). Accordingly, any attempt to establish a hydromechanical envelope must account for critical hydraulic gradient (i) and effective stress (σ').

The role of effective stress (σ') on mobility of the finer fraction was recognized by Skempton and Brogan (1994), who postulated the stress reduction concept (α concept). Previous work at UBC (Moffat, 2005) has confirmed experimentally a linear relation between critical hydraulic gradient and mean vertical effective stress for four soils. Given the additional data of the current study and those of the compiled experimental database, then it is an opportunity to use Skempton and Brogan's α concept to establish whether a hydromechanical threshold truly exists, and if so, define its characteristics.

6.3.1 The α concept: stress reduction

Skempton and Brogan (1994) reported findings from tests on well-graded and gap-graded sandy gravels. They found that for unstable sandy gravels, onset of internal instability of the sand grains occurred at hydraulic gradients one third to one fifth of the theoretical gradient for a uniform granular material of the same porosity, where,

$$i_{cr} = \alpha\, i_c \tag{6.12}$$

where, i_{cr} = the critical gradient for an internally unstable soil, and i_c = the gradient for an internally stable soil.

The phenomenon was attributed to a stress reduction on particles of the finer fraction. They postulated that effective stress in the finer particles of an internally unstable soil ($\sigma'_{f,vm}$) is only a proportion of the effective stress in the coarser particles (σ'_{vm}), where:

$$\sigma'_{f,vm} = \alpha\sigma'_{vm} \tag{6.13}$$

From this concept of stress reduction, the critical gradient is believed stress-dependent. A higher value of α for the soil yields a higher resistance to seepage-induced instability. Extending this concept, a theoretical hydromechanical envelope for seepage failure is now defined in the following section.

6.3.2 The concept of a hydromechanical envelope

The conditions at which seepage failure initiates are most easily illustrated using the concept of a hydromechanical path (Section 5.4). First, consider the response of an internally stable soil under seepage flow. Consider a soil layer with effective stress σ'_{t0} (Figure 6.26a), at hydrostatic condition ($i = 0$), the initial effective stress distribution is shown schematically in Figure 6.26b. The effective stress at the bottom of the layer is:

$$\sigma'_{b0} = \sigma'_{t0} + \gamma' \Delta z \tag{6.14}$$

At upward seepage flow ($i > 0$), the effective stress at the bottom of the layer decreases:

$$\sigma'_{b} = \sigma'_{t0} + \gamma' \Delta z - i\gamma_w \Delta z \tag{6.15}$$

It is assumed that the effective stress is linearly distributed with depth; therefore, the mean vertical effective stress in the soil layer can be expressed as,

$$\sigma'_{vm0} = 0.5\ (\sigma'_{t0} + \sigma'_{b0}) \tag{6.16}$$

$$\sigma'_{vm} = 0.5\ (\sigma'_{t0} + \sigma'_{b}) \tag{6.17}$$

Substituting Eqs.6.14 and 6.15 into Eqs.6.16 and 6.17, variation of mean vertical effective stress as a result of seepage flow is obtained:

$$\sigma'_{vm} = \sigma'_{vm0} - 0.5 i\gamma_w \Delta z \tag{6.18}$$

Eq.6.18 is a general expression for hydromechanical path, written in the normalized form as,

$$\bar{\sigma}'_{vm} = \bar{\sigma}'_{vm0} - 0.5i \qquad (6.19)$$

where, $\bar{\sigma}'_{vm} = \dfrac{\sigma'_{vm}}{\gamma_w \Delta z}$ = normalized mean vertical effective stress (see Chapter 5)

With help of hydromechanical path, the hydromechanical envelope can be developed. First, consider the response of a soil under self-weight loading ($\sigma'_{t0} = 0$) in a frictionless cell. With no flow (i = 0), the initial mean normalized effective stress ($\bar{\sigma}'_{vm0}$) is $0.5\gamma'\Delta z / \gamma_w \Delta z = 0.5\gamma'/\gamma_w$ (point A_i) (see Figure 6.28). With the imposition of upward seepage flow (i > 0), $\bar{\sigma}'_{vm}$ will decrease. When the seepage and resistance forces (self-weight) reach limit equilibrium ($\bar{\sigma}'_{vm}$ = 0), the hydraulic gradient is given by Terzaghi's theoretical value of γ'/γ_w (point A_s), and heave failure occurs. The line of A_iA_s represents the hydromechanical path of an internally stable specimen under seepage flow, with heave failure at A_s.

Now consider the normalized response of a series of stable specimens subject to upward seepage flow at different values of mean vertical effective stress. According to Eq.6.19, all hydromechanical paths are parallel to each other, with a slope $\Delta i / \Delta \bar{\sigma}'_{vm}$ = - 2 (see Figure 6.28). Heave failure initiates at the points A_s, B_s, C_s, etc. A line through these points defines the hydromechanical envelope for an internally stable soil, and can be expressed as,

$$i = 2(\bar{\sigma}'_{vm} + 0.5\gamma'/\gamma_w) \qquad (6.20)$$

Similarly, for an internally unstable soil, the condition at which instability occurs can also be illustrated with the aid of the hydromechanical path (Section 5.4). Stress distributions for an internally unstable material are illustrated in Figure 6.27. Consider a specimen subject to self-weight only ($\sigma'_{t0} = 0$), for which the hydromechanical path again starts at Point A_i (Figure 6.28). Prior to the onset of internal instability, the specimen behaves in the same manner as a stable material, and its hydromechanical path coincides with that defined earlier at a given vertical effective stress. Therefore, the hydromechanical path advances from A_i towards A_u. At point A_u, internal instability occurs at a hydraulic gradient = $\alpha \gamma'/\gamma_w$ (Figure 6.28), based on the postulation of Skempton and Brogan (1994).

Consider now the normalized response of a series of unstable specimens at different values of mean vertical effective stress, each with the same gradation. Based on the relation of $i_{cr} = \alpha\, i_c$, onset of internal instability occurs at points A_u, B_u, C_u, etc. (Figure 6.28). A line through these points defines the hydromechanical envelope for an internally unstable specimen. If α is constant for that gradation, based on the relation of Eq.6.12, the hydromechanical envelope for the internally unstable soil can be simply expressed as,

$$i = \frac{\alpha}{1-0.5\alpha}(\bar{\sigma}'_{vm} + 0.5\gamma'/\gamma_w) \qquad (6.21)$$

Eq.6.21 suggests the hydromechanical envelope is a function of α, and implies the slope of the envelope increases with the value of α. Furthermore, when α = 1, the envelope becomes $i = 2(\bar{\sigma}'_{vm} + 0.5\gamma'/\gamma_w)$, namely the boundary for internally stable specimen. When α = 0, the

slope of envelope $\Delta i / \Delta \bar{\sigma}'_{vm}$ = 0, and the specimen cannot bear any seepage gradient. For 0< α <1, stability of the specimen is governed by effective stress and hydraulic gradient.

As discussed in Chapter 5, mobilization of friction on the sidewall of the permeameter will influence the magnitude and distribution of vertical effective stress along the specimen in laboratory element tests. Therefore, a modification is required to establish the hydromechanical envelope in order to account for sidewall friction (see Appendix B). It causes Eq.6.21 to become,

$$i = \frac{\alpha}{1 - 0.5\alpha / A_c}(\bar{\sigma}'_{vm} + 0.5 A_c \frac{\gamma'}{\gamma_w}) \qquad (6.22)$$

where $A_c = 1 + 2 f_c \Delta z / D$, f_c = soil-wall friction at critical condition = K_0 *tan*(δ), D = diameter of specimen, Δz = thickness of soil layer. It is noted that for f_c = 0, A_c = 1, and Eq.6.22 reduces to Eq.6.21.

In concept the hydromechanical envelope establishes the boundary between the stable and unstable state in a soil that is potentially unstable and subject to seepage flow. If the seepage gradient in an element of soil reaches the boundary, internal instability will be triggered.

This theoretical analysis for the onset of internal instability using an extension to the α concept suggests a hydromechanical envelope exists for each soil gradation. A re-evaluation of previous work at UBC (Moffat, 2005,) and analysis of the current experimental data (see Chapter 5), confirm this hypothesis (Figures 5.31 and 6.29). These envelopes are governed

by α, and the slope of envelope increases with the value of α. Hence α appears a useful parameter for the idea of a hydromechanical index.

6.4 The onset of internal instability

Testing the hypothesis suggests there is a unique boundary in $i : \bar{\sigma}'_{vm}$ space for each gradation that is governed by a hydromechanical index (α). For practical purposes, it is attractive to correlate this hydromechanical index to the companion geometric index, for which three candidate measures have been evaluated ($(H/F)_{min,}$ D'_{15}/d'_{85}, d'_{85}/O_{50}). The objective is to devise an approach to evaluate conditions for the onset of internal instability knowing the grain size distribution of a soil. In order to do this, the value of α is required for a soil gradation. In this section, a method to determine α is first presented, whereupon a relation between α and various geometric indices is then examined. Finally, an approach is proposed to unify the geometric index and hydromechanical index in order to evaluate the internal instability of a soil.

The value of α can be determined only from a permeameter test in which the critical hydraulic gradient is measured. Current experimental results described in Chapter 5 show that a linear hydromechanical envelope exists for all 5 gradations tested at various stress loading (see Figure 5.31). The slope of the envelope is governed by the gradation shape. Based on the theoretical envelope defined by Eq. 6.22, a value of α for each gradation can be back-calculated from the corresponding envelope. The summary of these results is given in Table 6.8a, based on Figure 5.31, and a re-plotting of the Moffat (2005) data using the normalized mean effective stress against critical gradient (Figure 6.29).

Skempton and Brogan (1994) and Liu (2005) reported critical hydraulic gradient (i_{cr}) and specimen properties in their seepage flow tests, which are compiled in Table 6.8b. The top of the specimen was not subject to any stress (σ'_{t0} = 0) in these tests. Gradation HF01 of the current study is also in Table 6.8b since it was conducted in order to replicate the Skempton and Brogan (1994) gradation A. The theoretical critical gradient (i_c) at the appropriate void ratio is calculated based on Terzaghi's theory, using

$$i_c = (G_s\text{-}1)(1\text{-}n) \qquad (6.23)$$

The value of α was again back-calculated for each gradation, using Eq.6.12, and the results reported in Table 6.8b.

6.4.1 Relation between α and geometric indices

Studies show that the grain size distribution curve of a soil has influence on the initiation of internal instability (Skempton and Brogan, 1994, Moffat, 2005). Skempton and Brogan (1994) described a tentative relation between critical hydraulic gradient to cause 'segregation piping' and the geometric index $(H/F)_{min}$ (see Chapter 2). Moffat (2005) established the concept of a hydromechanical envelope, and found it to vary with grain size distribution curve. The current study has extended that finding to a normalized plot, from testing of additional gradations in two permeameters (see Figure 5.31 and Figure 6.29). As explained in Section 6.3, the hydromechanical envelope of a particular gradation is believed a function of α. Therefore, α influences the initiation of internal instability. In this section, the analysis is further advanced to identify a relation between α and three geometric indices, namely

$(H/F)_{min}$ (from Kenney and Lau, 1985), D'_{15}/d'_{85} (from Kezdi, 1979) and d'_{85}/O_{50} (from Kovacs, 1981).

6.4.1.1 Relation between α and $(H/F)_{min}$

A plot of α against $(H/F)_{min}$ for the current test data is shown in Figure 6.30. Inspection shows an apparent linear relation between α and $(H/F)_{min}$: α increases with increase of $(H/F)_{min}$. Gradation HF10, a 'Fuller' curve, is internally stable. It exhibits $\alpha = 1.0$. Gradations FR8 and FR7 are gap-graded, yielding $(H/F)_{min} = 0$, and $\alpha < 0.1$. It seems that α is strongly dependent on the ratio of $(H/F)_{min}$.

This relation between α and $(H/F)_{min}$ is further examined with reference to three other studies see Figure 6.31. Inspection now shows considerable scatter in the test data and, in contrast to Figure 6.30, a definite relation between α and $(H/F)_{min}$ cannot be discerned easily. Moffat (2005) and the current study use the same specimen reconstitution technique (described in Chapter 3); interestingly, a nearly linear relation is found between α and $(H/F)_{min}$ in those two data sets (triangle and square points). Skempton and Brogan (1994) used a moistened specimen reconstitution technique without compaction; three of the four test data fit well with the current study, while one of them is much lower than the postulated trend line (circle points). The specimen reconstitution technique used by Liu (2005) is unknown: five of eight test data from that study yield reasonable agreement with the trend line of the current study (Figure 6.30). It seems the relation between α and $(H/F)_{min}$ is not unique, a finding that is attributed to the influence of specimen reconstitution technique, porosity or other matters.

6.4.1.2 Relation between α and D'_{15}/d'_{85}

A plot of α against D'_{15}/d'_{85} for the current test data is shown in Figure 6.32. Inspection again reveals some scatter in the data and a non-linear relation between α against D'_{15}/d'_{85}, wherein α decreases with increase of D'_{15}/d'_{85}. Values of α for the two glass beads specimens (FR8 and FR7) plot below those for the soils. The difference is tentatively attributed to a relatively lower shear resistance in these rounded particles compared to the more angular soil particles. Notwithstanding the scatter it seems that α is dependent on the D'_{15}/d'_{85} for a certain type of soil.

This relation between α and D'_{15}/d'_{85} is further examined with reference to the same three other studies, see Figure 6.33. The D'_{15}/d'_{85} ratio is calculated at $(H/F)_{min}$ location for a widely-graded material or at the gap location for a gap-graded material. Inspection again shows a non-linear relation between α and D'_{15}/d'_{85}: α decreases with increasing D'_{15}/d'_{85}. A relatively good correlation between α and D'_{15}/d'_{85} can be observed for soils. The relation between α and D'_{15}/d'_{85} yields $\alpha = 6/(D'_{15}/d'_{85})^{1.5}$, with a correlation coefficient $R^2 = 0.63$.

6.4.1.3 Relation between α and d'_{85}/O_{50}

A plot of α against d'_{85}/O_{50} for the current test data is shown in Figure 6.34. Considering the boundary between the unstable and stable gradations defined by the capillary tube model (Eq. 6.11), the relation is established though $d'_{85}/O_{50} = 0.42$ at $\alpha = 1$. Inspection shows a nearly linear relation between α and d'_{85}/O_{50}: α increases with increasing d'_{85}/O_{50}. It seems that α is strongly dependent on the ratio of d'_{85}/O_{50}.

This relation between α and d'_{85}/O_{50} is once again examined with reference to the other three studies, see Figure 6.35. The d'_{85}/O_{50} ratio is calculated at $(H/F)_{min}$ location for a widely-graded material or at the gap location for a gap-graded material. Inspection confirms the same linear relation between α and d'_{85}/O_{50}, which appears to describe the data for soils and also glass beads. It can be expressed as $\alpha = 3.85(d'_{85}/O_{50}) - 0.616$, and yields a the correlation coefficient $R^2 = 0.74$. This improved correlation is attributed to a consideration of porosity and particle shape in the formulation of the capillary tube model.

From the above discussion, it can be seen that α is a function of geometric index. By inspection, the d'_{85}/O_{50} and D'_{15}/d'_{85} indices yield a better correlation than $(H/F)_{min}$. The index d'_{85}/O_{50} index takes account of the effect of grain size distribution, porosity and particle shape, and therefore yields the best correlation with α.

6.4.2 Unified approach for evaluation of internal stability

The tentative relation between the hydromechanical index α and the various geometric indices described in Section 6.4.1 provides a means to evaluate the onset of internal instability. The basis for this unified approach is illustrated in Figure 6.36. Knowing the shape of grain size distribution curve, the division point between its coarser and finer fraction (F_n) can be determined based on a simple rule: for gap-graded soils, F_n is taken at the gap location; for widely-graded soils, F_n is taken at the $(H/F)_{min}$. The relevant geometric index, D'_{15}/d'_{85} or d'_{85}/O_{50} (if porosity n is known), is then determined for that division point on the gradation curve. Knowing the relation between D'_{15}/d'_{85} and α (Figure 6.33) or d'_{85}/O_{50} and α

(Figure 6.35), enables the relevant value of α to be established. Knowing the α-value permits the hydromechancial boundary for the gradation to be determined (based on Eq. 6.21) in the i : $\bar{\sigma}'_{vm}$ space. If the imposed seepage gradient in an element reaches this boundary, then internal instability is expected to occur.

6.5 Summary

In this chapter, three commonly used geometric criteria, those of Kezdi (1979), Kenney and Lau (1986) and Burenkova (1993), are assessed using an experimental database of 62 gradations. It is found that the Kezdi method proves relatively more successful in the evaluation of gap-graded soils, and the Kenney and Lau method proves relatively more successful in the evaluation of widely graded soils. A combination of the Kezdi and the Kenney and Lau methods yields a moderate improvement in the success of both of methods. The Burenkova method proves less conservative than both the Kezdi and the Kenney and Lau methods.

A modified Kovacs's capillary tube model is proposed to assess the potential for internal instability in a soil. A constriction ratio of d'_{85}/O_{50} is suggested as a geometric index. The narrow boundary between the internally stable and unstable materials is identified as $d'_{85}/O_{50} = 0.42$.

In this chapter, α, a stress reduction factor, is proposed as a hydromechanical index. Hydromechanical envelope is found to be a function of α. The relation between α and geometric index D'_{15}/d'_{85} or d'_{85}/O_{50} is established by examining the experimental database

(Figures 6.33 and 6.35). Therefore, the hydromechancial envelope for a soil can be determined knowing the gradation of soil. The approach combining the geometric and hydromechanical indices is proposed to evaluate the onset of internal instability.

Table 6.1 Assessment of internal stability on current specimens

Test code	Laboratory results	Assessment of internal stability		
		Kezdi (1979)	Kenney & Lau (1986)	Burenkova (1993)
FR8	U	U	U	U
FR7	U	U	U	U
HF01	U	U	U	U
HF03	U	U	U	S
HF05	U	U	U	U
HF10	S	U	S	S

Note: The values of D'_{15}/d'_{85} and $(H/F)_{min}$ are reported in Tables 6.2 and 6.3. U = Unstable and S = Stable;

Table 6.2 Evaluation of internal stability of gap-graded soils by Kezdi (1979) and Kenney and Lau (1986) methods

Reference	Unstable				Stable			
	Gradation	$(D'_{15}/d'_{85})_{max}$	(D'_{15}/d'_{85}) at gap	$(H/F)_{min}$	Gradation	$(D'_{15}/d'_{85})_{max}$	(D'_{15}/d'_{85}) at gap	$(H/F)_{min}$
Skempton & Brogan (1994)	A	12.7@5	10.9@15	0.1@15				
Honjo et al. (1996)	G3-a	6.7@6	5.2@20	0@20	G2-a	3.4@6	2.6@20	2.7@20
	G3-b	5.6@18	5.2@30	0@30	G2-b	2.8@18	2.6@30	1.6@30
	G3-c	5.2@40	5.2@40	0.3@30	G2-c	2.6@40	2.6@40	1.3@30
	G4-a	9.3@6	7.4@20	0@20	G1-a	4.7@5	3.7@10	1.0@5
	G4-b	7.8@8	7.4@30	0@30	G1-b	4.7@6	3.7@20	1.0@10
	G4-c	7.4@40	7.4@40	0.3@30	G1-c	4@18	3.7@30	0.8@30
					G1-d	3.7@40	3.7@40	0.7@30
Khan (2003)	4.4S25	4.4@40	4.4@40	0.3@30				
	5.9S25	5.9@40	5.9@40	0.3@30				
	7.4S25	7.4@40	7.4@40	0.3@30				
	8.7S25	8.7@40	8.7@40	0.3@30				
Mao (2005)	A	25@18	10.3@30	0@30				
	B	34@14	10.5@25	0.1@25				
	C	38@10	13.8@20	0@20				
	D	12@18	7.1@30	0@30				
Moffat) (2005	T0	13.7@30	13.7@30	0.3@30				
	T5	14.3@30	14.3@30	0.3@30				
Current study	FR8	7.9@30	7.9@30	0@30				
	FR7	7.1@30	7.1@30	0@30				
	HF01	10.6@14	10.0@15	0.1@15				
	HF03	4.9@30	4.9@30	0.3@30				
	HF05	14.6@6	5.4@20	0.5@18				

Note: Value @ F represents mass passing, F% corresponding to $(D'_{15}/d'_{85})_{max}$ or $(D'_{15}/d'_{85})_{at\ gap}$ or $(H/F)_{min}$

Table 6.3 Evaluation of internal stability of widely graded soils by Kezdi (1979) and Kenney and Lau (1986) methods

Reference	Unstable				Stable			
	Gradation	$(D'_{15}/d'_{85})_{max}$	$(H/F)_{min}$	$(D'_{15}/d'_{85})_{Fn}$	Gradation	$(D'_{15}/d'_{85})_{max}$	$(H/F)_{min}$	$(D'_{15}/d'_{85})_{Fn}$
Kenney &Lau (1985)	A	3.5@36	1.0@20	2.6	As	3.7@5	0.9@25	3.2
	D	6.7@18	0.5@20	6.0	Ds	4.0@5	3.0@5	4.0
	X	51.0@5	0.6@10	13.5	K	3.2@5	3.4@5	3.2
	Y	6.5@5	0.7@20	5.0	1	4.9@5	1.2@24	2.4
	Ys	8.0@5	0.9@15	5.1	2	4.8@5	1.4@20	2.5
					3	10.5@5	1.3@15	3.6
					Cu=3	1.4	2.1@30	1.4
					Cu=6	1.7	1.9@20	1.7
					Cu=12	2.1	1.4@20	2.1
Skempton & Brogan (1994)	B	9.7@5	1.0@10	7.0	C	4.7@5	1.5@10	3.9
					D	4.0@5	2.8@6	3.6
Mao (2005)	b	5.0@14	0.8@18	4.7				
	c	7 .0@8	0.8@12	6.0				
	a	6.0@24	0.5@22	5.7				
	d	22.0@6	0.3@12	14.5				
Liu (2005)	1	35@5	0.46@15	13.0	5'	7.5@10	0.72@20	4.4
	2	18@5	0.45@22	8.8	6	3.3@5	1.0 @20	2.9
	4	35@5	0.48@15	9.5				
	29B	9.1@20	0.37@22	8.8				
	4'	25.3@15	0.26@15	25.3				
	3*	9.9@10	0.58@20	6.3				
	26*	13@5	0.9@8	8.7				
Moffat (2005)	C-20	7.7@5	0.67@20	4.2				
	C-30	10@6	0.42@30	5.6				
Current study					HF10	16@6	1.0@20	3.7

Note: * Transition soils

F_n = F at $(H/F)_{min}$

Table 6.4 Evaluation of internal stability of gap-graded soils by Burenkova method (1993)

Reference	Unstable					Stable				
	Gradation	h' (d_{90}/d_{60})	h" (d_{90}/d_{15})	lower limit	upper limit	Gradation	h' (d_{90}/d_{60})	h" (d_{90}/d_{15})	lower limit	upper limit
Skempton & Brogan (1994)	A	1.54	19.13	1.97	3.38					
Honjo et al. (1996)	G3-a	1.47	11.66	1.81	2.88	G2-a	1.47	5.82	1.58	2.42
	G3-b	1.55	13.61	1.86	3.11	G2-b	1.55	6.80	1.63	2.56
	G3-c	1.67	14.48	1.88	3.16	G2-c	1.67	7.24	1.65	2.60
	G4-a	1.48	16.49	1.92	3.26	G1-a	1.42	2.38	1.29	1.70
	G4-b	1.56	19.25	1.98	3.39	G1-b	1.48	8.37	1.70	2.72
	G4-c	1.68	20.48	2.00	3.44	G1-c	1.56	9.77	1.75	2.84
						G1-d	1.68	10.39	1.77	2.89
Khan (2003)	4.4S25	1.54	11.96	1.82	3.00					
	5.9S25	1.30	12.68	1.84	3.05					
	7.4S25	1.55	20.04	1.99	3.42					
	8.7S25	1.40	20.71	2.00	3.45					
Mao (2005)	3A	1.34	45.70	2.26	4.09					
	3B	1.32	41.38	2.23	4.01					
	3C	1.30	30.57	2.13	3.76					
	3D	1.34	22.85	2.03	3.53					
Moffat) (2005	T0	4.03	242.63	2.81	5.43					
	T5	4.03	242.63	2.81	5.43					
Current study	FR8	1.34	14.36	1.88	3.15					
	FR7	1.38	14.54	1.88	3.16					
	HF01	1.69	26.67	2.08	3.65					
	HF03	2.77	37.71	2.20	3.93					
	HF05	8.87	124.14	2.59	4.89					

Note: lower limit = 0.76 log (h") +1; upper limit = 1.86 log (h") +1

Table 6.5 Evaluation of internal stability of widely graded soils by Burenkova method (1993)

Reference	Unstable					Stable				
	Gradation	h' (d_{90}/d_{60})	h" (d_{90}/d_{15})	lower limit	upper limit	Gradation	h' (d_{90}/d_{60})	h" (d_{90}/d_{15})	lower limit	upper limit
Kenney & Lau (1985)	A	1.90	36.16	2.18	3.74	As	1.79	21.77	2.02	3.35
	D	1.70	22.88	2.03	3.39	Ds	1.87	4.24	1.78	2.10
	X	1.81	16.33	1.92	3.13	K	1.40	3.98	1.46	2.06
	Y	2.34	90.06	2.48	4.44	1	1.49	11.68	1.81	2.98
	Ys	2.14	47.98	2.28	3.96	2	3.62	36.22	2.18	3.90
						3	1.57	13.42	1.86	2.98
						Cu=3	1.93	5.20	1.54	2.33
						Cu=6	2.93	14.70	1.89	3.17
						Cu=12	4.44	41.57	2.23	4.01
Skempton & Brogan (1994)	B	1.54	7.46	1.66	2.62	C	1.54	7.10	1.65	2.58
						D	1.45	3.88	1.45	2.10
Mao (2005)	b	2.83	56.47	2.33	4.26					
	c	1.58	14.69	1.89	3.17					
	a	1.86	31.66	2.14	3.79					
	d	1.41	10.19	1.77	2.88					
Liu (2005)	1	1.25	22.29	2.02	3.51	5'	4.30	220.98	2.78	5.36
	2	1.40	71.62	2.41	4.45	6	7.13	158.12	2.67	5.09
	4	2.40	79.56	2.44	4.54					
	29B	1.24	100.61	2.52	4.72					
	4'	1.65	140.48	2.63	4.99					
	3*	2.75	191.83	2.74	5.25					
	26*	2.62	24.56	2.06	3.58					
Moffat (2005)	C-20	9.22	140.72	2.63	5.00					
	C-30	8.06	175.16	2.70	5.17					
Current study						HF10	2.26	35.12	2.17	3.87

Note: lower limit = 0.76 log (h") +1; upper limit = 1.86 log (h") +1

Table 6.6 Sandy gravels from Skempton and Brogan (1994)

Site	River	C_u	S_f : %	D'_{15}/d'_{85}	$(H/F)_{min}$	Reference for grading curve
Tarbela	Indus	130	15	25	0.16	Lowe(1978)
Mangla	Jhelum	200	18	32	0.18	Skempton & Catin (1963)
Wanapum	Columbia	100	15	13	0.38	Russo(1963)
Serre-Poncon	Durance	70	23	6.5	0.42	Maigre(1955)
Phoenix	Salt	40	18	7.3	0.50	Li & Fullerton (1987)
Kumagaya	Tone	38	22	5.1	0.57	Goto etc (1992)

Table 6.7 Summary of results for capillary tube model

Reference	Gradation	F_n	e	D^c_h (mm)	α_D	O_{50} (mm)	d'_{85} (mm)	d'_{85}/O_{50}	Laboratory results
Honjo et al (1996)	G1-a	10	0.54	0.97	8	0.35	0.19	0.55	Stable
	G1-b	20	0.48	0.97	8	0.41	0.19	0.46	Stable
	G1-c	30	0.46	0.97	8	0.52	0.19	0.37	Stable
	G2-a	20	0.55	0.68	8	0.32	0.19	0.60	Stable
	G2-b	30	0.52	0.68	8	0.40	0.19	0.48	Stable
	G3-a	20	0.46	1.36	8	0.56	0.19	0.34	Unstable
	G3-b	30	0.38	1.36	8	0.66	0.19	0.29	Unstable
	G4-a	20	0.35	1.90	8	0.65	0.19	0.29	Unstable
	G4-b	30	0.40	1.90	8	0.95	0.19	0.20	Unstable
Kenney and Lau (1986)	A	30	0.39	5.32	8	1.96	0.86	0.44	Unstable
	X	10	0.35	18.14	8	4.84	1.36	0.28	Unstable
	Y	20	0.28	11.05	8	3.10	1.03	0.33	Unstable
	Ys	15	0.39	13.90	8	4.41	1.41	0.32	Unstable
	Ds	5	0.4	7.91	8	1.87	1.39	0.74	Stable
	1	24	0.23	10.14	8	0.35	0.19	0.55	Stable
	2	20	0.28	10.41	8	3.12	2.00	0.64	Stable
	3	15	0.30	8.01	8	2.12	1.25	0.59	Stable
	As	25	0.35	7.86	8	3.14	1.54	0.49	Stable
Skempton and Brogan (1994)	A	15	0.51	3.13	8	1.22	0.23	0.19	Unstable
	B	10	0.59	2.7	8	1.04	0.29	0.28	Unstable
	C	10	0.60	3.14	8	1.28	0.56	0.44	Stable
	D	6	0.57	3.10	8	1.04	0.63	0.61	Stable
Current study	FR8	30	0.37	1.39	6	0.88	0.14	0.16	Unstable
	FR7	30	0.34	1.35	6	0.81	0.14	0.18	Unstable
	HF01	15	0.32	3.59	8	0.99	0.23	0.23	Unstable
	HF03	20	0.33	2.29	8	1.03	0.26	0.25	Unstable
	HF05	30	0.32	0.50	8	0.16	0.048	0.30	Unstable
	HF10	20	0.26	3.42	8	0.98	0.53	0.54	Stable
Moffat (2005)	C20	20	0.39	0.35	8	0.13	0.044	0.35	Unstable
	C30	30	0.39	0.39	8	0.18	0.045	0.25	Unstable
	T5	30	0.30	3.63	8	1.50	0.33	0.22	Unstable
	T0	30	0.33	3.63	8	1.64	0.33	0.20	Unstable
Liu (2005)	1	15	0.37	45.27	8	13.77	2.97	0.22	Unstable
	2	22	0.29	36.06	8	11.67	2.96	0.25	Unstable
	3	20	0.34	8.56	8	2.87	0.66	0.23	Unstable
	4	15	0.23	12.48	8	2.92	0.82	0.28	Unstable
	26	8	0.42	6.34	8	1.83	0.48	0.26	Unstable
	29B	22	0.29	8.31	8	2.52	0.58	0.23	Unstable
	5	20	0.21	4.59	8	1.18	0.46	0.39	Stable
	6	20	0.26	4.20	8	0.36	0.18	0.50	Stable

Note: Density of specimen is not given in gradations D, K, Cu=3, Cu=6, Cu=12 from Kenney and Lau (1985), gradation 4' from Liu (2005).

Table 6.8a Values of α ($\sigma'_{t0} > 0$)

Reference	Gradation	α	$(H/F)_{min}$	D'_{15}/d'_{85}	d'_{85}/O_{50}
Current study	FR8	0.01	0	7.9	0.16
	FR7	0.07	0	7.1	0.18
	HF03	0.30	0.30	4.9	0.25
	HF05	0.60	0.50	5.4	0.30
	HF10	1.0	0.98	4.0	0.54
Moffat (2005)	T-0	0.18	0.29	13.7	0.20
	T-5	0.40	0.29	14.3	0.22
	C-30	0.65	0.42	5.6	0.25
	C-20	0.73	0.67	4.2	0.35

Note: σ'_{t0} = effective stress at top of specimen (kPa)

Table 6.8b Values of α ($\sigma'_{t0} = 0$)

Reference	Gradation	n	i_{cr}	i_c	α	$(H/F)_{min}$	D'_{15}/d'_{85}	d'_{85}/O_{50}
Current study	HF01	0.24	0.17	1.25	0.13	0.14	10.0	0.23
Skempton and Brogan (1994)	A	0.34	0.20	1.09	0.18	0.14	11.0	0.19
	B	0.37	0.34	1.04	0.33	0.98	7.0	0.28
	C	0.375	1.0	1.03	0.97	1.6	3.9	0.44
	D	0.365	1.0	1.05	0.95	2.8	3.6	0.92
Liu (2005)	1	0.26	0.16	1.22	0.13	0.46	13.0	0.22
	2	0.17	0.17	1.36	0.12	0.45	8.8	0.25
	3	0.25	0.59	1.23	0.48	0.58	7.3	0.23
	4	0.19	0.44	1.34	0.33	0.48	9.5	0.28
	26	0.29	0.54	1.17	0.46	0.9	8.7	0.26
	29B	0.22	0.26	1.28	0.20	0.37	8.8	0.23
	5	0.17	1.01	1.36	0.74	0.72	4.4	0.39
	6	0.20	1.31	2.54	1.0	1.0	2.9	0.51

Note: σ'_{t0} = effective stress at top of specimen (kPa).

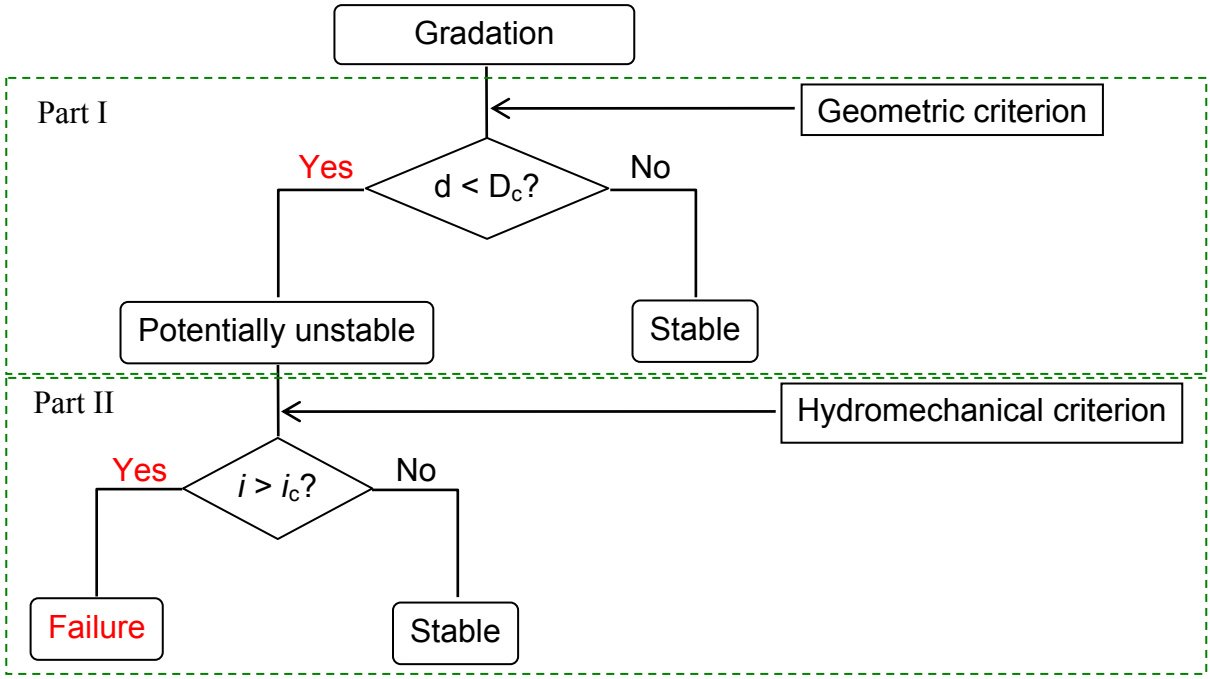

Figure 6.1 Assessment of internal stability of granular materials

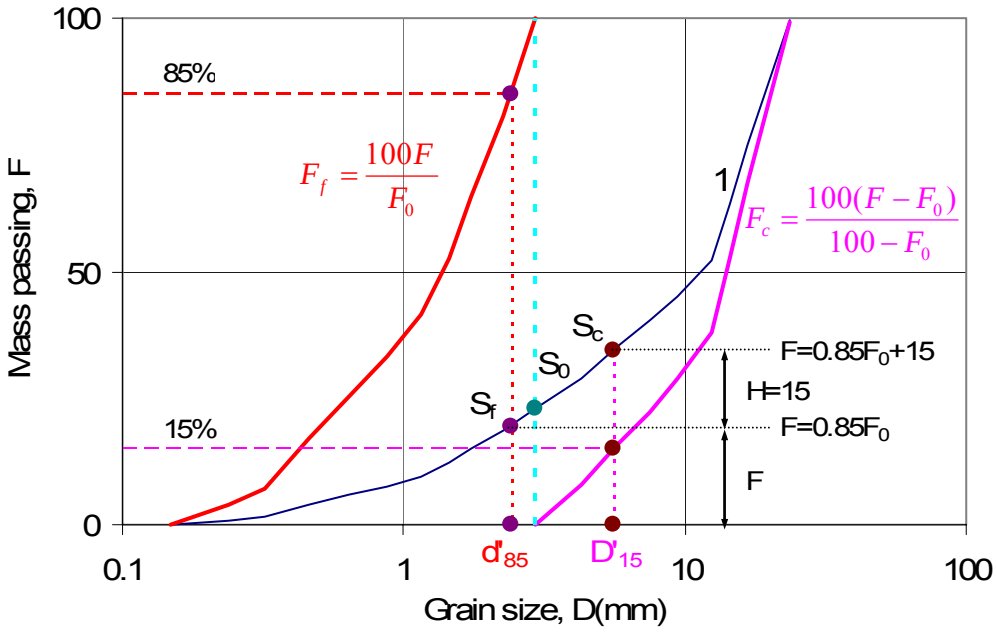

Figure 6.2 Approach of the Kezdi method

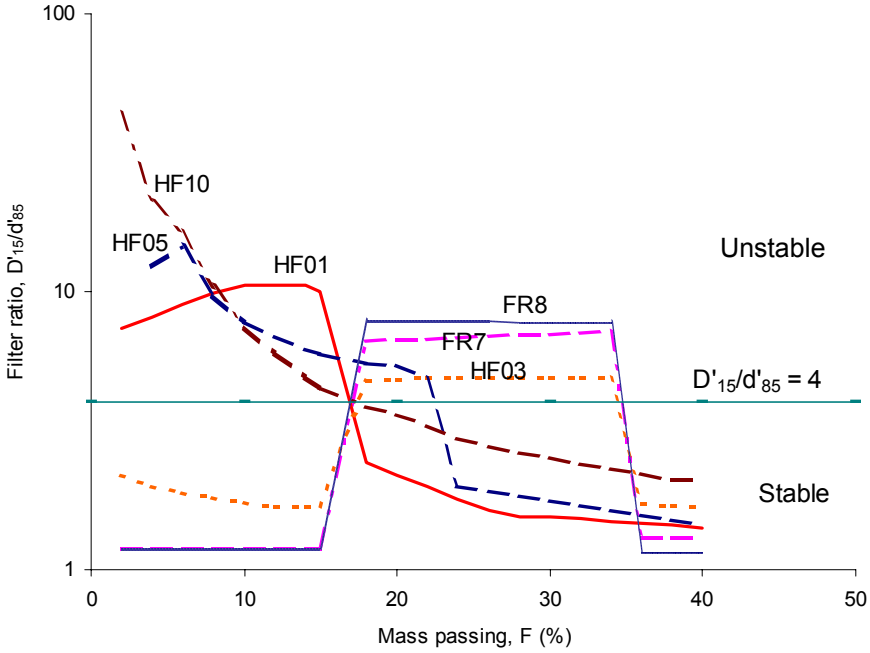

Figure 6.3 Assessment of internal stability by Kezdi method (1979)

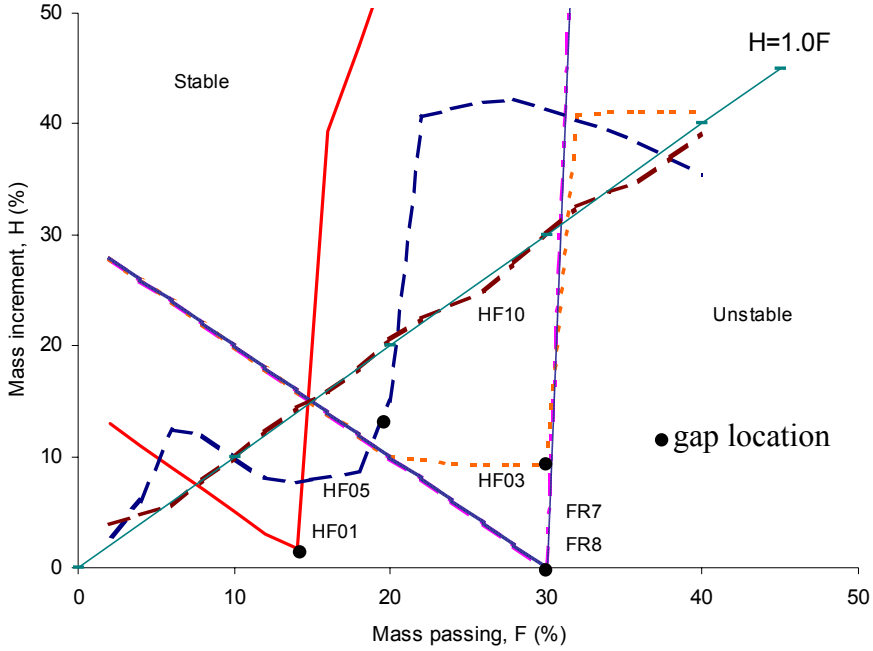

Figure 6.4 Assessment of internal stability by Kenney and Lau method (1986)

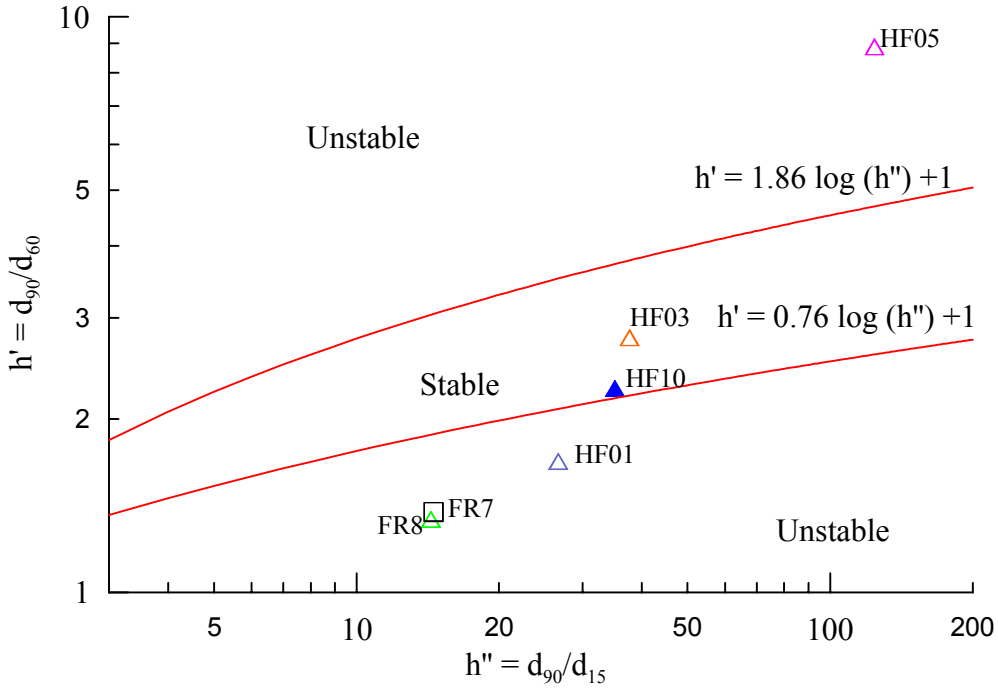

Figure 6.5 Assessment of internal stability by Burenkova method (1993)

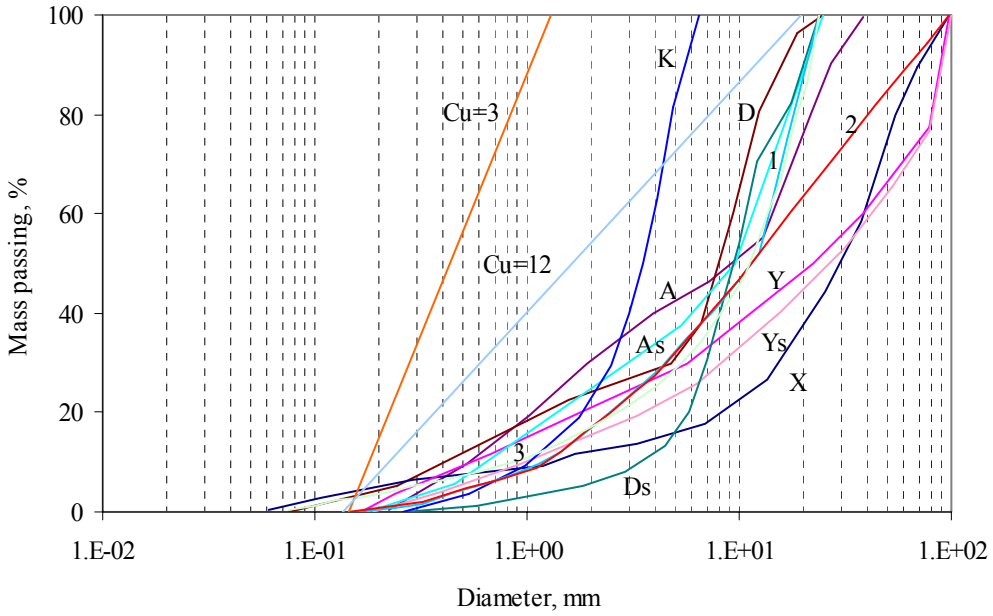

Figure 6.6 Gradations from Kenney and Lau (1985)

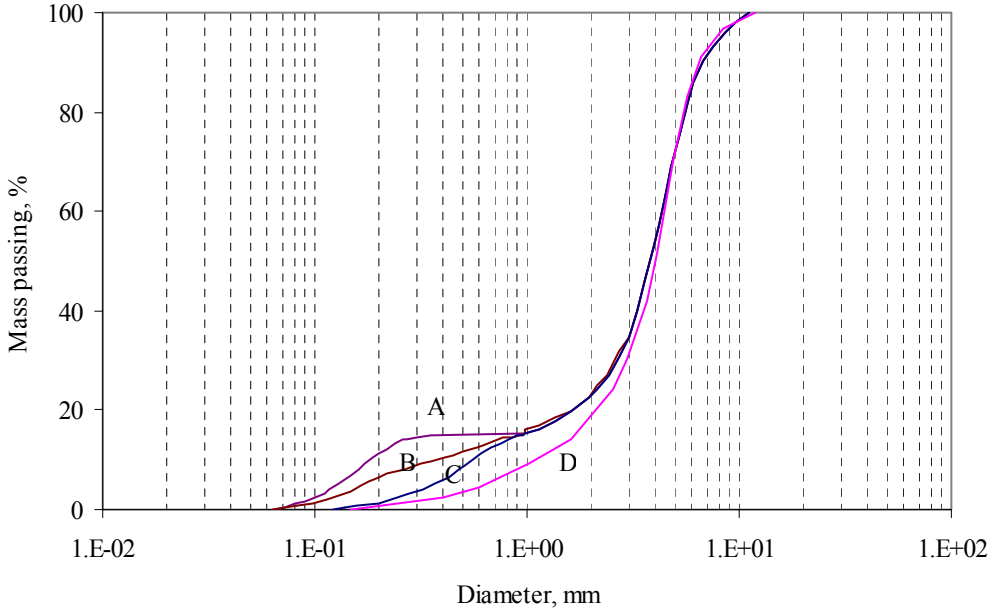

Figure 6.7 Gradations from Skempton and Brogan (1994)

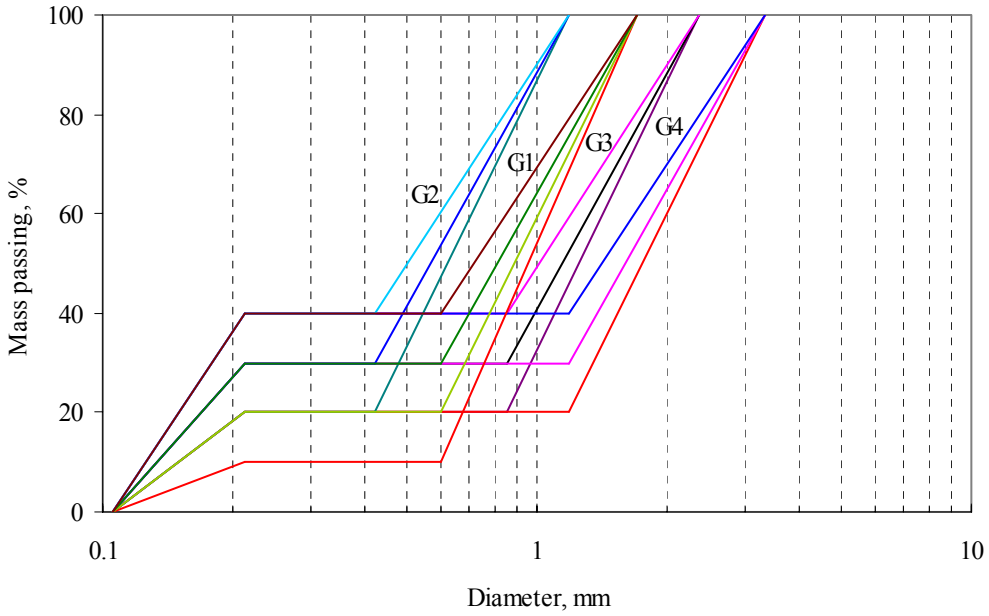

Figure 6.8 Gradations from Honjo et al. (1996)

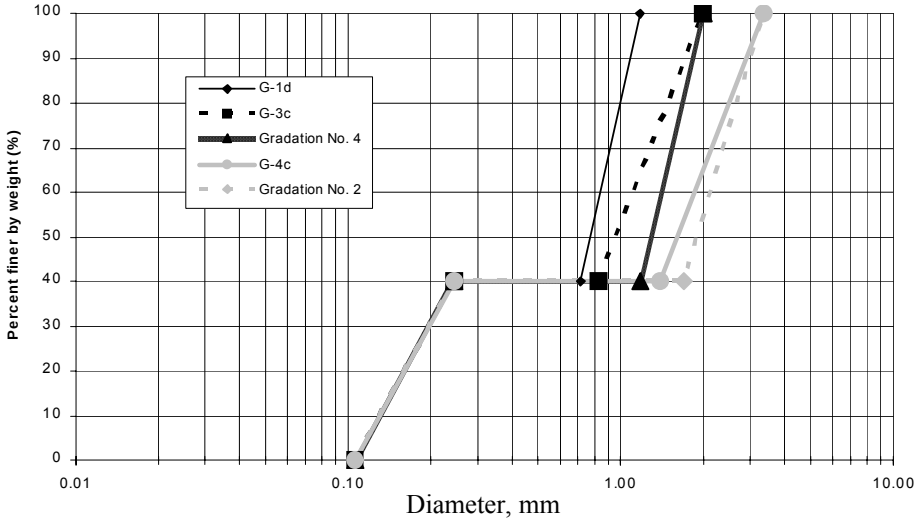

Figure 6.9 Gradations from Khan (2003)

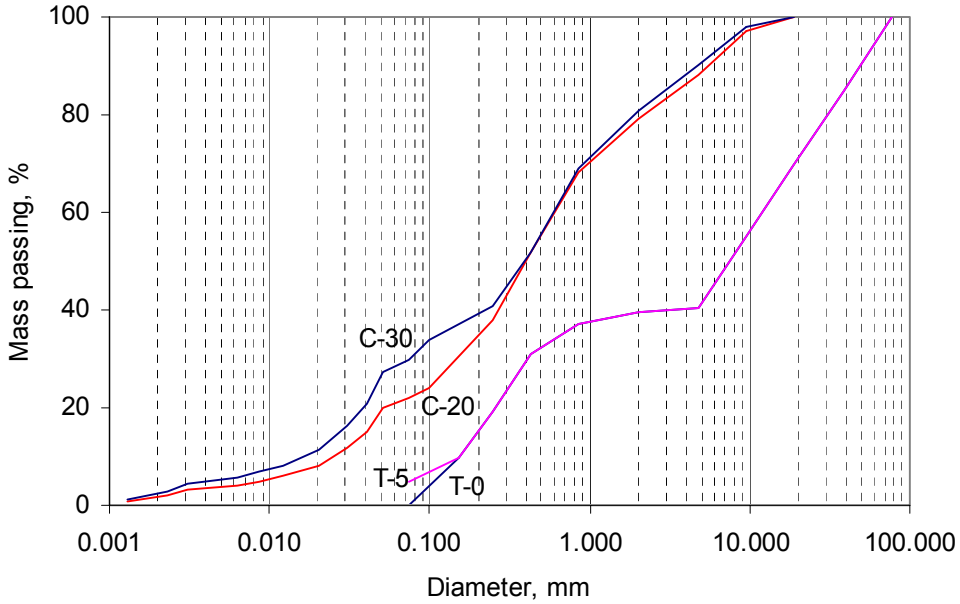

Figure 6.10 Gradations from Moffat (2005)

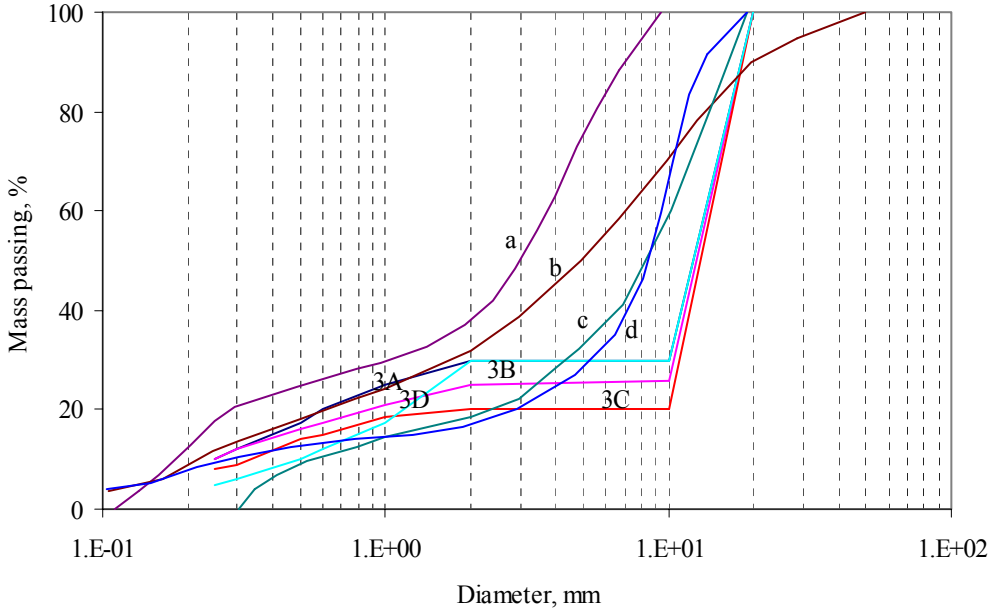

Figure 6.11 Gradations from Mao (2005)

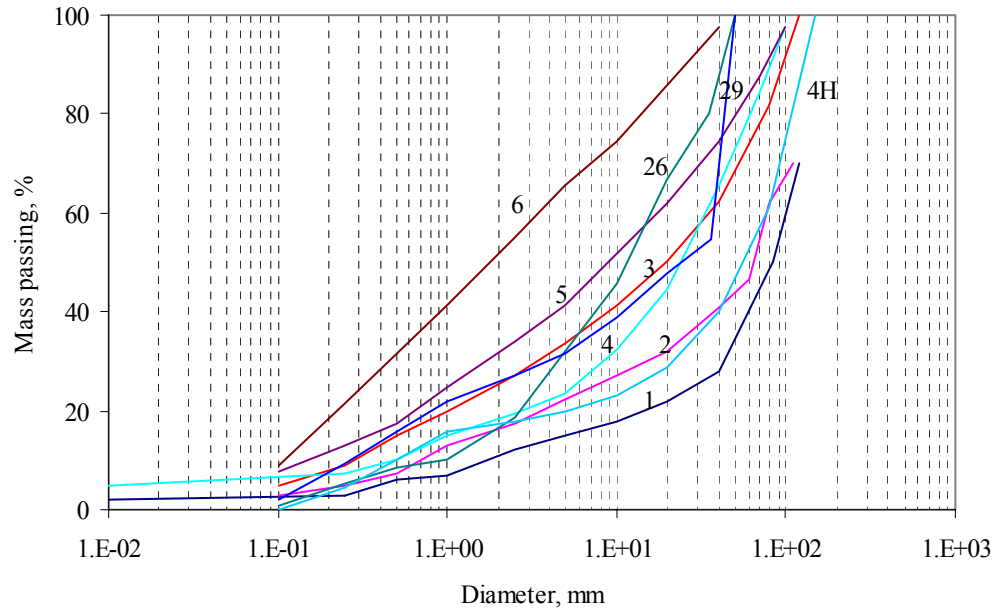

Figure 6.12 Gradations from Liu (2005)

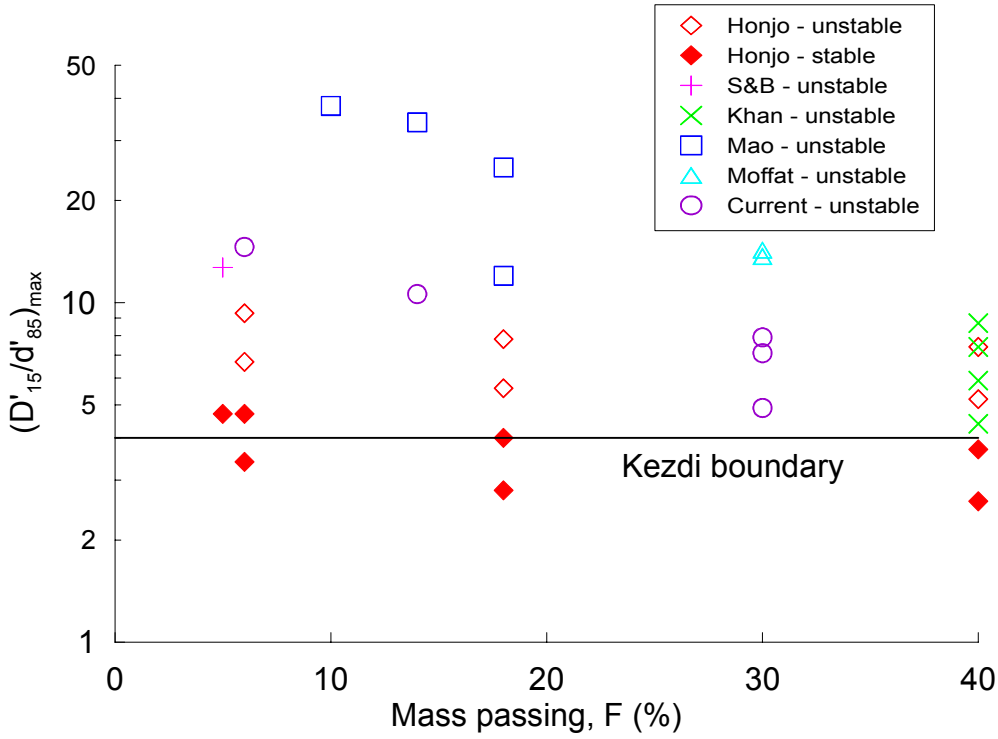

Figure 6.13 Assessment of internal stability of gap-graded soils: Kezdi method at maximum D'_{15}/d'_{85} ratio

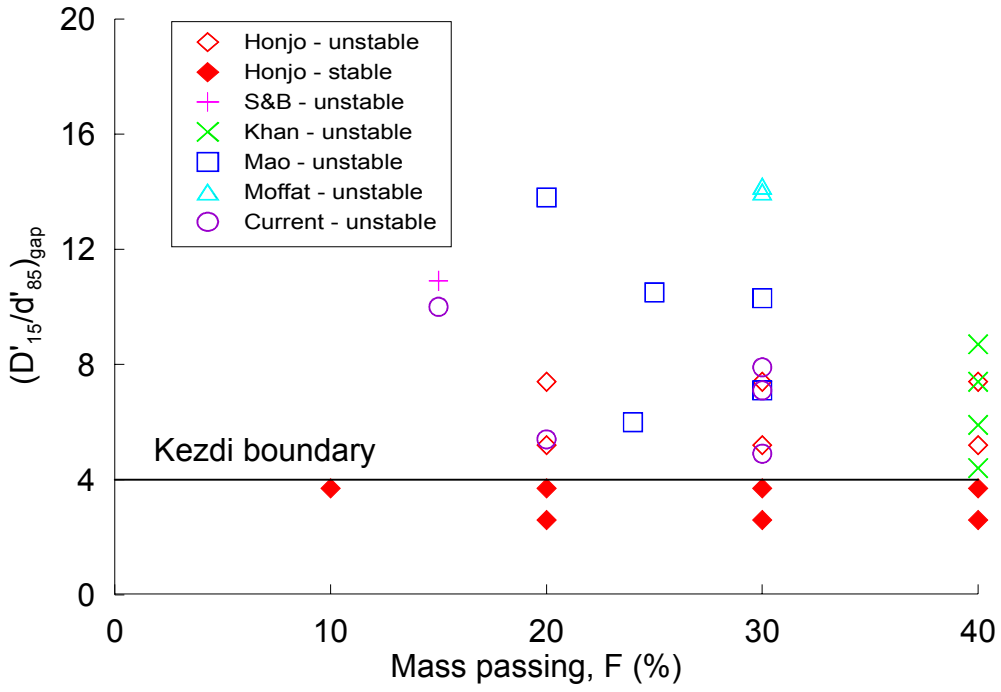

Figure 6.14 Assessment of internal stability of gap-graded soils: Kezdi method at gap location

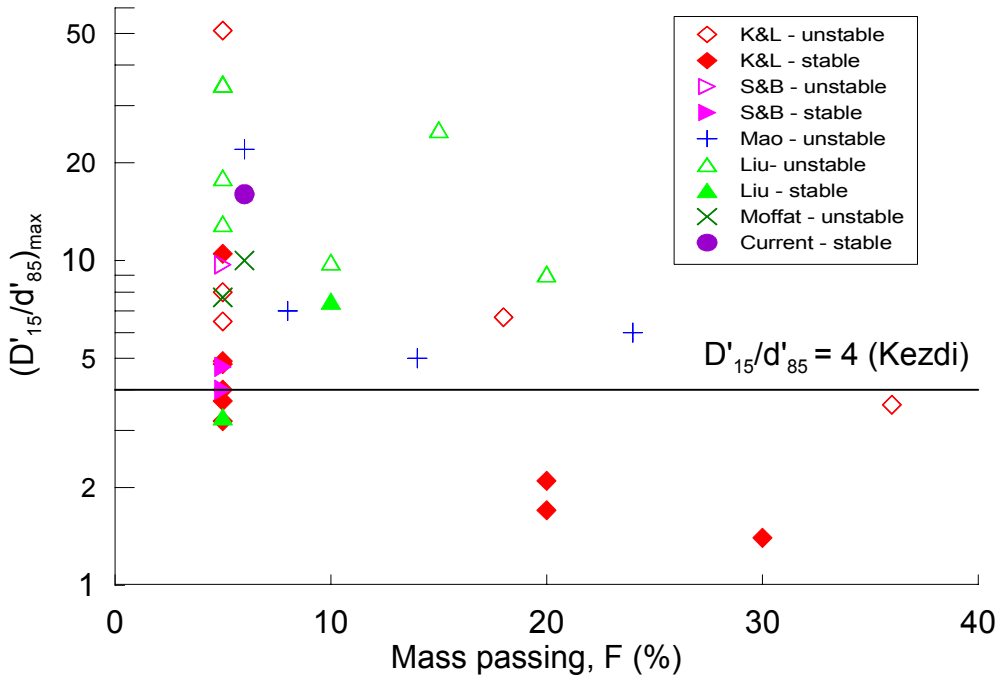

Figure 6.15 Assessment of internal stability of widely-graded soils: Kezdi method at maximum D'_{15}/d'_{85} ratio

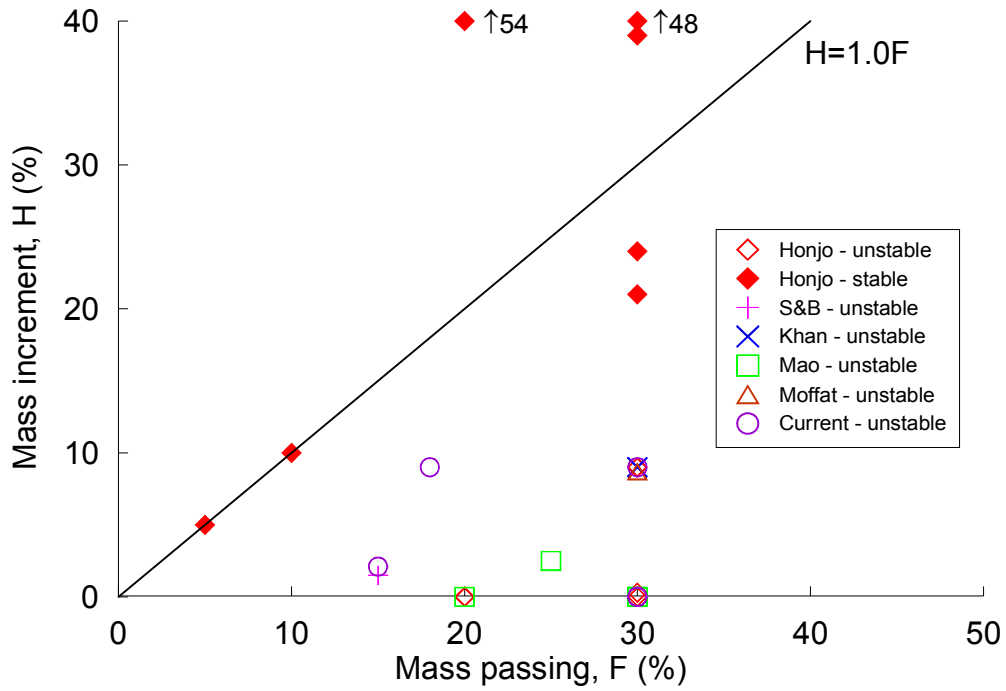

Figure 6.16 Assessment of internal stability of gap-graded soils: Kenney and Lau method at minimum H/F ratio

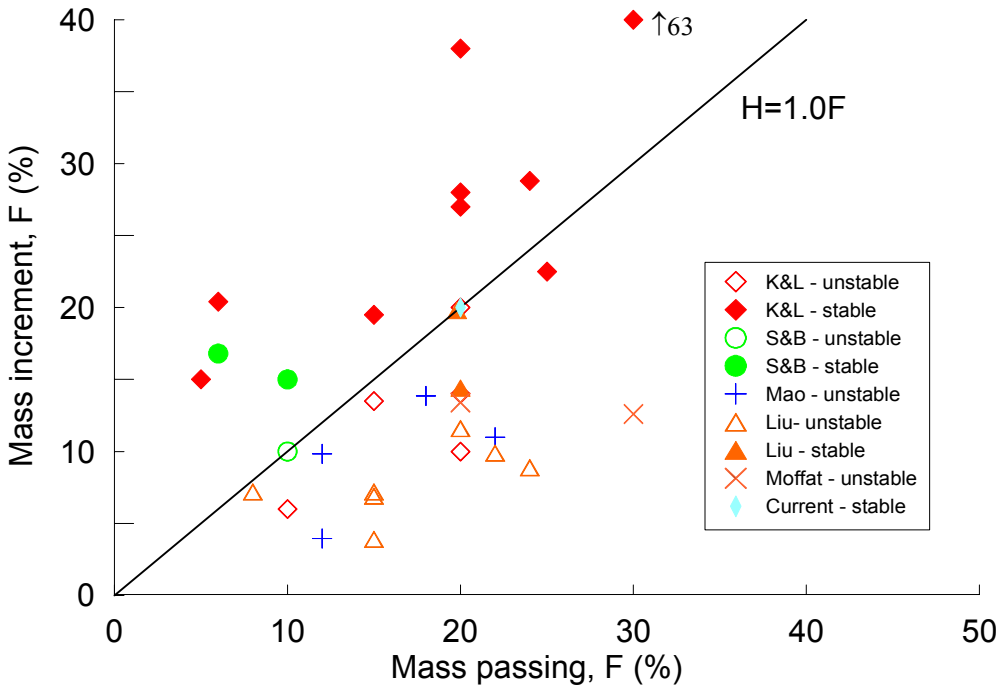

Figure 6.17 Assessment of internal stability of widely-graded soils: Kenney and Lau method at minimum H/F ratio

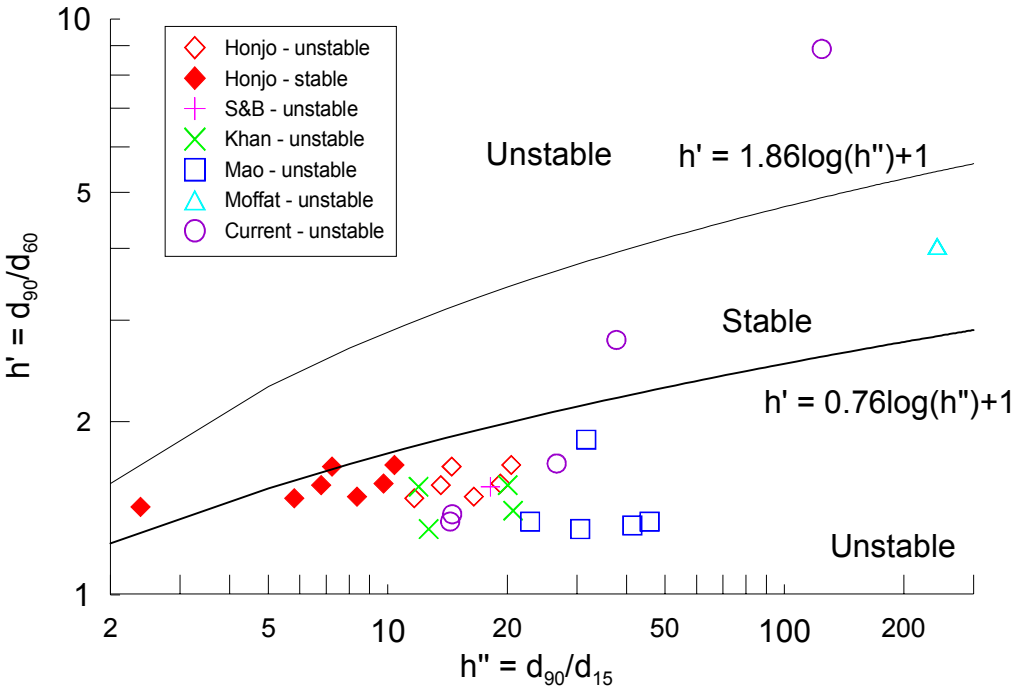

Figure 6.18 Assessment of internal stability of gap-graded soils: Burenkova method

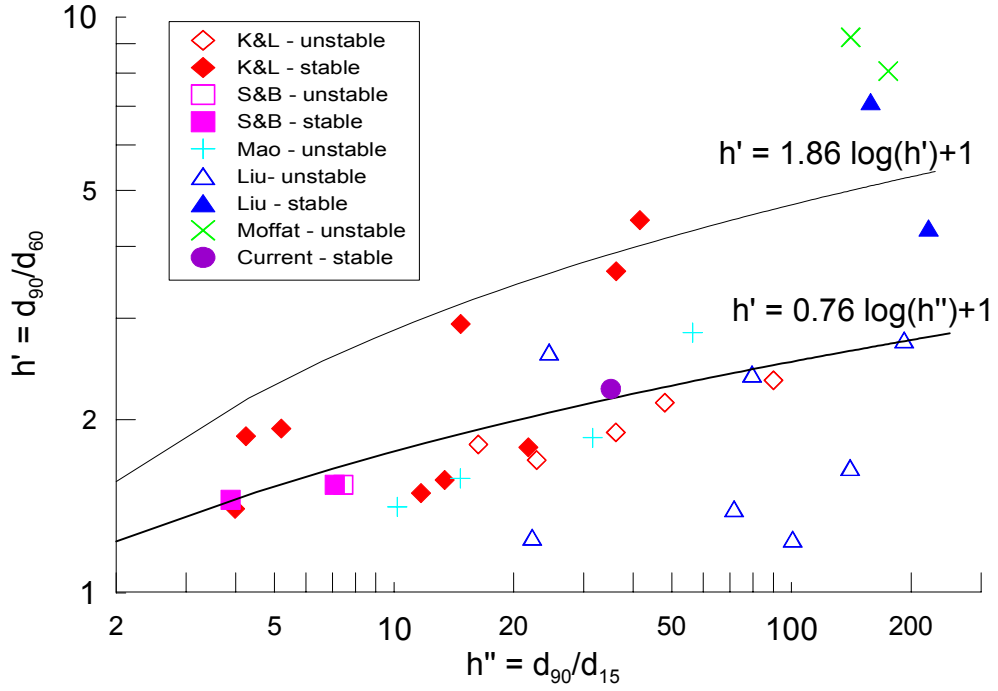

Figure 6.19 Assessment of internal stability of widely-graded soils: Burenkova method

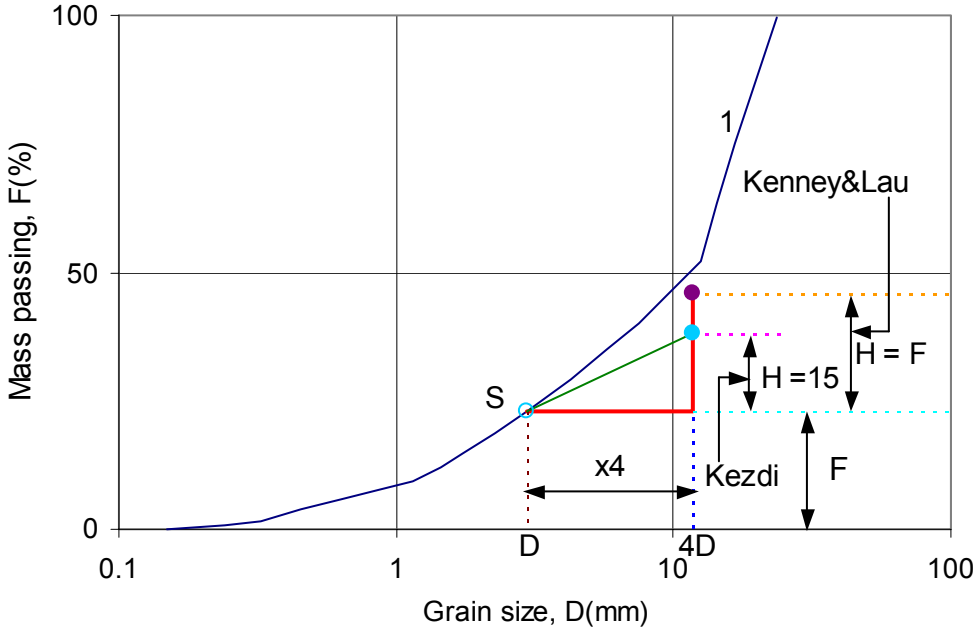

Figure 6.20 Comparison of the Kezdi and the Kenney and Lau methods

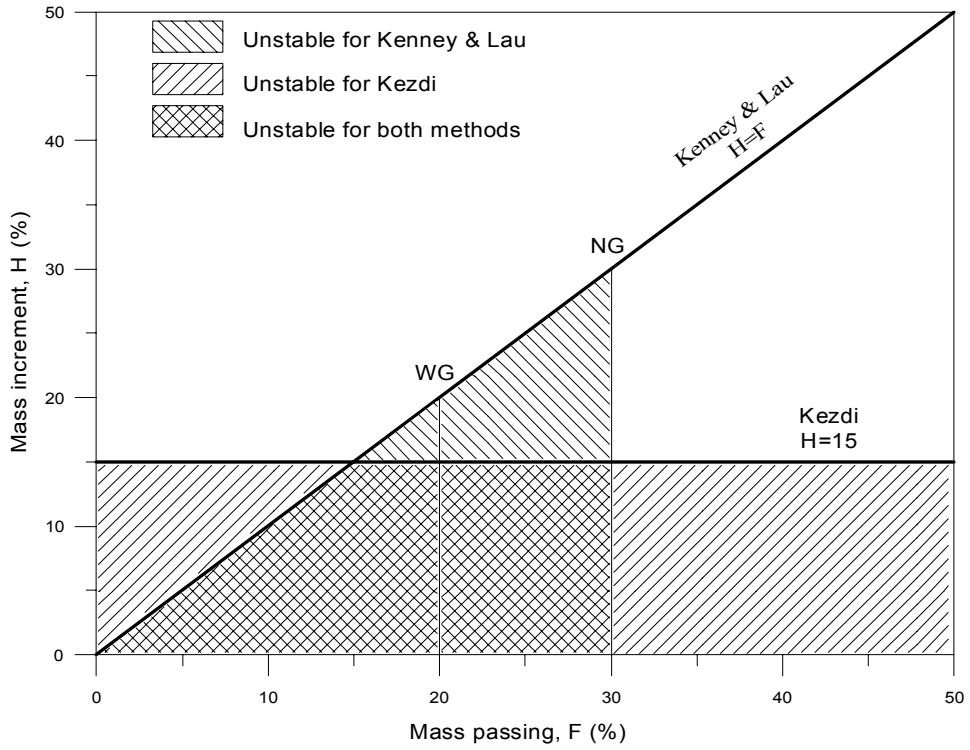

Figure 6.21 Synthesis of the Kezdi and the Kenney and Lau criteria
(Note: NG=narrowly graded; WG= widely graded)

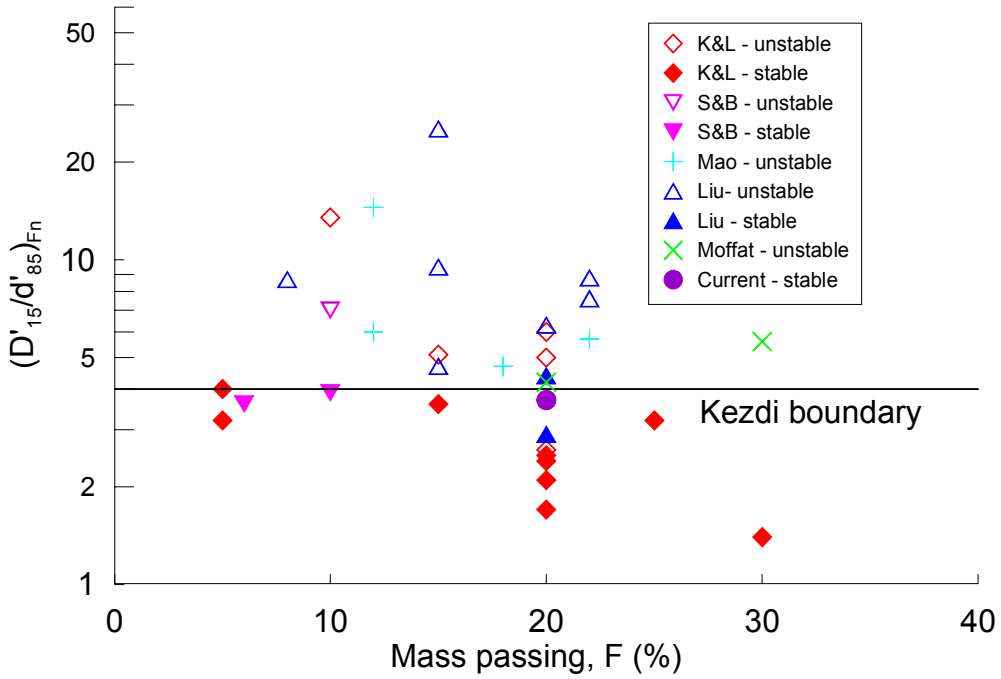

Figure 6.22 Assessment of internal stability of widely-graded soils: Kezdi method at minimum H/F ratio

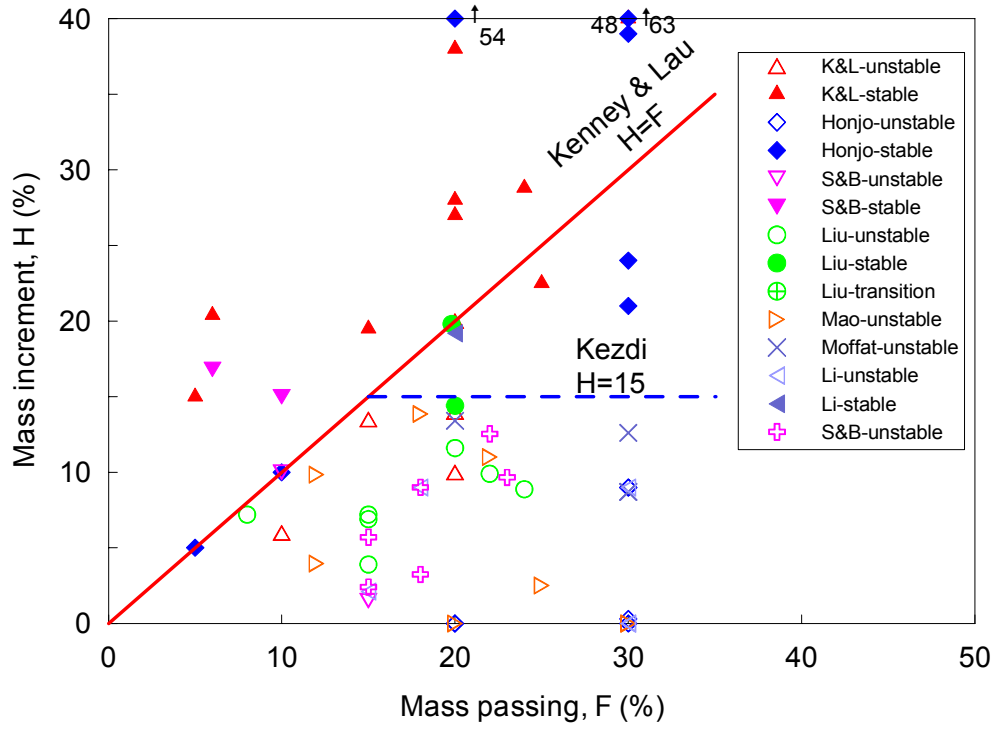

Figure 6.23 Comparative analysis of empirical criteria

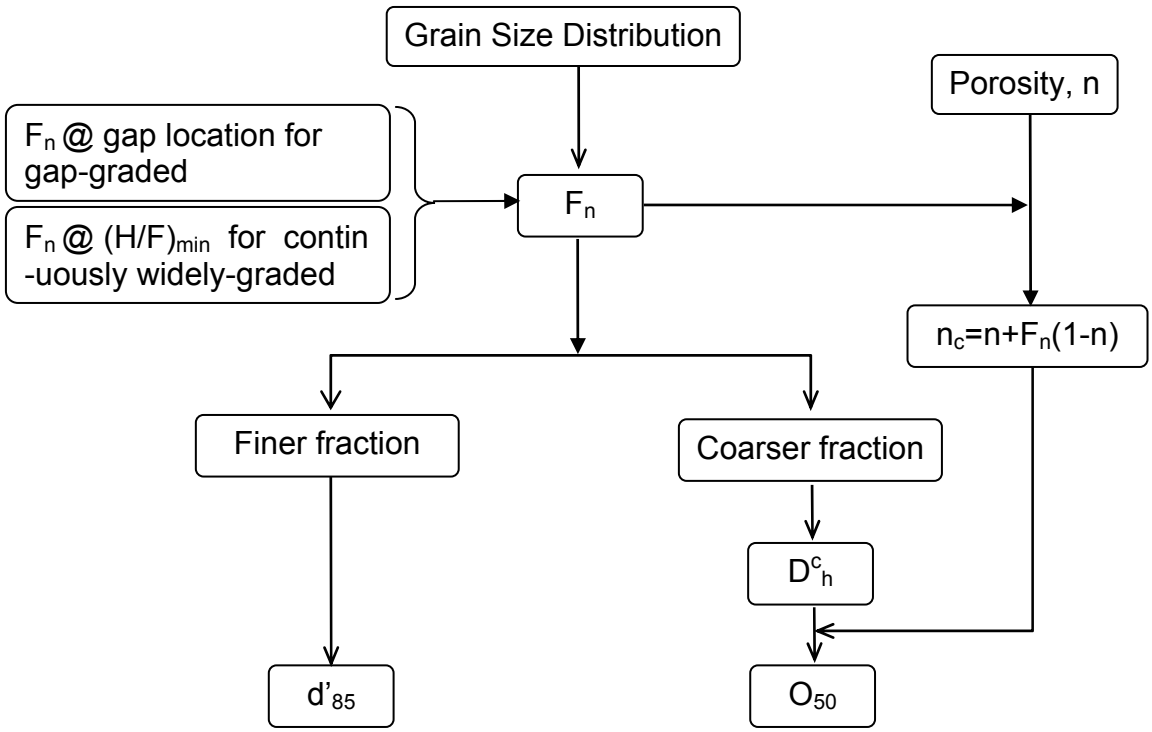

Figure 6.24 The procedure for capillary tube model

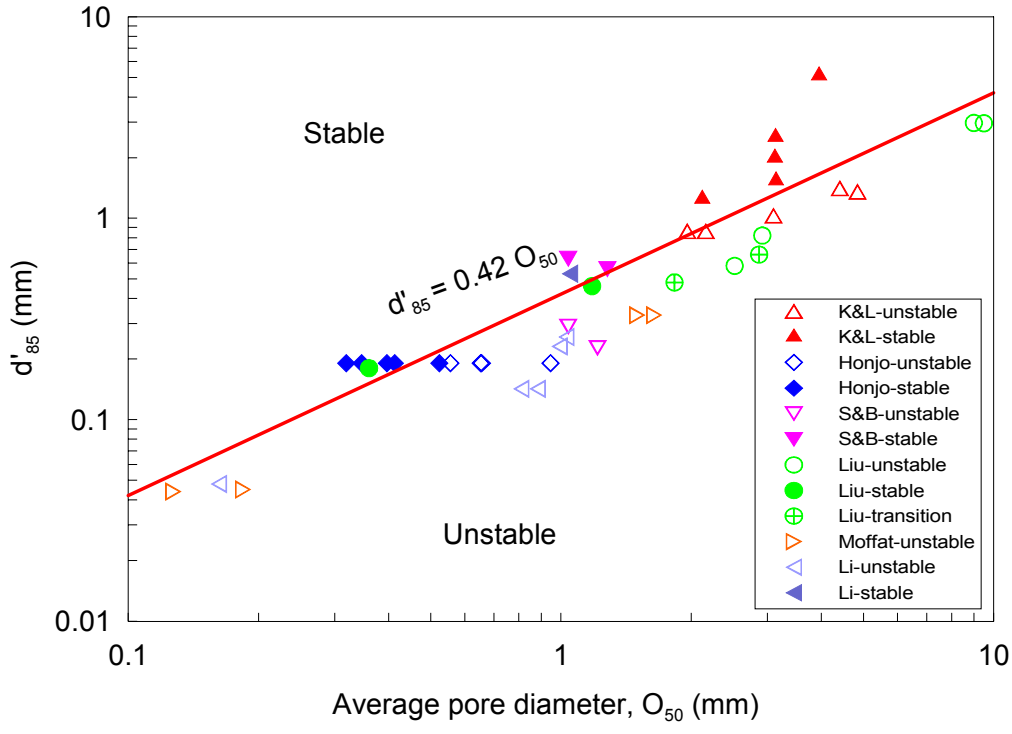

Figure 6.25 The boundaries for capillary tube model

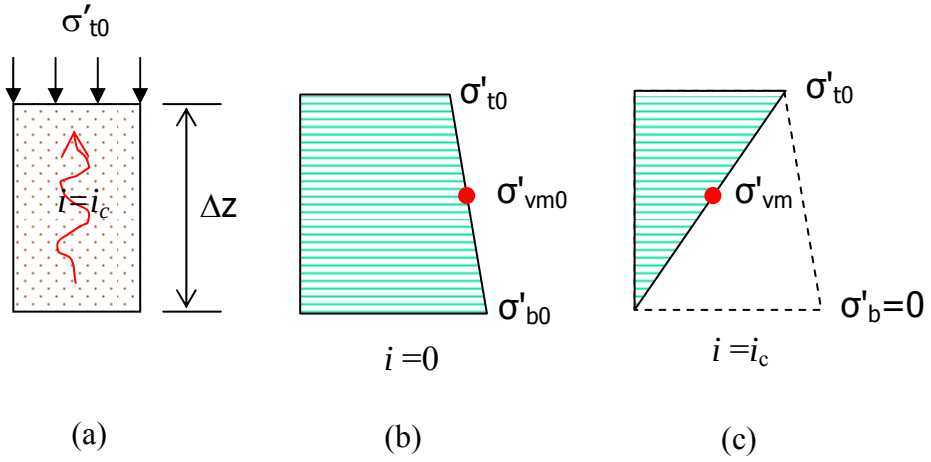

Figure 6.26 Schematic stress distributions for an internally stable material

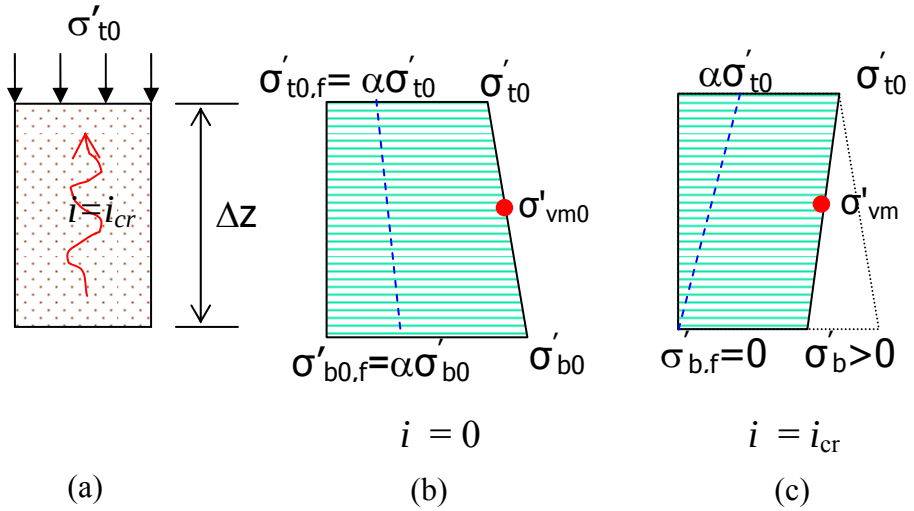

Figure 6.27 Schematic stress distributions for an internally unstable material

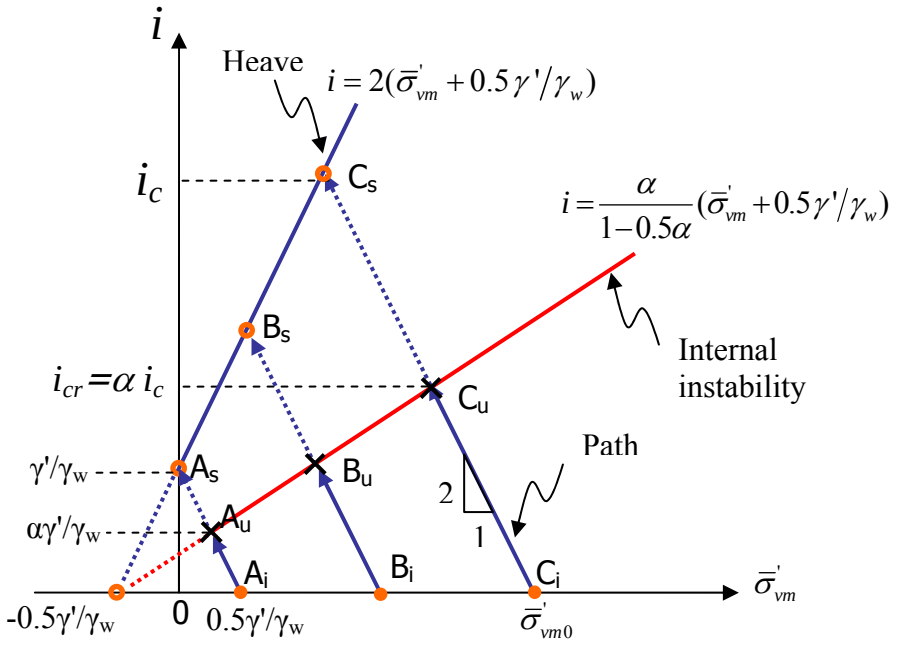

Figure 6.28 Hydromechanical path and hydromechanical envelope (f_c = 0)

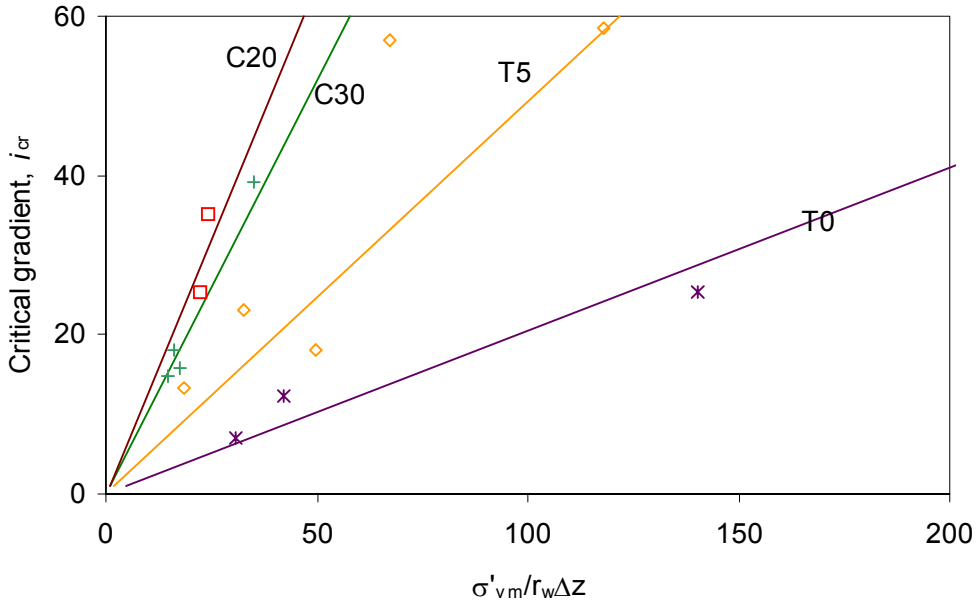

Figure 6.29 Hydromechanical envelopes (reworked from Moffat, 2005)

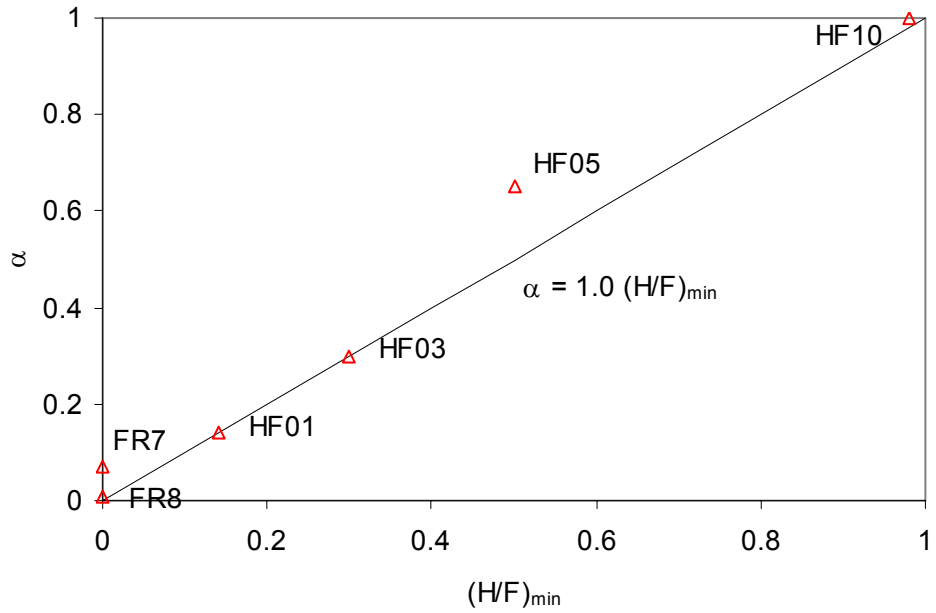

Figure 6.30 Variation of α with $(H/F)_{min}$ for current data

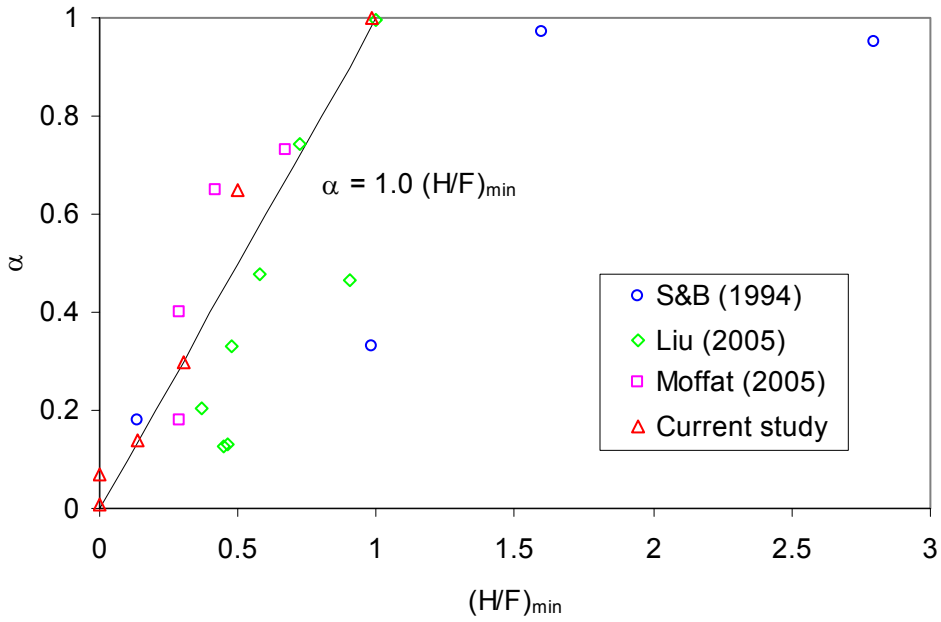

Figure 6.31 Variation of α with $(H/F)_{min}$

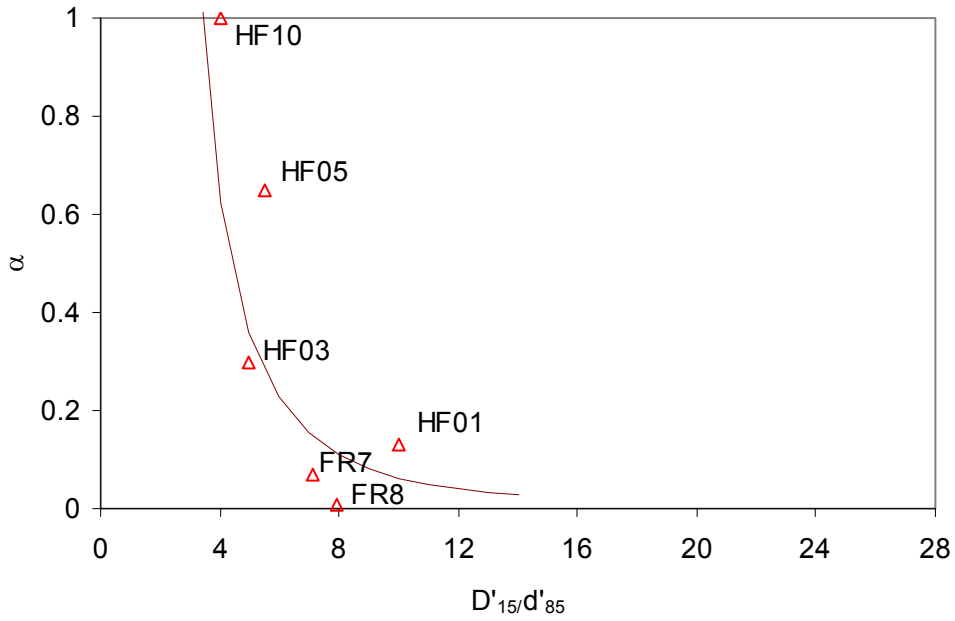

Figure 6.32 Variation of α with D'_{15}/d'_{85} for current data

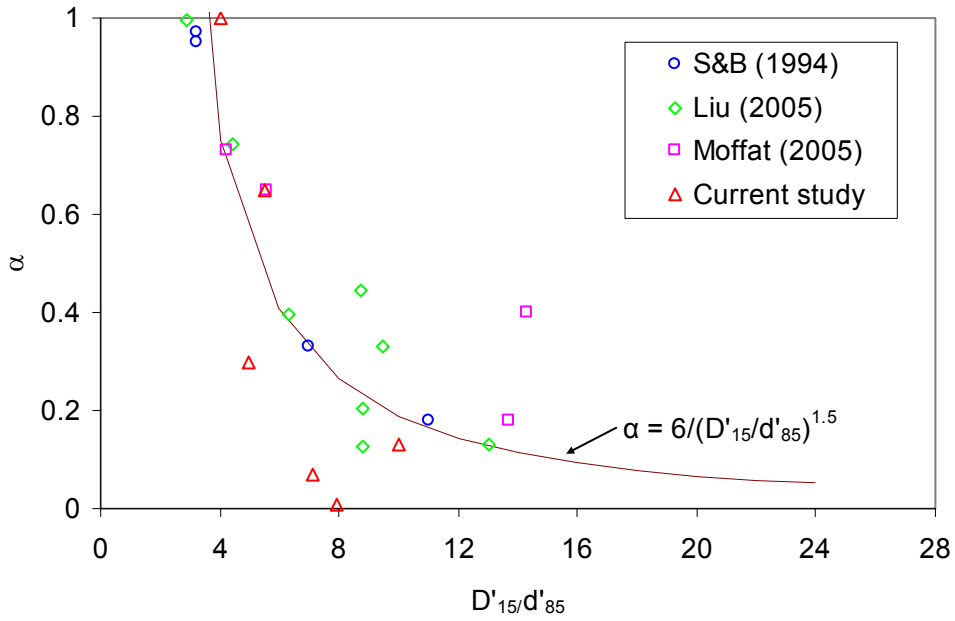

Figure 6.33 Variation of α with D'_{15}/d'_{85}

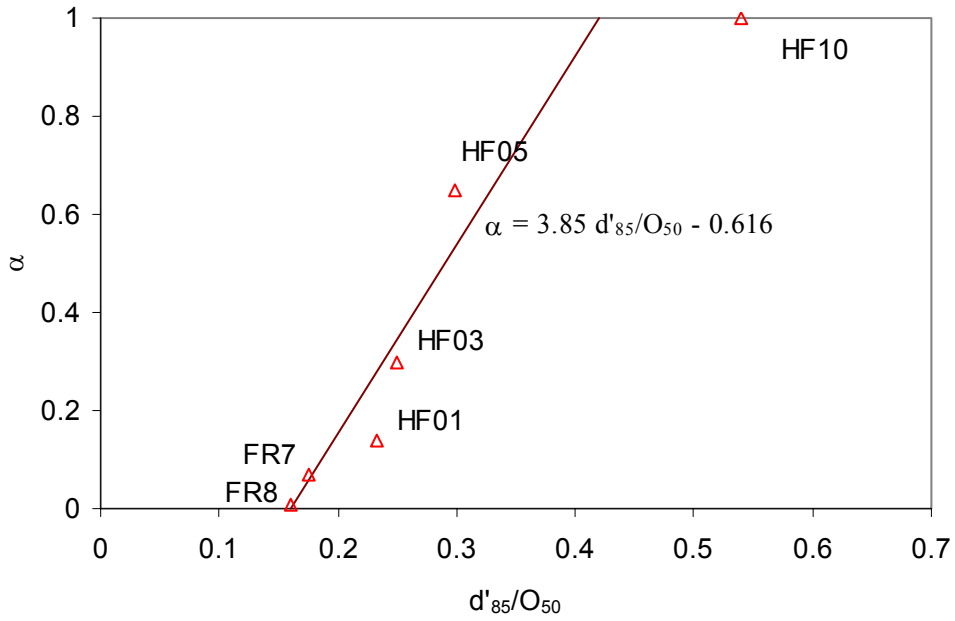

Figure 6.34 Variation of α with d'_{85}/O_{50} for current data

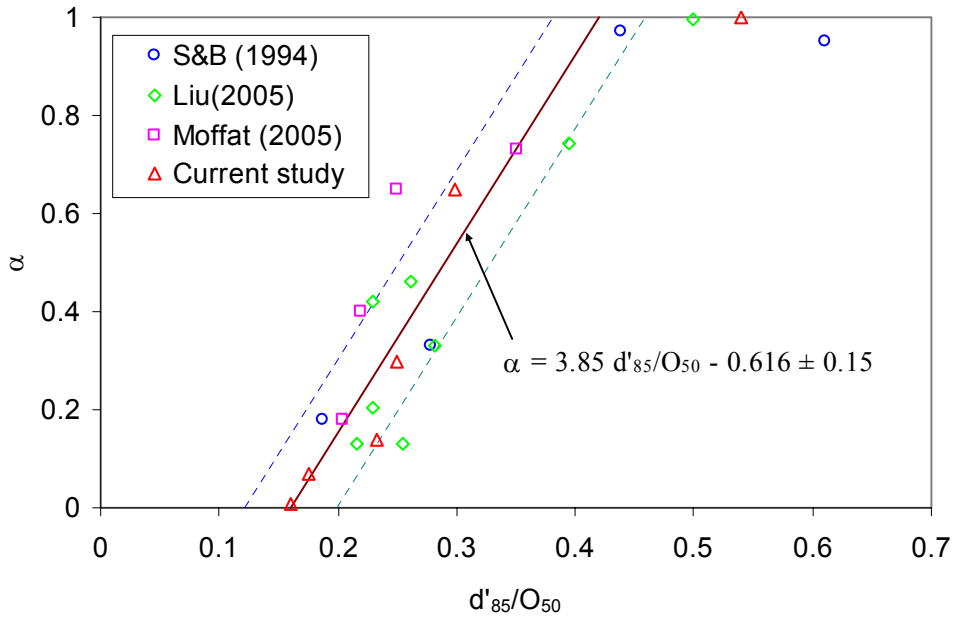

Figure 6.35 Variation of α with d'_{85}/O_{50}

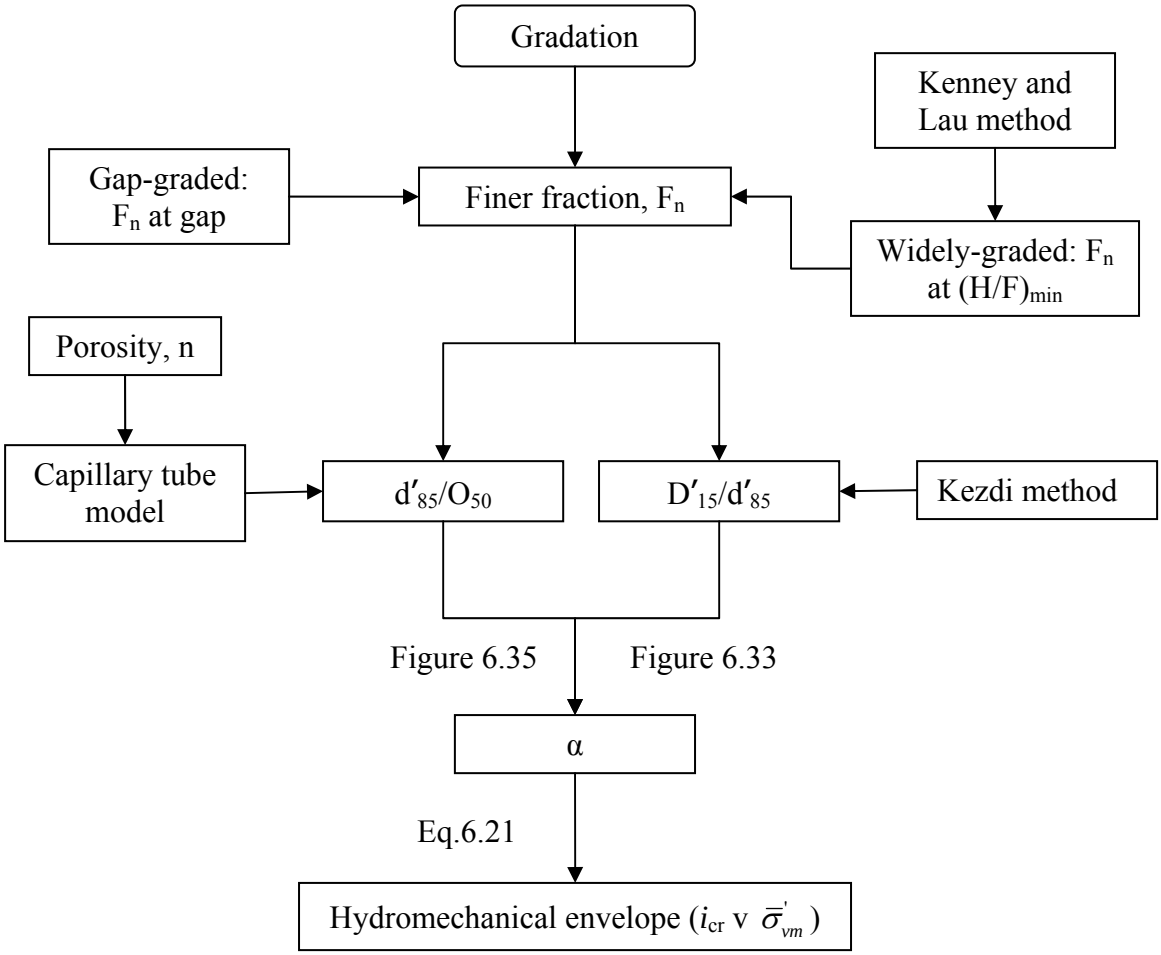

Figure 6.36 A framework for evaluation of internal instability

7 Conclusions and Recommendations

7.1 Conclusions

Internal stability of widely-graded cohesionless soils has been investigated. Onset of internal instability is governed by (i) grain size distribution curve of a soil, and (ii) a combined effect of effective stress and critical hydraulic gradient. In this study, three commonly used empirical geometric criteria are critically reviewed with respect to experimental database from the literature. The relative conservatism of these criteria is examined so that confidence is improved in using them in the engineering practice. A new geometric criterion based on capillary tube model is proposed to evaluate the internal instability. A hydromechanical envelope, the relation between critical hydraulic gradient and normalized effective stress, is defined based on the concept of stress reduction in finer particles, and then verified by the experimental observations. The relation between a hydromechanical index (α) and the geometric indices is established, thus making it possible to evaluate conditions governing the onset of internal instability knowing the grain size distribution curve of a soil. A summary of the findings is presented below that addresses the experimental observations, geometric indices and hydromechanical index in evaluating internal instability of cohesionless soils.

7.1.1 Experimental observations

A modified technique of slurry mixing and discrete deposition was used for testing of six soil gradations (FR8, FR7, HF01, HF03, HF05, and HF10), which was found satisfactory for reconstitution of a specimen of widely-graded soil. Multi-stage testing was conducted, wherein the hydraulic gradient across the soil specimen was increased in each stage until the

onset of instability was observed, or the specimen exhibited a heave failure. Test results yield a greater understanding of the onset of internal instability of soils subjected to seepage flow. The most important insights are summarized below:

- Onset of internal instability (suffosion) or heave was successfully identified based on (1) a change in slope of the $v \sim i_{av}$ curve; (2) a temporal variation of local hydraulic gradient, i_{jk}; and (3) companion visual observations.
- In suffosion, a distinction is made between internal suffosion and external suffosion. External suffosion is associated with an increase in slope of the $v \sim i_{av}$ curve (i.e., increase in hydraulic conductivity), and decrease in local hydraulic gradient. A contractive displacement, and a mass loss, usually accompanied the onset of external suffosion. In contrast, internal suffosion is associated with a decrease in slope of the $v \sim i_{av}$ curve (i.e., decrease in hydraulic conductivity), no displacement or mass loss was.
- Heave failure is associated with an increase in slope of the $v \sim i_{av}$ curve, and a decrease in local hydraulic gradient. However, in contrast to suffosion, an expansive displacement was observed with no mass loss.
- A combination of effective stress and critical gradient influences the onset of internal instability. A hydromechanical path is defined, from the variation of effective stress with seepage gradient. Under seepage flow, the hydromechanical path approaches a boundary at which the onset of internal instability occurs. This boundary to internal instability is deemed the hydromechanical envelope.
- The hydromechanical envelope is defined by a relation between critical gradient (i_{cr}) and normalized effective stress ($\overline{\sigma}'_{vm}$). It is different for each gradation tested. The difference is attributed to the grain size distribution of a soil. The greater the susceptibility to internal

instability, the lower the slope of the hydromechanical envelope.

7.1.2 Geometric criteria (potential to internal instability)

Three commonly used geometric criteria, those of Kezdi (1979), Kenney and Lau (1986) and Burenkova (1993), were assessed using an experimental database of 62 gradations from 8 studies (including the current study). The following conclusions are drawn:

- The Kezdi method proves relatively more successful in distinguishing between stable and unstable gradations in the evaluation of gap-graded soils; however, it is conservative in the evaluation of widely-graded soils.
- The Kenney and Lau method proves relatively more successful in the evaluation of widely graded soils. It is conservative in the evaluation of gap-graded soils (for F > 15%).
- The Burenkova method proves less conservative than both the Kezdi and the Kenney and Lau methods.

By comparison of the Kezdi and the Kenney and Lau methods on the basis of theoretical analysis and also experimental evaluation, the following conclusions are drawn:

- The two methods are predicated on a similar approach that involves quantifying the shape of the grain size distribution curve over a defined interval, but differ in how that interval is determined. The Kezdi method establishes it with reference to a constant increment of mass passing, whereas it is established by a variable increment in grain size in the Kenney and Lau method. This yields one point on the grain size curve where both methods converge to give to give the same index value, at F ≈ 15 %.
- Theoretical comparison indicates the filter ratio (D'_{15}/d'_{85}) of the Kezdi method is relatively

more conservative for F < 15 % and the stability index $(H/F)_{min}$ of the Kenney and Lau method is more conservative for F > 15 %. Assessment of the experimental database of 62 gradations also verifies this observation.

- A combination of the Kezdi and the Kenney and Lau methods yields a moderate improvement in the success of both of methods. Applying the Kezdi method to the point on the gradation curve deemed most critical by the Kenney and Lau method causes it to be very successful in distinguishing between stable and unstable gradations in the evaluation of widely-graded soils (Figure 6.22). Combining the boundaries of two methods, as shown in Figure 6.23, in application of the Kenney and Lau method yields a more reliable evaluation in internal stability of soils.

Finally, a new semi-empirical approach is proposed to assess the potential for internal instability in a soil. It invokes the theoretical capillary tube model in order to describe the pore size constriction of the coarse fraction: a constriction ratio of d'_{85}/O_{50} is suggested as a geometric index. The narrow boundary between the internally stable and unstable materials is identified by examining the experimental database of 40 gradations, whose porosities were given in the reference, to give $d'_{85}/O_{50} = 0.42$.

7.1.3 Hydromechanical envelope (onset of internal instability)

The hydromechanical envelope is defined with reference to the concept of stress reduction and verified by experimental findings. The most important findings are summarized below:

- Critical hydraulic gradient is found proportional to the normalized mean vertical effective stress ($\bar{\sigma}'_{vm}$).

- A linear theoretical hydromechanical envelope exists for the onset of internal instability, and it conforms to the experimental findings. The slope of the hydromechanical envelope is proportional to the stress reduction factor (α). The slope of hydromechanical envelope increases with increasing α-value.
- The α-value depends on the shape of the soil gradation curve. The relation between the α-value and geometric indices ($(H/F)_{min}$, D'_{15}/d'_{85} and d'_{85}/O_{50}) was examined. Although there is no definite relation between α and $(H/F)_{min}$, a general correlation exists between α and d'_{85}/O_{50} and also D'_{15}/d'_{85}. The α-value exhibits a linear increase with increase of d'_{85}/O_{50}, and nonlinear decrease with increase of D'_{15}/d'_{85}.
- A unified approach is proposed to assess the onset of internal instability by combining the geometric indices (d'_{85}/O_{50} or D'_{15}/d'_{85}) and the hydromechanical index (α). Given the grain size distribution of a soil, the stress reduction factor (α) can be estimated based on the postulated relation between α and d'_{85}/O_{50} or D'_{15}/d'_{85}, and hence the location of the hydromechanical envelope is determined in $\bar{\sigma}'_{vm}$ v. i_{cr} space. If the seepage gradient in an element of soil reaches this boundary condition at a given effective stress, it is expected that internal instability will be triggered.

7.1.4 Summary of novel research findings

This study systematically examined the influence of geometric and hydromechanical conditions on the internal instability of widely graded soils. Original contributions of the research are summarized as follows:

- In evaluating the potential for internal instability in a cohesionless soil, the general success of the Kenney and Lau and the Kezdi methods has been verified by Skempton

and Brogan (1994). Findings of this thesis yield an advance upon that verification of the two methods, by establishing the Kenney and Lau method is relatively conservative at F > 15% while the Kezdi method is relatively conservative at F < 15%.

- Kovacs (1981) conceived a capillary tube model. Application of that model to analysis of data in this thesis demonstrates the capillary tube model can be used to provide a science-based explanation to the phenomenon of internal instability.
- Moffat (2005) found the relation between effective stress and hydraulic gradient defines hydromechanical envelope to the onset of internal instability, from testing of four soils. The findings of this thesis confirm the hydromechanical envelope also exists for an additional five soil gradations. Skempton and Brogan (1994) postulated a stress reduction concept, whereby stress in the finer fraction of a soil is less than that in the coarser matrix, and this concept is advanced in the thesis to interpret the test data.
- Skempton and Brogan (1994) acknowledged "further work is required to define the relation of critical gradient and stability index". The major contribution of this thesis is to establish an empirical correlation between a hydromechanical index (α) and several geometric stability indices. A unified approach is provided to evaluate the onset of internal instability in widely graded soils.

7.2 Recommendations for future studies

In this study, the theoretical analysis and experimental evaluation are based on unidirectional seepage flow tests in the vertical direction. These tests were performed on reconstituted soil specimens, using a rigid-wall permeameter cell. In further studies, it is recommended that consideration be given to:

- Performing tests in a flexible-wall permeameter, in order to more accurately control

stresses imposed on the specimen.

- Examining internal instability in horizontal flow, which is likely more representative of field conditions (for example, in an earth dam).
- Examining the effect of specimen reconstitution technique on the response to seepage flow.
- Further verifying the boundary between internally stable and unstable soils for which $0.5 < (H/F)_{min} < 1.0$ at $F > 15\%$.
- Use of Discrete Element Methods (for example, Particle Flow Code (PFC), HCItasca) to better understand the stress in the finer fraction, and hence the concept of a stress reduction factor.
- Using Bender Elements technique into the large permeameter to measure shear wave velocity during the permeameter tests, to establish possible correlations to field data.
- Developing a numerical model to simulate the phenomenon of internal instability.

BIBLIOGRAPHY

Aberg, B. (1992), Void ratio of noncohesive soils and similar materials, Journal of Geotechnical Engineering, Vol. 118, No. 9, pp. 1315-1334

Aberg, B. (1992), Hydraulic conductivity of noncohesive soils, Journal of Geotechnical Engineering, Vol. 118, No. 9, pp. 1335-1347

Aberg, B. (1993), Washout of grains from filtered sand and gravel materials, Journal of Geotechnical Engineering, Vol. 119, No. 1, pp. 36 – 53

Aberg, B. (1996), Void sizes in granular soils, Journal of Geotechnical Engineering, Vol. 122, No. 3, pp. 36 – 53

Adel, H.D, Bakker, K.J. and Breteler, M.K. (1988), Internal stability of minestone, Modelling Soil-Water-Structure Interactions: SOWAS 88, Kolkman et al (eds), pp. 225-231, Rotterdam: A.A. Balkema

ASTM (1996), Standard Test Method for Measuring the Soil-Geotextile Clogging Potential by the Gradient Ratio (D5101-96), in the Annual Book of ASTM Standards, Vol. 04.09, ASTM Philadelphia, USA.

Atmatzidis, D.K. (1987), An experimental study of sand migration in gravel. In Proceedings of the 9th ECSMFE, Dublin, pp. 887-890.

Atmatzidis, D.K. (1989), A study of sand migration in gravel. In Proceedings of the 12th ICSMFE, Rio de Janeiro, vol.1, pp. 683-686.

Bertram, G.E. (1940), An Experimental Investigation of Protective Filters, Soil Mechanics Series No. 7, Graduate school of Engineering, Harvard University, Cambridge, MA, USA.

Campbell, J. (2006) On the use of shear wave velocity to characterize changes in fines content of a silty sand, M.A.Sc Thesis, University of British Columbia, Vancouver, BC, Canada.

Charles, J.A. (2001), Internal Erosion in European Embankments Dams, Proceedings of Hydropower 01, ICOLD European Symposium, June 25-27, Geiranger, Norway.

Chapuis, R.P. (1992), Similarity of internal stability criteria for granular soils. Canadian Geotechnical Journal, 29: 711-713.

Chapuis, R.P., Contant, A., and Baass, K.A. (1995), Migration of fines in 0-20 mm crushed base during placement, compaction, and seepage under laboratory conditions, Canadian Geotechnical Journal, Vol. 33, pp. 168-176

Chapuis, R.P. and Aubertin, M. (2004) On the use of the Kozeny-Carman equation to predict the hydraulic conductivity of soils, Reply, Canadian Geotechnical Journal, Vol. 41, pp. 994-996

Chapuis, R.P. and Tournier, J. P. (2006) Simple graphical methods to assess the risk of internal erosion, Proceedings 12th ICOLD Congress, Q86, Barcelona 2006, pp. 319-334

Daniel, D.E. (1994), State-of-the-Art: Laboratory hydraulic conductivity tests for saturated soils, Hydraulic Conductivity and Waste Contaminant Transport in Soil, ASTM STP 1142, David, E. Daniel and Stephen J. Trautwein, Eds., American Society for Testing and Materials, Philadelphia, 1994, pp. 30-78

De Mello, F.B. (1975) Some lessons learned from unsuspected, real and fictitious problems in earth dam engineering in Brazil. 6th Regional Conference for Africa on Soil Mechanics and Foundation Engineering, Durban, S. Africa, 285-304.

Fannin, R.J., Vaid, Y.P., and Shi, Y.C. (1994), Filtration behaviour of nonwoven geotextiles, Canadian Geotechnical Journal, Vol. 31, No. 4, pp.555-563

Fannin, R.J., Vaid, Y.P., and Shi, Y.C. (1994), A critical evaluation of the Gradient Ratio test, Geotechnical Testing Journal, Vol. 17, No. 1, pp.35-42

Fannin, R.J., Vaid, Y.P., Palmeira, E. M. and Shi, Y.C. (1996) A Modified Gradient Ratio Test Device, Recent Developments in Geotextile Filters and Prefabricated Drainage Geocomposites, ASTM STP 1281, Shobha K. Bhatia and L. David Suits, Eds., pp. 100-111

Fannin, R.J. and Moffat, R. (2002) On the internal stability of granular soils, CDA 2002 Annual Conference, Victoria, BC, Canada, pp.1-10.

Fannin, R.J. and Moffat, R. (2006) Observations on internal stability of cohensionless soils, Geotechnique, 56, No. 7, pp.497-500.

Fannin, R.J. and Li, M. (2006) A comparison of two criteria for internal stability on granular soil, 59th Canadian Geotechnical Conference, Vancouver, Oct. 1-4, p.1178-1184

Fisher, G.R., Mare, A.D. and Holtz, R.D. (1999) Influence of procedural variables on the Gradient Ratio Test, Geotechnical Testing Journal, Vol. 22, pp.22-31

Foster, M., Fell, R., and Spannagle, M. (2000) A method for assessing the relative likelihood of failure of embankment dams by piping, Canadian Geotechnical Journal Vol. 37 No. 5 pp. 1025-1061.

Foster, M. and Fell, R. (2001) Assessing embankment dam filters that do not satisfy design criteria, ASCE Journal of Geotechnical and Geoenvironmental Engineering, Vol. 127, No. 5, pp.398-407

Frost, J.D. and Park, J.Y. (2003) A critical assessment of the moist tamping technique, Geotechnical Testing Journal, Vol. 26, No. 1, pp.1-14

Fuller, W.B. and Thompson, S.E. (1907) The laws of proportioning concrete, Transactions American Society of Civil Engineering, 59

Garner, S.J. and Sobkowicz, J.C. 2002. Internal Stability in Gap-Graded Cores and Filters, Proceeding of Canadian Dam Association Annual Conference, October 6-10, Victoria, BC, Canada.

Giroud, J.P. (1996) Granular filters and geotextile filters, Geofilters'96, pp. 565-680

Harney, M.D. and Holtz, R.D. (2001) A flexible wall gradient ratio test, Geosynthetics Conference 2001, pp. 409-422

Head, K.H., (1992) Manual of soil laboratory testing, London, Pentech Press,

Honjo, Y., Haque, M.A. and Tsai, K.A. (1996) Self-filtration behaviour of broadly and gap-graded cohesionless soils. Geofilters' 96, BiTech Publishers, Montreal, Canada, 227-236.

ICOLD (1994) Embankment dams: granular filters and drains Bulletin No. 95. International Commission on Large Dams, Paris, France, 256p

Indraratna, B. and Vafai, F. (1997) Analytical model for particle migration within base soil-filter system, ASCE Journal of Geotechnical and Geoenvironmental Engineering, Vol. 123, pp. 100-109.

Indraratna, B. and Radampola, S. (2002) Analysis of critical hydraulic gradient for particle movement in filtration, ASCE Journal of Geotechnical and Geoenvironmental Engineering, Vol. 128, pp. 347-350

Jones, J.A.A. (1981) The nature of soil piping: a review of research, Geo Books, Norwich. 301p

Karpoff, K.P. (1955) The use of Laboratory Tests to Develop Design Criteria for Protective Filters, Proceedings of American Society for Testing Materials 5, pp. 1183-1198.

Kenney, T.C., Chacal R., Chiu, E., Ofeogbu, G.I., Omanga, G.N., and Ume, C.A. (1985), Controlling constriction sizes of granular filters, Canadian Geotechnical Journal, Vol.22, No.1 pp.32-43

Kenney, T.C. and Lau, D. (1985) Internal stability of granular filters. *Canadian Geotechnical Journal*, 22: 215-225.

Kenney, T.C. and Lau, D. (1986) Internal stability of granular filters: Reply. Canadian Geotechnical Journal, 23: 420-423.

Kezdi, A. (1979) Soil physics – selected topics. Elsevier Scientific Publishing Company, Amsterdam, 160p.

Khan, A. S. (2003) Experimental Study for Evaluating the Internal Stability of Gap-Graded Soils, M.A.Sc Thesis, University of British Columbia, Vancouver, BC, Canada.

Kovacs, G. (1981) Seepage hydraulics. Elsevier Scientific Publishing Company, Amsterdam, 730p.

Kuerbis, R.H. Vaid, Y.P (1988) Sand Sample Preparation – The Slurry Deposition Method, Soils and Foundations, Vol. 28, No. 4, pp. 107-118.

Ladd, R.S (1978) Preparing Test Specimens Using Undercompaction, Geotechnical Testing Journal, GTJODJ, Vol.1, No.1, pp. 16-23.

Lafleur, J. (1984) Filter Testing of Broadly Graded Cohesionless Tills, Canadian Geotechnical Journal, Vol. 21, No. 4, pp. 634-643.

Lafleur, J., Mlynarek, J., and Rollin, A.L. (1989) Filtration of Broadly Graded Cohesionless Soils, ASCE, Journal of Geotechnical Engineering, Vol. 115, No.12, December 1989, pp. 1747-1769.

Lafleur, J., T. Eichenauer and G.Werner (1996) Geotextile Filter Retention Criteria for Well Graded Cohesionless Soils, Geofilters' 96, pp. 429-438.

Lafleur, J., Montes, P., Alicescu. V., and Phuong, N. (2000) Laboratory Simulations of Filtration through Dam Cores made of Broadly Graded Moraines, Proceedings of Geofilters 2000 Conference, Warsaw, Poland, June 5-7, pp. 135-144.

Li, G.X., Jie, Y.X. and Li, Q.Y. (2004) Yangtze dyke and its strengthening, Lowland Technology International, Vol. 5, No. 2, pp. 39-46

Li, M. (2006) Personal communication with C.X. Mao and X.B. Duan, e-mail correspondence, August 26, 2006

Liu, J. (2005) Seepage control of earth-rock dams: theoretical basis, engineering experiences and lessons (in Chinese), China Waterpower Press, Beijing, 219p.

Locke, M., Indraratna, B. and Adikari, G., (2001) Time-dependent particle transport through granular filters, ASCE Journal of Geotechnical and Geoenvironmental Engineering, Vol. 127, No.6, pp.521-529

Lubochkov, E.A. (1969) The calculation of suffosion properties of noncohesive soils when using the non-suffosion analog (in Russian). International Conference on Hydraulic Research, Brno, Czechoslovakia, 135-148.

Lowe, J. (1988) Seepage analysis, in advanced dam engineering, for design, construction and rehabilitation. ed. Robert B. Jansen, Van Nostrand Rheinhold, 270-275.

Mao, C.X. (2005) Study on piping and filters: Part I of piping (in Chinese). Rock and Soil Mechanics, Vol.26, No.2: 209-215.

Milligan, V. (1986) Internal stability of granular filters: Discussion. Canadian Geotechnical Journal, 23: 414-418.

Minister of Water Resource, (2005) Code of geological investigation for levee project (SL188-2005), China Waterpower Press, Beijing, China, 49p.

Minister of Water Resource, (2001) Design specification for sluice (SL265-2001) (2001), China Waterpower Press, Beijing, China, 128p.

Morgan, G.C. and Harris, M.C. (1967) Portage mountain dam II Materials, XIXth Canadian Soil Mechanics Conference, II, Vol. IV, No.2 pp.142-166

Moffat, R. (2002) A Laboratory Study of Particle Migration in Cohesionless Soils, M.A.Sc Thesis, University of British Columbia, Vancouver, BC, Canada.

Moffat, R. (2005) Experiments on the internal stability of widely graded cohesionless soils, PhD thesis, the University of British Columbia, Vancouver, Canada.

Moffat, R. and Fannin, R.J. (2006) A large permeameter for study of internal stability in cohensionless soils, Geotechnical Testing Journal, Vol. 29, No. 4, pp.1-7

Molenkamp, F., Calle, E.O.F., Heusdens, J.J. and Koenders, M.A. (1979), Cyclic filter tests in a triaxial cell, 7th European Conference on Soil Mechanics and Foundation Engineering, Brighton, England, 2: 97-101.

Richards, K., and Reddy, K.R. (2007), Critical Appraisal of Piping Phenomena in Earth Dams, Bulletin of Engineering Geology and the Environment, Vol.66, No.4, pp.381-402

Sherard, J.L. (1979) Sinkholes in Dams of Coarse, Broadly Graded Soils. In Proceedings of the 13th ICOLD, New Dehli, India. Vol.2, pp.25-34

Sherard, J.L., Dunnigan, L.P., Talbot, J.R. (1984). Basic Properties of Sand and Gravel Filters, Journal of Geotechnical Engineering, Vol. 110, No. 6, pp. 684-700.

Sherard, J.L., Dunnigan, L.P., Talbot, J.R. (1984). Filters for silts and clays, Journal of Geotechnical Engineering, Vol. 110, No. 6, pp. 701-718.

Sherard, J.L. and Dunnigan, L.P. (1986) Internal stability of granular filters: Discussion. Canadian Geotechnical Journal, 23: 418-420.

Sherard, J.L. and Dunnigan, L.P. (1989) Critical filters for impervious soils. Journal of Geotechnical Engineering, Vol. 115, No. 7, pp. 927-947

Shi, Y.C. (1993) Filtration Behaviour of Non-Woven Geotextiles in the Gradient Ratio Test, M.A.Sc Thesis, University of British Columbia, Vancouver, BC, Canada.

Silveira, A. (1965), An analysis of the problem of washing through in protective filters. In Proceedings of the 6th ICSMFE, Montreal, vol.2, pp. 551-555.

Skempton, A.W. and Brogan, J.M. (1994) Experiments on piping in sandy gravels. Geotechnique, 44: 449-460.

Sterpi, D. (2003) Effects of the erosion and transport of fine particles due to seepage flow, Internatioal Journal of Geomechanics, Vol. 3, No. 1, pp.111-122.

Stewart, R.A. and Watts, B.D., (2000). The WAC Bennett Dam sinkhole incident, Canadian Geotechnical Society, Proceedings of 53rd Canadian Geotechnical Conference, Montreal, October 15-18.

Tanaka, T. and Toyokuni, E. (1991) Seepage-failure experiments on multi-layered sand columns, Soils and Foundations, Vol. 31, No. 4, pp. 13-36

Terzaghi, K. (1922) Failuare of dam foundations by piping and means for preventing it (in German), Die Wasserkraft, Special Forchheimer Issue, 17, pp. 445-449

Terzaghi, K. (1939) Soil mechanics: a new chapter in engineering science. J. Instn. Civ. Engrs, 12: 106-141.

Terzaghi, K., Peck, R.B. and Mesri, G. (1996) Soil mechanics in engineering practice, 3rd edition, New York, NY: John Wiley and Sons, 592p.

Tomlinson, S.S. and Vaid, Y.P. (2000) Seepage Forces and Confining Pressure Effects on Piping Erosion, Canadian Geotechnical Journal, Vol. 37, pp. 1-13.

U.S. Army Corps of Engineers (1953), Filter experiments and design criteria, Technical Memorandum, No. 3-360, Waterways Experiment Station, Vicksburg

Vallejo, L.E. (2001) Interpretation of the limits in shear strength in binary granular mixtures, Canadian Geotechnical Journal, Vol. 38, pp. 1097-1104

Valdes, R. (2002), Fines migration and formation damage – microscale studies, PhD thesis, the Georgia Institute of Technology, Atlanta, USA

Van ZYL, D. and Harr, M.E. (1981), Seepage erosion analysis of structures, Proceedings of 10th International Conference on Soil Mechanics and Foundation Engineering, Vol. 1, pp. 503-509

Vaughan, P.R. (2000) Filter Design for Dam Cores of Clay, A Retrospect, Proceedings of Geofilters 2000 Conference, Warsaw, Poland, June 5-7, pp. 189-196.

Wan, C.F. and Fell, R. (2004a) Experimental investigation of internal instability of soils in embankment dams and their foundations, UNICIV Report No. R-429, the University of New South Wales, Sydney, Australia, 223p

Wan, C.F. and Fell, R. (2004b) Experimental investigation of internal erosion by the process of suffusion in embankment dams and their foundations, ANCOLD Bulletin No. 126, pp.69-78

Zhang, L.M and Chen Q. (2006) Seepage failure mechanism of the GouHou rockfill dam during reservoir water infiltration, Soils and Foundations, Vol. 46, No. 5, pp. 557-568

APPENDICES

Appendix A Effective stress model

A.1 Formulations

A simple model was used to analyse the distribution of vertical effective stress with seepage flow. It considers the influence of sidewall friction and also accommodates variations of hydraulic gradient along the specimen length. The soil column is divided into n layers (Figure A.1a). Consider a layer of thickness dz (Figure A.1b), for which equilibrium of the element is given by:

$$-\pi R^2 \frac{d\sigma}{dz} dz + 2\pi R\mu K_0 \sigma' dz + \pi R^2 dz\gamma = 0 \qquad \text{(A.1)}$$

Where, σ and σ' are total stress and effective stress respectively; γ = unit weight of a soil; R = radius of specimen; μ = friction between sidewall and soil = $\tan(\delta)$; K_0 = coefficient of earth pressure at rest.

According to the principle of effective stress, $\sigma = \sigma' + u$, hence A.1 may be re-written as:

$$-\pi R^2 \frac{d\sigma'}{dz} dz - \pi R^2 \frac{du}{dz} dz + 2\pi R\mu K_0 \sigma' dz + \pi R^2 dz\gamma = 0 \qquad \text{(A.2)}$$

where, u = pore water pressure.

According to Bernoulli's equation, the total head (h) at a point can be represented by,

$$h = z - \frac{u}{\gamma_w} \tag{A.3}$$

$$i_z = \frac{dh}{dz} = 1 - \frac{1}{\gamma_w}\frac{du}{dz} \tag{A.4}$$

where, i_z = hydraulic gradient across the element; and γ_w = unit weight of water.

Knowing $\gamma' = \gamma - \gamma_w$, and substituting Eqs. A.3 and A.4 into Eq. A.2, enables the governing equation for seepage flow to be obtained:

$$-\frac{d\sigma'}{dz} + \frac{2\mu K_0}{R}\sigma' + \gamma' + i_z\gamma_w = 0$$

or

$$-\frac{d\sigma'}{dz} + \frac{4f}{D}\sigma' + \gamma' + i_z\gamma_w = 0 \tag{A.5}$$

Where, D = diameter of specimen = 2R; i_z is positive for downward flow and negative for upward flow; $f = \mu K_0$ = soil-wall friction, and f is positive when the friction force acts downward and negative when it acts upward.

A.2 Solution for the hydrostatic condition

The hydrostatic condition is the case for no seepage flow (i = 0). Eq. A.5 reduces to:

$$\frac{d\sigma'}{dz} - \frac{4f}{D}\sigma' = \gamma' \tag{A.6}$$

It is assumed that γ', and f are constant along the specimen. The boundary condition, namely the effective stress on the top of specimen, σ'_{t0}, is also known. A solution for the first

order ordinary differential equation is applied to Eq.A.6. Therefore, the effective stress at any depth z ($\sigma_z^{'}$), can be obtained,

$$\sigma_z^{'} = -\frac{\gamma^{'} D}{4f} + (\sigma_{t0}^{'} + \frac{\gamma^{'} D}{4f}) e^{-\frac{4fz}{D}} \tag{A.7}$$

The effective stress at the bottom of the specimen, $\sigma_{b0}^{'}$, is obtained for z = L (Figure A.1a),

$$\sigma_{b0}^{'} = -\frac{\gamma^{'} D}{4f} + (\sigma_{t0}^{'} + \frac{\gamma^{'} D}{4f}) e^{-\frac{4fL}{D}} \tag{A.8}$$

$$\sigma_{b0}^{'} = -\frac{\gamma^{'} D}{4f} (1 - e^{-\frac{4fL}{D}}) + \sigma_{t0}^{'} e^{-\frac{4fL}{D}} \tag{A.9}$$

By inspection, and ignoring the first term in the right side of Eq. A.9, the ratio of effective stress between the bottom (z = L) and top (z = 0) of specimen is given by:

$$\sigma_{b0}^{'} \Big/ \sigma_{t0}^{'} = e^{-\frac{4fL}{D}} \tag{A.10}$$

A.3 Solution for seepage condition (*i* >0)

In the experimental tests, measurements reveal the seepage gradient may not be uniformly distributed along the specimen length. Considering the variation of seepage gradient, there is no analytical solution for Eq. A.5. A sub-layer method is used to solve the problem.

Written in finite difference form, Eq. A.5 becomes

$$-\frac{\Delta\sigma'}{\Delta z} + \frac{4f}{D}\bar{\sigma}' + \gamma' + i_z\gamma_w = 0$$

or in the layer j

$$-\frac{\sigma_j^{'}-\sigma_{j-1}^{'}}{z_j}+\frac{4f}{D}\bar{\sigma}_{vmj}^{'}+\gamma'+i_j\gamma_w=0 \qquad \text{(A.11)}$$

Once again, γ' and f are assumed constant along the specimen length, and the effective stress in any sub-layer is assumed linearly distributed. In layer j (Figure A.1a), the relation between effective stress at the bottom and top of the layer, $\sigma_j^{'}$ and $\sigma_{j-1}^{'}$, can be expressed as,

$$\sigma_j^{'}=\sigma_{j-1}^{'}+i_j\gamma_w z_j+\gamma_j^{'}z_j+\sigma_{vmj}^{'}\frac{4f}{D}z_j \qquad \text{(A.12)}$$

Where, $\sigma_{vmj}^{'}$ = vertical mean effective stress in layer j. Linear distribution in effective stress in layer j leads to $\sigma_{vmj}^{'}=\frac{1}{2}(\sigma_{j-1}^{'}+\sigma_j^{'})$. Therefore, Eq. A.12 becomes,

$$\sigma_j^{'}=a_jb_j\sigma_{j-1}^{'}+b_ji_j\gamma_w z_j+b_j\gamma_j^{'}z_j \qquad \text{(A.13)}$$

Where, $a_j=1+\frac{z_j}{D}2f$; $b_j=1\Big/(1-\frac{z_j}{D}2f)$ (A.14)

There are two unknown variables for each layer, hence for an n-layer system, there are 2n unknown variables. Since the soil-wall friction (f) is also assumed, there are 2n+1 unknown variables in total. There are n equilibrium equations (Eq. A.13) and (n+1) boundary conditions. The boundary conditions include: (1) the known effective stress on the top and bottom of specimen ($\sigma_{t0}^{'}$ and $\sigma_{b0}^{'}$); (2) the stress continuity at the interface of two sub-layers. Therefore, the governing equation Eq. A.11 can be solved, yielding the distribution of effective stress along the specimen length.

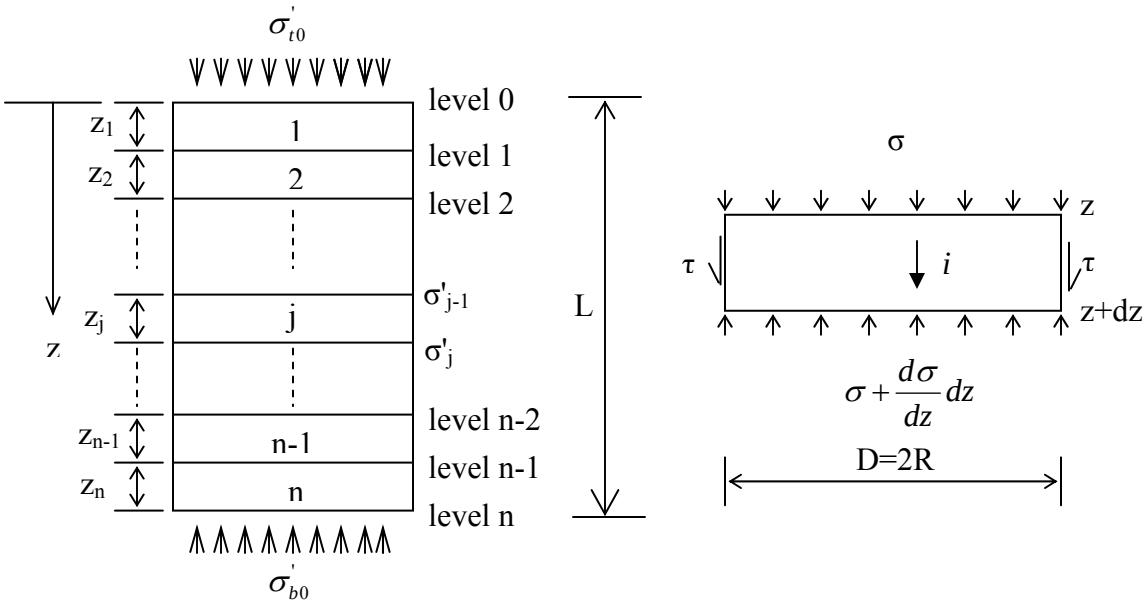

(a) (b)

Fig. A.1 Schematic soil column and representative soil element

Appendix B Theoretical hydromechanical envelope

B.1 Introduction

Seepage failure is believed to be governed by effective stress. Terzaghi (1933) analyzed seepage failure in a uniform sand column subject to upward flow and found that, at critical hydraulic gradient, the sand was in a liquefied or quick state at which the effective stress in the soil mass was zero. Tanaka & Toyokuni (1991) studied seepage failure of sand columns with overburden pressure. They observed a horizontal crack at the bottom of the sand column when seepage failure took place, and defined seepage failure to occur when effective stress became zero at a certain horizontal plane. Skempton and Brogan (1994) studied the internal instability of gap-graded sandy gravels and suggested that finer particles in the soil mass carried much less effective stress than coarser particles, which resulted in seepage failure at a much lower hydraulic gradient than the theoretical gradient for heave failure. The findings implied that the effective stress in the finer particles became zero for internal instability to occur. Moffat (2005) conducted tests on widely graded gravel-sand-silt mixes with different overburden stresses, and found a linear relation exists between mean vertical effective stress σ'_{vm} and local critical hydraulic gradient i_{cr}, termed the hydromechanical envelope.

The above observations indicate the onset of seepage failure is governed by a combination of critical gradient and effective stress. In this study, the relation between the normalized mean vertical effective stress $\overline{\sigma}'_{vm}$ and critical gradient i_{cr} is examined. More specifically, advances are made to the concept of a theoretical hydromechanical envelope at which internal instability initiates based on Skempton and Brogan's α concept.

B.2 Critical hydraulic gradient for internally stable materials

Heave failure will occur when sufficient upward seepage flow is applied to an internally stable material. In an internally stable material, effective stresses are believed to be uniformly distributed among the finer particles and coarser particles (Skempton and Brogan, 1994). When subjected to upward seepage flow, effective stress at a certain horizontal plane reduces to zero, at which the resistance forces (for example, self-weight) in the soil mass cannot resist the seepage force, the soil mass will be pushed upward resulting in heave failure.

Consider a soil layer with effective stress σ'_{t0} (Figure B.1a). For hydrostatic conditions (i = 0), the initial effective stress distribution is shown schematically in Figure B.1b. The effective stress at the bottom of the layer is:

$$\sigma'_{b0} = \sigma'_{t0} + \gamma' \Delta z \tag{B.1}$$

For upward seepage flow, at hydraulic gradient i, the effective stress at the bottom of the layer decreases:

$$\sigma'_{b} = \sigma'_{t0} + \gamma' \Delta z - i\gamma_w \Delta z \tag{B.2}$$

At the critical condition (Figure B.1c), σ'_b becomes zero, and the critical hydraulic gradient is given by:

$$i_c = \frac{\sigma'_{t0}}{\gamma_w \Delta z} + \frac{\gamma'}{\gamma_w} \tag{B.3}$$

In a thin layer of soil, it is reasonable to assume that the effective stress is linearly distributed with depth; therefore, the mean vertical effective stress in the soil layer can be expressed as,

$$\sigma'_{vm0} = 0.5\ (\sigma'_{t0} + \sigma'_{b0}) \quad \text{(B.4)}$$

$$\sigma'_{vm} = 0.5\ (\sigma'_{t0} + \sigma'_{b}) \quad \text{(B.5)}$$

Substituting Eqs. B.4 and B.5 into Eqs. B.1 and B.2 yields,

$$\sigma'_{vm0} = \sigma'_{t0} + 0.5\gamma'\Delta z \quad \text{(B.6)}$$

$$\sigma'_{vm} = \sigma'_{t0} + 0.5\gamma'\Delta z - 0.5i\gamma_w\Delta z \quad \text{(B.7)}$$

Substituting Eq. B.6 into Eq. B.7, establishes the variation of mean vertical effective stress as a result of seepage flow:

$$\sigma'_{vm} = \sigma'_{vm0} - 0.5i\gamma_w\Delta z \quad \text{(B.8)}$$

Substituting Eq. B.6 into Eq. B.3, the critical gradient in terms of mean effective stress is obtained,

$$i_c = \frac{\sigma'_{vm0} + 0.5\gamma'\Delta z}{\gamma_w\Delta z} \quad \text{(B.9)}$$

At the critical condition, $\sigma'_b = 0$ while $\sigma'_{vm} \geq 0$, yielding:

$$\sigma'_{vm} = 0.5\sigma'_{t0} = 0.5(\sigma'_{vm0} - 0.5\gamma'\Delta z) \quad \text{(B.10)}$$

By inspection, for the case of self-weight loading only, $\sigma'_{t0} = 0$, $\sigma'_{vm0} = 0.5\gamma'\Delta z$, Eq. B.10 gives:

$$\sigma'_{vm} = 0 \quad \text{(B.11)}$$

B.3 Critical hydraulic gradient for internally unstable materials

In an internally unstable material, the effective stress is not uniformly distributed between finer and coarser particles, and it has been postulated the finer particles only carry a reduced portion of the effective stress (Skempton and Brogan, 1994). Consider now a soil layer with overburden pressure σ'_{t0}, for which the effective stress in the finer particles ($\sigma'_{f,x}$) is given by (Figure B.2):

$$\sigma'_{f,x} = \alpha\sigma'_{x} \tag{B.12}$$

where α is a stress reduction factor proposed by Skempton and Brogan (1994), and the subscript x = b, t, and vm describes the bottom, top, and mean vertical effective stress, respectively.

For upward seepage flow, the effective stress in the finer particles ($\sigma'_{f,b}$), becomes

$$\sigma'_{f,b} = \alpha(\sigma'_{t0} + \gamma'\Delta z) - i\gamma_w\Delta z \tag{B.13}$$

At the critical gradient i_{cr}, effective stress in the finer particles ($\sigma'_{f,b}$), becomes zero, while effective stress in the coarser particles is still greater than zero. The finer particles are able to move into the interstices of coarser particles or alternatively, to move from the exit face. Accordingly, critical hydraulic gradient, i_{cr} for internal instability can be expressed as:

$$i_{cr} = \alpha\left(\frac{\sigma'_{t0}}{\gamma_w\Delta z} + \frac{\gamma'}{\gamma_w}\right) \tag{B.14}$$

By inspection, the critical hydraulic gradient increases with increase of effective stress.

Substituting Eq. B.6 into Eq. B.14, the critical gradient can be expressed in terms of mean effective:

$$i_{cr} = \alpha \left(\frac{\sigma'_{vm0} + 0.5\gamma'\Delta z}{\gamma_w \Delta z} \right) \tag{B.15}$$

A comparison of Eq. B.9 with Eq. B.15, or Eq. B.3 with Eq. B.14, shows the general relation of critical hydraulic gradient with a given overburden pressure (between unstable and stable soils) is defined by:

$$i_{cr} = \alpha \, i_c \tag{B.16}$$

Eq. B.16 establishes the critical hydraulic gradient in an unstable soil is only a part of the critical hydraulic gradient in a stable soil. When α=1, the soil is internally stable, and the critical hydraulic gradient is equal to the theoretical value for heave failure. In contrast, when α=0, the soil is physically unstable and prone to catastrophic segregation. Hence it is reasonable to expect the value of α is a function of the geometric characteristics of the grain size distribution.

B.4 Hydromechanical envelope

B.4.1 Theoretical description without sidewall friction

The successive values of effective stress that exist in a soil mass, as it is subject to seepage flow, can be depicted using a hydromechanical path. Specifically, the hydromechanical path describes the variation of mean vertical effective stress with the hydraulic gradient (see

Eq.B.8). Written in a non-dimensional form by dividing $\gamma_w \Delta z$, the hydromechanical path is given by:

$$\bar{\sigma}'_{vm} = \bar{\sigma}'_{vm0} - 0.5i \tag{B.17}$$

where, $\bar{\sigma}'_x = \dfrac{\sigma'_x}{\gamma_w \Delta z}$ = normalized effective stress (B.18)

The variation of normalized mean vertical effective stress with upward hydraulic gradient is illustrated in i : $\bar{\sigma}'_{vm}$ space (Figure B.3). Mean vertical effective stress decreases with increase of hydraulic gradient. Based on Eq. B.17, the hydromechanical path starts at $\bar{\sigma}'_{vm0}$ (point O, for i = 0), and progresses at a slope = $\Delta i / \Delta \bar{\sigma}'_{vm}$ = -2. It terminates at $\bar{\sigma}'_{vm}$ = $0.5\,(\bar{\sigma}'_{vm0} - 0.5\gamma'/\gamma_w)$, at which state heave failure occurs (point P_s). Since all candidate hydromechanical paths are parallel with a slope of -2, by examining the geometric relation in the $\bar{\sigma}'_{vm}$ -i diagram, the hydromechanical envelope can be simply expressed as,

$$i = 2(\bar{\sigma}'_{vm} + 0.5\gamma'/\gamma_w) \tag{B.19}$$

As the hydromechanical path for an internally stable material reaches this envelope (Figure B.3), heave failure occurs.

Now consider internally unstable materials. Prior to the onset of internal instability, an internally unstable material behaves in the same manner as an internally stable material, therefore, at a given vertical effective stress, the hydromechanical path for an internally unstable material coincides with that for an internally stable material. The hydromechanical path starts at $\bar{\sigma}'_{vm0}$ (point O), and moves toward the envelope given by

$i = 2(\bar{\sigma}'_{vm} + 0.5\gamma'/\gamma_w)$. However, the hydromechanical path of an unstable material does not reach this envelope. Prior to attaining point P_s, the effective stress in finer fraction particles diminishes to zero. Based on the relation $i_{cr} = \alpha\, i_c$, the hydromechanical path for an unstable material terminates at point P_u.

At different values of mean vertical effective stress, various parallel hydromechanical paths plot in the i : $\bar{\sigma}'_{vm}$ space. The relation bounding all of these hydromechanical paths defines the corresponding hydromechanical envelope. If α is constant and stress-independent for a given soil within a certain stress range, the hydromechanical envelope will be a straight line. By examining the relation in the $\bar{\sigma}'_{vm}$ -i diagram, the hydromechanical envelope can be simply expressed as,

$$i = \frac{\alpha}{1 - 0.5\alpha}(\bar{\sigma}'_{vm} + 0.5\gamma'/\gamma_w) \qquad \text{(B.20)}$$

Eq. B.20 defines that the hydromechanical envelope as a function of α. When α = 1, the envelope becomes $i = 2(\bar{\sigma}'_{vm} - 0.5\gamma'/\gamma_w)$, namely the boundary for internally stable material. When α = 0, as before the materials is prove to catastrophic segregation. For $0 < \alpha < 1$, the material is deemed a hydraulically unstable material for which instability is initiated by the critical gradient.

By inspection of Eq. B.20, the interception of a hydromechanical envelope at "i" axis is $0.5\frac{\alpha}{1-0.5\alpha}\frac{\gamma'}{\gamma_w}$, which varies with the value of α. When α = 1, the interception is γ'/γ_w, namely the critical gradient for heave failure from Terzaghi's piping theory. Although the intercept varies with the value of α, the intercept on the "$\bar{\sigma}'_{vm}$" axis is constant, since all envelopes converge to the point at $\bar{\sigma}'_{vm} = -0.5\gamma'/\gamma_w$ at i = 0 (Figure B.3).

B.4.2 Influence of sidewall friction

In the permeameter tests of the current study, sidewall friction is recognized to influences the distribution of effective stress along the specimen. Therefore, the hydromechanical path (Eq. B.17) and the corresponding hydromechanical envelope (Eq. B.20) should be modified accordingly.

Considering the soil element shown in Figure B.4, for which the limit equilibrium equations (Eqs. B.1 and B.2) become,

$$\sigma'_{b0} = \sigma'_{t0} + \gamma'\Delta z - 4f_0\frac{\Delta z}{D}\sigma'_{vm0} \qquad \text{at i = 0} \qquad \text{(B.21)}$$

and

$$\sigma'_b = \sigma'_{t0} + \gamma'\Delta z - 4f_c\frac{\Delta z}{D}\sigma'_{vm} - i\gamma_w\Delta z \qquad \text{at upward seepage flow i > 0} \qquad \text{(B.22)}$$

where D = diameter of specimen, Δz = thickness of soil layer, f_0, f_c = frictional resistance between the sidewall and specimen at the hydrostatic condition and for seepage flow *i*, respectively.

Again, it is assumed the effective stress within the layer is linearly distributed, and therefore the relations of Eqs. B.4 and B.5 remain valid. Substituting Eqs. B.4 and B.5 into Eqs.B.21 and B.22, the hydromechanical path considering the influence of sidewall friction can be expressed as,

$$(1+2f_c\Delta z/D)\sigma'_{vm} =(1+2f_0\Delta z/D)\sigma'_{vm0} - 0.5i\gamma_w\Delta z \quad \text{(B.23)}$$

Written in short form, Eq. B.23 becomes

$$A_c\sigma'_{vm} =A_0\sigma'_{vm0} - 0.5i\gamma_w\Delta z \quad \text{(B.24)}$$

where $A_c = 1+2f_c\Delta z/D$ (B.25a)

$$A_0 = 1+2f_0\Delta z/D \quad \text{(B.25b)}$$

Written in non-dimensional form by dividing $\gamma_w\Delta z$, Eq. B.24 becomes,

$$A_c\bar{\sigma}'_{vm} = A_0\bar{\sigma}'_{vm0} - 0.5i \quad \text{(B.26)}$$

At the critical condition, $\sigma'_b =0$, and the critical gradient i_c is given by:

$$i_c = A_0(2-A_c)\bar{\sigma}'_{vm0} + 0.5A_c\frac{\gamma'}{\gamma_w} \quad \text{(B.27)}$$

and corresponding normalized mean vertical effective stress

$$\bar{\sigma}'_{vm} = 0.5(A_0\bar{\sigma}'_{vm0} - 0.5\frac{\gamma'}{\gamma_w}) \quad \text{(B.28)}$$

Eq. B.26 indicates the slope of hydromechanical path that takes friction in account is $-2A_c$ rather than -2. By examining the two boundary relations, the hydromechanical envelope for an internally stable material can be expressed as:

$$i = 2(2 - A_c)\bar{\sigma}'_{vm} + \frac{\gamma'}{\gamma_w} \tag{B.28}$$

and that for an internally unstable material, as:

$$i = \frac{\alpha A_c(2 - A_c)}{1 - 0.5\alpha(2 - A_c)}(\bar{\sigma}'_{vm} + \frac{0.5}{2 - A_c}\frac{\gamma'}{\gamma_w}) \tag{B.29}$$

From Eq. B.25a, it is evident that $A_c(2 - A_c) = 1 - (2f_c\frac{\Delta z}{D})^2$. Furthermore, when $f_c < 0.3$, $\Delta z/D \approx 0.25 \sim 0.4$, and then $A_c(2 - A_c) \approx 1$. Therefore, the hydromechanical envelope for internally stable and unstable materials (Eqs. B.28 and B.29) can be simplified as (Figure B.5),

$$i = \frac{2}{A_c}(\bar{\sigma}'_{vm} + 0.5A_c\frac{\gamma'}{\gamma_w}) \tag{B.30}$$

$$i = \frac{\alpha}{1 - 0.5\alpha / A_c}(\bar{\sigma}'_{vm} + 0.5A_c\frac{\gamma'}{\gamma_w}) \tag{B.31}$$

When $f_c = 0$, then $A_c = 1$, and Eqs. B.30 and B.31 become Eqs.B.19 and B.20, respectively. By inspection, Eq.B.30 is a special case of Eq.B.31 when $\alpha = 1$.

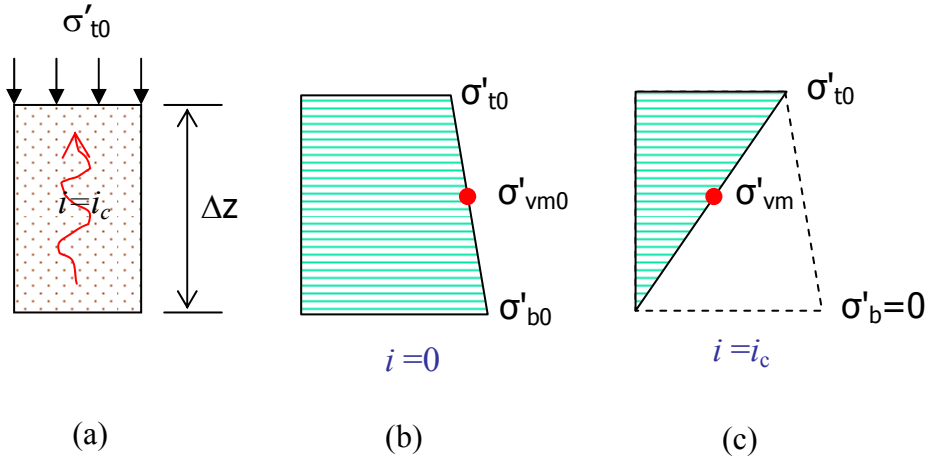

Figure B.1 Schematic stress distributions for an internally stable material

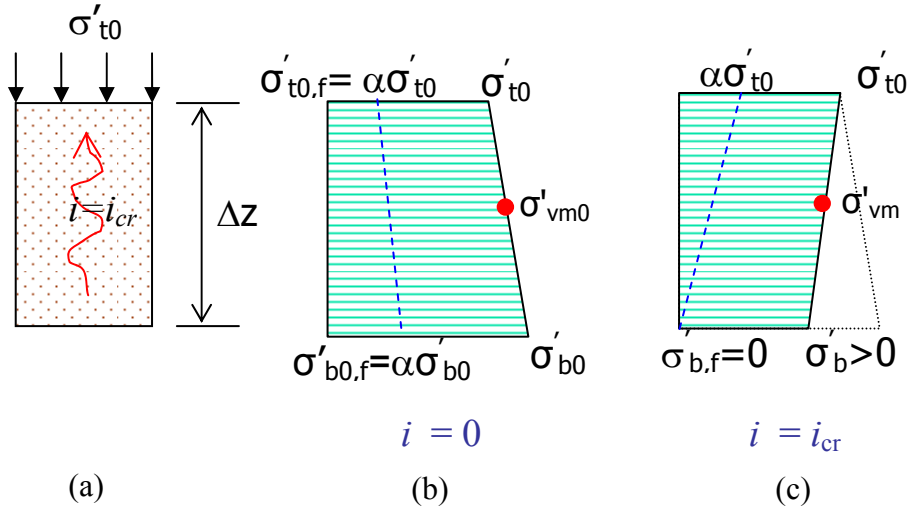

Figure B.2 Schematic stress distributions for an internally unstable material

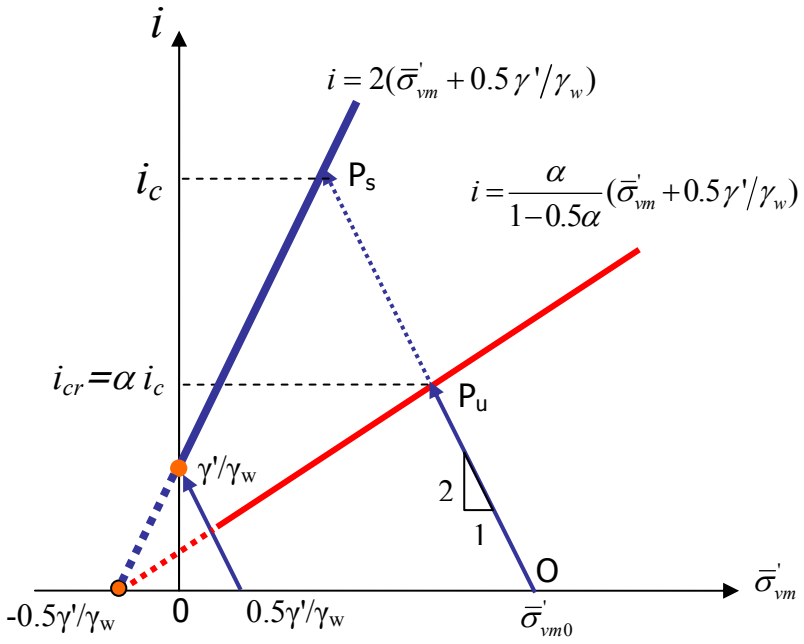

Figure B.3 Theoretical hydromechanical envelope ($f = 0$)

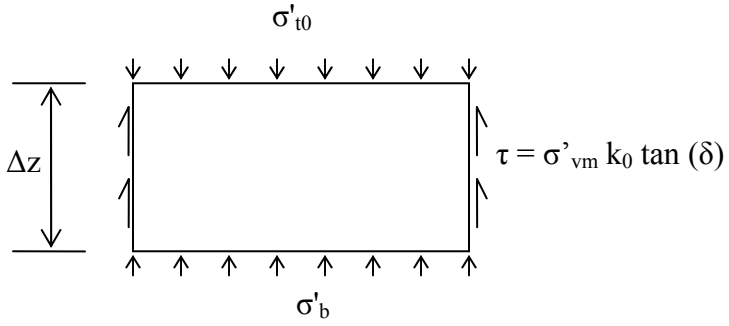

Figure B.4 Representative soil layer

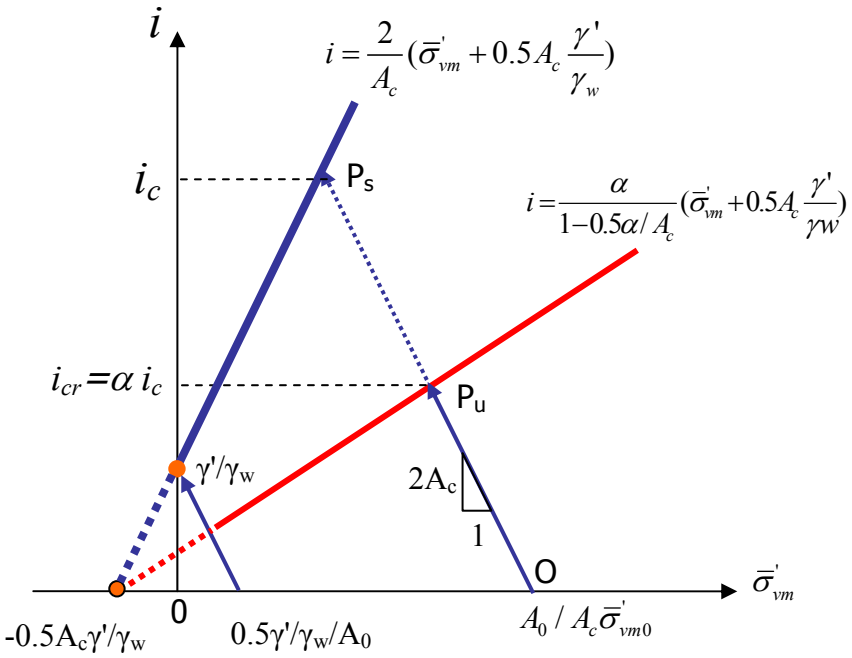

Figure B.5 Theoretical hydromechanical envelope ($f > 0$)

Appendix C Water head distribution

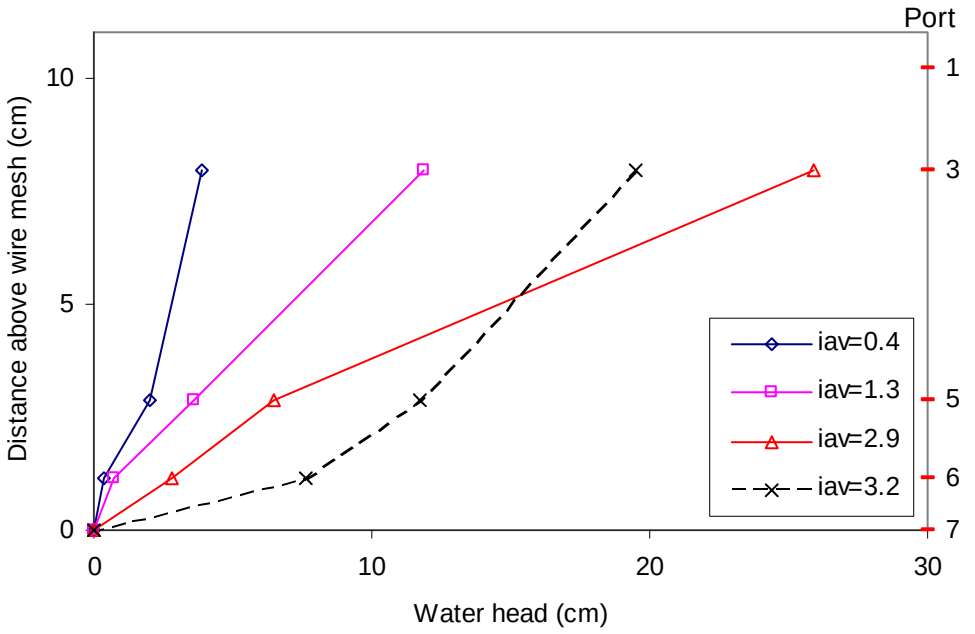

Figure C.1 Water head distribution in the test FR8-25-D0

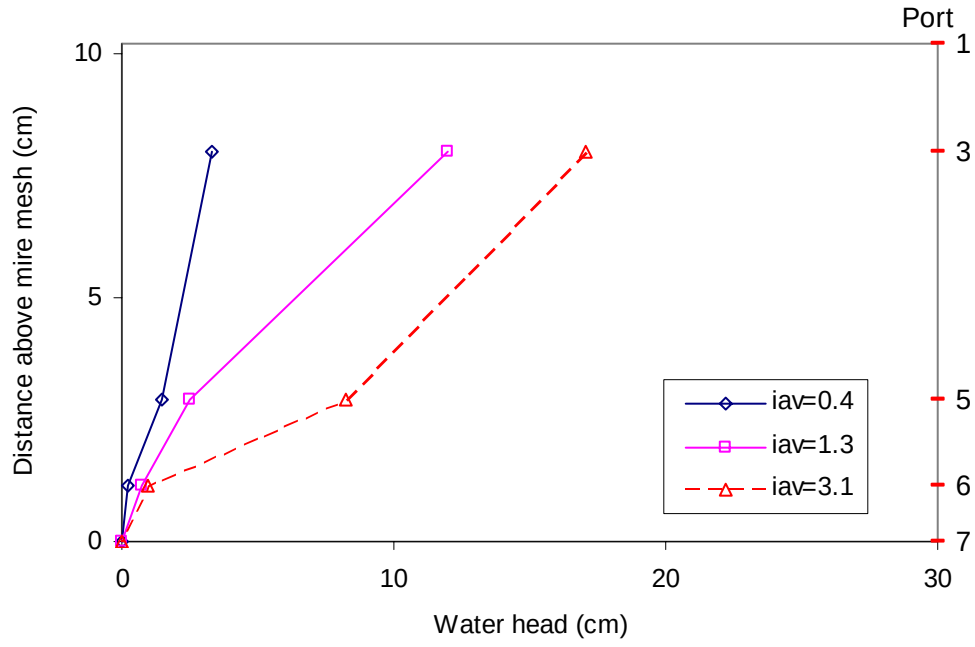

Figure C.2 Water head distribution in the test FR8-25-D1

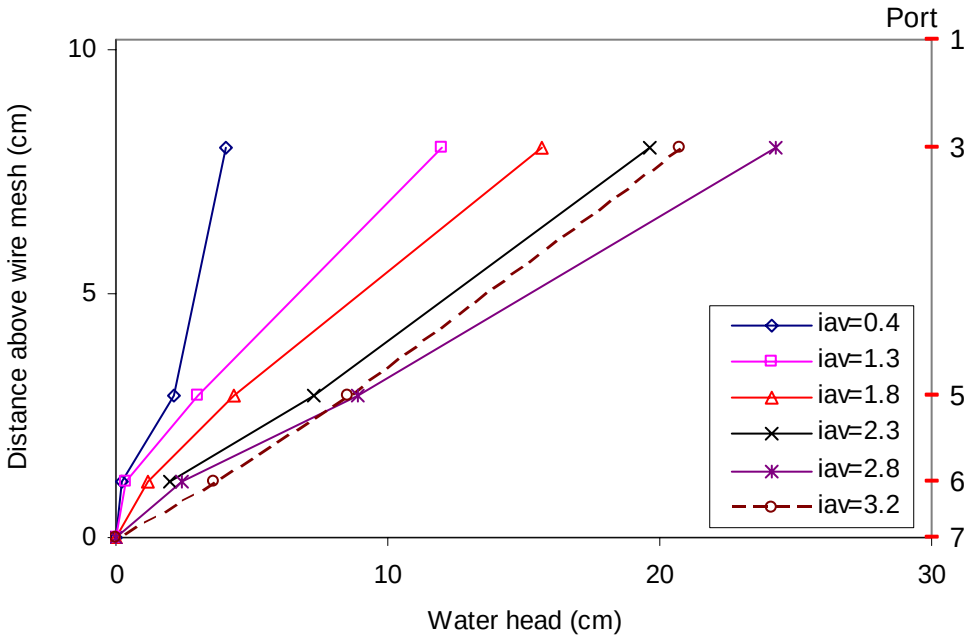

Figure C.3 Water head distribution in the test FR8-25-D2

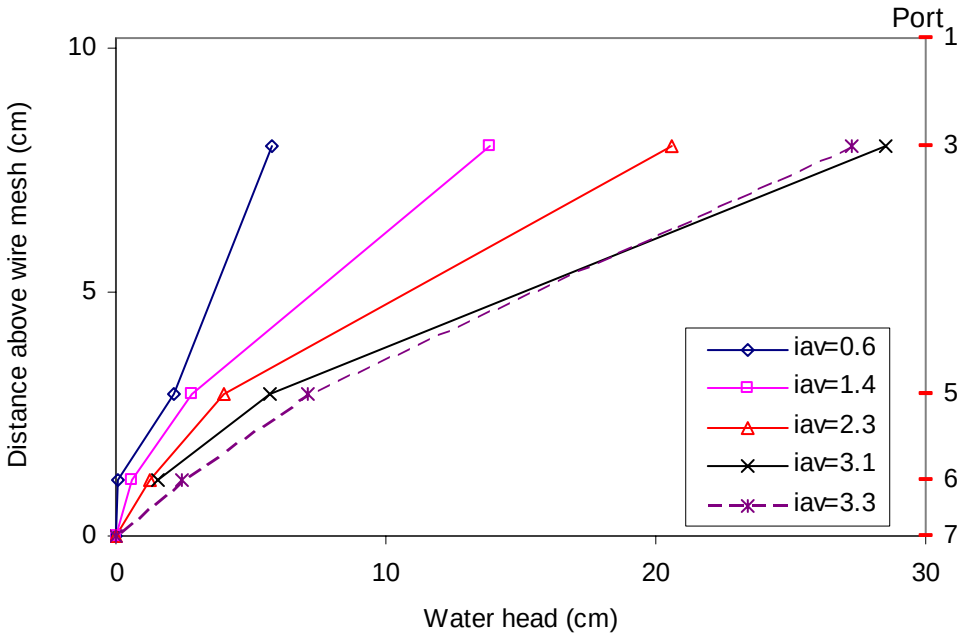

Figure C.4 Water head distribution in the test FR8-50-D

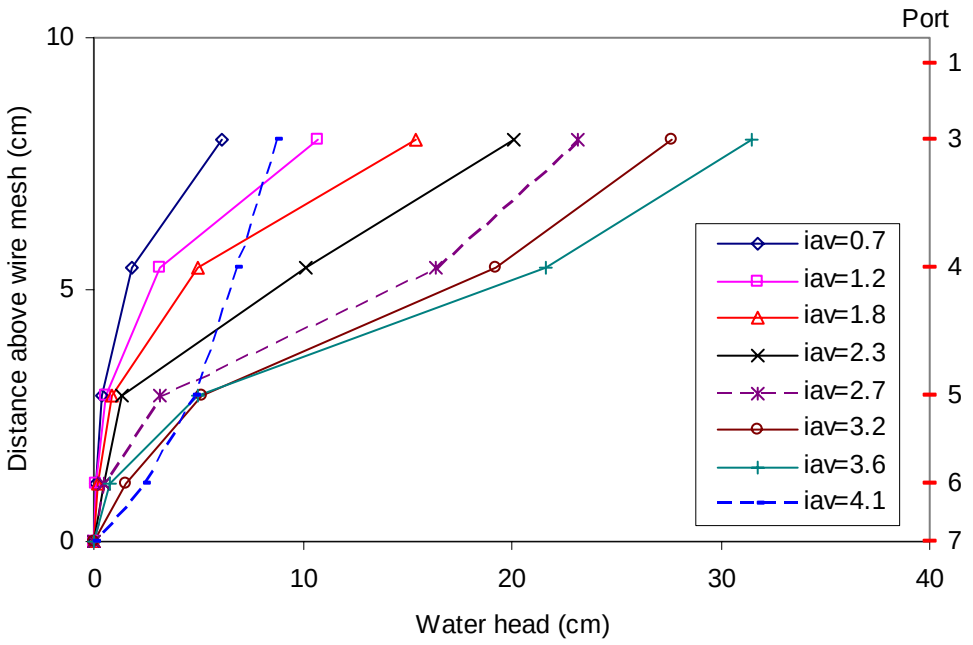

Figure C.5 Water head distribution in the test FR8-100-D

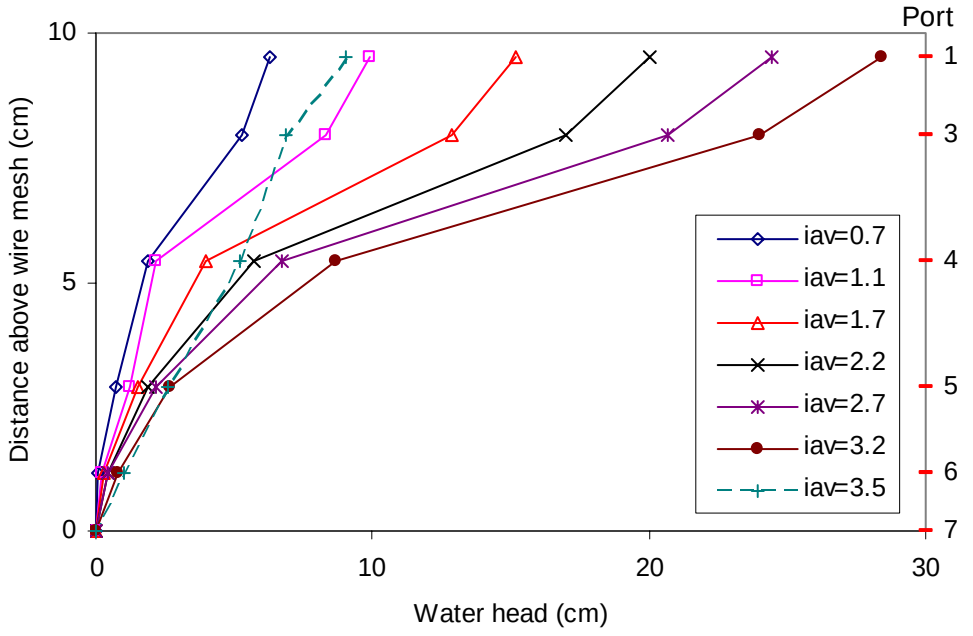

Figure C.6 Water head distribution in the test FR8-200-D

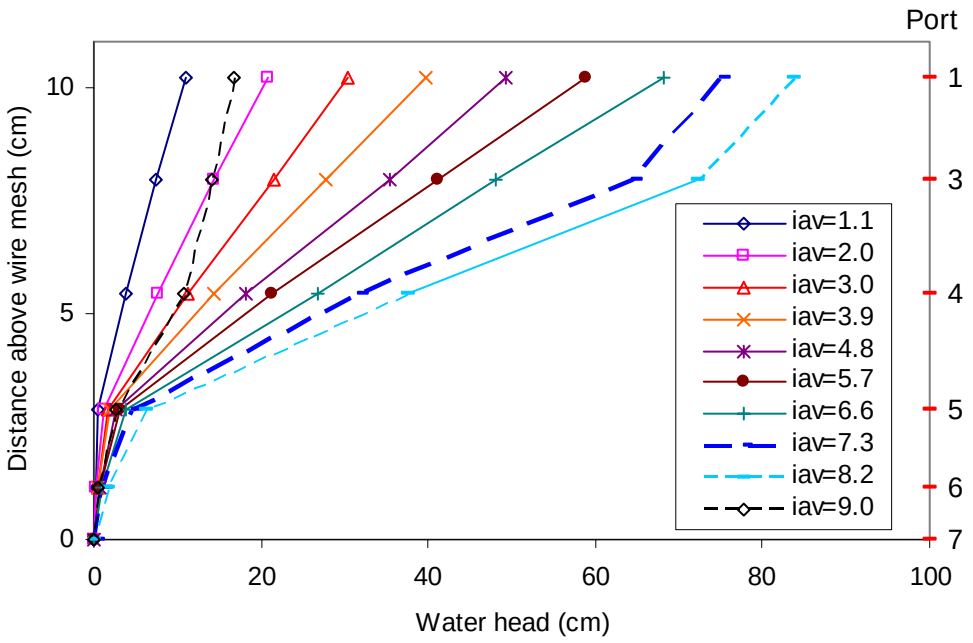

Figure C.7 Water head distribution in the test FR7-25-D

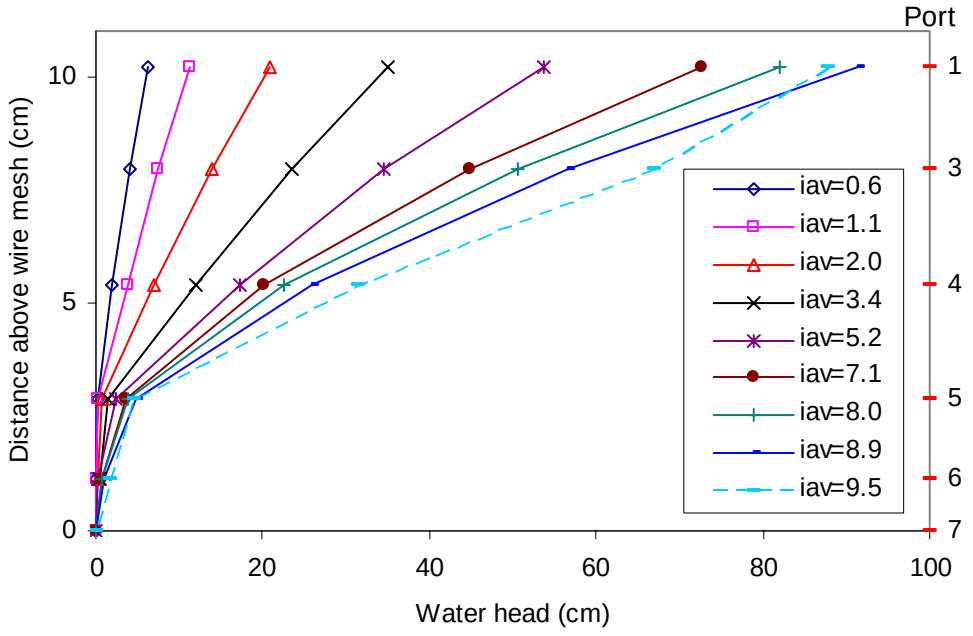

Figure C.8 Water head distribution in the test FR7-50-D

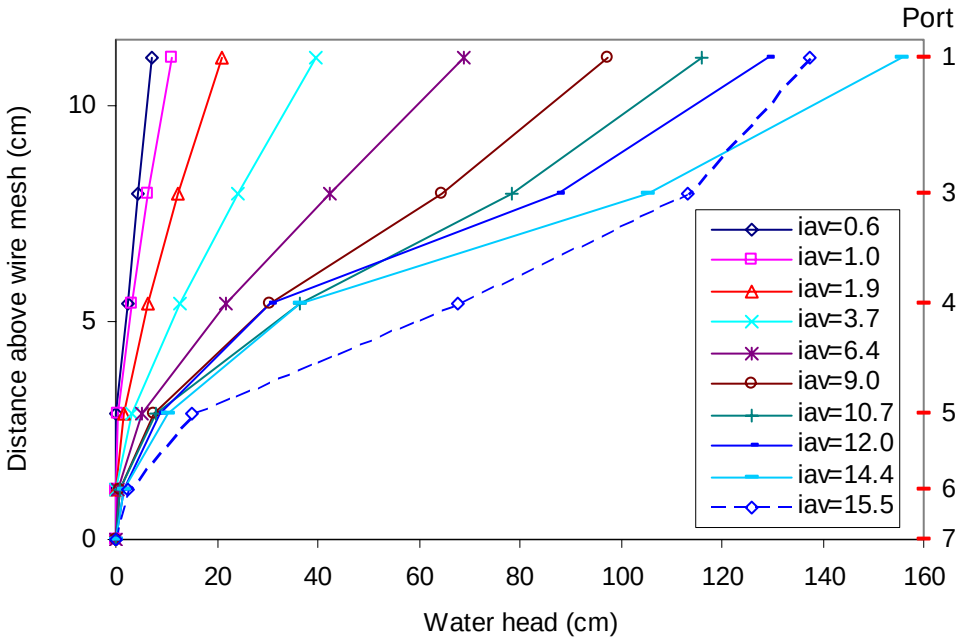

Figure C.9 Water head distribution in the test FR7-100-D

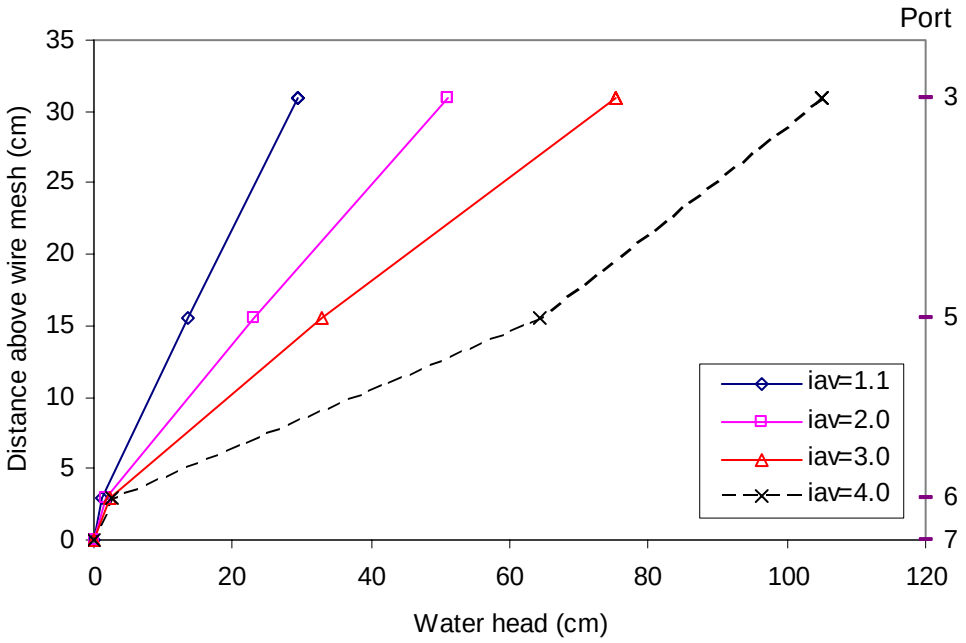

Figure C.10 Water head distribution in the test FR7-150-D

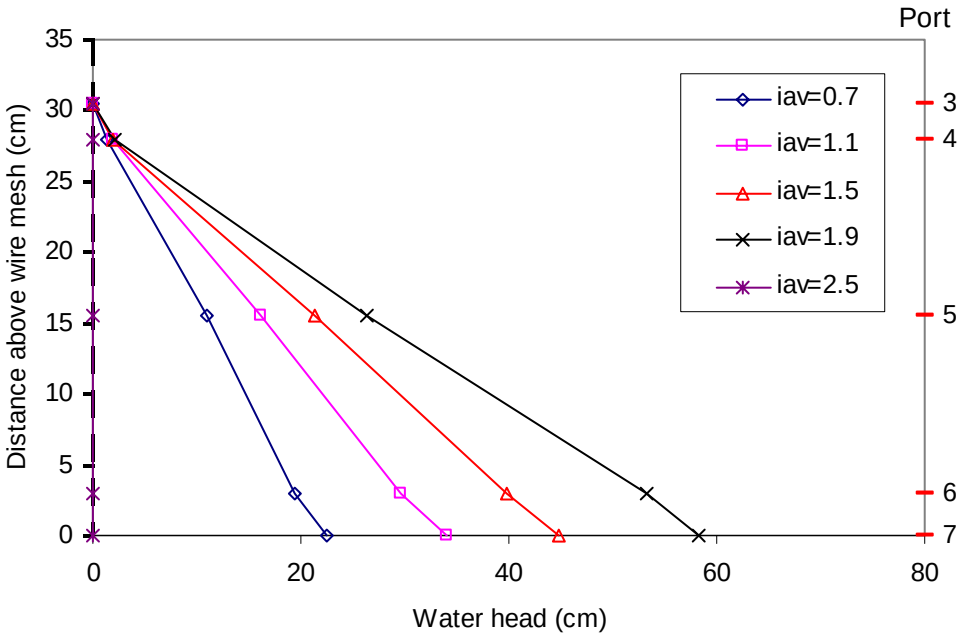

Figure C.11 Water head distribution in the test FR7-150-U

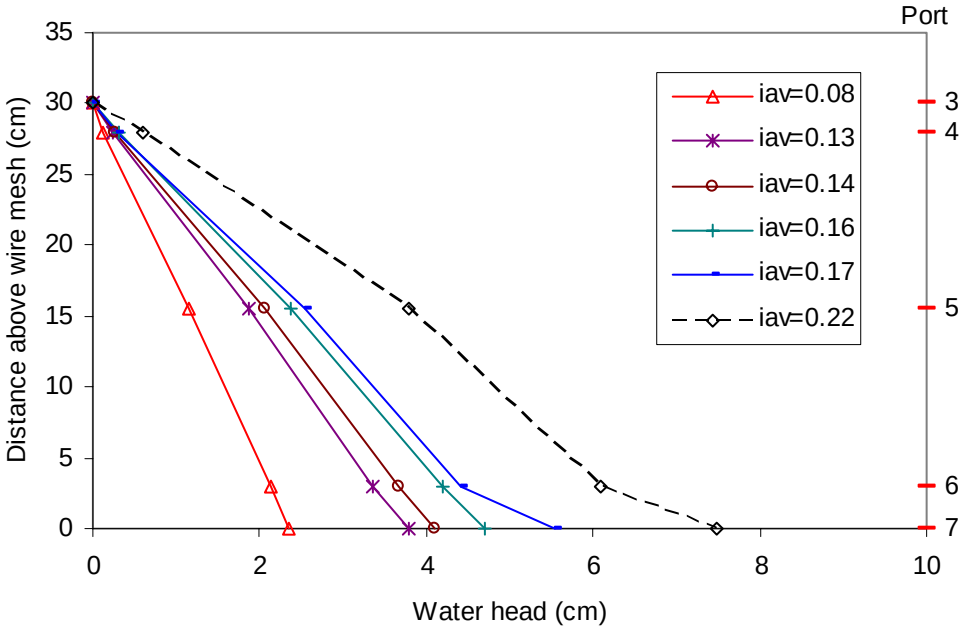

Figure C.12 Water head distribution in the test HF01-0-U

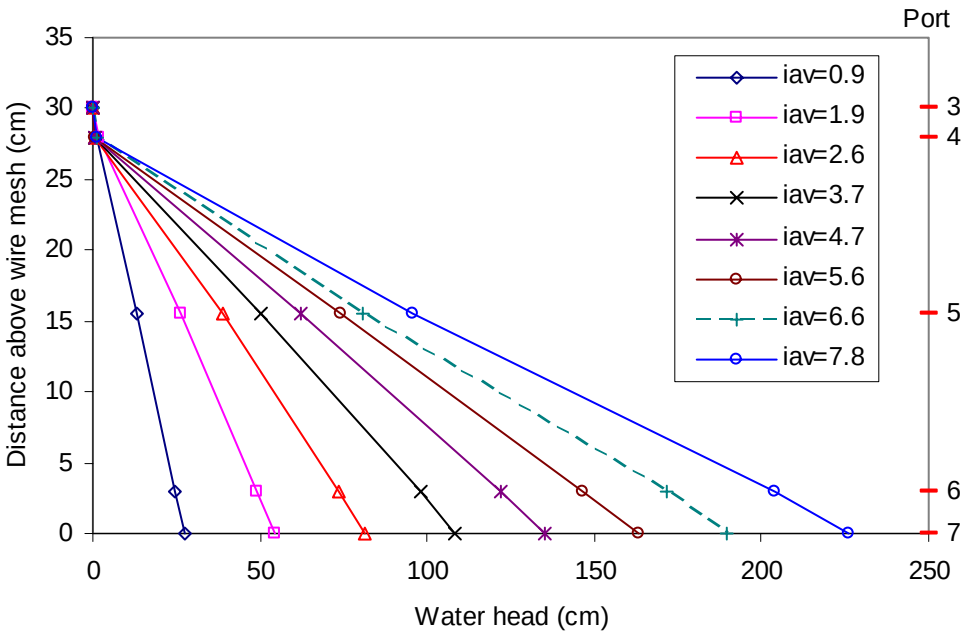

Figure C.13 Water head distribution in the test HF03-25-U

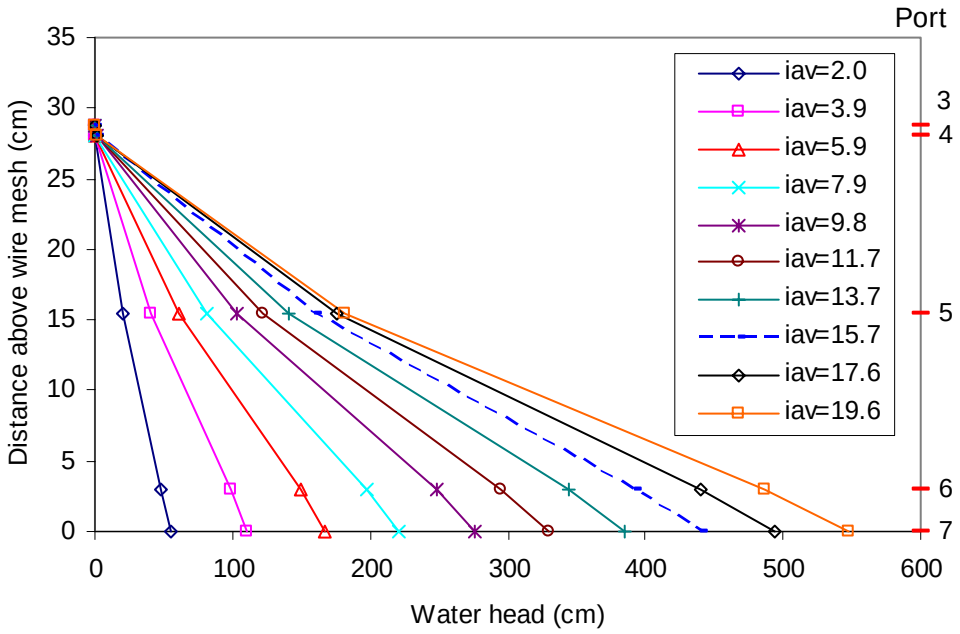

Figure C.14 Water head distribution in the test HF03-50-U

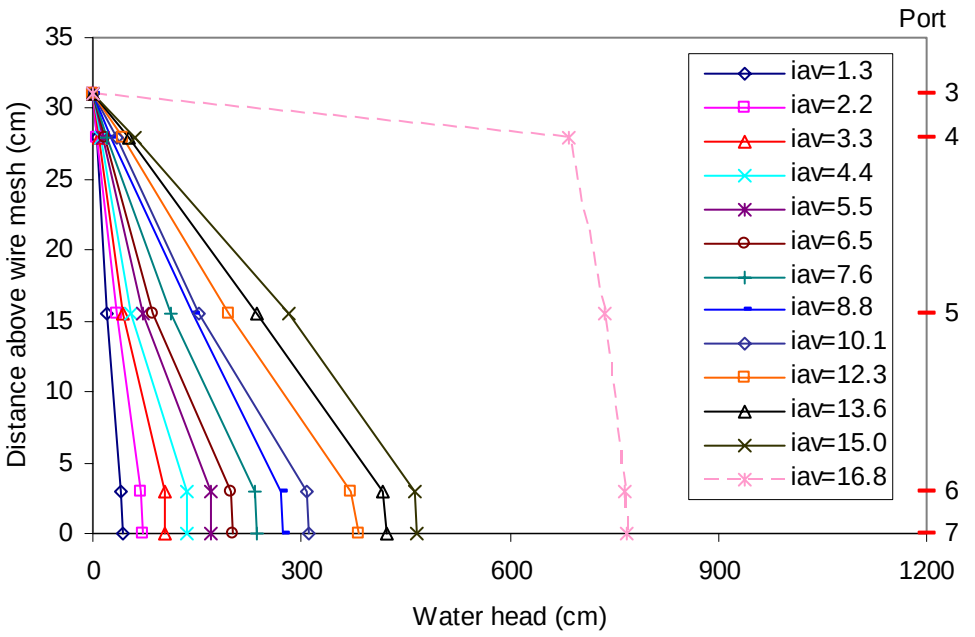

Figure C.15 Water head distribution in the test HF05-25-U1

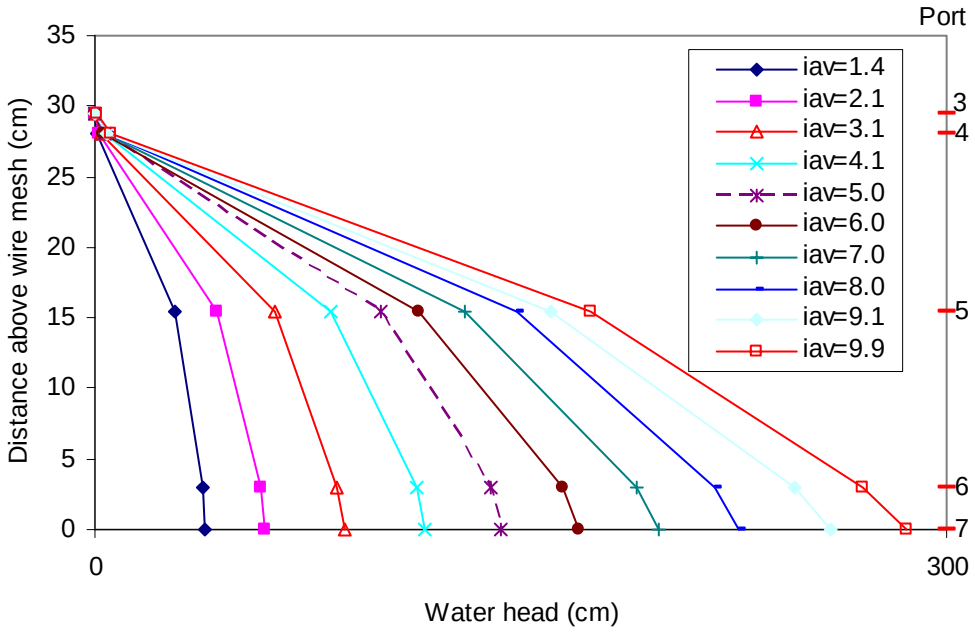

Figure C.16 Water head distribution in the test HF05-25-U2

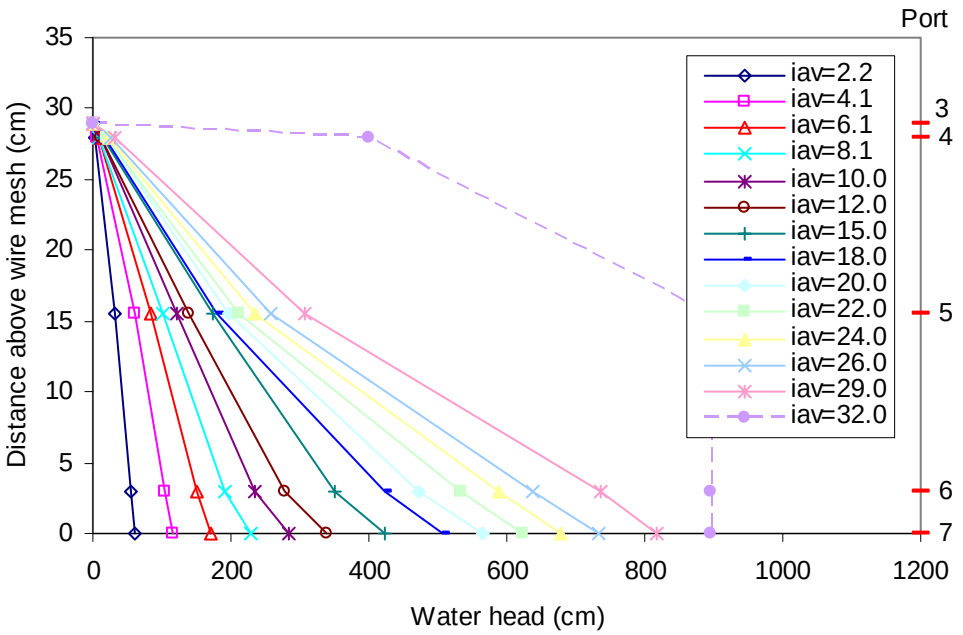

Figure C.17 Water head distribution in the test HF05-50-U

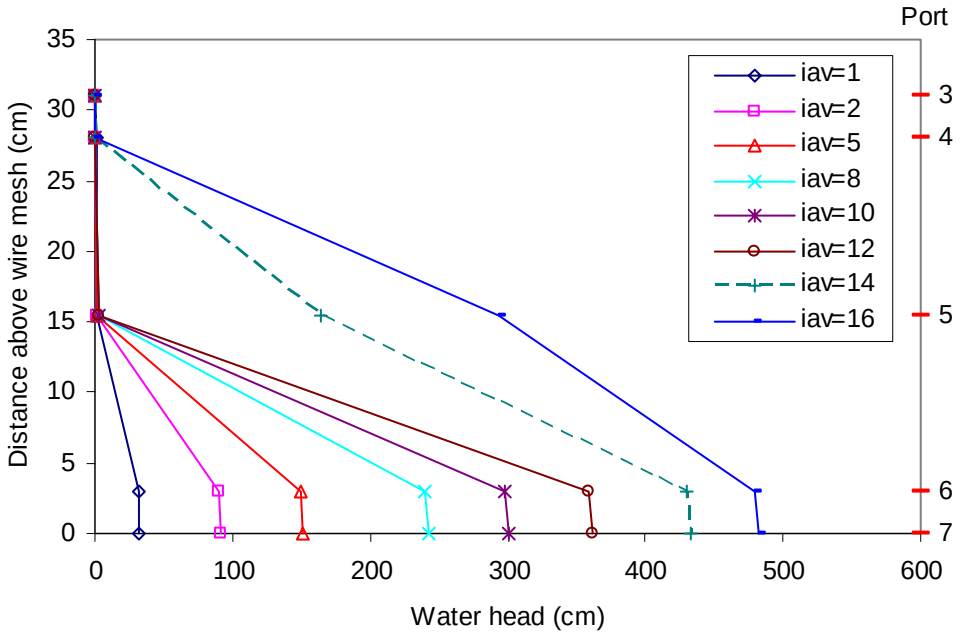

Figure C.18 Water head distribution in the test HF10-15-U

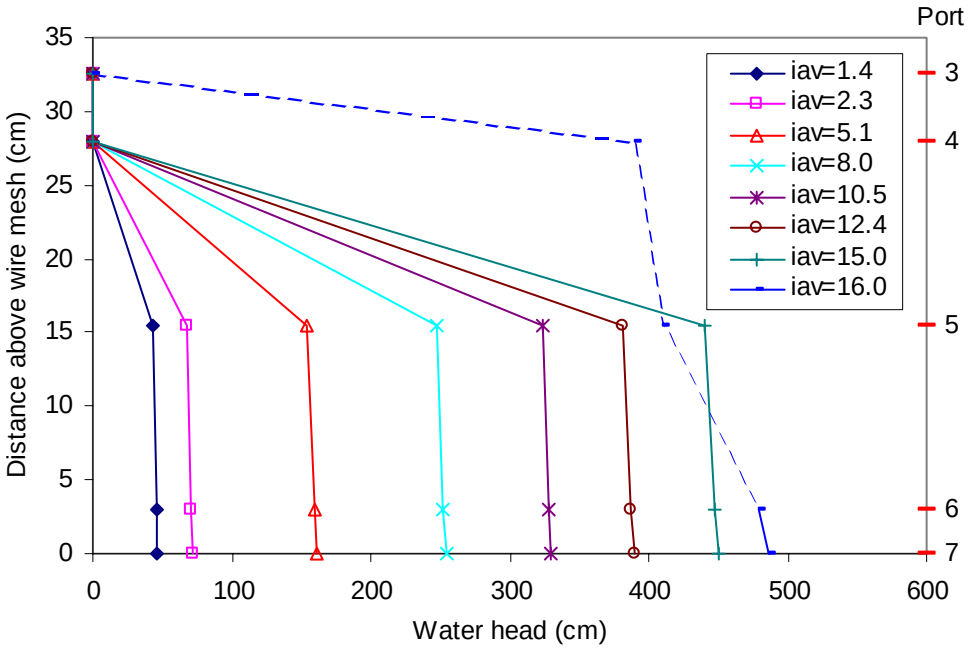

Figure C.19 Water head distribution in the test HF10-25-U

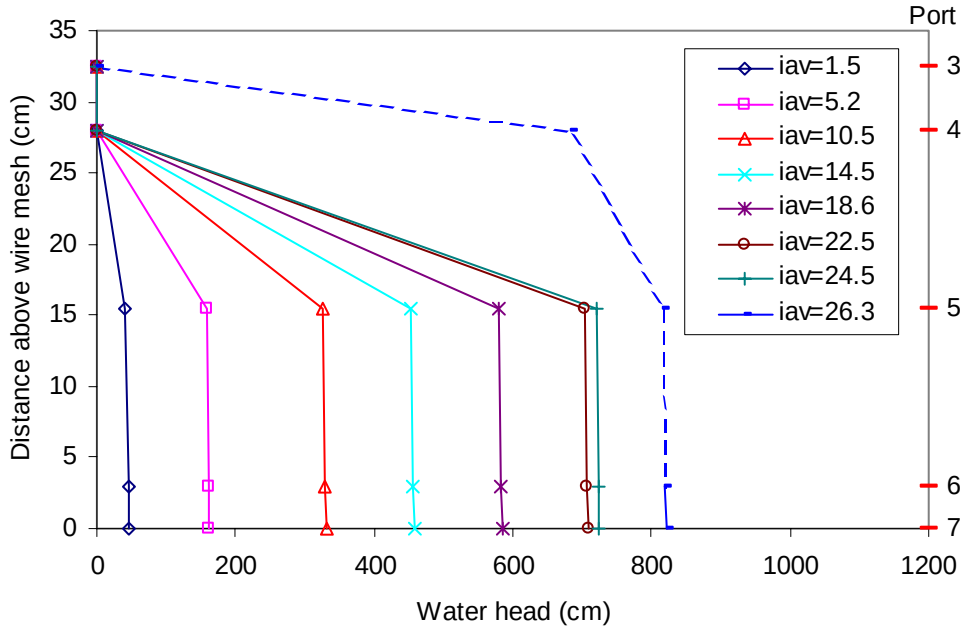

Figure C.20 Water head distribution in the test HF10-50-U

Appendix D Local hydraulic conductivity

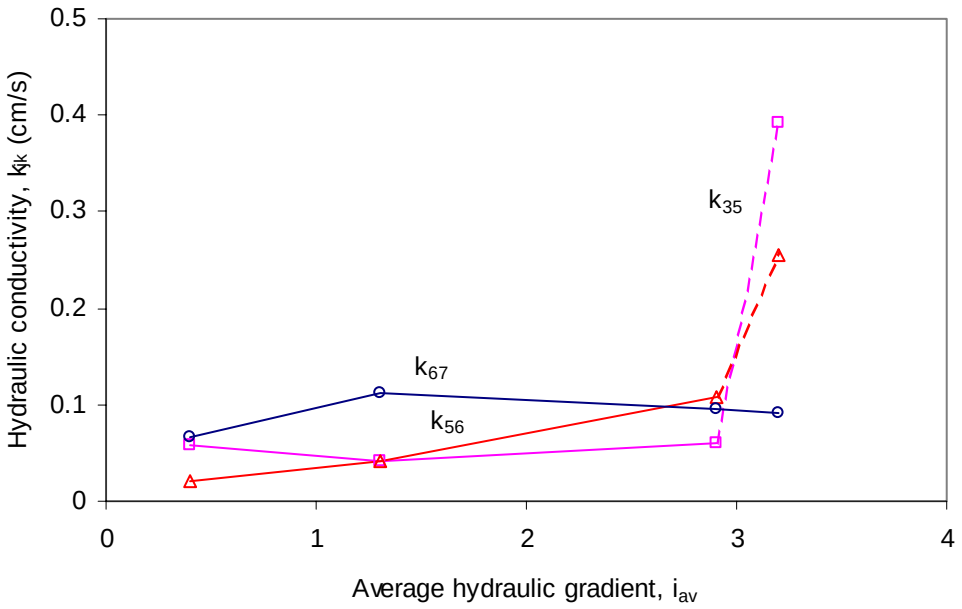

Figure D.1 Variation of hydraulic conductivity with gradient in the test FR8-25-D0

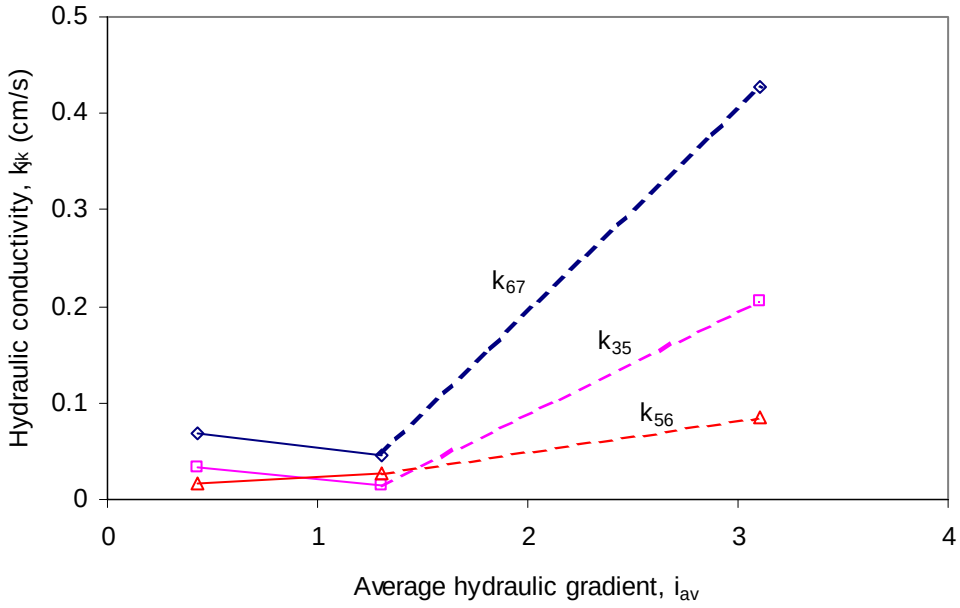

Figure D.2 Variation of hydraulic conductivity with gradient in the test FR8-25-D1

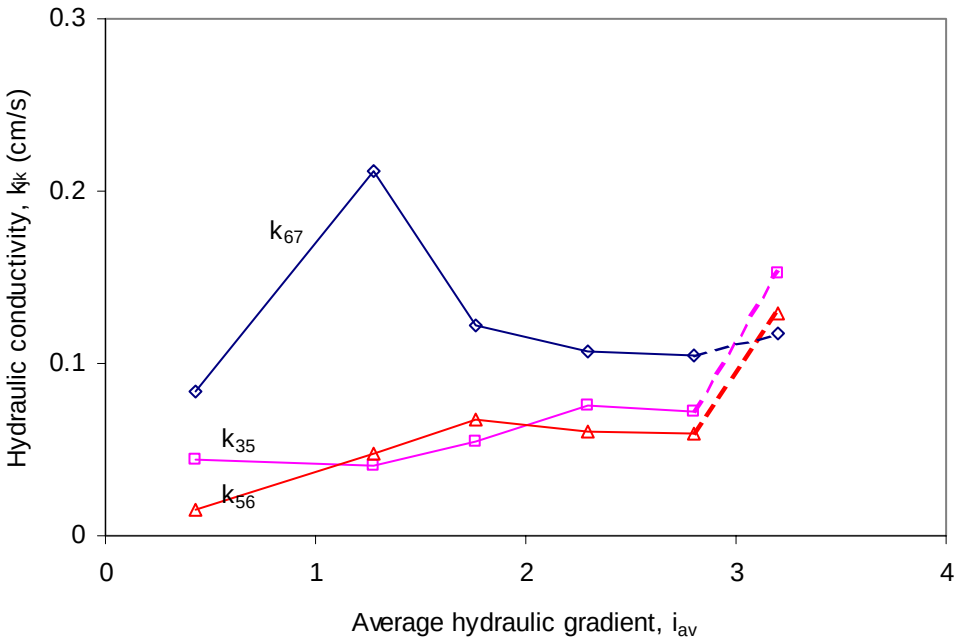

Figure D.3 Local Variation of hydraulic conductivity with gradient in the test FR8-25-D2

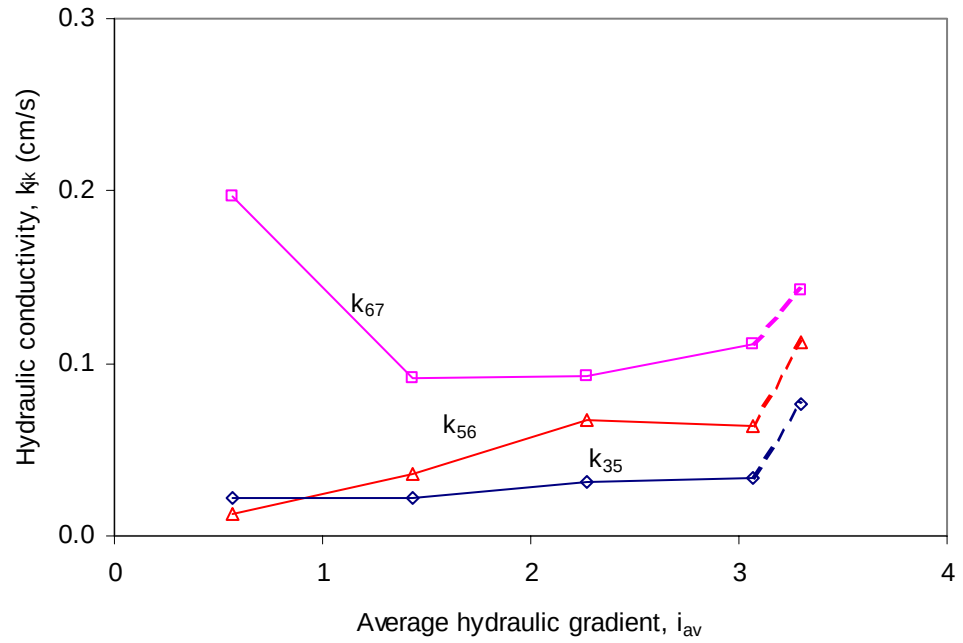

Figure D.4 Variation of hydraulic conductivity with gradient in the test FR8-50-D

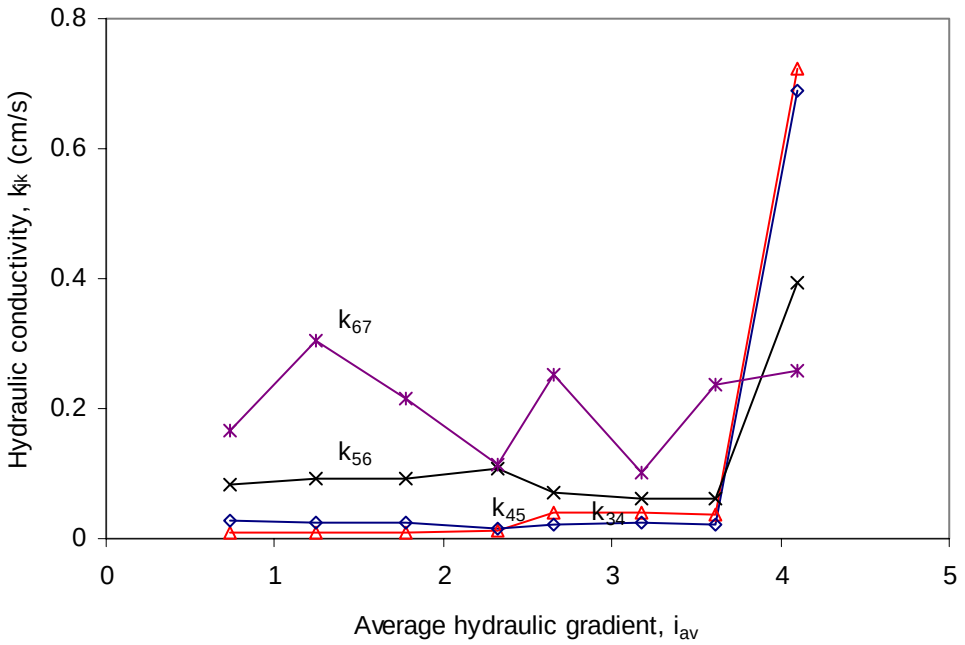

Figure D.5 Variation of hydraulic conductivity with gradient in the test FR8-100-D

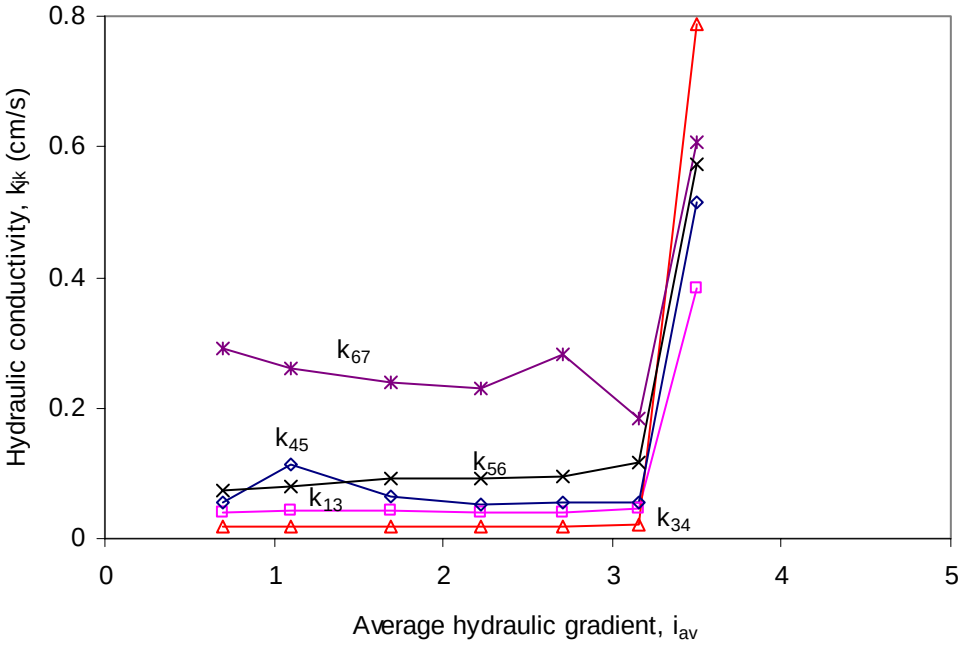

Figure D.6 Variation of hydraulic conductivity with gradient in the test FR8-200-D

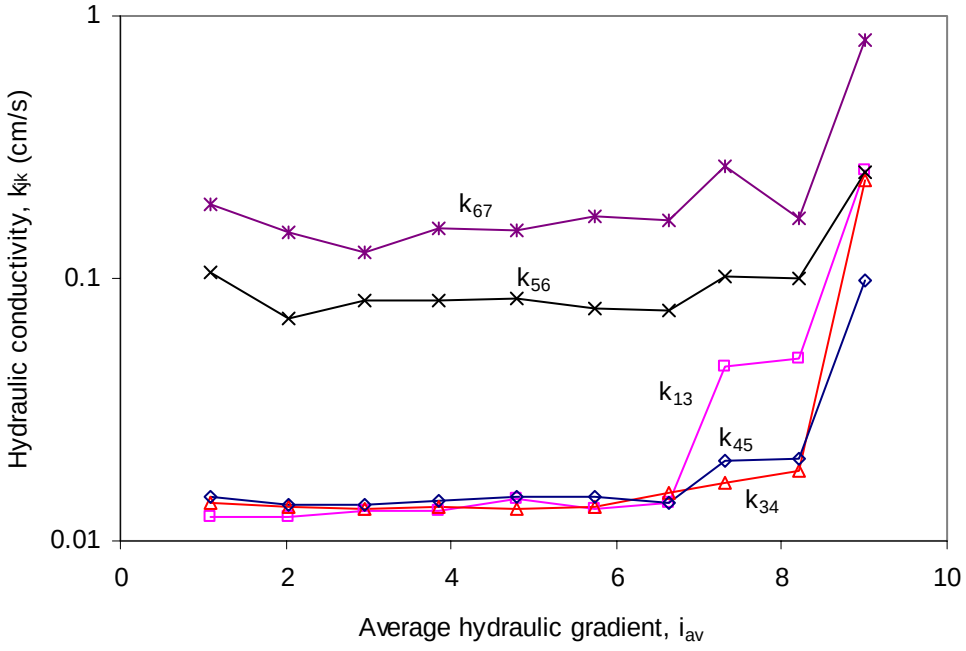

Figure D.7 Variation of hydraulic conductivity with gradient in the test FR7-25-D

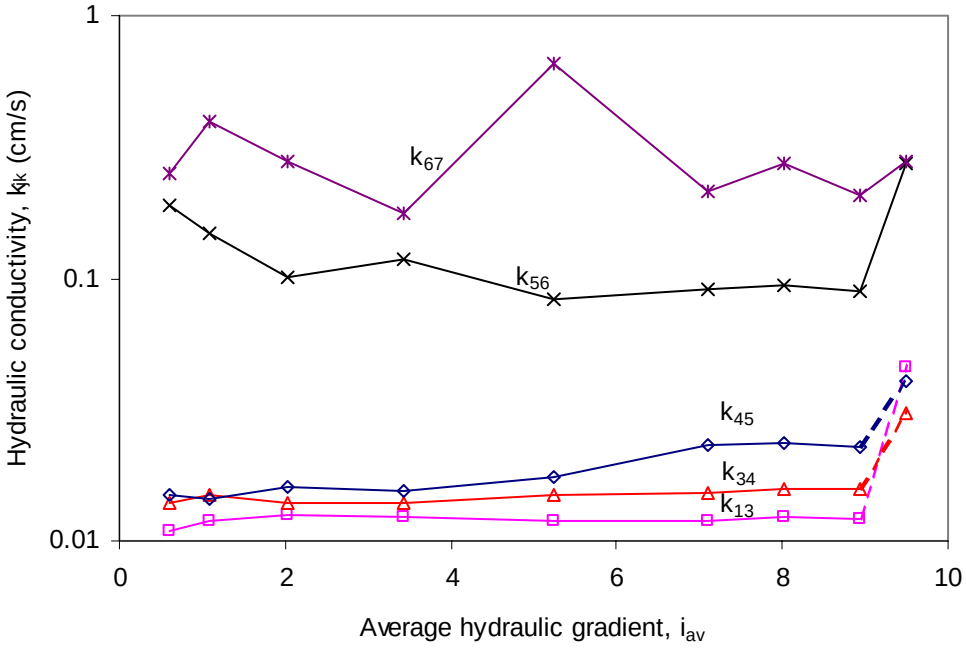

Figure D.8 Variation of hydraulic conductivity with gradient in the test FR7-50-D

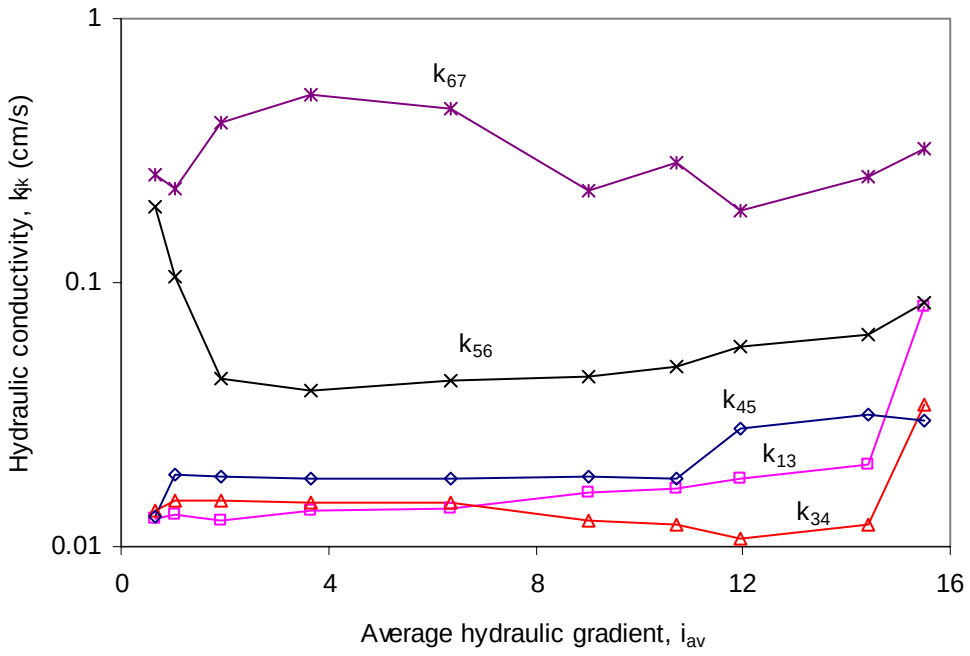

Figure D.9 Variation of hydraulic conductivity with gradient in the test FR7-100-D

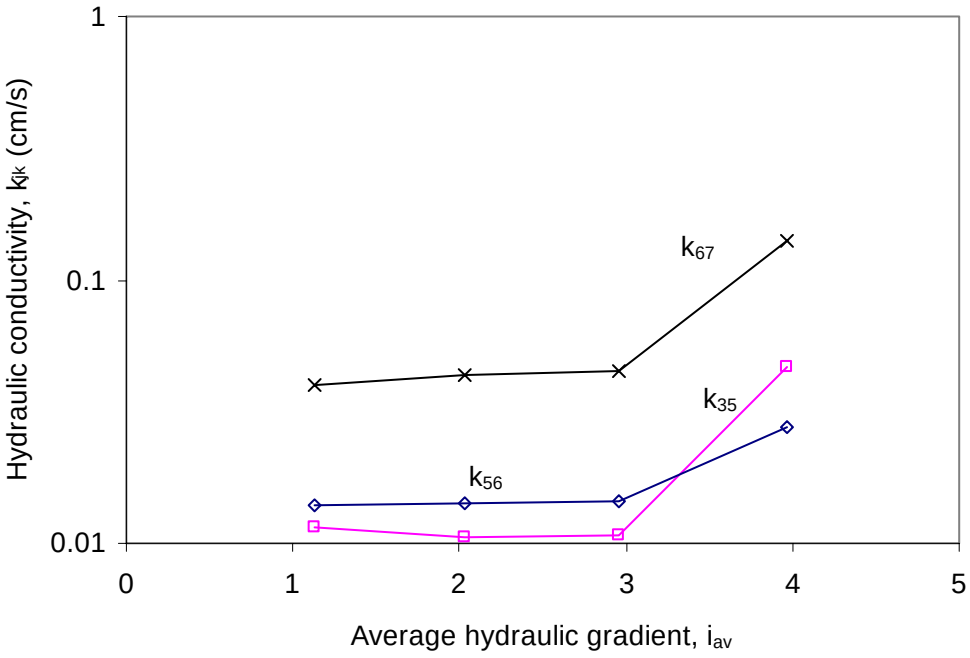

Figure D.10 Variation of hydraulic conductivity with gradient in the test FR7-150-D

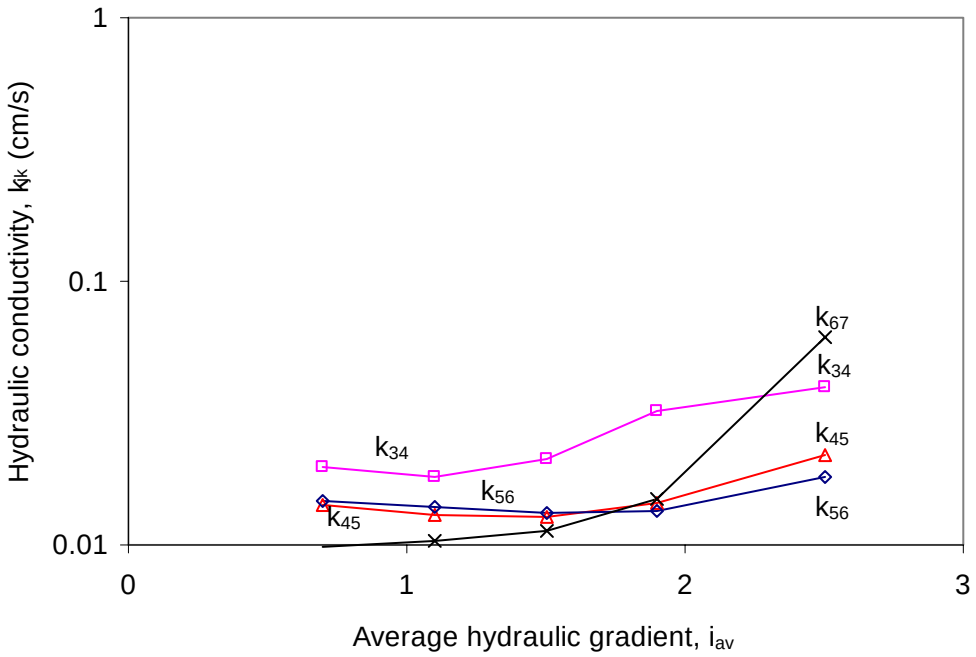

Figure D.11 Variation of hydraulic conductivity with gradient in the test FR7-150-U

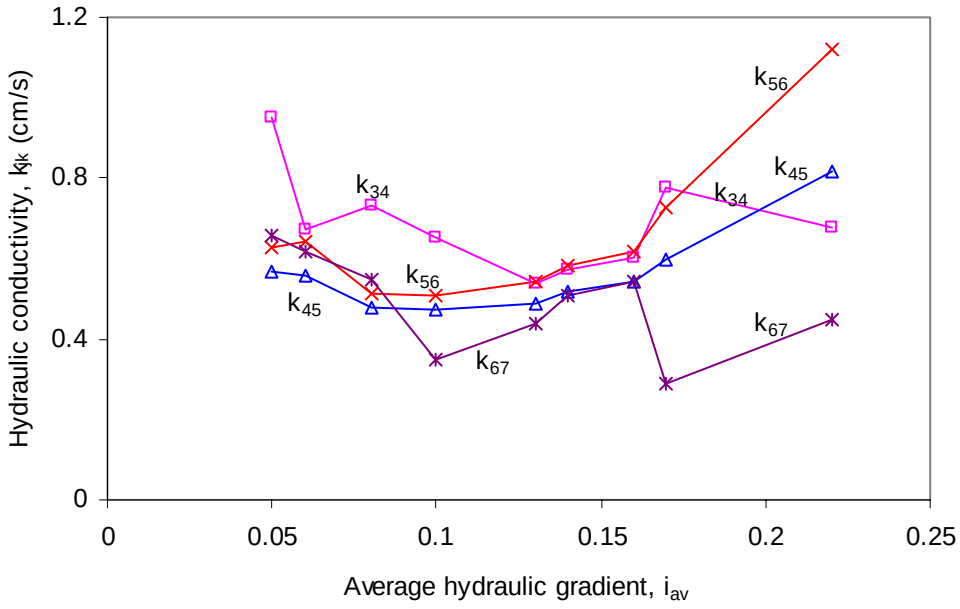

Figure D.12 Variation of hydraulic conductivity with gradient in the test HF01-0-U

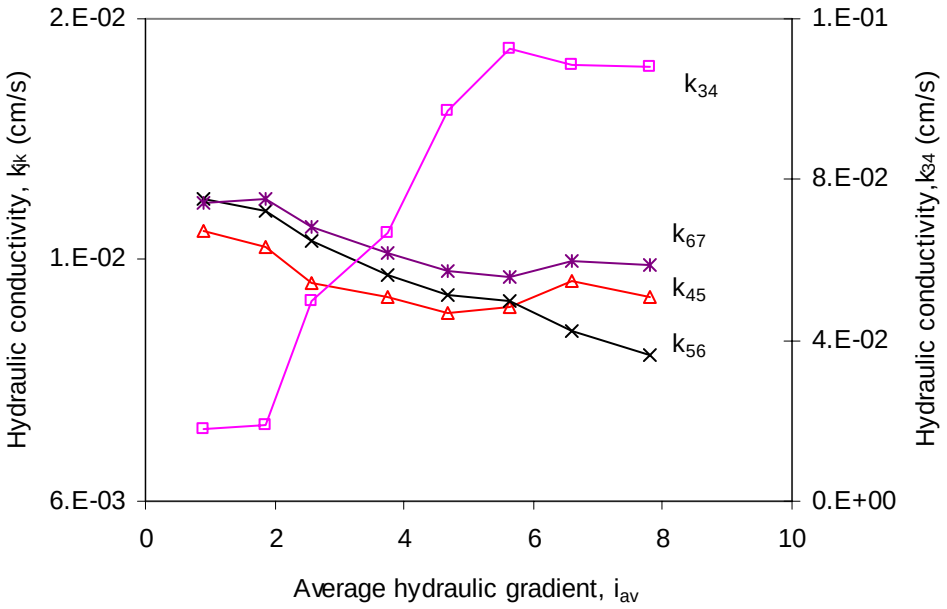

Figure D.13 Variation of hydraulic conductivity with gradient in the test HF03-25-U

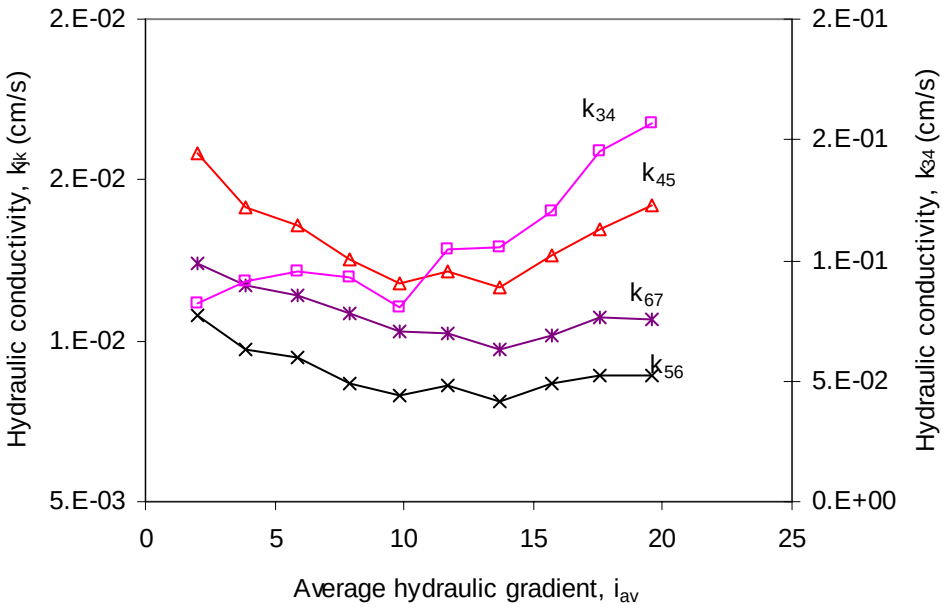

Figure D.14 Variation of hydraulic conductivity with gradient in the test HF03-50-U

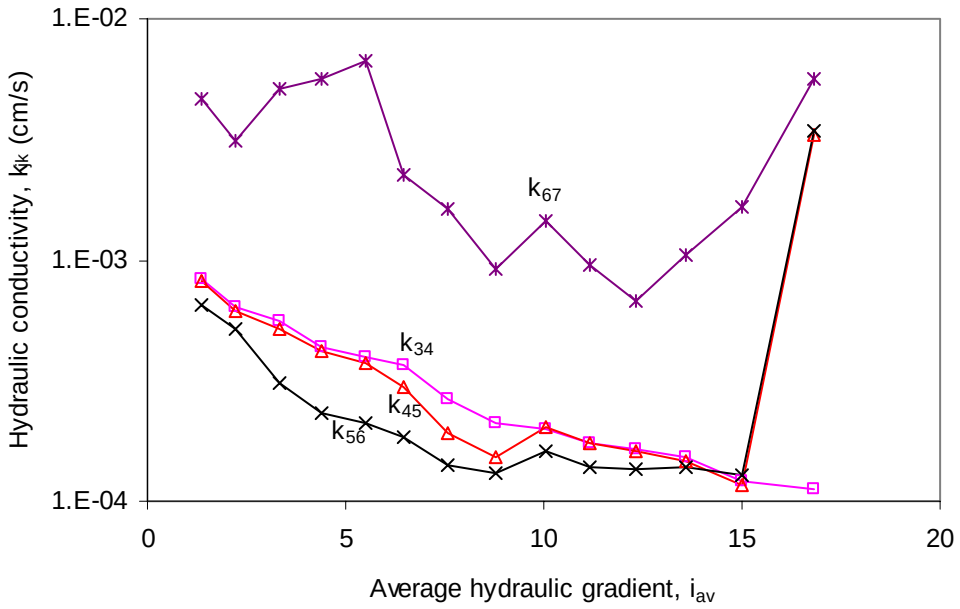

Figure D.15 Variation of hydraulic conductivity with gradient in the test HF05-25-U1

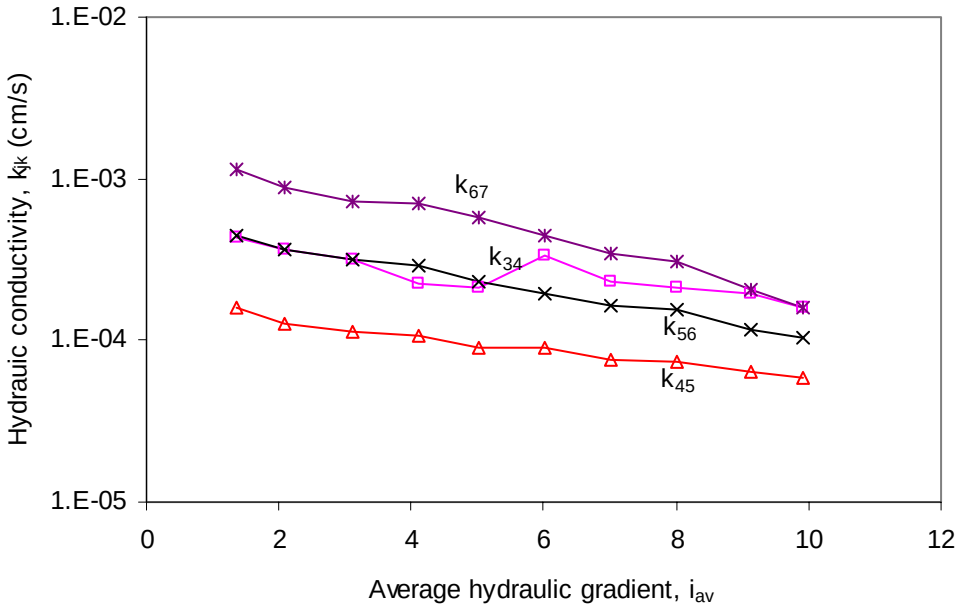

Figure D.16 Variation of hydraulic conductivity with gradient in the test HF05-25-U2

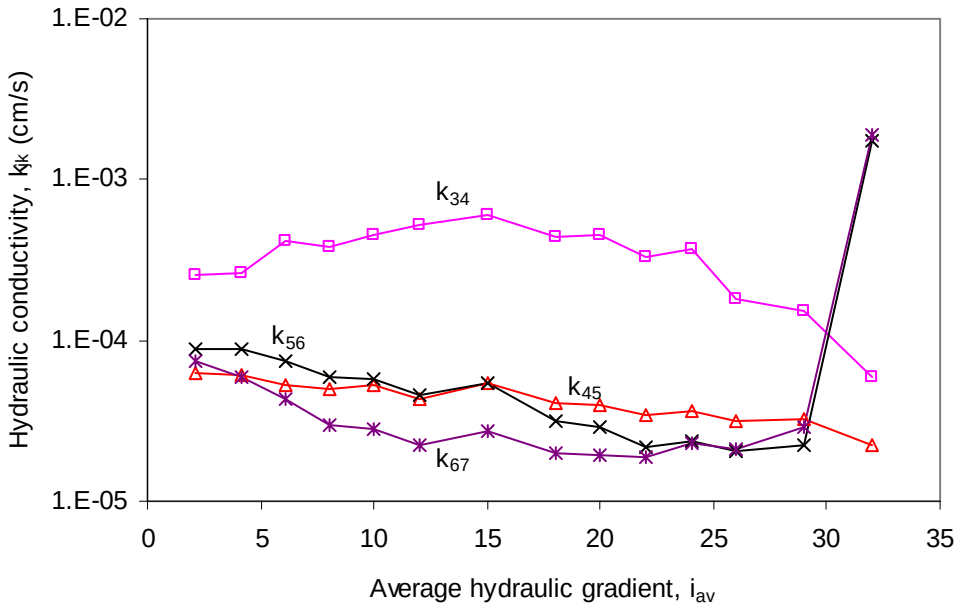

Figure D.17 Variation of hydraulic conductivity with gradient in the test HF05-50-U

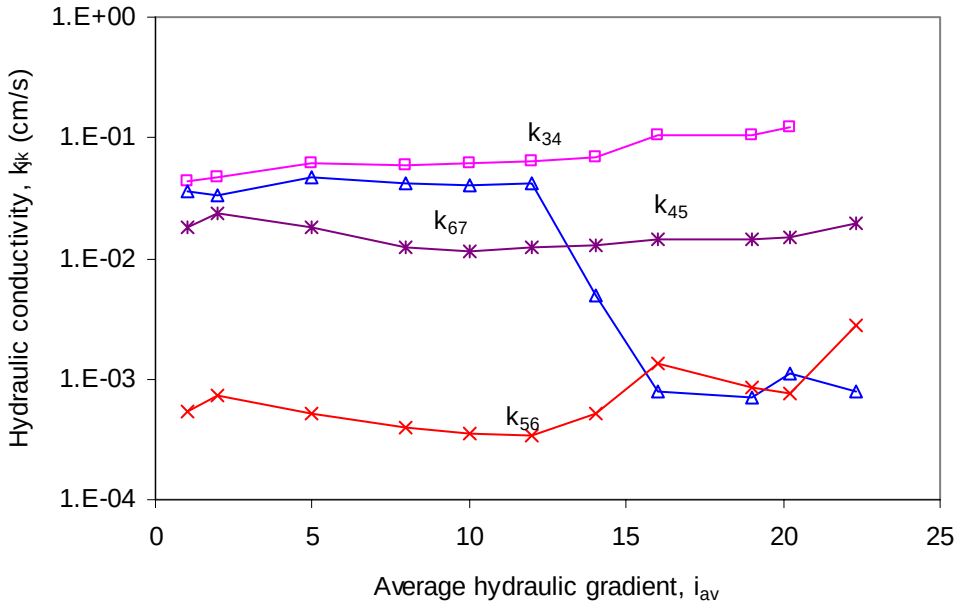

Figure D.18 Variation of hydraulic conductivity with gradient in the test HF10-15-U

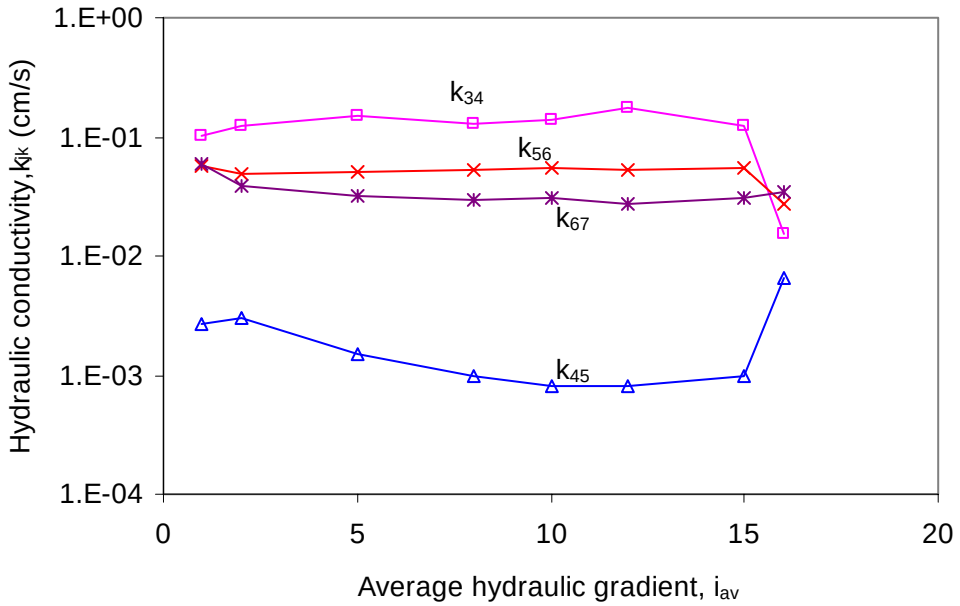

Figure D.19 Variation of hydraulic conductivity with gradient in the test HF10-25-U

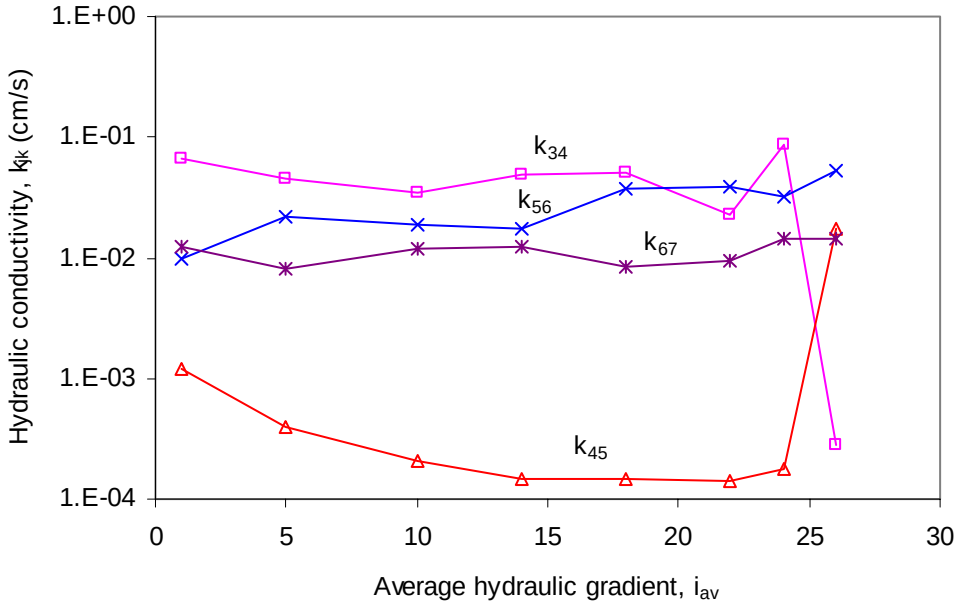

Figure D.20 Variation of hydraulic conductivity with gradient in the test HF10-50-U

Appendix E Test specimen

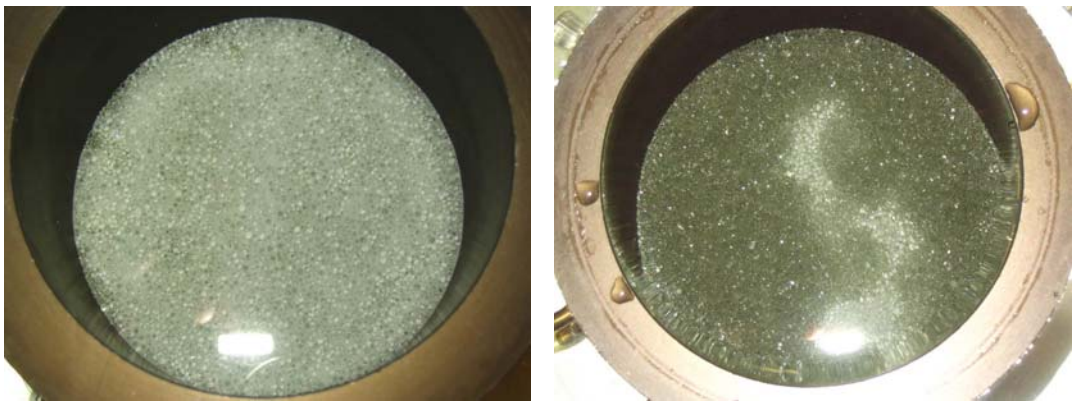

Figure E.1 Top surface before/after test in FR8-100-D

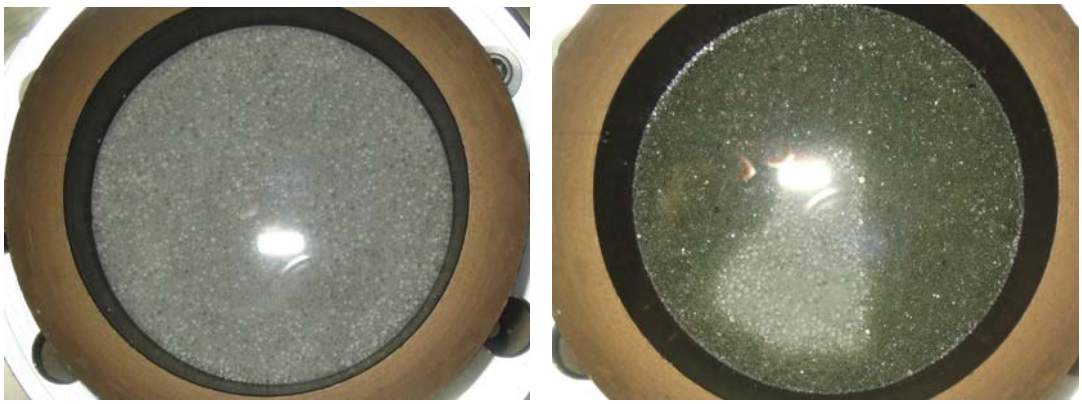

Figure E.2 Top surface before/after test in FR8-200-D

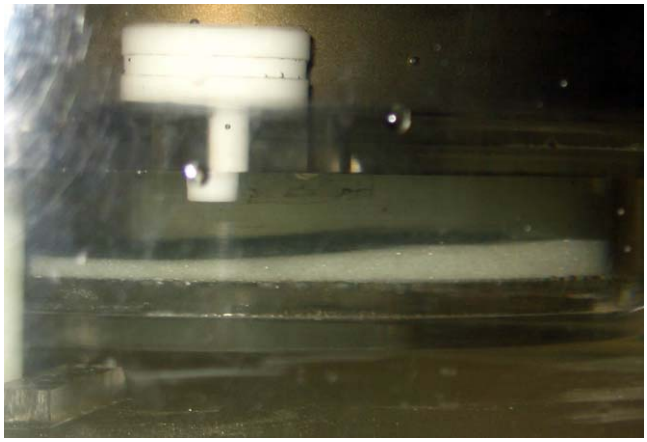

Figure E.3 Finer particles collected in the bottom trough in FR7-25-D

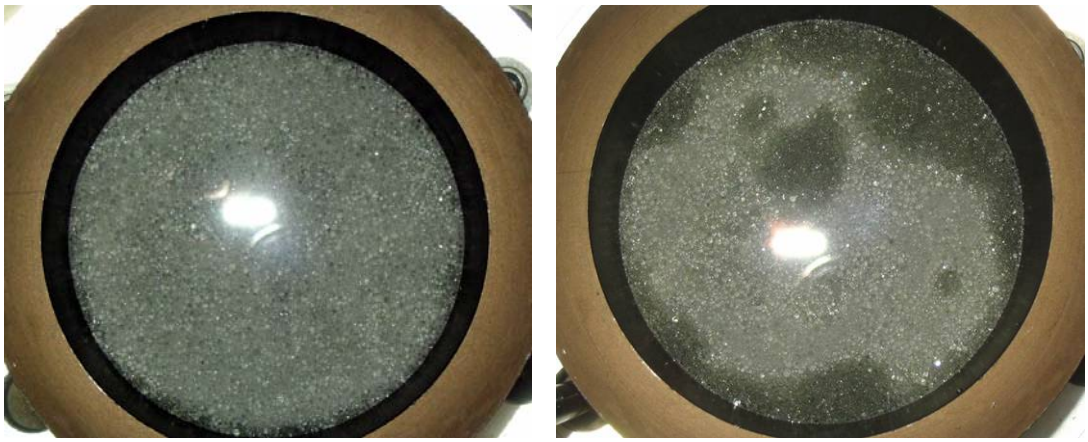

Figure E.4 Top surface before/after test in FR7-25-D

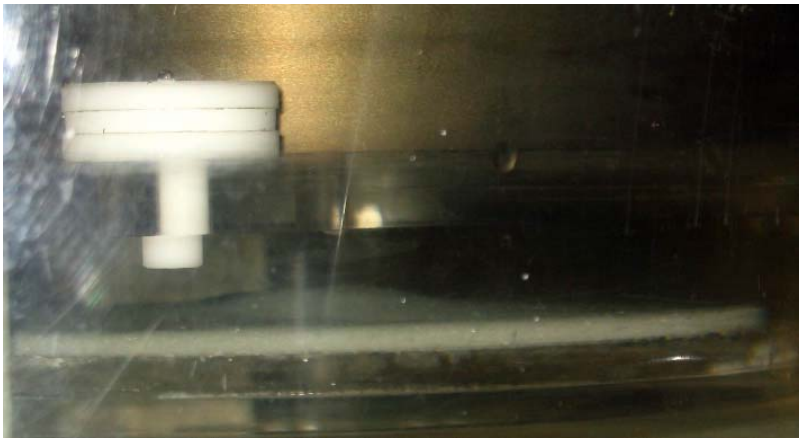

Figure E.5 Finer particles collected in the bottom trough in FR7-50-D

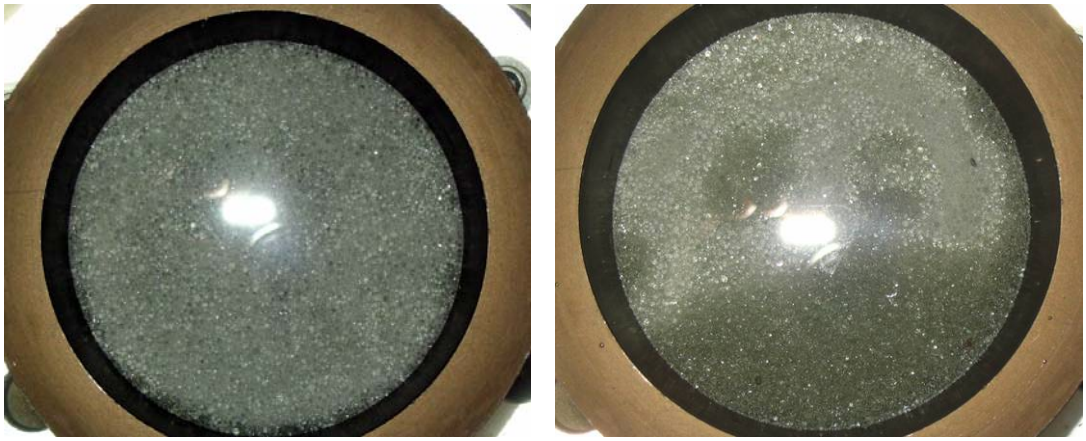

Figure E.6 Top surface before/after test in FR7-50-D

Figure E.7 Finer particles collected in the bottom trough in FR7-100-D

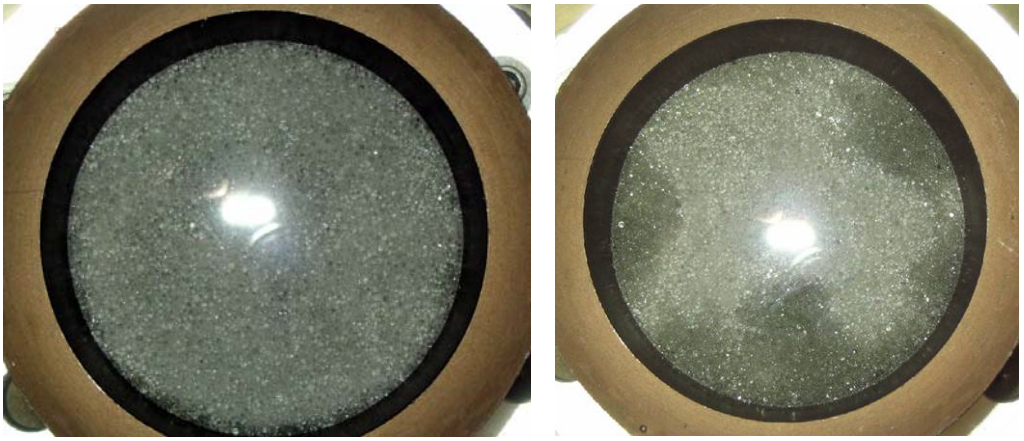

Figure E.8 Top surface before/after test in FR7-100-D

Figure E.9 Finer particles was continually lost through the exit screen in FR7-150-D

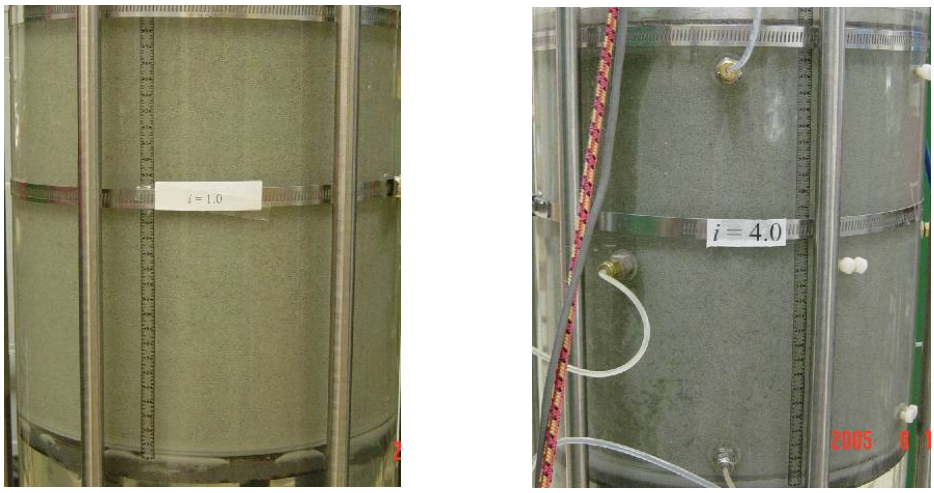

Figure E.10 Specimen before and after test in FR7-150-D

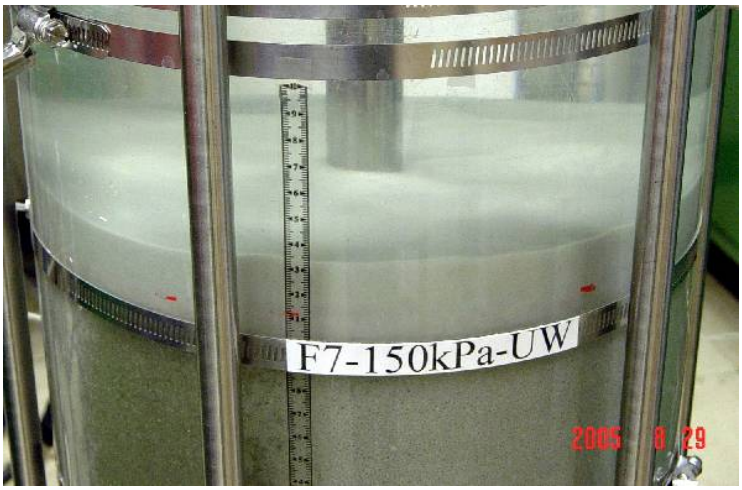

Figure E.11 Loss of finer particles collected on the top surface of specimen in FR7-150-U

Figure E.12 Specimen before and after test in FR7-150-U

Figure E.13 Finer particle boiling at the top surface of specimen in HF01-0-U

Figure E.14 Finer particle collected at the top surface of specimen in HF01-0-U

Figure E.15 Soil specimen before/after internal instability in HF03-25-U

(a) (b)

Figure E.16 Finer particles boiling at the top surface in HF03-25-U

Figure E.17 Finer particle boiling at the top surface of specimen in HF03-50-U

Figure E.18 Finer particle collected at the top surface of specimen in HF03-50-U

Figure E.19 Soil specimen before/after internal suffosion in HF05-25-U1

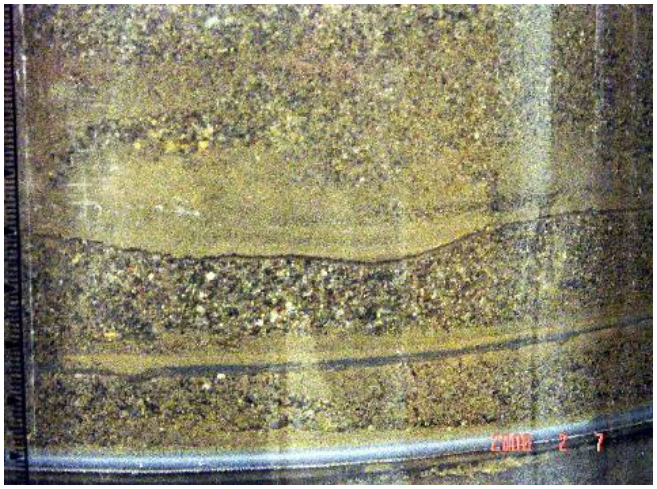

Figure E.20 Horizontal crack between ports 5 and 6 in HF05-25-U1

Figure E.21 Specimen after heave failure in HF05-25-U1

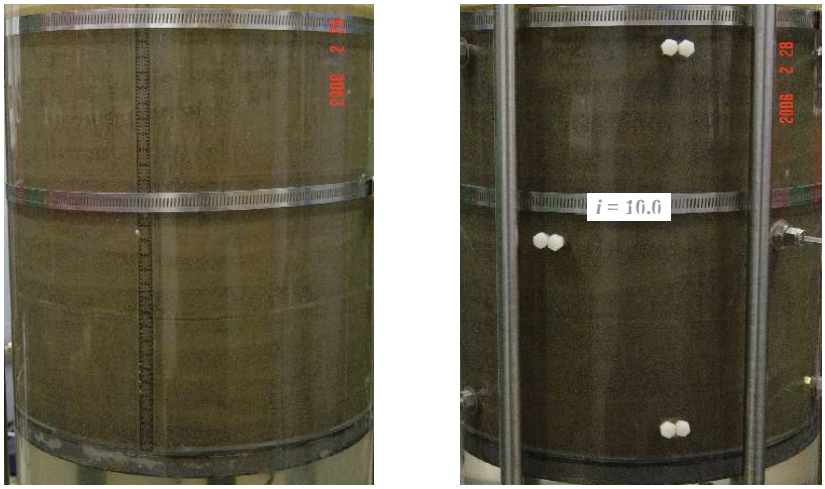

Figure E.22 Specimen before/after test in HF05-25-U2

Figure E.23 Specimen before/after internal instability in HF05-50-U

Figure E.24 Horizontal crack between ports 5 and 6 in HF05-50-U

Figure E.25 Specimen after heave failure in HF05-50-U

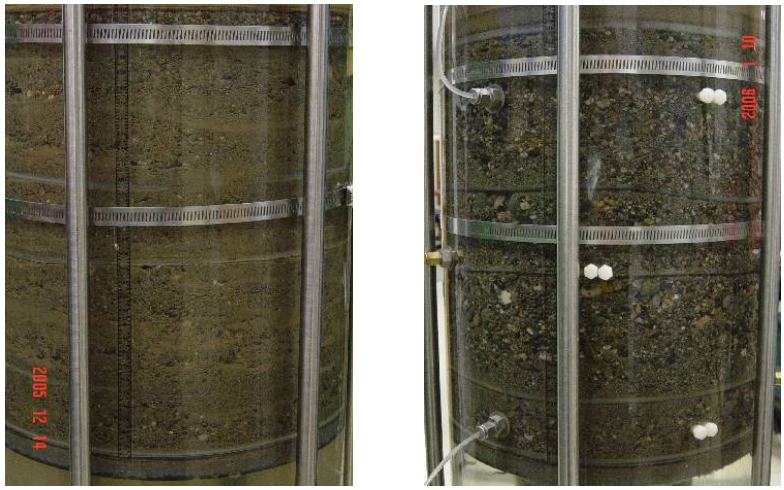

Figure E.26 Specimen before/after heave failure in HF10-15-U

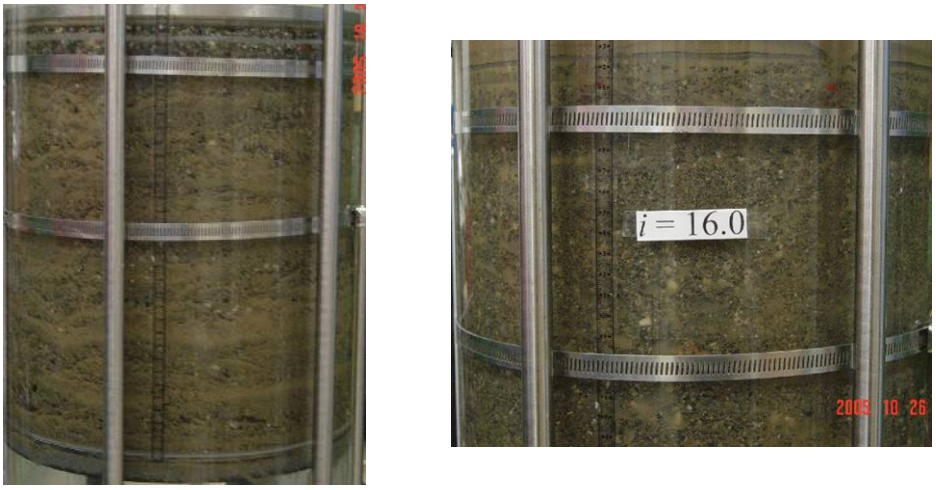

Figure E.27 Specimen before/after heave failure in HF10-25-U

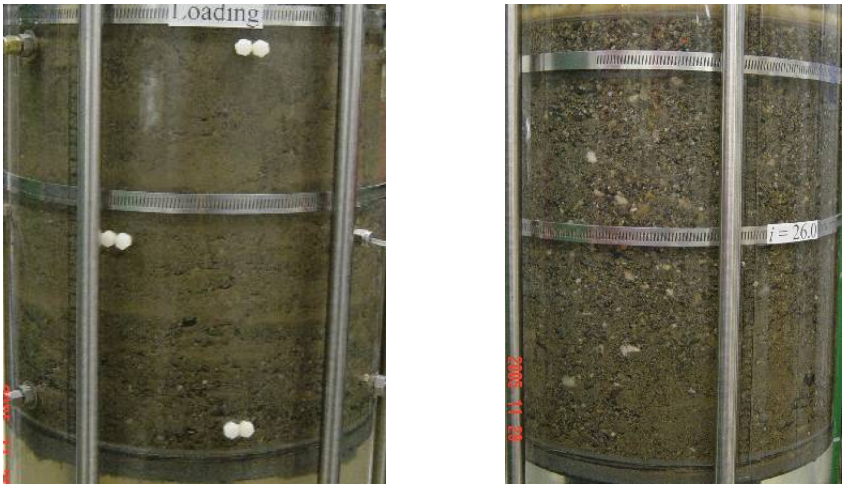

Figure E.28 Specimen before/after heave failure in HF10-50-U

Appendix F Capillary Tube Model (Kovacs, 1981)

The capillary tube model is a simple model for porous media in which the pore space is represented as an array of cylinder tubes. The crucial assumption of the model is that the tubes do not intersect each other. Often it is assumed that the tubes are straight or parallel to each other (Figure F.1). The diameter of the tubes (d_0) forming the models is believed to be proportional to the characteristic diameter of a sample. Kozeny's effective diameter is mostly used to describe the heterodisperse sample in seepage hydraulics.

Kozeny (1953) investigated the hydrodynamically equivalent tube-diameter for the heterodisperse samples. He has proved that the surface-volume ratio has to be identical in the original sample and the model system, because in these cases, the sufficient ratio of the two most important forces (i.e. gravity and friction) is ensured. This is the basis of the determination of Kozeny's effective diameter for a heterodisperse sample. According to the original definition, this is the diameter of a sphere, whose homodisperse sample (a sample of particles having the same diameter) has the same surface-volume ratio as the investigated homodisperse sample. The determination of the effective diameter can be given as follows. The distance between the maximum and minimum diameter is divided into n equidistant intervals. D_i = average diameter in the i-th interval of the particle size distribution curve and ΔS_i = the weight of grains in the i-th interval of the particle size distribution curve. Assuming the grains to be spheres in both systems, and the surface-volume ratio of the solid phase to be identical for both the model and the investigated sample, the following relationship can be given:

$$\frac{A}{V}=\frac{ND_h^2\pi}{ND_h^3\pi/6}=\frac{6}{D_h}=\frac{\sum\frac{\Delta S_i}{\gamma_s}\frac{6}{D_i}}{\sum\frac{\Delta S_i}{\gamma_s}}$$

$$D_h=\frac{1}{\sum\frac{\Delta S_i}{D_i}} \tag{F.1}$$

where N is the number of spheres in the homodisperse sample, and γ_s is the specific weight of the solid grains.

Considering the shape coefficient, the quotient of the effective diameter and the average shape coefficient can be calculated:

$$\frac{D_h}{\alpha_D}=\frac{1}{\sum\Delta S_i\frac{\alpha_i}{D_i}} \tag{F.2}$$

The general surface-volume ratio can be expressed as,

$$\frac{V}{A}=\frac{D}{\alpha_D} \tag{F.3}$$

where α_D = average shape coefficient = 6 for sphere, =7-11 for sand and gravel.

As shown in Figure F.1, these capillary tubes are parallel to the flow direction, and average pore diameter (d_0) for the tubes is determined using the Kozeny's concept of identical surface-volume ratio. The surface of the pipe-wall related to its inner volume should be equal to the ratio of the grain surface (A) in the sample to the pore volume (V_p):

$$\frac{ld_0\pi}{ld_0^2\pi/4}=\frac{4}{d_0}=\frac{A}{V_p}=\frac{1-n}{n}\frac{A}{V}=\frac{1-n}{n}\frac{\alpha_D}{D_h}; \tag{F.4}$$

Consequently, average pore diameter (d_0) can be expressed as,

$$d_0 = 4\frac{n}{1-n}\frac{D_h}{\alpha_D} \qquad \text{(F.5)}$$

where n = porosity;

This model is ideal model. Some differences do not take account of the actual sample including the followings:

(a) The cross section of the actual channels is not circular;

(b) The channels in the network are longer than the length of the sample, and the tubes do not cross the cross section (which is directed at right angles to the main flow direction) perpendicularly (i.e. tortuosity);

(c) The cross-sectional areas of the channels are not constant, but change continuously.

Therefore, correction has to be made between the real sample and this model based on experimental results. In the calculation of hydraulic conductivity, the measurement of actual sample is 2.5 times smaller than that of a bundle of straight capillary tubes. Therefore, Irmay's parameter, i.e. 0.4, is multiplying to eliminate the difference (Kovacs, 1981).

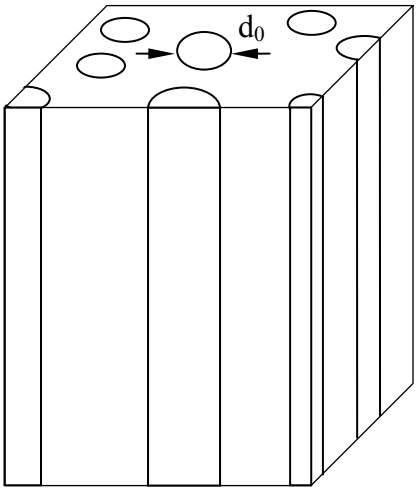

Figure F.1 Capillary tube model